Nanoengineered Titanium as Protein-Releasing Implants: A Molecular Adjunct to Reduce Craniofacial Surgery

A thesis submitted in fulfilment of the requirement for the degree of

Doctor of Philosophy

Bioengineering and Nanomedicine

Manpreet Bariana

January 2017

THE UNIVERSITY of ADELAIDE

School of Dentistry

Faculty of Health Sciences

The University of Adelaide

Table of Contents

List of Figures

LIST OF TABLES

ABSTRACT

Craniosynostosis is a developmental disorder characterised by the premature fusion of skull sutures in children, necessitating repetitive surgical interventions throughout infancy. A major goal of craniosynostosis research is to develop molecular adjunctive treatments to reduce the morbidity and complications associated with multiple craniofacial surgery. Recent progress in molecular biology has highlighted the regulatory effects of bone morphogenetic protein 2 (BMP2) antagonists, including glypicans (GPC1 and GPC3), on suture morphogenesis and cellular functions. Moreover, the availability of genetically-engineered murine models of human craniosynostosis and drug-delivery systems (DDS) has assisted towards investigation of the glypican-based therapeutics *in vivo*. However, the conventional DDS are limited by their uncontrolled release patterns and undesired pharmacokinetics. The development of clinically viable implantable DDS, prior to human trials, require preclinical studies to investigate their characterisation, efficacy, pharmacokinetics and toxicity both *in vitro* and *in vivo* (in animal models).

Medical Titanium (Ti) implants nanoengineered with Titania nanotubes (TNTs) have been recognised as a superior delivery platform in complex bone therapies (*i.e.* orthopaedics, cancer *etc*.) to localise the release of therapeutics in a controlled and sustained manner. This thesis presents the use of therapeutic-releasing TNT/Ti implant technology in a murine model, to address a key clinical challenge of delaying post-operative sutural bone growth in craniosynostosis. This interdisciplinary project has three aspects and specific aims including: (i) engineering and *in vitro* study: to fabricate and optimise TNT/Ti implants to study glypican release *in vitro* and bioactivity

in murine C2C12 cells, (ii) pre-*in vivo* cell study: to evaluate the biological response at TNT-cell interface of heterogeneous (human) suture mesenchymal cells (SMCs) and (iii) *in vivo* study: to assess *in vivo* implant biocompatibility and efficacy as a glypican delivery system in wildtype and Crouzon murine models.

TNT/Ti implants with controllable nanotube dimensions were fabricated via electrochemical anodisation process, and their protein-releasing capability and protein functionality were tested spectrophotometrically in physiological buffer and transfected C2C12 cells (BMP reporter cells), respectively. A metabolic activity assay was performed to investigate human SMC behavior at TNT-cell interface. The *in vivo* performance was assessed using micro-CT and histology in a surgical cranial defect model to verify TNT/Ti implant biocompatibility and glypican release efficiency.

A protein loaded, mechanically robust TNT/Ti implant (120 ± 10 nm pore-diameter) displayed a biphasic *in vitro* release profile, with high loading efficiencies and prolonged release durations, spanning across 1 to 4 weeks. The pharmacokinetic modelling, based on the protein release parameters, showed an anomalous burst release and a zero-ordered sustained release. GPC1 and GPC3 released from TNTs were biologically active and reduced the BMP2-osteogenic activity in C2C12 cells. A decrease in adhesion and proliferation of SMCs at the TNT-cell interface, rendered the implant nanotopography and surface chemistry suitable for craniosynostosis therapy. The murine studies confirmed the implant biocompatibility and reiterated the sustained delivery of glypicans *in vivo*, demonstrated by decreased bone volume and surface area in therapeutically-intervened cranial defects.

These findings confirm the potential of the nanoengineered TNT/Ti implants as an effective glypican delivery system to delay rapid post-operative bone re-growth in a murine model. This approach may evolve into a non-surgical molecular adjunct to minimise the need for recurrent re-operations in human craniosynostosis management.

PREFACE

This thesis is submitted as a "Combined Conventional Publication format" in accordance with "Specifications for Thesis 2015" of the University of Adelaide. It contains an introduction, a detailed literature review and six experimental chapters followed by conclusion and appendices. The research that was carried out during the three and a half years of this PhD program has resulted in successful publication and/or submission of two articles in reputed journals. Additionally, two other journal articles are under preparation. Also, the research findings of this PhD study have been presented at 7 national and international conferences. A complete list of publications is provided in following pages (p. xxii-xxv).

LIST OF PUBLICATIONS

Peer-reviewed Journal Articles Published:

1. **M. Bariana**, P. Dwivedi, S. Ranjitkar, J. Kaidonis, D. Losic, P.J. Anderson , "Biological Response of Human Suture Mesenchymal Cells to Titania Nanotube-Based Implants for Advanced Craniosynostosis Therapy", *Colloids and Surfaces: B*, 2017, 150, 59-67.

Journal Articles Submitted/In Preparation:

2. **M. Bariana**, P. Dwivedi, S. Ranjitkar, J. Kaidonis, D. Losic, P.J. Anderson, " Glypican-Based Drug Releasing Titania Implants to Regulate BMP2 Bioactivity as a Potential Approach for Craniosynostosis Therapy", *Nanomedicine: Nanotechnology, Biology and Medicine*, 2016. (Invited article under peer-review)

3. **M. Bariana**, S. Ranjitkar, J. Kaidonis, D. Losic, P.J. Anderson , " Titania Nanotube-based Glypican-3 delivery Implants inhibit Cranial Defect Healing in Crouzon Model of Craniosynostosis" 2016. (Under preparation for Nature Communications)

4. **M. Bariana**, S. Ranjitkar, J. Kaidonis, D. Losic, P.J. Anderson , "Assessment of *in vivo* Tissue Response to Titania Nanotube-based Cranial implants" 2016. (Under preparation for Journal of Biomedical Materials Research Part A)

Conference Presentations:

1. **M. Bariana**, P. Dwivedi, S. Ranjitkar, J. Kaidonis, D. Losic, P.J. Anderson , "Cellular response of Human Suture Cells on Titania Nanotube-based Implants for Craniosynostosis Therapy", International Conference on Nanoscience and Nanotechnology 2016, Canberra, Australia, February 2016. (Poster presentation)

2. **M. Bariana**, P. Dwivedi, S. Ranjitkar, J. Kaidonis, D. Losic, P.J. Anderson , "Nanoengineered Protein-Delivery System for Craniosynostosis Therapy", IADR ANZ Division 55th Annual Scientific Meeting, Dunedin, New Zealand, August 2015. (Poster and oral presentation)

3. **M. Bariana**, S. Ranjitkar, J. Kaidonis, D. Losic, P.J. Anderson, "Titania Nanotubes-based Protein-release Studies to Delay Suture Fusion in Re-synostosis Murine Model", 6th International Nanomedicine Conference, Sydney, Australia, July 2015. (Oral presentation)

4. **M. Bariana**, S. Ranjitkar, J. Kaidonis, D. Losic, P.J. Anderson, "A Nano-approach for Craniosynostosis Therapy" Asia Pacific Craniofacial Association 2014 Biennial Meeting, Adelaide, Australia, October 2014. (Oral presentation)

5. **M. Bariana**, S. Ranjitkar, J. Kaidonis, D. Losic, P.J. Anderson, "A Novel Treatment to Prevent Re-operation in Craniosynostosis" 2014 Joint Australian-New Zealand CRS Student Workshop Development of Pharmaceutical Therapeutics: From Biological Imaging to Delivery System Optimisation, Adelaide, Australia, October 2014 (Oral presentation)

6. **M. Bariana**, S. Ranjitkar, J. Kaidonis, D. Losic, P.J. Anderson, "Protein-eluting Titania Nanotube-based Implants for Craniosynostosis Therapy" 5th International Nanomedicine Conference, Sydney, Australia, June 2014. (Poster presentation)

7. **M. Bariana**, T. Kumeria, A. Santos, S. Ranjitkar, J. Kaidonis, D. Losic, P.J. Anderson, "Nanoporous Anodic Alumina as Protein-Delivery System for Localised Therapy: Controlling Release Characteristics by Structural modifications" International Conference on Nanoscience and Nanotechnology 2014, Adelaide, Australia, February 2014. (Poster presentation)

Awards:

1. International Association for Dental Research (IADR) ANZ Division: Joan Chong Award in Dental Materials 2014 for early career researchers (October 2014).

2. The Colgate Travel Award from the School of Dentistry, The University of Adelaide to present at the IADR ANZ Division meeting in Dunedin, New Zealand (August 2015).

3. Best Presentation Award at Research Day organised by the Faculty of Health Sciences, The University of Adelaide (July 2015).

Additional Publications:

Book Chapter:

1. M. S. Aw, **M. Bariana**, D. Losic, "Nanoporous Anodic Alumina for Drug Delivery and Biomedical Applications", *Nanoporous Alumina: Fabrications, Structure, Properties and Applications* 2015, Springer International Publishing AG- Germany, Springer Series in Materials Science 219, DOI: 10.1007/978-3-319-20334-8.

Review Articles:

2. A. Santos, M. Sinn Aw, **M. Bariana**, T. Kumeria, Y. Wang., D. Losic, "Drug-releasing implants: Current progress, challenges and perspectives", J*ournal of Materials Chemistry B*, 2014, 2, 6157-6182.

3. D. Losic, M. Sinn Aw, A. Santos, K. Gulati, **M. Bariana**, "Titania nanotube arrays for local drug delivery: Recent advances and perspectives", *Expert Opinion on Drug Delivery*, 2015, 12, 103-127.

DECLARATION

I certify that this work contains no material which has been accepted for the award of any other degree or diploma in my name, in any university or other tertiary institution and, to the best of my knowledge and belief, contains no material previously published or written by another person, except where due reference has been made in the text. In addition, I certify that no part of this work will, in the future, be used in a submission for any other degree or diploma in any university or other tertiary institution without the prior approval of the University of Adelaide and where applicable, any partner institution responsible for the joint-award of this degree. I acknowledge the support I have received for my research through the provision of an Australian Government Research Training Program Scholarship.

I give consent to this copy of my thesis when deposited in the University Library, being made available for loan and photocopying, subject to the provisions of the Copyright Act 1968.

 The author acknowledges that copyright of published works contained within this thesis resides with the copyright holder(s) of those works.

I also give permission for the digital version of my thesis to be made available on the web, via the University's digital research repository, the Library catalogue and also through web search engines, unless permission has been granted by the University to restrict access for a period of time.

MANPREET BARIANA

AKNOWLEDGEMENTS

"Nothing worth having comes easy" and this amazingly daunting yet worthy PhD journey was no different. This unique milestone in my life would have been impossible to achieve without my professional and personal support system. First and foremost, I would like to thank my principal supervisor Prof. Peter Anderson for his unwavering support and encouragement over the years, from introducing me to the world of craniofacial biology to putting the "bio" in my engineering. I have been constantly amazed by his passion, enthusiasm and dedication for research which may only be eclipsed by his commitment to the students. He was always an email away to discuss new ideas, problems with research, or even for a "pep talk", no matter how busy his schedule was! He has worked equally hard (if not more) to get me across the finish line and I would not be overstating when I say, I owe this thesis to him.

I would also like to thank my co-supervisor Prof. Dusan Losic for giving me my first break as a naïve researcher 5 years ago and supporting me till the end of my PhD. He gave me freedom to explore the exciting field of biomaterials and believed in my ability to handle this exciting interdisciplinary project. I would also like to acknowledge my co-supervisor A/Prof. John Kaidonis for always having full confidence in me (even when I doubted myself). His kind and insightful comments (both work and life-related) have helped me stay motivated and sane. He has always guided me with patience and a big smile on his face. I cannot express my gratitude towards Dr. Sarbin Ranjitkar for being a tremendous mentor in more ways than one. His valuable feedback and attention to detail has turned hundreds of my imperfect drafts into well-crafted manuscripts/chapters. His prompt and timely advice has kept this thesis on schedule, even if it

meant spending the weekends to help me run statistics, chase paper submissions, or just pick up typos and spelling errors. Besides being an ace advisor, he's also a great friend. I could not have asked for a better supervisory panel to work with. I would like to extend a big thank you to the University of Adelaide for giving me the opportunity and financial support to pursue this research.

The friendly staff at Women's and Children's hospital deserve a special mention. More specifically, I would like to thank Dr. Prem Dwivedi for training me in cell culture and related bioassays, all the while reminding me the importance of being organised and planned during the experiments. I am also extremely grateful to Kerry Lymm for her infallible help with all things related to bone histology, and to Lynn Marsden and Steve for managing and taking care of my mice and patiently helping me out in the unfamiliar animal house territory.

The support from characterisation facility at Adelaide microscopy is of paramount importance to this research. I would like to acknowledge Ruth Williams, Ken Nuebauer, Lyn Waterhouse and Agatha Labrinidis for their constant help and guidance (even after hours and on weekends). Ruth has been an absolute legend, forever staying positive to help me tackle the never ending list of problems related to micro-CT (she called me "trouble" for a reason). I also appreciate the help provided by the IPAS (at OptoFab node of the Australian National Fabrication Facility) during Implant fabrication. I would like to extend my gratitude to workshop staff from the School of Chemical Engineering, particularly Jason Peak, Michael Jung and Jeffrey Hiorns, for assistance with the fabrication of the electrochemical set-up.

I would like to thank my 6th floor dentistry family for accepting me as one of their own; Special thanks to Prof. Grant Townsend for his valuable fatherly advice whenever I was in distress; Karen

Most importantly, I would like to convey my utmost gratitude towards my family; Mum for her unconditional love, genuine care and constant prayers, Dad for believing in me and my dreams and off course for the "brainy genes", my big brother for being my hero and stress-buster, and my sis-in-law for being my personal cheerleader. You guys mean the world to me and I know I can always count on you for anything and everything.

"Being a PhD student is like becoming all of the Seven Dwarfs. In the beginning you're Dopey and Bashful. In the middle, you are usually sick (Sneezy), tired (Sleepy), and irritable (Grumpy). But at the end, they call you Doc, and then you're Happy." (Adapted from Azuma, 2002, p.2)

I dedicate this thesis to these very special people in my life:

My Mum

My Dad

My Brother

And my fur-baby Dazzle.

I love you all dearly.

xxx

CHAPTER 1

INTRODUCTION

CHAPTER 1: Introduction

1.1. Thesis Introduction

Craniosynostosis is a developmental disorder characterised by the premature fusion of one or more cranial sutures, affecting approximately 1 in 2500 children [1-3]. If left untreated, craniosynostosis can result in severe complications, including increased intracranial pressure, impaired cerebral blood flow, airway obstruction, restricted brain growth, impaired vision and hearing, cognitive disabilities, seizures and adverse psychological effects, along with deformed head shape and asymmetrical facial features [4-8]. The current management in most cases requires complex cranial vault reconstruction to release the synostosed suture, restore the normal intracranial volume and correct the craniofacial deformities. However, patients often experience rapid post-operative bone re-growth at craniectomy site, necessitating repetitive invasive interventions as the dysmorphic growth continues [5, 9, 10]. A major goal of craniosynostosis research is to develop molecular adjunctive treatment to decrease the potential morbidity and mortality associated with multiple high-risk operations. **Figure 1.1** shows the digital and radiographic image of an infant before surgery for unicoronal synostosis (*i.e.* suture fusion on the right side of the skull).
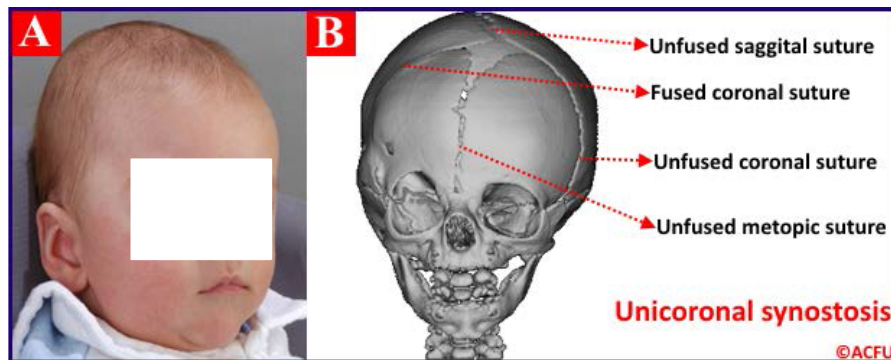
Figure 1.1. Digital (A) and radiographic (B) images of an infant skull with unicoronal synostosis

before undergoing a cranial vault reconstruction surgery at the Australian Craniofacial Unit.

Recent advancements in cranial bone biology and genetic micro-array techniques have led to identification of biochemical pathways involved in normal and pathological suture morphogenesis, unravelling the aetiopathology of craniosynostosis [1, 11-13]. The osteogenically potent bone morphogenetic protein 2 (BMP2) signalling pathway has been reported to play a key role in regulation of sutural bone formation and cellular functions, whereas a faulty/mutated BMP2 pathway has been linked to craniosynostosis. Moreover, bone antagonising molecules such as glypicans (GPC1 and GPC3), expressed in patent sutures and decreased in prematurely fusing sutures, have been shown to downregulate the BMP2-mediated osteogenic activity. To this end, manipulation of BMP2 pathway via glypican delivery can act as potential therapeutic intervention to control the bone re-growth after the primary surgery [1, 2, 11, 14, 15]. Moreover, the design and development of genetically-modifed murine models analoguos to human syndromic craniosyntosis have contributed towards studying suture fusion and testing the glypican-based therapeutics *in vivo*. Typically, a critical-sized defect (CSD) is created onto the mouse cranium, lateral to the suture of interest, to observe and quantify the bone re-growth pattern. The CSD does not heal completely without a positive therapuetic intervention in both normal and pathological models [16, 17].

A major challenge in translating the molecular findings into a therapeutically viable strategy is the lack of suitable drug delivery systems (DDS). The development of clinically viable implantable DDS, prior to human trials, requires preclinical studies to investigate their characterisation, efficacy, pharmacokinetics and toxicity both *in vitro* and *in vivo* (in animal models). Medical Titanium (Ti) implants electrochemically anodised with Titania nanotubes (TNTs) have been recognised as a superior delivery platform in complex bone therapies, especially

in orthopaedics to localise the release of in-bone therapeutics in controlled and sustained manner for severe conditions, including osteomyelitis and bone cancer [18-23]. TNTs have also been tested to deliver chemotherapeutics into the brain and anti-inflammatory and antibiotic payloads to various target sites in the body [18, 24]. Extending the scope of this nanoengineered delivery system to craniosynostosis treatment may provide a molecular adjunct to reduce the number of cranial reconstruction surgery and potentially avoid primary fusion.

Figure 1.2 presents the two different murine models investigated in this study to evaluate the protein-eluting ability of the TNT/Ti implants: (i) a pathological Crouzon model with $Fgfr2^{c342y/+}$ mutated genes presenting phenotypic similarity to human Crouzon patients, including dome-shaped skull, proptotic eyes, underdeveloped maxilla, mandibular prognathism and prematurely fused coronal sutures in majority of cases [25-27] and (ii) the wildtype littermates without the mutation.

Phenotypic Difference between Crouzon and Wildtype mouse

(a)   (b)   (c)
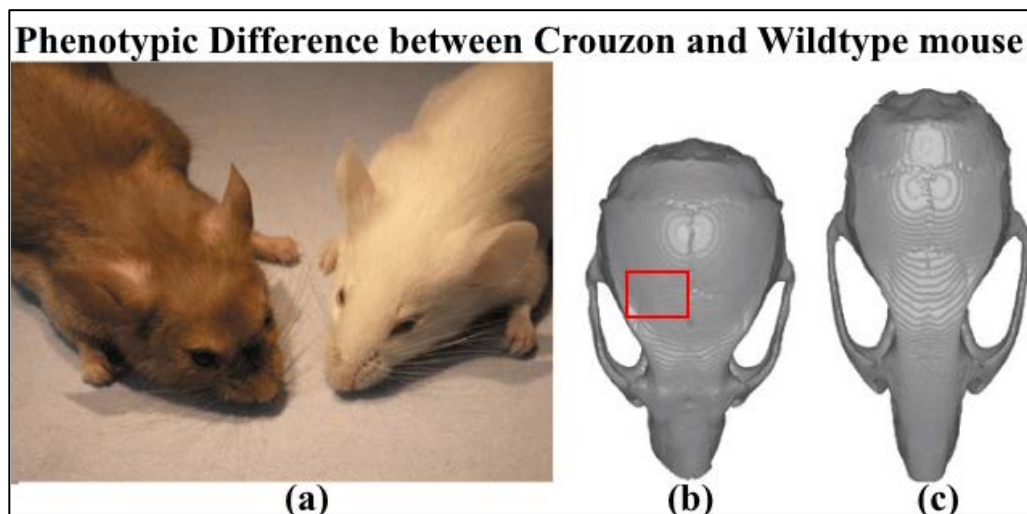
Figure 1.2. (a) Digital photographs of a Crouzon mouse (left) and a wildtype mouse (right). Micro-CT images of the skull of (b) a Crouzon mouse and (c) a wildtype mouse. The inset with red borders shows the fused coronal suture (adapted with permission from [27]).

1.2. Objectives

The broad aim of the work described in this thesis was to investigate the potential of glypican-releasing TNT/Ti implant technology in a murine model, to address a key clinical challenge of delaying post-operative sutural bone growth in craniosynostosis. This interdisciplinary project combines nanofabrication, surface engineering, craniofacial biology, molecular biology and nanomedicine to develop a molecular adjunct for craniosynostosis treatment. A schematic of the proposed TNT/Ti based implantable glypican delivery system is presented in **Figure 1.3**.
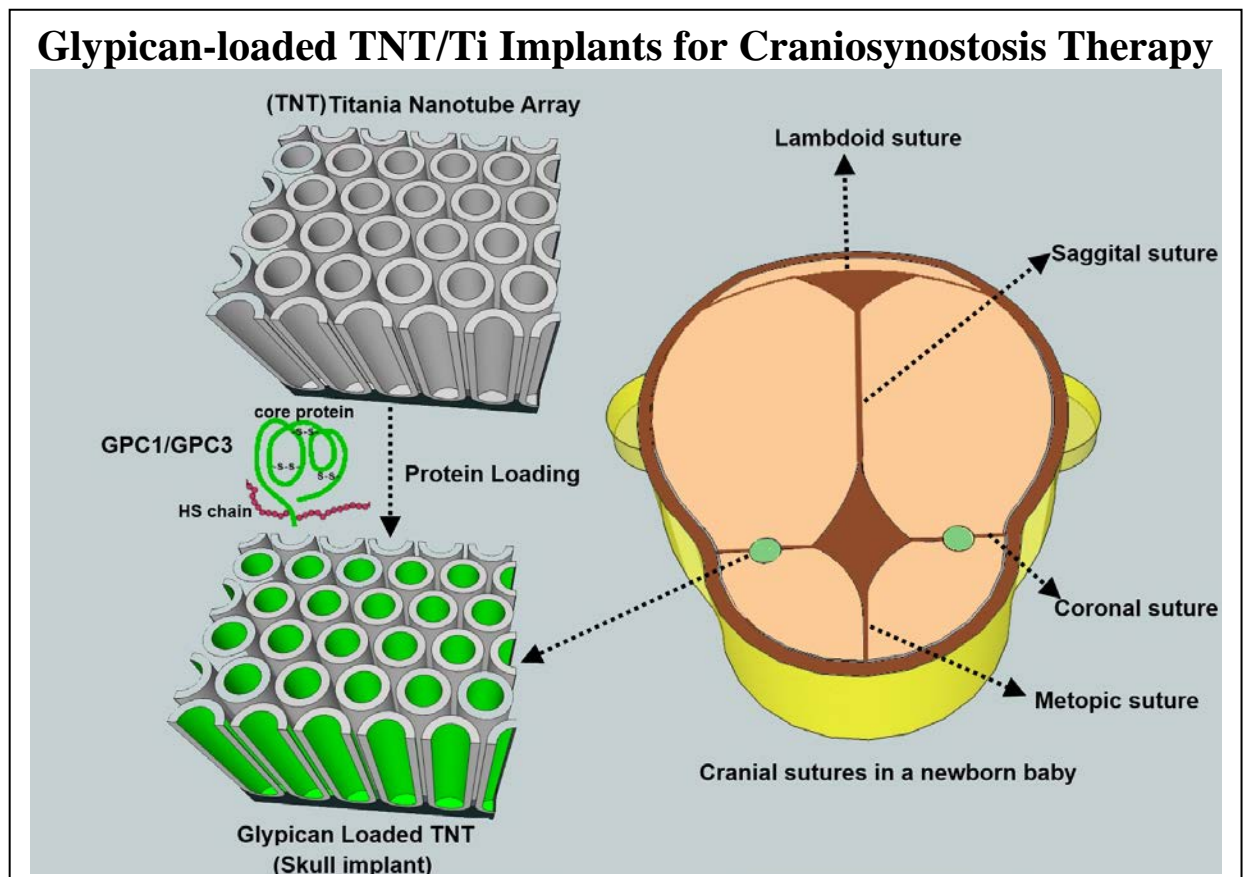
Figure 1.3. Application of electrochemically anodised Titania nanotubes (TNTs) as glypican-releasing skull implants for craniosynostosis therapy.

These are the list of aims of this research and the specific objectives relating to them:

1. **Implant engineering**: To fabricate and refine TNT/Ti based cranial implants with improved structural properties for developing an effective protein delivery system. The specific research objectives are:

   - to design and produce 3 mm circular Ti discs via ultrasonic milling to act as implant base for anodisation and to fit into critical-sized defects in murine models,

   - to optimise electrochemical anodisation conditions to fabricate stable and high quality TNTs with controllable and reproducible dimensions,

   - to compare the effect of two different electrolyte conditions on the TNT surface and mechanical characteristics, and

   - to modify and characterise the TNT/Ti implant surface with biopolymer coatings (Chitosan and Pluronic-F127) of variable thickness.

2. *In vitro* **study**: To investigate the *in vitro* protein release characteristics of biopolymer-coated and uncoated TNT/Ti implants in phosphate buffer (PBS, pH 7.4). The specific research objectives are:

   - to measure the physical characteristics (hydrodynamic diameter and charge) of model proteins (control- Bovine Serum Albumin and experimental- GPC1 and GPC3),

   - to establish the release characteristics of control protein by exploring the effects of loading amounts, techniques (in vacuum or air), and different biopolymer coatings,

   - to establish release profiles for GPC1 and GPC3 entrapped within polymer-coated and uncoated TNTs at room temperature and 37 $^{\circ}$C, and

   - to mathematically model the glypican release kinetics.

3. *In vitro* **cell study**: To demonstrate the ability of chitosan-coated TNT/Ti implants to slow release bioactive recombinant glypicans. The specific research objectives are:

   - to measure the *in vitro* release of rGPC1 and rGPC3 independently and synergistically (rGPC1+3) in phosphate buffer (PBS, pH 7.4),

   - to transfect the murine myoblasts, C2C12 cells with experimental (BMP2-responsive luciferase) and control plasmid constructs to functionally analyse the BMP2 activity using Dual luciferase reporter (DLR) assay, and

   - to analyse the inhibitory effects of rGPC1, rGPC3 and rGPC1+3 released from proposed TNT-based cranial implants on BMP2 bioactivity in the transfected cells using DLR assay.

4. **Pre-*in vivo* cell study**: To evaluate the biological response of heterogeneous (human) suture mesenchymal cells (SMCs) at TNT-cell interface. The specific research objectives are:

   - to investigate the initial human SMC interaction at the implant surfaces,

   - to compare the human SMC behaviour (adhesion, spreading and proliferation) within and between the polymer-coated (with Chitosan and Pluronic-F127), uncoated TNT and control surfaces, and

   - to investigate the effects of surface chemistry and wettability on human SMC viability between the polymer-coated and uncoated TNT/Ti implants.

5. ***In vivo* implant response**: To assess the *in vivo* tissue response to TNT/Ti implants (polymer-coated and uncoated) in wildtype murine model, after 12 weeks of implantation. The specific research objectives are:

- to histologically evaluate the skin and bone tissue (around the implantation site) to establish the biocompatibility of TNT/Ti implants inserted either subcutaneously or within the CSD,

- to quantify (via micro-CT imaging) the undesired/excessive bone or cartilage formation inside the CSD, and

- to surface characterise the TNT/Ti discs retrieved at the end of the study.

6. **Implant protein release potential *in vivo***: To test the delivery potential of chitosan-coated and uncoated TNT/Ti implants to locally release the biologically active model proteins (control-BSA and experimental- GPC3) within the murine cranial CSDs, over the 12 weeks implantation period. The specific research objectives are:

- to analyse the *in vivo* degradation of chitosan film covering the TNT/Ti surface,

- to evaluate the effect of BSA and GPC3 released form TNT/Ti implants on bone re-growth within the defect site in a wildtype mouse model, and

- to assess the bone-antagonising effect of GPC3 released from TNT/Ti implants in a Crouzon defect model (Fgfr2$^{c342y/+}$ mutated) and compare it with the wildtype littermates.

1.3. Thesis Structure

This thesis includes 10 chapters and the following summary briefly describes how specific objectives (as defined in the previous section) are addressed by each chapter, towards developing a TNT-based molecular adjunct to craniosynostosis therapy.

Chapter 1 provides an outline of the work performed throughout the course of this project. It briefly describes the craniofacial disorder (craniosynostosis), its symptoms and current management technique. It emphasises on the need to develop minimally invasive alternative treatments for craniosynostosis, based on molecular bone inhibition, to reduce the associated morbidity. Most importantly, it describes the potential of nanoengineered Ti implants for localised cranial bone inhibition.

Chapter 2 offers detailed literature review related to the pathological condition and the nanoengineered implants, to bridge the knowledge gap and substantiate the applicability of this interdisciplinary treatment approach.

Chapter 3 provides details on the materials, electrochemical set-up and methodologies used for TNT/Ti implant fabrication and surface modifications.

Chapter 4 reports loading of model protein molecules into the TNT nanocarriers and their subsequent release characteristics under different conditions and parameters. This work formed the basis for future cell and animal experiments.

Chapter 5 demonstrates the biological response of human suture mesenchymal cells to the TNT/Ti implant surface. The cell morphology, adhesion, proliferation and viability characteristics were considered to evaluate the effects of different surface-modified TNT implants. This work is an important contribution towards pre-clinical assessment of TNT/Ti implants in heterogeneous cell population.

Chapter 6 presents the ability of TNT/Ti implants to release biologically active protein molecules that inhibit BMP2 activity in C2C12 cell cultures. This study analyses the encapsulation and preservation of the labile and sensitive therapeutics within the nanotubes.

A common experimental section extensively describing the materials and methods used in all *in vivo* investigations precedes Chapter 7 and 8.

Chapter 7 compares the *in vivo* performance of the polymer-coated and uncoated TNT/Ti cranial implants to establish their biocompatibility, when implanted subcutaneously or within a surgically created critical-sized defect. This work tested the implantation, surgical and analysis techniques in a normal bone healing model (wildtype mouse).

Chapter 8 provides the successful preliminary testing of the bone-inhibiting potential of GPC3-releasing TNT/Ti implants in both wildtype and Crouzon murine model. This study transcends from the previous *in vitro* work as it manifests the practical application of the designed implants in a successful surgical setting.

Chapter 9 presents a consolidative discussion articulating the investigations carried throughout this project, reiterating the key findings of the studies in Chapter 3-8. It also provides a perspective for future applications of TNT/Ti protein-delivering cranial implants.

Appendix A describes the detailed procedures for histological labelling with H&E, Movat Pentachrome, Picro-Sirius Red, Periodic Acid- Schiff and TRAP stains. **Appendix B** contains Animal Ethics Approval certificates from The University of Adelaide (first page of the approved application) and Women's and Children's Animal Ethics Committee. **Appendix C** shows the grant approval acknowledgement for this project from Australian Dental Research Foundation (ADRF).

1.4. References

1. Coussens, A.K., Wilkinson, C.R., Hughes, I.P., Morris, C.P., Van Daal, A., Anderson, P.J., and Powell, B.C. Unravelling the molecular control of calvarial suture fusion in children with craniosynostosis. *BMC Genomics*, **2007**. 8, 458-83.

2. Dwivedi, P., Grose, R., Hii, C., Filmus, J., Anderson, P., and Powell, B. Regulation of bone morphogenetic protein signalling and osteogenesis by glypicans in human cranial suture cells. *Bone*, **2011**. 48, 243.

3. Wilkie, A.O. Craniosynostosis: genes and mechanisms. *Human Molecular Genetics*, **1997**. 6, 1647-56.

4. Gault, D.T., Renier, D., Marchac, D., and Jones, B.M. Intracranial pressure and intracranial volume in children with craniosynostosis. *Plastic and Reconstructive Surgery*, **1992**. 90, 377-81.

5. Panchal, J. and Uttchin, V. Management of craniosynostosis. *Plastic and Reconstructive Surgery*, **2003**. 111, 2032-48.

6. Gosain, A.K., McCarthy, J.G., and Wisoff, J.H. Morbidity associated with increased intracranial pressure in Apert and Pfeiffer syndromes: the need for long-term evaluation. *Plastic and Reconstructive Surgery*, **1996**. 97, 292-301.

7. Gonsalez, S., Hayward, R., Jones, B., and Lane, R. Upper airway obstruction and raised intracranial pressure in children with craniosynostosis. *European Respiratory Journal*, **1997**. 10, 367-75.

8.   Khong, J.J., Anderson, P., Gray, T.L., Hammerton, M., Selva, D., and David, D. Ophthalmic findings in apert syndrome prior to craniofacial surgery. *American Journal of Ophthalmology*, **2006**. 142, 328-30.

9.   Ghali, G., Sinn, D.P., and Tantipasawasin, S. Management of nonsyndromic craniosynostosis. *Atlas of the Oral and Maxillofacial Surgery Clinics*, **2002**. 10, 1-41.

10.   Mehta, V.A., Bettegowda, C., Jallo, G.I., and Ahn, E.S. The evolution of surgical management for craniosynostosis. *Neurosurgical Focus*, **2010**. 29, E5.

11.   Mooney, M.P., Moursi, A.M., Opperman, L.A., and Siegel, M.I. Cytokine therapy for craniosynostosis. *Expert Opinion on Biological Therapy*, **2004**. 4, 279-99.

12.   Derderian, C. and Seaward, J. Syndromic craniosynostosis. in *Seminars in Plastic Surgery*. **2012**. Thieme Medical Publishers.

13.   Kimonis, V., Gold, J.-A., Hoffman, T.L., Panchal, J., and Boyadjiev, S.A. Genetics of craniosynostosis. in *Seminars in Pediatric Neurology*. **2007**. Elsevier.

14.   Warren, S.M., Brunet, L.J., Harland, R.M., Economides, A.N., and Longaker, M.T. The BMP antagonist noggin regulates cranial suture fusion. *Nature*, **2003**. 422, 625-29.

15.   Dwivedi, P., Lam, N., and Powell, B. Boning up on glypicans—opportunities for new insights into bone biology. *Cell Biochemistry and Function*, **2013**. 31, 91-114.

16.   Cooper, G.M., Usas, A., Olshanski, A., Mooney, M.P., Losee, J.E., and Huard, J. Ex vivo Noggin gene therapy inhibits bone formation in a mouse model of postoperative resynostosis. *Plastic and Reconstructive Surgery*, **2009**. 123, 94-103.

17.   Ye, J.-H., Xu, Y.-J., Gao, J., Yan, S.-G., Zhao, J., Tu, Q., Zhang, J., Duan, X.-J., Sommer, C.A., and Mostoslavsky, G. Critical-size calvarial bone defects healing in a mouse model with silk scaffolds and SATB2-modified iPSCs. *Biomaterials*, **2011**. 32, 5065-76.

18.   Gulati, K., Aw, M., and Losic, D. Nanoengineered drug-releasing Ti wires as an alternative for local delivery of chemotherapeutics in the brain. *International Journal of Nanomedicine,* **2012**. 7, 2069-76.

19.   Gulati, K., Aw, M.S., Findlay, D., and Losic, D. Local drug delivery to the bone by drug-releasing implants: perspectives of nano-engineered titania nanotube arrays. *Therapeutic Delivery*, **2012**. 3, 857-73.

20.   Gulati, K., Aw, M.S., and Losic, D. Drug-eluting Ti wires with titania nanotube arrays for bone fixation and reduced bone infection. *Nanoscale Research Letters*, **2011**. 6, 1-6.

21.   Aw, M.S., Khalid, K.A., Gulati, K., Atkins, G.J., Pivonka, P., Findlay, D.M., and Losic, D. Characterization of drug-release kinetics in trabecular bone from titania nanotube implants. *International Journal of Nanomedicine*, **2012**. 7, 4883-92.

22.   Losic, D., Aw, M.S., Santos, A., Gulati, K., and Bariana, M. Titania nanotube arrays for local drug delivery: recent advances and perspectives. *Expert Opinion on Drug Delivery*, **2015**. 12, 103-27.

23.   Neupane, M.P., Park, I.S., Bae, T.S., Yi, H.K., Uo, M., Watari, F., and Lee, M.H. Titania nanotubes supported gelatin stabilized gold nanoparticles for medical implants. *Journal of Materials Chemistry*, **2011**. 21, 12078-82.

24.   Aw, M.S., Gulati, K., and Losic, D. Controlling drug release from titania nanotube arrays using polymer nanocarriers and biopolymer coating. *Journal of Biomaterials and Nanobiotechnology*, **2011**. 2, 477-84.

25.   Eswarakumar, V.P., Horowitz, M.C., Locklin, R., Morriss-Kay, G.M., and Lonai, P. A gain-of-function mutation of Fgfr2c demonstrates the roles of this receptor variant in osteogenesis. *Proceedings of the National Academy of Sciences of the United States of America*, **2004**. 101, 12555-60.

26.   Perlyn, C.A., DeLeon, V.B., Babbs, C., Govier, D., Burell, L., Darvann, T., Kreiborg, S., and Morriss-Kay, G. The craniofacial phenotype of the Crouzon mouse: analysis of a model for syndromic craniosynostosis using three-dimensional MicroCT. *The Cleft palate-Craniofacial Journal*, **2006**. 43, 740-48.

27.   Ólafsdóttir, H., Darvann, T.A., Hermann, N.V., Oubel, E., Ersbøll, B.K., Frangi, A.F., Larsen, P., Perlyn, C.A., Morriss-Kay, G.M., and Kreiborg, S. Computational mouse atlases and their application to automatic assessment of craniofacial dysmorphology caused by the crouzon mutation Fgfr2C342Y. *Journal of Anatomy*, **2007**. 211, 37-52.

CHAPTER 2

LITERATURE REVIEW

CHAPTER 2: Literature Review

2.1. Bone structure and ossification

Bones forming the skeletal framework of all vertebrates are dense connective tissues which serve crucial roles relating to structural support, body movement, blood cell production, maintenance of body chemistry, endocrine signalling and storage depot for vital minerals. The bony milieu consists of organic matrix, inorganic minerals, cells, and water. The organic component is mainly Type I collagen, which interacts with the inorganic crystalline calcium phosphate, entrapping the bone cells and hardening into a bone [1, 2].

Bone development is a dynamic process which remodels throughout the lifespan to repair fractures and accommodate variable mechanical loads. Bone ossification or osteogenesis depends on two primary cell types, osteoclasts and osteoblasts. Osteoclasts are multinucleated bone-resorbing cells that have originated from hematopoietic precursors such as monocytes and macrophages. Osteoclasts located in tiny resorptive pits on bones latch onto the breakdown sites along the surface of the bone and dissolve the bone matrix by enzymatic action [3, 4]. They are often balanced by osteoblasts that are responsible for new bone production. Osteoblasts are small mononucleated cells of mesenchymal origin. They synthesise and secrete collagen fibres and calcium salts to form immature bone matrix called osteoid, which later becomes fully mineralised by hydroxyapatite deposition [5]. Once the bone calcifies, the osteoblasts get trapped inside the matrix. These mature and quiescent bone cells are termed as osteocytes and they maintain the bone tissue, mineral homeostasis and metabolic activities [6].

Bones regenerate by two distinct developmental processes: intramembranous ossification and endochondral ossification [7]. Intramembranous ossification is common to skull and other flat bones in the body, wherein the progenitor cells differentiate directly to form a sheet-like dense connective tissue membrane which calcifies as the tissue develops. Endochondral ossification occurs in development and repair of long bones. It involves replacement of a hyaline cartilaginous intermediate which prefigures future skeletal elements, within a developing bone [8]. During this process, the chondrocytes undergo proliferation, followed by hypertrophy and death. This is succeeded by vascular invasion, spongy bone formation and eventually calcification with hydroxyapatite to form mature bone [9-11].

2.2. Normal mammalian skull vault development

The basic structure of a mammalian cranial vault consists of five free-floating flat bones: a pair of frontals and parietals, and a singular occipital, which abut at fibrous junctions called sutures [12, 13]. According to Gray's Anatomy a suture is "an articulation in which contiguous margins of adjacent bone are united by a thin layer of fibrous tissues" [14]. These intervening flexible sutures in infants, separating the bony cranial plates, serve as the most important centers of appositional growth in the skull [15]. The also play pivotal roles in early life, permitting head malleability during passage through the birth canal, helping in the relative movement of the separate bones during volumetric expansion of infant skull and in absorbing mechanical trauma in childhood [16]. An infant human vault typically forms with an interfrontal (metopic) suture between the frontal bones and the sagittal suture situated between the parietal bones. Along the transverse axis, the paired coronal sutures are located between the two frontal and two parietal bones and the paired lambdoid sutures form between the parietal and occipital bones. The junctional boundaries of two or more

sutures comprising of larger non-mineralised areas of connective tissue are termed as fontanelles, which close when the sutures fuse together during normal development [12, 13, 16, 17]. The patency of sutures and production of the new bone is position and age specific, with anterior midline metopic suture closing a few months after birth [18]. The other three sutures obliterate between 22 to 39 months of age [17]. The arrangement of the bones and sutures in newborn human is shown in **Figure 2.1**.
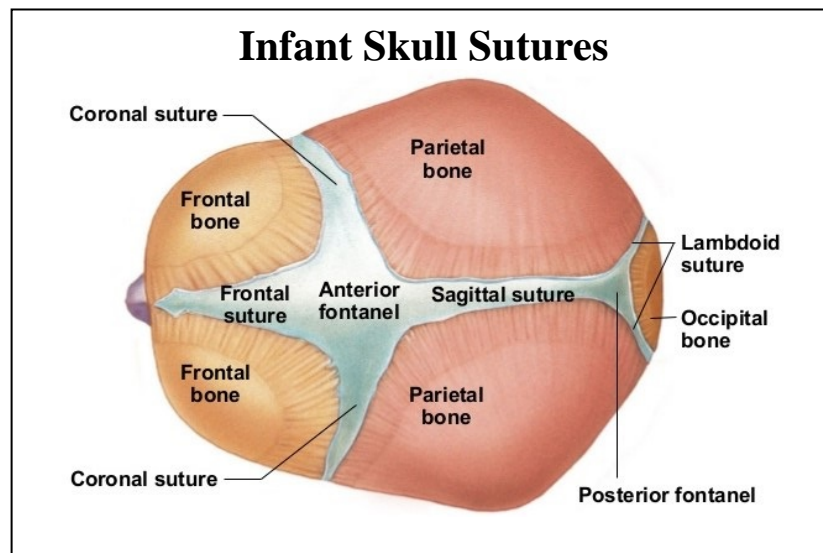
Figure 2.1. The Skull of an Infant with major patent sutures (© 2012 Pearson Education, Inc.).

The mineralisation of the cranial vault at the osteogenic fronts, along the suture boundaries occurs by intramembranous ossification without a pre-existing cartilaginous matrix (**Figure 2.2**). Cranial skeletogenesis is a unique phenomenon derived from multipotent mesenchymal cells located under the dermal mesenchyme and above the meninges covering the brain. Calvaria formation initiates from the primary centre of ossification where progenitor cells undergo rapid proliferation, which allows the cranial vault to expand and accommodate the rapidly growing brain. This is followed by subsequent differentiation into osteoblasts at the osteogenic fronts. The

ossification proceeds radially from the condensation centres to form the skull bones until the two calvaria approximate each other, leading to suture formation during craniofacial development. A fine balance exists between the proliferation and differentiation processes, which along with programmed apoptosis, governs the regulation of suture fusion. Disruption of any of these processes can result in various types of skull distortion and defects [12, 13, 15, 19].
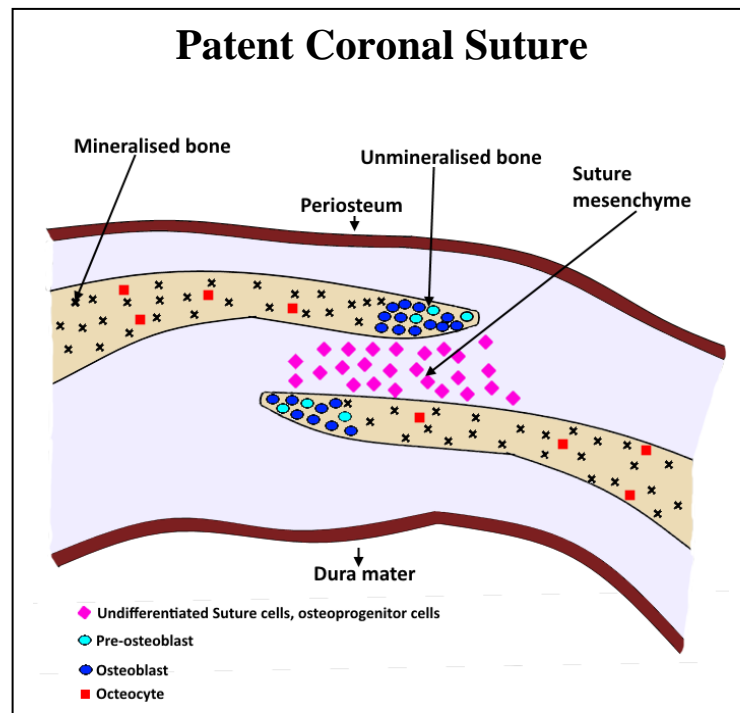
Figure 2.2. Cross-section through a patent coronal suture.

2.3. Craniosynostosis

Craniosynostosis is a debilitating and disfiguring pediatric abnormality that is characterised by the premature fusion of one or more skull sutures, resulting in cessation of bone growth at the affected site [15, 18, 20, 21]. It represents a highly unknown but significant medical problem, occurring in ~ 1 in 2500 live births [22]. The early ossification of cranial sutures is associated with morphologic

abnormalities such as dysmorphic head and asymmetric facial features, causing significant morbidity. Other sequelae include raised intracranial pressure, impaired cerebral blood flow, mental retardation, impaired vision and hearing, airway obstruction, abnormal mastication, intellectual disability, seizures and long-term psychological effects [23-30].

2.3.1. Classification
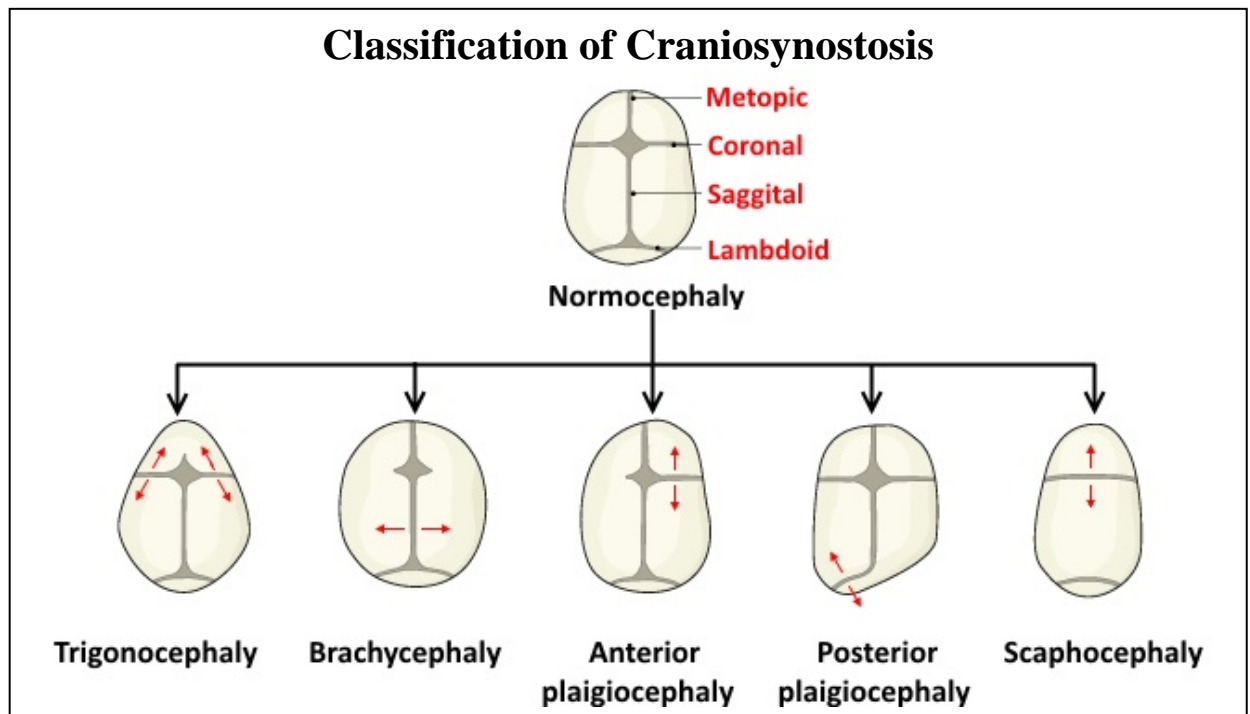
Figure 2.3. Craniofacial growth patterns in craniosynostosis.

Craniosynostosis can be divided into two main groups: syndromic and non-syndromic. The non-syndromic types account for approximately 60% of the cases and usually occur as an isolated event. These types of sporadic craniosynostosis can be predicted phenotypically based on the site of obliterated sutures as well as the rate of progression of synostosis. The shape alteration is dictated by Virchow's law *i.e.*, the compensatory growth of the vault enhances in a plane parallel to the

closed suture, instead of the regular perpendicular dimension, thus causing overexpansion of the cranium [31, 32]. The diagnostic phenotypic classification of the craniofacial anomalies is summarised in **Figure 2.3**.

Sagittal synostosis

Sagittal sutures are most commonly prone to synostosis and comprise of 40% to 58% of the non-syndromic patients. Sagittal synostosis is characterised by a broad forehead, increased anterior-posterior dimension and decreased lateral dimension, leading to an elongated skull. The condition is clinically termed as scaphocephaly (boat head in Greek) [31, 33].

Coronal synostosis

Coronal synostosis accounts for 20% to 29% of the cases and is the second most common type of craniosynostosis. Unilateral coronal fusion causes anterior plagiocephaly typically associated with a skewed head/ facial twist, ipsilateral flattening of the forehead at the side of closed suture and contralateral bulging of the skull in frontoparietal direction [33, 34]. In case of bilateral fusion or brachycephaly, skull shortens anteriorly to posteriorly with bilateral forehead retrusion [33].

Metopic synostosis

According to epidemiologic studies, metopic synostosis occurs only in 4% to 10% of the non-syndromic cases. Resultant trigonocephaly leads to narrowing of the frontal bones, prominence of the posterior parietal and occipital bones and a typical triangular-shaped forehead [33].

Lambdoidal synostosis

This is the rarest type of non-syndromic craniosynostosis (2% to 4%) and is characterised by occipital/posterior plagiocephaly. The resultant phenotype shows ipsilateral flattening and widening of the occipital bone with the cranial base titled toward the affected side [31].

Syndromic craniosynostosis

Craniosynostosis with extracranial dysmorphic features or developmental defects is categorised as the syndromic type. The additional anomalies associated with phenotypical changes in the face, skeleton, nervous system, heart or respiratory tract have been attributed to specific genetic mutations causing clinically recognised syndromes [31, 35].

The most common syndromic form involves a gain-of-function mutation in the fibroblast growth factor receptor family (FGFR 1 to 3) which plays a vital role in cell proliferation and differentiation from the earliest embryonic stages. The FGF receptors are tyrosine kinase like receptors which in mutated state, tend to remain active and cross phosphorylate, even in the absence of a target FGF ligand [12, 36]. This results in Pfeiffer, Apert, Crouzon, Beare-Stevenson, Jackson-Weiss, and Muenke syndromes which are mostly characterised by bicoronal suture fusion or cloverleaf skull, distinctive mid-face deformities and limb abnormalities [31].

Apart from the FGF mutations, certain transcription factors have been known to cause craniosynostosis of variable severities. Boston-type craniosynostosis is caused by mutation in the *MSX2* which is associated to BMP signalling and osteoblast differentiation. This is highly penetrant, autosomal dominant disorder, confined to a single family with variable phenotype from metopic ridging to cleft palate, extra teeth and digital abnormalities [37].

By contrast, Saethre-Chotzen syndrome, an autosomal dominant form results from loss-of-function mutations in TWIST1 gene which is a basic-helix-loop-helix transcription (bHLH) factor expressed early in suture development. The majority of patients display bicoronal synostosis, facial asymmetry, low frontal hairline, drooping eyelids, syndactyly and abnormal ears. Twist 1 has also been held responsible for negatively regulating signalling pathways related to FGFR1, 2 and 3, MSX2 and *Runx2*.

2.3.2. Aetiology

Apart from genetics being a potential cause of premature suture closure, it has been observed that several other factors are likely to play a role, especially in non-syndromic cases. Some of them include biomechanical, environmental and hormonal factors. Increased intrauterine head constraint during pregnancy has been implicated as a risk factor for premature suture fusion. The abnormal forces on the foetal cranial vault inside the womb triggered changes in gene expressions and signalling pathways crucial to bone development. In addition, twins have been documented to be more prone to craniosynostosis compared to singletons [38, 39]. Maternal smoking has been linked to craniosynostosis possibly by affecting the FGFR genes. Furthermore, exposure to teratogenic factors such as amine-containing drugs or epilepsy medication can elevate the risks during pregnancy [40-43]. Moreover, in hyperthyroidism, it is presumed that the bone matures faster due to high levels of thyroid hormone thus mediating premature closure [44].

2.3.3. Diagnostics and management

The preliminary diagnosis is based upon physical examination or cephalometrics that enable precise longitudinal measurements of head growth. Ultrasonographic and radiographic investigations, including X-ray reports and computed tomography (CT) scans, can further aid to visualise the patency of the skull sutures. Three-dimensional CT can clearly document the extent and severity of the deformity and its effect on adjacent craniofacial region. These techniques help in comparing pre-, intra- and post-operative measurements of the bony landmarks. Sophisticated software can be used to reconstruct a CT scan and determine the type of craniofacial abnormality, quantify the skeletal deformity, calculate the changes in intracranial volume and plan a treatment accordingly. Furthermore, molecular screening can be performed by early gene testing in case of syndromic craniosynostosis [23, 45-48].

Moreover, magnetic resonance imaging (MRI) has been applied to measure the flattening of brain foldings. It can anatomically delineate the pattern of cortical gyri and sulci underlying the fused suture. The pre- and post- operative scans that are taken a year apart, can be compared as a follow-up study. But, a lack of centralised database for these MRI scans makes this study unreliable [23].

The management of craniosynostosis is highly dependent on the timing, area and extent of sutural fusion. While the optimal approach for managing craniofacial anomalies involves a multidisciplinary set of skills, surgical intervention has been the most common treatment [23, 49]. Over the past 100 years, craniofacial surgery have evolved from strip craniectomies to a traditional cranial vault reconstruction/remodelling and endoscopic suturectomies [50]. The extended reconstruction surgery involves surgical excision of the fused suture by dividing the cranial bones

artificially and removing, remodelling and repositioning the cranial bone segments. This procedure is usually performed at late infancy, 6-12 months of age because the cranium bones are malleable and easier to reshape. Also, most of the dynamic brain growth is completed by the end of first year and the surgical bony gaps can re-ossify without the need of external fillers. In most cases, fixation hardware such as titanium screws, plates and absorbable implants *etc*. is required to reshape the skull. Though the morbidity rate from the initial operation is low, these surgery are typically 4-5 hours in duration and may require blood transfusion as well as prolonged post-operative hospital care. The surgical intervention helps to improve both aesthetics and function by securing greater room for the brain to expand and eliminating the risks of neurologic and cognitive impairment [23, 50-52].

For infants younger than 3 months, a minimally invasive endoscopic method is adapted to avoid the massive blood loss and trauma associated with a traditional surgery. The surgeon makes small incisions in the scalp, inserts an endoscope for good access and opens the sutures to enable brain growth. This approach is quicker and requires overnight observation in intensive care unit. However, the surgeon cannot alter the cranial shape and these surgery are usually followed by the use of molding helmets therapy. Additional follow-ups and a series of customised helmets are required to mechanically reshape the skull vault [50, 53, 54].

Even after a successful primary operation, cranial vault reconstruction has to be repeated to accommodate the changes with age. In 40% of the cases, the extirpated bones rapidly re-fuse resulting into a condition termed as resynostosis. Thereafter, multiple operative interventions are needed to release the resynostic constraint and normalise the cranial shape, especially in syndromic cases such as Apert, Crouzon and Pfeiffer syndromes [55, 56].

As with all surgical procedures, there are severe mortality and morbidity risks associated with craniectomies. The complications include excessive intra-operative bleeding, infection, dural tears, subdural haemorrhages, scarring, seizures, cerebral edema, stoke and death in extreme circumstances [55, 57-59]. Alternate rationale and solutions to minimise the number of invasive re-operations have been the main focus of craniofacial research over the past few decades. An intra-operative image of a child undergoing cranial vault remodelling is depicted in **Figure 2.4**.

Cranial Vault Reconstruction Surgery
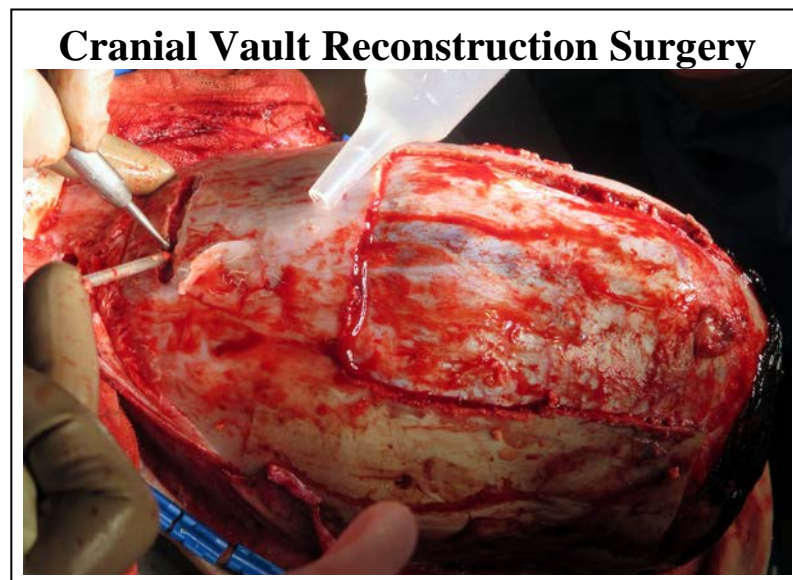
Figure 2.4. Cranial vault reconstruction surgery at Australian Craniofacial Unit (ACFU).

2.3.4. Research based findings for craniosynostosis therapy

2.3.4.1. Animal models in craniofacial research

Craniofacial malformations are among the most heterogeneous but frequent birth defects in humans. An appropriate animal model forms the basis of all the surgical manipulations required for craniosynostosis therapy. It helps to understand the molecular mechanisms involved in normal and abnormal suture development and function. Preclinical investigations of new therapeutics have

been conducted in a number of small and large animal model systems. The rabbit, rat and mice are the most commonly used animals in cranial suture research [60, 61].

Mouse is an excellent model due to its easy maintenance and low cost. The craniofacial development in mice is predictable and comparable to humans, with the posterior frontal suture fusing between 7-12 days postnatally which is analogous to human metopic suture [61]. The rest of the mouse sutures remain patent throughout the adult life unlike in human skull [16, 61]. Furthermore, availability of sophisticated cellular and molecular analysis tools with high reproducibility makes the use of mouse models ideal. Typically, to study the bone healing/re-growth, a critical-sized defect is introduced onto the cranial skeleton around the suture of interest, which, if left untreated, will not heal in a normal as well as pathological mouse model [62]. This provides an effective model to understand the causative mechanisms and to test therapeutic interventions to delay bone re-fusion.

The rat is another common model which aids towards technically better craniectomies due to larger size. In this model, each animal can be used as its own control by introducing bilateral defects on both sides of the suture [62, 63]. Investigators have developed specific animal models which help focus on the phenomenon to be studied. Firstly, a stress induced murine model has recently been tested for intrauterine constraint causing suture fusion [64]. It elucidated the effect of up- or down-regulation of specific molecules in fusing/fused sutures. The presence of bone promoters such as bone morphogenetic protein 4 (Bmp4), Indian hedgehog (Ihh), RunX2 or antagonists such as noggin can alter the suture patency. A rat organ culture system with micro-distraction device showed that mechanical stress influences both physiologically fused and normally patent sutures [38, 64].

The second type of model involved transgenic mouse models which have been genetically engineered with a mutation associated with a craniosynostosis syndrome in humans. This includes various models with knock-outs genes, under- or overexpressing certain proteins [16]. A Crouzon mouse model with mutated $Fgfr2^{c342y/+}$ genes has been well-researched to study cellular, molecular and biochemical mechanisms of Crouzon syndrome, and also to test pharmacological interventions [65-67].

Mooney and co-workers have been actively involved in investigating a rabbit model with familial, congenital non-syndromic craniosynostosis of the coronal suture [68]. They identified the mutated strain in affected New Zealand white rabbits and interbred them to develop and sustain a colony with craniosynostosis. These animals demonstrate autosomal dominant transmission with a vast range of phenotypic expressions, from unilateral or bilateral suture fusion (early or pre-natal onset) to delayed-onset (post-gestational) synostosis [69, 70]. Due to paucity of molecular tools for genetic disorder mapping in rabbits, the underlying mutation is currently unknown. The primary benefit of larger animals is better precision and control during surgery but they are more expensive to use and maintain. Other models such as mini-pigs, sheep or non-mammalian ones (zebra-fish, frog *etc*.) have also been utilised to study suture morphogenesis [68-71].

2.3.4.2. Molecular regulation of suture morphogenesis

Although several growth factor receptor and transcription factor mutations have been implicated in craniosynostosis, the underlying mechanisms leading to sutural obliteration remain unclear. Cranial vault sutures are the prime site of intramembranous bone growth due to rapid neurocranium expansion. The underlying mechanisms for sutural patency or obliteration are implicated to the major signalling pathways in bone formation and their corresponding mutations. It involves a

complex interplay and balance of transcription factors, growth factor receptors, cytokines and extracellular matrix molecules. The fibroblast growth factor (FGF) and transforming growth factor (TGF)-β pathways are most extensively studied in craniofacial development and suture patency. These pathways participate in morphogenetic, proliferative and differentiative processes during intramembranous ossification involved in cranial development and repair [16, 72, 73].

Mutations involving these pathways account for the syndromic cases of craniosynostosis (with known genetic causes) [22, 24]. Studies involving microarray analysis have reported a large number of genes (MSX2, FGFR1, FGFR2, FGFR3, TWIST genes *etc.*) that form part of complex molecular network controlling suture morphogenesis [27]. The functions of these genes have been assessed by gene knock-out approach in animal models, with a significant difference in expression of these genes being observed in fused and unfused sutures [73].

The (TGF)-β superfamily comprising of bone morphogenetic proteins (BMP 2-8), transforming growth factor beta (TGF-β1-3), activins, inhibins and growth differentiation factors (GDF 1, 5, 8, 10) regulate osteoblast proliferation, angiogenesis, and production of extracellular matrix proteins [16, 74]. Experimental evidence shows the variable expression of TGF-β isoforms in cranial sutures. Opperman et al. elucidated down-regulation of TGF-β3 and upregulation of TGF-β1 and 2 in fusing posterior frontal suture in a murine model. An inverse pattern was observed in patent coronal sutures [75]. The knock-out and TGF-β2 null mouse models further supported the findings, where conditional inactivation of TGF-β2 caused developmental defects [76, 77].

The FGF members and receptors also have profound effects on suture morphogenesis. The family consists of 22 members but FGF2 has been frequently implicated in several aspects of suture formation. Transgenic mouse model with overexpression of FGF2 exhibited mineralisation defects,

flattening and shortening of long bones while a FGF2 knock-out model has shown decreased bone mass [16, 73]. As stated earlier, a gain-of-function mutation in FGFR genes is a major cause of syndromic craniosynostosis.

2.3.4.3. BMP and BMP antagonists

The BMP proteins belonging to TGF-β family are one of the major growth factors responsible for bone development, regeneration and craniofacial and skeletal patterning. There are 20 BMPs identified till date which have been involved at different stages of bone formation. Although the BMP isoforms are structurally and functionally related, BMP2 and BMP4 are considered most osteogenically potent in cranial suture biology. During skull growth, BMP signalling pathway has been associated with down-streaming of FGF pathway, hence can be manipulated for treating cranial deformities. The BMP family members initiate signalling by dimerising and binding to tetramer transmembrane receptors on the mammalian cell surface which possess serine/threonine kinase activity intrinsically. There are mainly two types of BMP receptors, including type I (BMPR-I) and type II (BMPR-II) receptors. Typically, the signal transduction cascade is triggered by BMP binding to BMPR-I or II to form a ternary complex. This initiates the transphosphorylation of type I receptor from the activated type II receptor. The type I receptor consecutively phosphorylates the intracellular R-Smads (Smad1, 5 and 8) which then associates with the co-Smad (Smad4), and translocates to the nucleus, regulating the gene transcription [16, 73, 78, 79]. The BMP regulatory mechanism during bone formation is shown in **Figure 2.5**.
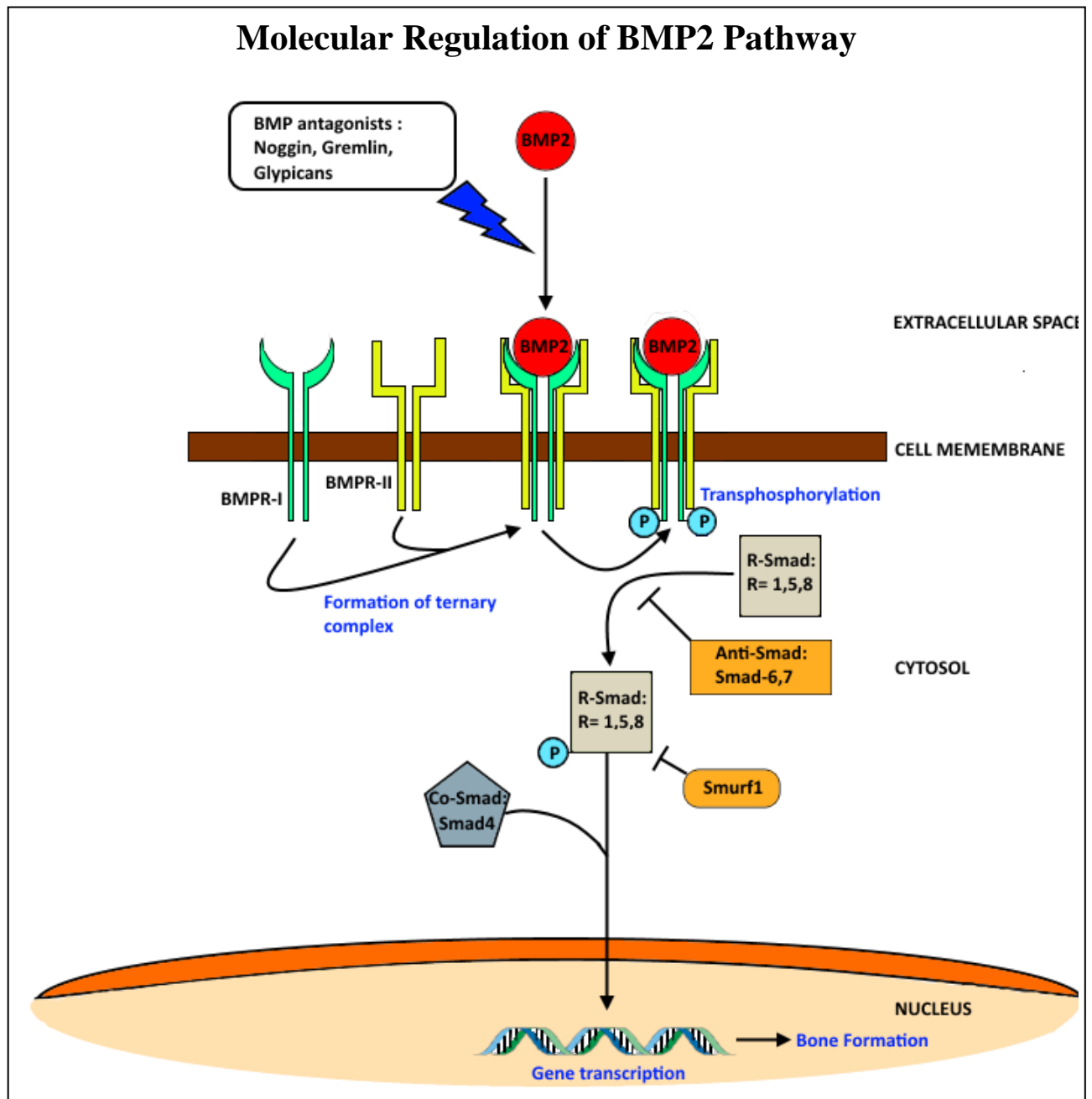
Figure 2.5. Regulation of the BMP signalling pathway during bone formation.

BMP signalling is critically regulated by a class of molecules called BMP antagonists. These regulators maintain a fine balance of cellular and developmental activities in the suture mesenchyme by providing negative feedback to the BMP production. The BMP antagonists can be both intracellular and extracellular and function through binding to the BMP complex. This prohibits BMPs to bind to the target receptors and regulates the pathway. In some cases, the antagonists bind directly to the receptor to block the signal transduction altogether [78, 80].

A number of proteins have been identified and documented as members of BMP antagonists, with noggin, gremlin and glypicans studied mainly in craniofacial literature. Noggin is a prominent antagonist which binds to BMPs 2, 4, 5, 6 and 7 complexes with different levels of affinity and inhibits their osteogenic potential and bone formation. It is also essential for embryonic neural tube development and skeleton patterning. A previous study has demonstrated the postnatal expression of noggin in patent, but not in synostosing cranial sutures. Moreover, it has been suggested that the FGFR-mediated craniosynostosis may be caused due to inappropriate downregulation of noggin in the suture mesenchyme [63, 71, 81].

Gremlin is another alternative to Noggin, which has shown higher specificity in blocking the BMP function. It is involved in kidney and limb development as well as in blocking osteoblast differentiation and function. A Grem-1 knock-out mouse model increased trabecular bone formation, whereas its overexpression caused osteopenia and short stature [80, 82].

Glypicans, a group of inhibitory molecules have been explored over the past decade by our group at Australian Craniofacial Unit in Adelaide, Australia. These BMP antagonists have been closely linked to suture patency and craniosynostosis. Glypicans have been described in detail in the following section.

2.3.4.4. Glypicans

Glypicans are cell-surface heparan sulfate proteoglycans that are bound to the exoplasmic surface, anchored by a glycosylphosphatidylinositol (GPI) linkage, localised to intracellular granules or secreted to the extracellular matrix (**Figure 2.6**) [73, 83-85].

Vertebrates typically contain six members of this family (GPC1-GPC6), measuring ~ 60-70 kDa in size [84]. Structurally, core proteins consist of a large, globular and stable α-helical domain with 14 invariant cysteine residues. This is followed by a glycosaminoglycan (GAG) attachment domain substituted with heparan sulfate (HS) chains, coiled into a folded, tertiary structure interacting via disulfide bridges [73, 86, 87]. X-ray crystallographic studies reveal that the compact cylinder of core protein is approximately 10 nm in length and 3 nm in diameter. Mature glypican attached to the GAG (unbranched oligosaccharide) chains in extended form measures around 50-150 nm, depending on number of chains [73].

Loss-of-function mutations in glypican core proteins and the GAG chains have revealed their importance in determining skeletal development [73, 85]. GPC3 mutations have been associated with a rare disorder in humans, Simpson-Golabi-Behmel Syndrome (SGBS), which is characterised by pre- and post-natal overgrowth and developmental delays [85]. Moreover, upregulation of GPC3 acts as an oncogene (molecular marker) in liver cancers. Over or under expression of other glypicans have also been observed in cancers pertaining to gliomas, ovary and breast. Furthermore, homozygous mutations in GPC6 can lead to a recessive genetic condition called Omodysplasia [73, 85].
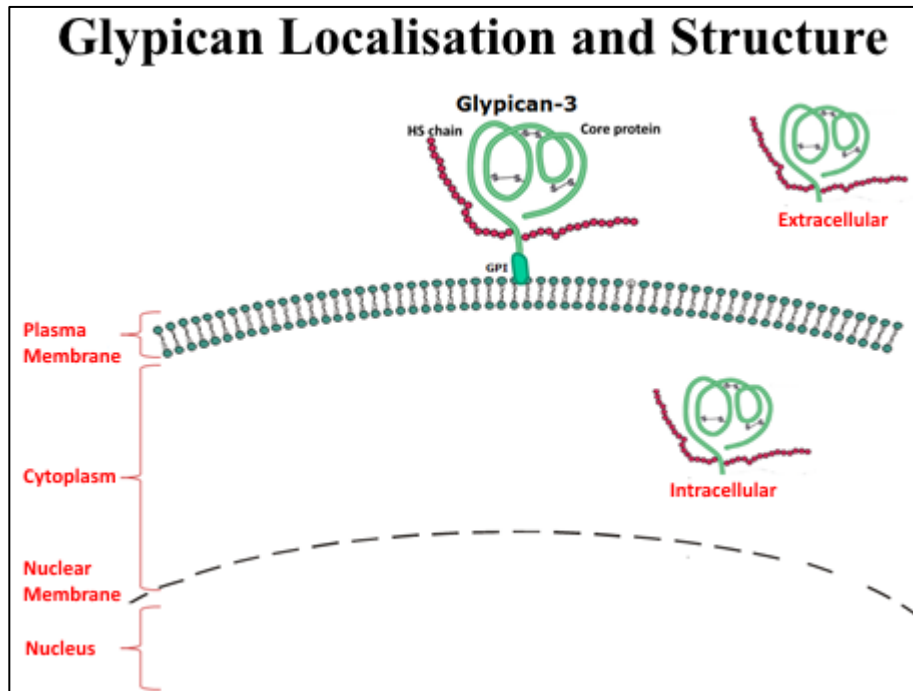
Figure 2.6. Schematic representation of localisation and structure of glypicans in the vertebrates. The multiple disulphide bridges (S-S) organise the core protein which is attached to a heparan sulfate (HS) chain. The glypicans are attached via a glycosylphosphatidylinositol (GPI) anchor to the outer surface of plasma membrane or located in the extracellular matrix after cleavage of the linkage.

2.3.4.5. Interaction of glypicans and BMPs

Apart from their association with various genetic abnormalities, glypicans play a vital role in receiving, modulating, trafficking and spreading the extracellular and intercellular signals [85]. They can have inhibitory or stimulatory actions depending on the pathway, cellular context and location. Recent studies have reported high levels of BMP2 in prematurely fusing sutures in craniosynostosis patients [18]. BMP signalling occurs downstream of FGF signalling, hence manipulation of BMP pathway has been reported to be effective for craniosynostosis therapy. A

complex interplay of molecules governs the BMP activity, with glypicans as co-regulators [18]. The exact mechanism by which glypicans regulate BMP activity is still unclear, but there is experimental evidence to suggest that GPC3 and/or GPC1 work at the level of signal reception by altering the physical interaction between BMP2 and BMPR signalling receptors [18, 73].

It has also been established that the expression of GPC3 and/or GPC1 in suture mesenchymal cells controls the BMP2 activity, and that the GPC1-GPC3-BMP axis synergistically regulates skull growth. A 7 fold decrease of GPC3 was observed in fusing sutures during luciferase reporter assay, with GPC1/GPC3 being noted to block BMP2 activity by binding to its receptors, whereas antibody blockade of these glypicans was found to potentiate BMP2 activity [18]. By increasing the concentration of GPC1/GPC3 in the affected sutures to inhibit BMP2 signalling, BMP2-mediated bone formation and premature fusion can be avoided [18].

2.3.5. Current therapies for delaying/avoiding premature fusion

Better understanding of suture pathogenesis, the regulatory mechanisms and the signaling pathways, along with availability of surgical animal models, provide meaningful insights to develop adjunctive non-surgical therapies to treat or delay post-operative resynostosis. Several molecular adjuncts have been proposed and tested to target potent bone-forming mechanisms by controlled delivery of bone antagonist proteins that inhibit the osteoblastic activity [15, 88, 89].

The animal craniectomies or suturectomies are simulated based on the corrective surgical intervention in human patients. Herein, a midline scalp incision is performed to expose the underlying calvaria and the sutures. After isolating the osteogenetically fused/fusing suture, the periosteum is carefully removed. This is followed by extirpating a region of the suture of interest,

leaving a critical-sized defect, similar to gaps created in craniosynostosis operations. The placebo group usually has an empty defect; while the experimental groups have a controlled delivery system with therapeutic proteins targeted locally [88, 89].

To this end, the researchers investigated the delivery of neutralising antibodies against TGF-β2 growth factors to the suturectomy sites in rabbit model of synostosis. This confirmed the hypothesis that disruption in TGF-β2 function and activity rescues suture obliteration [90]. This was followed by a study demonstrating the prevention of suture re-closure by controlled delivery of Tgf-β3 in rabbits with delayed-onset craniosynostosis [91, 92].

The BMP antagonist, noggin has been shown experimentally to block BMP function and avoid resynostosis in large as well as small animal models. Noggin was effective in delaying craniectomy site re-fusion and bone ossification, evidenced by presence of calvarial defects up to 84 days after treatment in well-established rabbit model of human coronal synostosis [70]. Another study showed that the administration of noggin to fusing sutural sites in rabbit models with delayed-onset synostosis did not inhibit suture fusion, suggesting that BMPs were not directly involved in disease pathogenesis and only regulated post-operative bony healing [69]. In a more elaborate set of experiments, cells overexpressing noggin protein seeded onto a scaffold were placed surgically over a defect in posterior interfrontal murine suture in a post-operative resynostosis model. The results confirmed that noggin was actively delivered to antagonise ectopic bone formation as well as membranous re-ossification [88]. Furthermore, in a weanling rat model xenotransplanted with FGFR2-mutant human osteoblasts (from Crouzon and Apert patients) under the coronal suture, the induced bridging synostosis was counteracted by placing acrylic beads with recombinant human noggin at the surgical site [63]. The pro-patency effects of bone inhibitors show a varied response in infant and adult mice, with the bone regenerative rates in the cranial defects higher in young

animals. This can be clinically translated into age-dependent severity of resynostosis [55, 93].

2.3.6. Delivery systems for suture regulation

As described in the previous section, the transcranial surgical outcomes can be improved by combining them with controlled release of therapeutic proteins that inhibit re-ossification. The desirable drug delivery system should provide an effective dosage for prolonged release of the bioactive proteins, with tailorable release pharmacokinetics, high bioavailability and biodistribution, high efficacy, minimal non-specificity, improved *in vivo* stability and shelf life [94-96]. So far, the localised administration of the cytokines and therapeutic proteins into the craniofacial regions has been done either directly using a carrier (polymer-based microspheres, hydrogels, and implants, lipid nanoparticles, ceramics, titanium fibre-mesh or porous glass) or gene based therapies (both viral and non-viral vectors) [71, 89, 94].

Collagen, a natural polymer, is the most common delivery vehicle used for multiple tissue regeneration and craniofacial studies. In early animal and clinical studies, collagen sponges were applied as vehicles owing to their resorbable nature [94, 97]. However, their high porosity, quick degradation, uncontrolled diffusion of proteins, dose dumping and large initial burst release deemed them undesirable. The sponges were replaced by another less porous, more retentive collagenous matrix, collagen hydrogel. This carrier provided better release kinetics but also induced osteogenesis in rat cranial defects [97]. A recent advancement over conventional hydrogel was made with the development of highly purified, bovine, type I collagen gel. This is a high density semi-viscous material which can be easily injected at the surgical site, solidifying into a gel at 37 °C. This formulation is biocompatible, slow-resorbing and non-osteogenic in nature. This scaffold has been extensively applied in animal model to deliver bone inhibitors and antibodies to

delay reossification of the suture site [70, 72, 94]. Although a collagen vehicle has its advantages, the little control over the rapid release parameters, associated inflammatory response and high fraction of protein retention even after release, makes it unsuitable for craniosynostosis treatment [94, 98, 99].

A synthetic polymer-based system facilitates better control and flexibility for maintaining a sustained release with tailored degradation rates. Biopolymers such as poly-lactic-co-glycolic acid (PLGA), poly-ethylene glycol (PEG) and poly-caprolactone (PCL) have been extensively used in many tissue-engineered orthopaedic and craniofacial models. These polymers can be fabricated into microspheres which can be injected directly onto the surgical site or into a gelatin carrier (Gelfoam) to deliver bioactive molecules [89, 100-102]. With advancements in polymer and material chemistry, synthetic polymeric vehicles can be modified into non-antigenic materials with controllable therapeutic encapsulation/adhesion and target specificity [103].

Injectable synthetic hydrogels are preferred over pre-formed scaffolds in craniofacial applications, but they require cross-linking to polymerise within an *in vivo* system. Traditionally, UV light or potentially harmful chemicals are used to cross-link the gel, which can have severe implications on neurological health [104, 105]. Recently, an injectable hydrogel (reactive PEG molecules) with rapid *in situ* "click-chemistry" crosslinking has been explored to deliver Gremlin to a critical-sized defect in a weanling mouse model of resynostosis. This hydrogel-based therapy showed bone growth inhibition dependent on the Gremlin dosage [106].

2.4. Nano-drug delivery Implants: Titania Nanotubes

Despite the development in innovative micro-scale delivery systems, the current techniques have some limitations. The conventional systems are unable to provide a long-term sustained delivery of bioactive proteins necessary for cranial suture regulation to prevent resynostosis. These proteins are also susceptible to enzymatic denaturation and instability if left unprotected (short half-lives). Moreover, protein dosage is critical in craniofacial delivery as the target cells (undifferentiated mesenchymal cells) in the suture mesenchyme can respond differently and adversely to the same biomolecule, depending on the concentration [72, 94].

To overcome these drawbacks, more efficacious and rational delivery systems based on nanotechnological approaches have been explored. These alternative nano-drug delivery systems have empowered the development of implantable drug releasing platforms providing targeted, controlled, sustained, programmable and localised administration of therapeutics. The current medical applications of these systems is summarised in **Figure 2.7** along with other microfabricated devices.

Advanced nanofabrication technology has led to emergence of a plethora of nanomaterial-based implants to deliver active agents in an optimal manner. Herein, nanoengineered surfaces have attracted much attention over the past few decades, due to their easy fabrication, controllable geometry, applicability and drug releasing capability. The inorganic nanoporous and nanotubular implants (such as nanoporous Alumina, porous Silicon and Titania nanotubes) generated by electrochemical etching/anodisation have emerged as a special niche in biomedical research due to their unique properties [96, 107-110]. Titania nanotubes (TNTs) in particular, have an edge over other biomaterials as they can be generated on pre-existing titanium and their alloyed medical

implants (plates, screws, wires *etc*.) which are the current gold standard for craniofacial and dental applications [89].
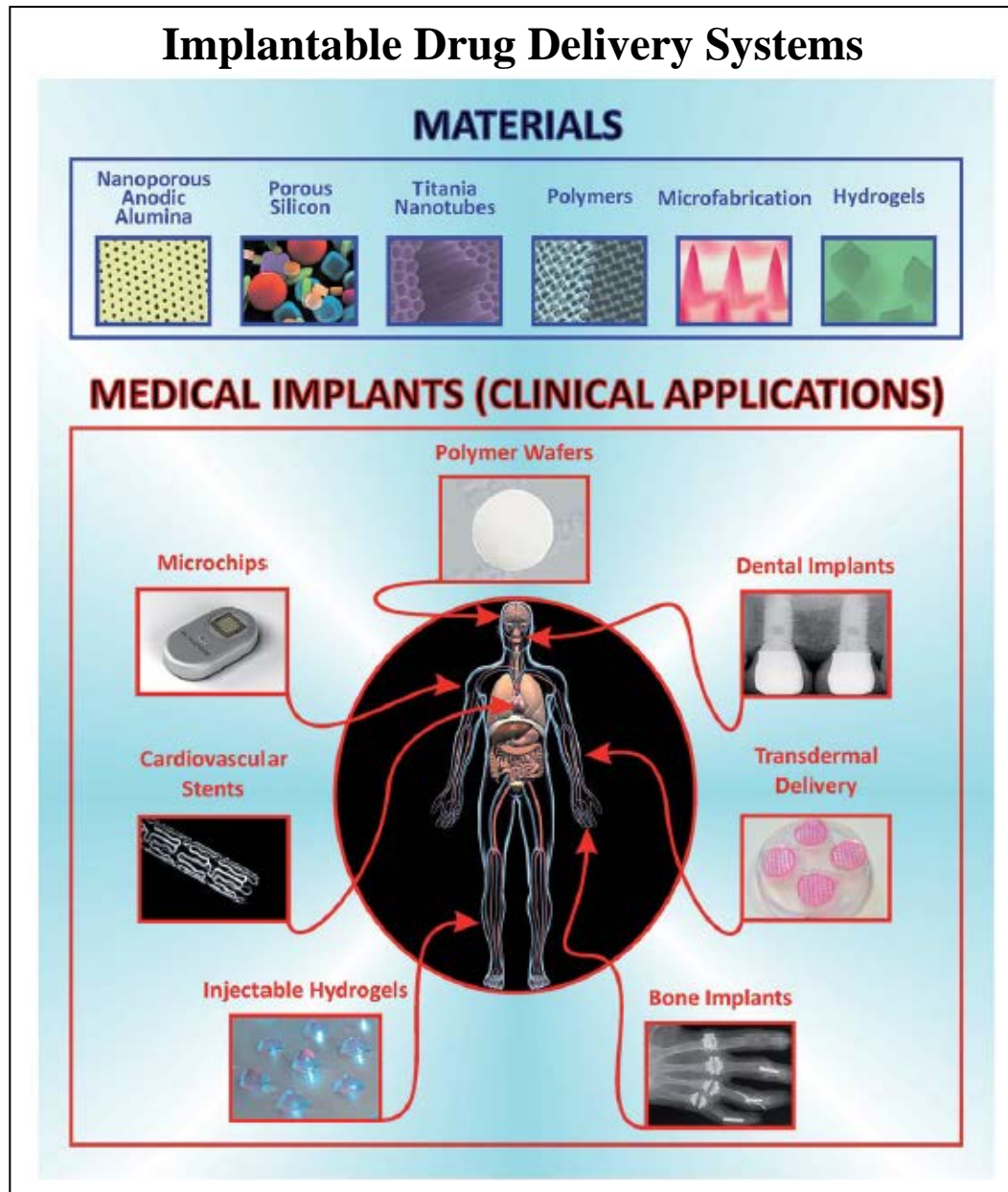
Figure 2.7. Current Drug-releasing implants based on micro-/nano-engineered strategies (reprinted with permission from [109]).

Self-organised nanostructured materials have attracted considerable interest due to their spontaneous generation and specific hierarchical organisation at micro- and nano-scales [107, 111-113]. TNTs are composed of arrays of vertically aligned, self-ordered nanotube structures with hexagonal arrangements and controllable dimensions. These novel nanoengineered structures demonstrate a low-cost fabrication, high surface-to-volume ratio (~1000-2000), high surface area (180-250 m^2/g), versatile nanotube geometry with controllable pore size (10-300 nm) and thickness (0.5-500 µm), high loading capacity, chemical and mechanical stability, ease of functionalisation, enhanced drug-releasing performance and excellent biocompatibility [107, 114-117]. These characteristics have made TNTs desirable for a number of applications. For instance, remarkable work has been done to explore the use of TNTs as photocatalysts (for water splitting, hydrogen generation, pollutant degradation) [118-121], dye-sensitised solar cells [122, 123], energy storage systems [124, 125], sensors (humidity, gas, bio–sensors) [126-129], interference coatings in optical devices [130], templates for secondary nanomaterials [130-132] and self-cleaning membranes. Furthermore, their use in biomedicine including cell interaction, tissue engineering implants [115, 133] and drug delivery systems [134, 135] has also been investigated owing to profound changes in performance dependent on nanotube length, diameter, wall thickness, crystallinity and the density of tubes/pores on the surface [136].

2.4.1. Fabrication of TNT

TNTs are hexagonally arranged one-dimensional tubular structures, with a closed bottom and an open top, that arrange themselves on Ti substrates or form loose agglomerates in a solution. Synthesis of these nanostructures can be achieved by different approaches involving template-assisted, sol-gel, hydro/ solvothermal and electrochemical methods.

For template assisted synthesis, a titanium alkoxide precursor undergoes acid-catalysed hydrolysis (to form a gel-type Ti-O-Ti chain) within a selected template, followed by hydrolysis into TiO_2 precipitates. Several templates from spherical or rod like micellar assemblies to nanoporous alumina have been used to facilitate TNT formation. An atomic layer deposition technique has also been applied to obtain TNTs with controlled thickness within the template. A major challenge of this approach is dissolution of the template, which results in low yield of loose agglomerated TNTs of non-uniform lengths. Another well-established template-free method is hydro/solvothermal synthesis, which involves autoclaving bulk TiO_2 powder in NaOH solution at high temperatures to obtain nanotubular bundles with wide size-distribution [114, 137].

A more recent fabrication technique based on electrospinning has been researched, wherein titanate precursors are electrospun onto polymeric fibres, followed by heat decomposition of the polymer to yield hollow titania nanofibers or TNTs [138]. In contrast, electrochemical anodisation of Ti involves the synthesis of highly-ordered nanotubes using localised chemical dissolution, with controlled field-assisted oxidation and dissolution reactions. This method is deemed most suitable for biomedical implants due to adjustable morphological control [139].

2.4.2. Electrochemical Anodisation (EA): Mechanistic model of nanotube array formation

There are a large number of reports regarding the mechanism underlying the formation of self-organised TNTs [107, 114, 117, 140-142]. The schematic of electrochemical set-up and the key processes involved in generation of self-ordered nanotubes is elucidated in **Figure 2.8**. The basic experimental setup involves an electrolyte, a target metal substrate (working electrode or anode), and a counter electrode (cathode). The electrochemical synthesis by anodic oxidation involves

application of current/voltage to oxidise an electrochemically active species in an appropriate electrolyte. Depending on the fluoride ion concentration in the electrolyte, three different electrochemical profiles can be attained. In a fluoride-free case, a stable compact oxide (CO) layer is formed whilst, in access of fluoride ions, electropolising of the surface occurs.

However, during a process with optimal fluoride ions in an electrochemical cell, initial oxide growth at the metal (anode) surface occurs due to interaction of titanium with the O_2/OH^- anions from the water content (field-aided deprotonation) in the electrolyte (eq. 1 and 2). This is followed by migration of Ti^{+4} cations from the oxide/metal interface to the electrolyte/oxide interface and finally into the solution (**Figure 2.8b**).

$$2\,H_2\,O \rightarrow O_2 + 4\,e^- + 4\,H^+ \tag{1}$$

$$Ti + O_2 \rightarrow TiO_2 \tag{2}$$

Simultaneously, chemical dissolution of the formed oxide as soluble fluoride complexes starts under the impact of focussed localised electric field due to surface morphological fluctuations (eq. 3). This leads to generation of pits (**Figure 2.8c**) which get converted into bigger pores that spread uniformly over the surface (steady-state condition)

$$TiO_2 + 6F^- + 4H^+ \rightarrow [TiF_6]^{2-} + 2H_2O \tag{3}$$
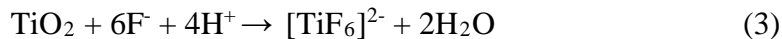
The pore growth occurs due to inward movement of oxide layer into the bulk metal. Thus, the dynamics of the pore formation can be described as a competitive process between electric-field assisted oxide dissolution at the electrolyte/oxide interface and field-driven oxidation/chemical dissolution of metal at the oxide/metal interface, leading to the final porous oxide layer. The driving force for self-assembly has been attributed to the repulsive forces generated due to inter-pore

compressive mechanical stress. It has also been reported that TNTs separate into individual tubular structures owing to the electric-field and localised heating-enhanced dehydration (volume contraction of hydroxide layer normal to the walls) [107, 143, 144].
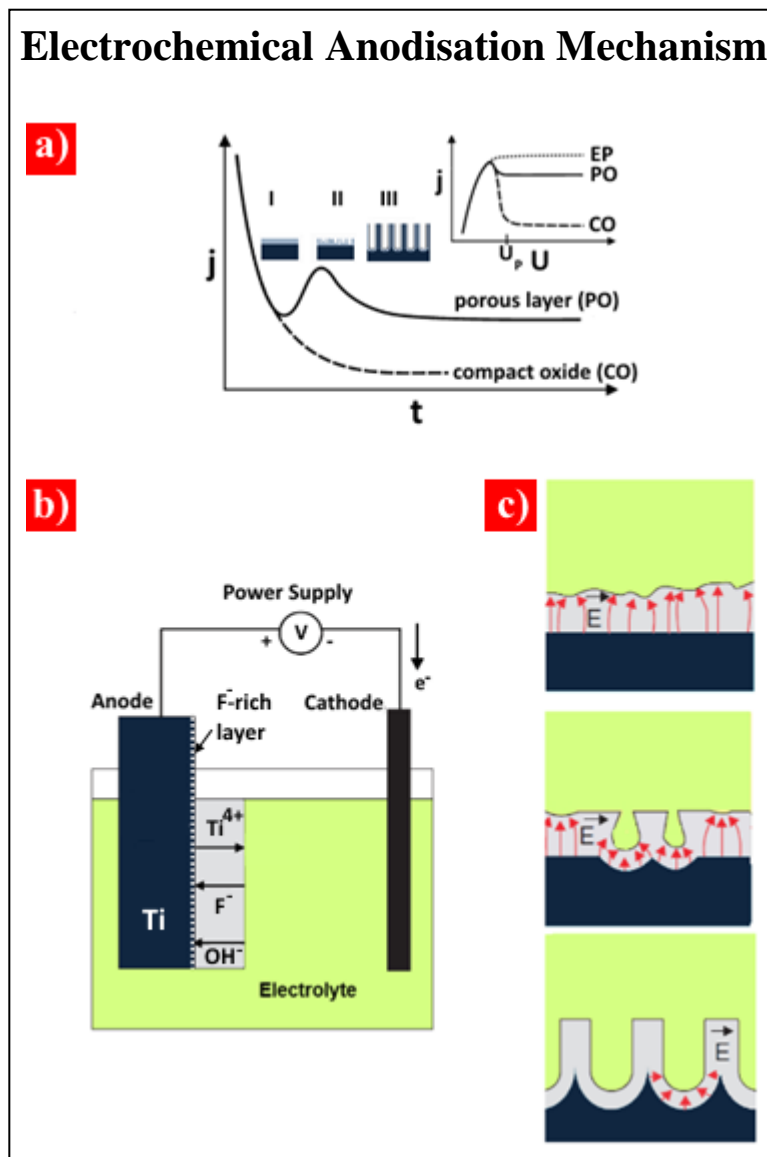
Figure 2.8. Characteristic features of EA for TNT fabrication. (a) Typical current-density (j) v/s time plot, compact-oxide-CO and PO-porous-oxide. Inset shows linear sweep voltammo-grams (j-U plots) for electrolytes, containing different fluoride concentrations [very high: electro-

polished/EP, very low: CO, intermediate: PO or TNT formation]. (b-c) Electrochemical set-up with mechanistic model for TNT fabrication (Adapted from [107] and [114]).

A typical EA reaction has a characteristic current density vs time curve as depicted in **Figure 2.8a**. It has three different regions corresponding to various stages of the process. Region I identifies with equation 1, where an exponential drop in anodic current is observed, suggesting formation of thick CO layer on titanium surface. At this time, this oxide layer is partially disturbed by 'nanopits' or etch channels, generating a porous initiation layer. In stage II, a sharp increase in anodic current is observed due to increased pore surface area. This is accompanied by competitive inter-pore widening until equilibrium is established, with each pore sharing equal current. This is followed by region III, which is a steady-state with constant current and stable pore growth.

2.4.3. Timeline: Progress in EA

Zwilling et al. in 1999 pioneered the electrochemical synthesis of titania nanostructures using fluorinated acidic electrolytes [145, 146]. The porous layer obtained was disordered and only a few hundred nanometres in length. This research led to so called "1st generation" of TNTs comprising of porous/tubular structures with sidewall inhomogeneity and short lengths due to excessive chemical dissolution in the HF electrolyte. Since then, many approaches have been proposed to better define growth conditions for longer and controllable nanotube dimensions. In 2001, Gong et al., demonstrated formation of well aligned and organised high-density uniform arrays of tubular structure by using the same technique [147].

The "2nd generation" of fabrication was based on crucial improvements to the tube morphology established by Macak et al. [148, 149], who reported a reduction in acidic dissolution of TiO_2

during anodisation by using pH controlled aqueous buffered electrolytes. Nanotube lengths up to 7 µm and aspect ratios of up to 50 were achieved using the modified conditions. These investigations confirmed the anodisation parameters (such as voltage/current, time, pH and electrolyte *etc*.) dependent growth of nanotube morphology (such as size, crystal structure *etc*.).

In later studies, almost ideally hexagonal tube layers with individual nanotube lengths up to approximately 1000 µm were achieved using non-aqueous polar organic solvents (such as dimethyl sulfoxide, formamide, ethylene glycol or diethylene glycol) which were termed as the "3rd generation" [150-156]. The longest close packed TNT structures were observed post-anodisation in organic viscous electrolytes using voltage of around 80-120V. More recently fabricated nanotube arrays in non-fluoride electrolytes forms the 4th generation, which still have a scope for further refinement [157, 158].

By controlling and tailoring various parameters of electrochemical anodisation of titanium (Ti), different nanoporous/nanotubular morphologies and characteristics can be obtained. Factors such as Ti substrate composition, applied potential [159], current density [160], anodisation time [161], temperature [136], voltage ramping rate [162] and electrolyte species (pH, aqueous or organic, age, viscosity, water and fluoride content) [114, 163-165] mutually influence geometry of TNTs. Optimising these conditions leads to formation of oxide structures with different order degrees. The obtained nanoarchitecture may be compact/disordered/ordered/porous or highly self-organised nanotubular layer, depending on both the rate of nanotube array formation and dissolution rate of resultant oxide. Advanced geometries like nanobamboo, nanolace, branched tube and double walled nanotubes can also be achieved by varying the basic parameters [142].

A recent study showed ultrafast fabrication of organised TNTs at high voltages by altering the chemistry of common ethylene glycol-based traditional anodisation electrolyte. A range of weak chelating organic acids were added individually into the anodisation solution, leading to an excellent increase in nanotube length (especially at high temperatures). This approach is discussed in detail in the following section [166].

2.4.4. Ultrafast nanotube formation

The anodisation time required to obtain good length TNTs in a fluoride containing ethylene glycol electrolyte depends on the applied voltage and the electrolyte constituents. Addition of efficient chelating agents such as EDTA, H_2O_2 and certain weak acids (oxalic, citric, malonic, glycolic and lactic acid) can help achieve extremely high nanotube growth rates, whilst maintaining the structural and functional properties of TNTs. This unprecedented growth rate is due to field supporting effect of the additives. Usually, applying a high voltage in a classic high field anodisation process across the growing oxide layer would cause a dielectric/avalanche breakdown (*i.e.* charge carrier injection from the electrolyte and multiplication towards the Ti metal). The breakdown, in general, can be triggered at different surface points, such as stress-induced local rupture, impurities, secondary entities or fissures in the oxide layer. It is assumed that the adsorption of additive ions onto the surface avoids the local breakdown (burning) of the formed TNT layer. The added organic components shift the breakdown threshold voltage to a higher value, thus allowing a thicker compact oxide or a faster anodisation rate. The extent of the upshift depends on the nature of the organic component [167, 168].

The addition of EDTA improves the process kinetics by releasing the free fluoride in the (EDTA+F$^-$) solution, but its low solubility renders it unsuitable for TNT fabrication. Another

additive and H_2O_2 provides an alternate oxygen source, probably through radical species [169-171]. Although many additives have shown beneficial effects, the addition of lactic acid (LA) has been shown to be most promising for exceptional anodisation behaviour. A standard LA-based anodisation (as researched by Schmuki et al.) can be carried out at extremely high voltages (120-150 V), which may otherwise lead to anodic breakdown [166]. **Figure 2.9** demonstrates the characteristic current density-time curve for LA electrolyte (1.5 M LA, 0.1 M NH_4F, 5 wt.% H_2O, ethylene glycol) and traditional (reference) electrolyte (0.1 M NH_4F, 5 wt.% H_2O, ethylene glycol) conditions at 60 °C and room temperature (RT). The LA assists fluoride to chelate Ti^{4+} ions, hence in a typical curve, the current drops to a steady state value (after an initial rise) with continuous tube formation. On the other hand, at 120V in reference electrolyte, a local breakdown occurs at distinct sites after a quick rise in current (**Figure 2.9d**). The anodisation phenomenon is both voltage and temperature dependent. For the sake of comparison, the average thickness of TNTs using a lactic acid electrolyte at RT and 60 °C as established by Schmuki et al. is depicted in the **Figure 2.9e** [166].

Anodisation Characteristics

	30s	60s	180s	600s	1800s	3600s
60 °C	8.47	12.73	35.10	73.85	112.81	145.04
RT	1.80	2.17	3.39	25.04	66.61	90.20
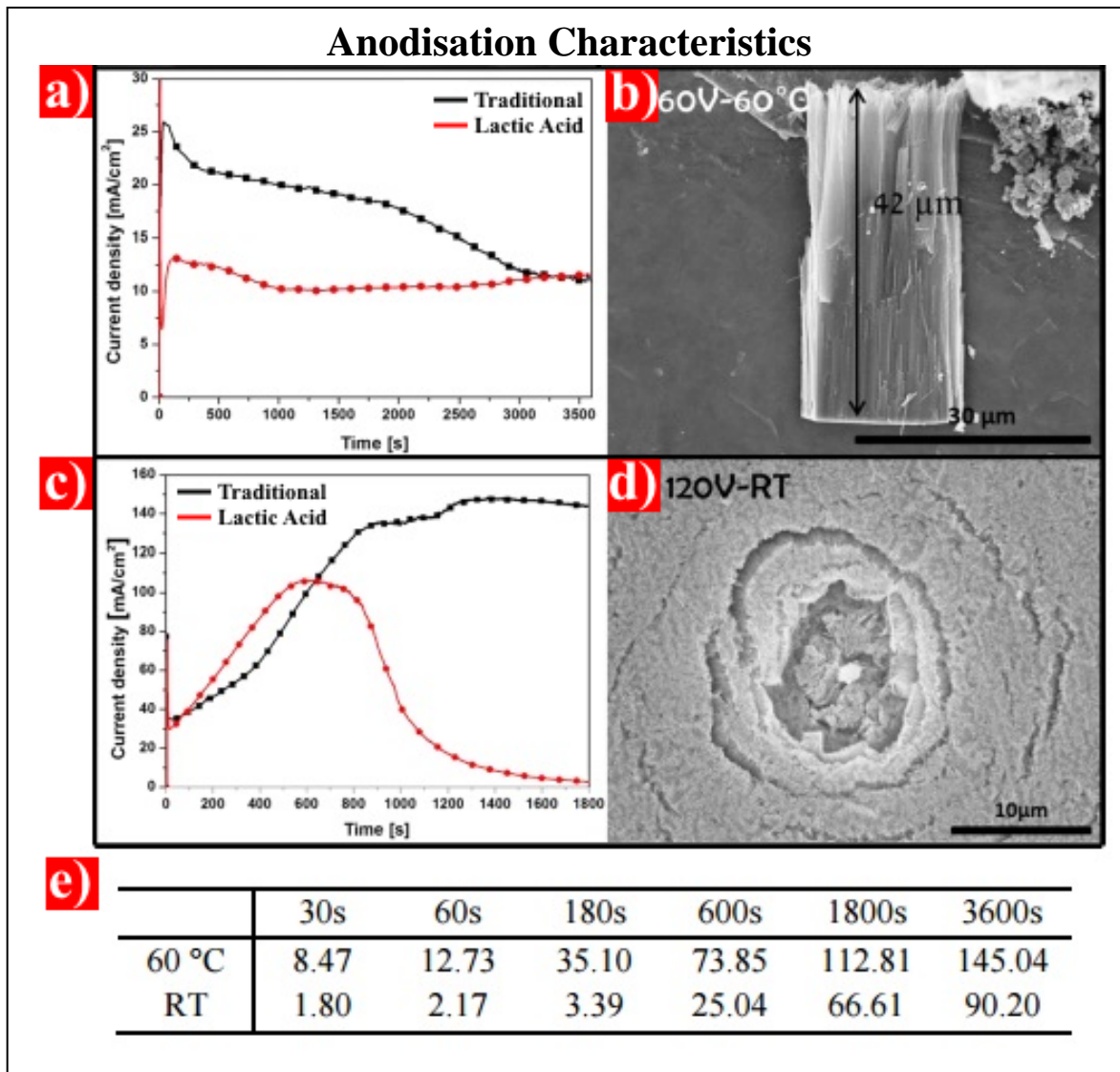
Figure 2.9. Current−time curves for anodisation (a) at 60 V and 60 °C and (b) at 120 V and room temperate (RT) in lactic acid and in the traditional (reference) electrolyte. SEM images of the TNT displaying the morphology after anodisation under the traditional electrolyte conditions (c) at 60 V and 60 °C after 1 h and (d) at 120 V and RT after 10 min (a typical breakdown morphology). (e) Average thickness of TNTs using a lactic acid electrolyte (adapted from [166]).

2.4.5. Therapeutic functions of Ti/TNT implants

Easy integration and adaptability of surface engineered Ti substrates into the current implant market make Ti/TNT implants an ideal candidate for localised drug delivery systems. Apart from their excellent biocompatibility and structural properties, the empty tubular structure can act as a nanoreservoir to hold broad range of active therapeutics such as antibiotics, anti-cancer, immunosuppressant, antifungal and anti-inflammatory drugs, proteins, growth factors, peptide chains, neurotransmitters and genes.

Multiple *in vitro* and *in vivo* studies have confirmed the use of TNT implants to precisely delivery the drugs at desired dosage and time points, with desirable pharmacokinetics. TNTs have predominantly been applied as orthopaedic and dental implants for post-surgical treatments of necrotic or avascular bone tissues. They have also been tested in coronary stents, bone-related cancer therapies and bone tissue engineering [96, 107, 109, 172, 173]. Currently, TNTs are considered as promising candidates for local drug delivery for extended periods of time, readily controlled by altering the nanotube dimensions and surface properties. **Table 2.1** summarises the most representative studies involving TNTs as drug releasing implants [109].

Implant	Therapeutic loaded	Application
Titanium implant with TNTs coating	None D-a-tocopheryl polyethylene glycol 1000 (TPGS) Pluronic F127 PEO_{260}–PPO_{400}–PEO_{260} 1,2-Distearoyl-sn-glycero-3-phosphoethanolamine-N-[methoxy (polyethylene glycol)-5000 1,2-Distearoyl-sn- glycero-3-phosphoethanolamine-N-[methoxy (polyethylene glycol)-2000]	Artificial joint replacement prostheses Design of porous therapeutic implants for an extended elution time of poorly water soluble drugs using polymer micelles as drug nanocarriers
TNTs on chips	Indomethacin BMPs Human osteoblasts	Orthopaedic applications and bone therapies (*e.g.* infections, local delivery of anabolic agents for bone repair, antiresorptive agents, bone cancer, osteomyelitis, *etc.*)
Sequential-step prepared biocompatible TNTs film	Dexamethasone	Design of anticoagulants, analgesics and antibiotics drug-releasing TNTs implants to prevent inflammatory reactions
TNTs on chips	Penicillin/streptomycin Dexamethasone	Prolonged drug delivery in orthopaedic implants to prevent infection, inflammation and to promote ossteointegration
TNTs on Ti and Ti6Al4V alloy **TNTs on Ti chips featuring various topologies**	Bone cells Marrow stromal cells (MSCs)	Long-term bone implant Antibacterial adhesion for controlled, guided, and rapid wound healing, prevent acute or chronic inflammation/ infection or fibrosis
Annealed TNTs on Ti chips	---	Biomimetic carbonated hydroxyapatite (CHA)
Titania bioceramic implants	Anti-epileptic drug	Treatment for epileptic seizures

Table 2.1. Summary of selected therapeutics and their applications using Titania nanotubes-based delivery system (Modified from [109]).

The release of potent therapeutics loaded into the TNTs is governed by Fick's first law of diffusion. This biphasic diffusion process not only depends on the size/mass and charge of the payload, their dissolution rates and interfacial affinity toward TNTs but also on the nanotubular dimensions, surface chemistry, diffusion coefficient and pH. A rapid burst release occurs as soon as the open pore TNTs interact with the physiological milieu *in vivo* or the buffer *in vitro,* due to high diffusion gradient at the surface, followed by a slower prolonged release of the molecules stored deep within the nanotube. The high burst release is undesirable as it results in quick release of almost 40-70 % of loaded therapeutics, causing dose dumping and tissue toxicity, thus making the release system ineffective [95, 96, 173].

Different strategies have been incorporated into the TNT-based delivery system to achieve sufficient local concentration and a sustained long-term release with zero-order kinetics. The zero-order kinetics yields minimal burst release and uniform release rate within the therapeutic window [96]. A schematic diagram summing up the strategies aimed at controlling the release of drugs from TNTs are presented in **Figure 2.10**.

In order to accommodate different drugs for different therapies and disease conditions, physiological modification of the TNT surface has been explored to provide hydrophilicity or hydrophobicity. Chemical functionalisation with versatile self-assembled monolayers (SAMs) has been studied to change the interfacial interactions of TNT and active molecules This allows attachment of various functionalities and target molecules to further improve drug attachment [174].

In recent past, several approaches have been presented by our group to advance the controlled release pattern from TNT implants. For instance, structural and dimensional (length and height)

modification by varying the anodisation time can lead to increased drug loading and improved release performance [108, 175]. Variable drug loading methods such as, soaking/immersion, drop-casting, vacuum assisted and loading from SBF, also alter the drug occupancy and the release duration. The vacuum loading method has been deemed the best as it loads the molecules deep within the TNT void and not superficially [174, 176].
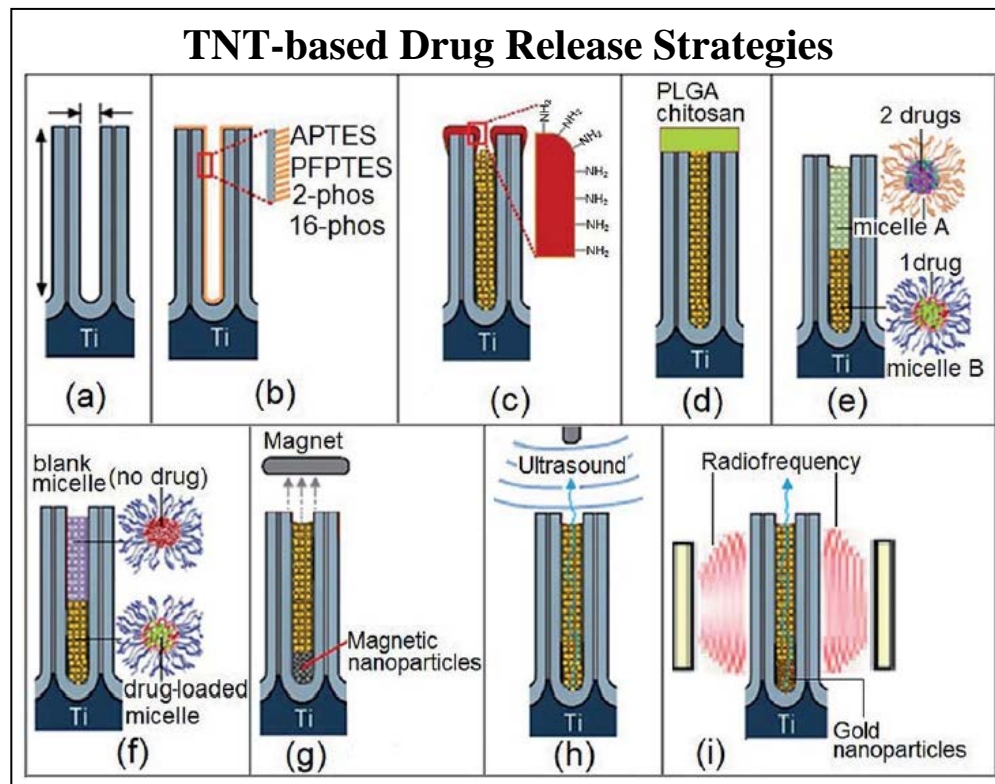
Figure 2.10. Strategies for controlling drug release from TNTs. (A) controlling the nanotube diameters and length; (b) surface chemistry (hydrophobic, hydrophilic, charged); (C) nanotube opening by plasma polymerisation; (D) degradation of polymer film closing nanotubes (PLGA or chitosan); (E) using drug nano-carriers (micelles) for multidrug delivery; (F-I) external field triggered drug release using temperature, magnetic field, ultrasound and radiofrequency. A single nanotube structure is shown to represent an array of TNTs (reprinted with permission from [109]).

Another approach to extend and control the release has been proposed by combing the TNT implants with biodegradable polymers. This technique imparts interesting characteristics to the delivery system by blocking/narrowing the pores and slowing down the release. The nanotube surface can be modified with various forms of polymeric coats, gels, fibres or nanoparticles. Our group extensively explored this concept by using spin-coating, dip-coating, micellar encapsulation and plasma-polymerisation to introduce new functionalities onto the TNTs. A reduction of the pore openings of TNTs by polymer (poly-(allylamine)) deposition using plasma polymerisation has been stated to delay the release from modified TNT implants. However, this technique is complex, time-consuming and costly [177, 178].

A simpler approach involving dip-coating of polymers such as PLGA and chitosan has been shown to reduce the burst release in multiple cases. The release kinetics can be fine-tuned based on the thickness of the polymeric layer. The release pattern is dependent on the degradation of the polymeric layer on exposure to the aqueous fluids. The chitosan layer also provides inherent antibacterial properties to the implant [135, 179, 180]. Moreover, labile molecules such as proteins and growth factors need protection against denaturation to maintain their bioactivity. To this end, polymeric micelles have been used as drug nano-carriers that encapsulate the therapeutics in a micellar structure before being loaded into the nanotubes. This enhances the TNT releasing capabilities and also helps device a multi-drug system [134, 181].

For rapid on-demand or time-programmed release, TNT-based systems have been designed with flexibility to stimulate delivery on an external trigger. Several approaches have been explored to provide high bursts of time-specific release, essential for treating urgent conditions, such as bacterial infections, unexpected inflammation, septic arthritis *etc*. One such strategy was to apply a temperature-responsive polymer ((Poly)N-isopropylacrylamide)) as a hydrogel coating onto the

TNT surface to control release of Vitamin B2. At high temperatures (such as in case of inflammation), the hydrogel structure collapses to trigger the drug release, thus acting as a direct temperature controlled therapy [182].

In another study, the TNTs loaded with magnetic nanoparticles were triggered magnetically or photocatalytically to release drug molecules anchored at the surface or as a therapy to kill cancer cells, respectively. Similar principle was applied to release micelles encapsulating drugs by applying a magnetic field to achieve 100% payload release in just 1.5 h [183, 184]. Other external stimuli, such as ultrasound, electric field and radio-frequency (coupled with gold nanoparticles), have also been successfully tested for triggered release applications [110, 185].

Robust drug molecules are easier to deliver than highly sensitive proteins, but there is evidence of efficient delivery of proteins and growth factors from TNT implants in *in vitro*, *ex vivo* and *in vivo* conditions. In such attempts, the loading and elution efficiencies of model proteins, such as bovine serum albumin (BSA) and lysozymes, from TNTs have demonstrated significant modulation of release kinetics (controlled by changing the tube length, diameter, and wall thickness) [115, 186]. A separate but related study elucidated the long-term BSA (up to 30 days) and sirolimus and paclitaxel elution (for few weeks) from within the TNTs with variable dimensions. Drugs eluted from TNTs were bioactive and decreased cell proliferation *in vitro* [175].

Efficacy of TNTs as drug-eluting implantable devices have also been explored in bone tissue engineering applications. For example, BMP2 conjugated on polydopamine modified TNTs were employed to investigate their influence on the behaviours of mesenchymal stem cells (MSCs). Cells cultured in the presence of BMP2 functionalised-TNTs displayed higher differentiation levels of ALP and mineralisation, suggesting diameter dependent benefit for cell proliferation and

differentiation [133]. Moreover, the deposition of multi-layered coating of bioactive polymers gelatin and chitosan led to delayed release of BMP2, hence improving implant ossteointegration [187]. In further investigations to modulate ossteointegration, alternative bioactive molecules, including CNN2 (connective tissue growth factor) fragment, peptide sequence KRSR (lysine-arginine-serine-arginine), and drugs raloxifene and alendronate, were incorporated inside TNTs [188-190]. In an *in vivo* model, TNTs loaded with bisphosphonates, pamidronate and ibadronate were implanted into the tibiae of Wistar rats. The study reported enhanced expression of collagen type-1 and osteocalcin after 2 and 4 weeks of implantation [191].

2.5. Significance of the Research Project

The review covered here summarises the recent progress and challenges in two main fields relevant to this PhD research project. These include: (i) the pathophysiology and current management of craniosynostosis; advancements in craniofacial and molecular biology (molecular and cellular mechanisms underlying premature fusion in craniosynostosis); availability of pertinent animal models (comparable to human syndromic craniosynostosis) and delivery systems for suture regulation, in order to develop a molecular adjunct for craniosynostosis treatment, and (ii) Titania nanotube-based delivery systems as promising candidate for implantable localised drug release (TNT fabrication and therapeutic applications). This project bridges a significant gap in our knowledge and advances the applications of the nanoengineered therapeutic delivery system towards targeting craniofacial disorders such as craniosynostosis. Improvements and fine-tuning of these techniques can provide valuable linearised drug elution kinetics at the craniectomy sites, especially for delivery of BMP antagonists to avoid bone regeneration. This thesis explores the protein-delivery potential (for release of bone antagonising glypicans) of TNT/Ti implants in a

wide range of *in vitro, pre-in vivo* and *in vivo* experiments (pertaining to objectives mentioned in **Chapter 1**). Extending the scope of the unique nanoengineered protein eluting system based on TNTs on titanium implants for treatment of craniosynostosis could lead to a potential breakthrough for adjunctive, generic therapy to reduce the number of invasive cranial reconstruction surgery.

2.4. References

1.   Allori, A.C., Sailon, A.M., and Warren, S.M. Biological basis of bone formation, remodeling, and repair-part II: extracellular matrix. *Tissue Engineering Part B: Reviews*, **2008**. 14, 275-83.

2.   Boskey, A.L. Mineral-matrix interactions in bone and cartilage. *Clinical Orthopaedics and Related Research*, **1992**. 281, 244-74.

3.   Boyce, B.F. and Xing, L. Biology of RANK, RANKL, and osteoprotegerin. *Arthritis Research and Therapy*, **2007**. 9, S1.

4.   Schett, G. and Teitelbaum, S.L. Osteoclasts and arthritis. *Journal of Bone and Mineral Research*, **2009**. 24, 1142-46.

5.   J Panetta, N., M Gupta, D., and T Longaker, M. Bone regeneration and repair. *Current Stem Cell Research & Therapy*, **2010**. 5, 122-28.

6.   Aarden, E.M., Nijweide, P.J., and Burger, E.H. Function of osteocytes in bone. *Journal of Cellular Biochemistry*, **1994**. 55, 287-99.

7.   Dimitriou, R., Tsiridis, E., and Giannoudis, P.V. Current concepts of molecular aspects of bone healing. *Injury*, **2005**. 36, 1392-404.

8.   Yamagiwa, H. and Endo, N. [Bone fracture and the healing mechanisms. Histological aspect of fracture healing. Primary and secondary healing]. *Clinical Calcium*, **2009**. 19, 627-33.

9.   de Crombrugghe, B., Lefebvre, V., and Nakashima, K. Regulatory mechanisms in the pathways of cartilage and bone formation. *Current Opinion in Cell Biology*, **2001**. 13, 721-28.

10.   Nakashima, K. and de Crombrugghe, B. Transcriptional mechanisms in osteoblast differentiation and bone formation. *Trends in Genetics*, **2003**. 19, 458-66.

11.   Anderson, H. Mechanism of mineral formation in bone. *Laboratory Investigation; A Journal of Technical Methods and Pathology*, **1989**. 60, 320-30.

12.   Morriss-Kay, G.M. and Wilkie, A.O. Growth of the normal skull vault and its alteration in craniosynostosis: insights from human genetics and experimental studies. *Journal of Anatomy*, **2005**. 207, 637-53.

13.   Opperman, L.A. Cranial sutures as intramembranous bone growth sites. *Developmental Dynamics*, **2000**. 219, 472-85.

14.   Williams, P.L., *Gray's Anatomy*. Vol. 378. **1989**: Churchill livingstone Edinburgh.

15.   Wilkie, A.O. Craniosynostosis: genes and mechanisms. *Human Molecular Genetics*, **1997**. 6, 1647-56.

16.   Slater, B.J., Lenton, K.A., Kwan, M.D., Gupta, D.M., Wan, D.C., and Longaker, M.T. Cranial sutures: a brief review. *Plastic and Reconstructive Surgery*, **2008**. 121, 170-78.

17.   Cunningham, M.L. and Heike, C.L. Evaluation of the infant with an abnormal skull shape. *Current Opinion in Pediatrics*, **2007**. 19, 645-51.

18.   Dwivedi, P.P., Grose, R.H., Filmus, J., Hii, C.S., Xian, C.J., Anderson, P.J., and Powell, B.C. Regulation of bone morphogenetic protein signalling and cranial osteogenesis by Gpc1 and Gpc3. *Bone*, **2013**. 55, 367-76.

19.   Furtwängler, J., Hall, S., and Koskinen-Moffett, L. Sutural morphogenesis in the mouse calvaria: the role of apoptosis. *Cells Tissues Organs*, **1985**. 124, 74-80.

20.   Liu, J., Kwon, T.-G., Nam, H., and Hatch, N. Craniosynostosis-associated Fgfr2C342Y mutant bone marrow stromal cells exhibit cell autonomous abnormalities in osteoblast differentiation and bone formation. *BioMed Research International*, **2013**. **Doi:**10.1155/2013/292506.

21.   Coussens, A.K., Wilkinson, C.R., Hughes, I.P., Morris, C.P., Van Daal, A., Anderson, P.J., and Powell, B.C. Unravelling the molecular control of calvarial suture fusion in children with craniosynostosis. *BMC Genomics*, **2007**. 8, 458-83.

22.   Wilkie, A.O. Epidemiology and genetics of craniosynostosis. *American Journal of Medical Genetics*, **2000**. 90, 82-83.

23.   Panchal, J. and Uttchin, V. Management of craniosynostosis. *Plastic and Reconstructive Surgery*, **2003**. 111, 2032-48.

24.   Gosain, A.K., McCarthy, J.G., and Wisoff, J.H. Morbidity associated with increased intracranial pressure in Apert and Pfeiffer syndromes: the need for long-term evaluation. *Plastic and Reconstructive Surgery*, **1996**. 97, 292-301.

25.   Gonsalez, S., Hayward, R., Jones, B., and Lane, R. Upper airway obstruction and raised intracranial pressure in children with craniosynostosis. *European Respiratory Journal*, **1997**. 10, 367-75.

26.   Gray, T.L., Casey, T., Selva, D., Anderson, P.J., and David, D.J. Ophthalmic sequelae of Crouzon syndrome. *Ophthalmology*, **2005**. 112, 1129-34.

27.   Khong, J.J., Anderson, P., Gray, T.L., Hammerton, M., Selva, D., and David, D. Ophthalmic findings in apert syndrome prior to craniofacial surgery. *American Journal of Ophthalmology*, **2006**. 142, 328-30.

28.   David, L.R., Wilson, J.A., Watson, N.E., and Argenta, L.C. Cerebral perfusion defects secondary to simple craniosynostosis. *Journal of Craniofacial Surgery*, **1996**. 7, 177-85.

29.   Renier, D., Sainte-Rose, C., Marchac, D., and Hirsch, J.-F. Intracranial pressure in craniostenosis. *Journal of Neurosurgery*, **1982**. 57, 370-77.

30.   Khong, J.J., Anderson, P., Gray, T.L., Hammerton, M., Selva, D., and David, D. Ophthalmic findings in Apert's syndrome after craniofacial surgery: twenty-nine years' experience. *Ophthalmology*, **2006**. 113, 347-52.

31.   Kimonis, V., Gold, J.-A., Hoffman, T.L., Panchal, J., and Boyadjiev, S.A. Genetics of craniosynostosis. in *Seminars in Pediatric Neurology*. **2007**. Elsevier.

32.   Delashaw, J.B., Persing, J.A., Broaddus, W.C., and Jane, J.A. Cranial vault growth in craniosynostosis. *Journal of Neurosurgery*, **1989**. 70, 159-65.

33.   Garza, R.M. and Khosla, R.K. Nonsyndromic craniosynostosis. in *Seminars in Plastic Surgery*. **2012**. Thieme Medical Publishers.

34.   Persing, J.A. MOC-PS (SM) CME article: management considerations in the treatment of craniosynostosis. *Plastic and Reconstructive surgery*, **2008**. 121, 1-11.

35.   Derderian, C. and Seaward, J. Syndromic craniosynostosis. in *Seminars in Plastic Surgery*. **2012**. Thieme Medical Publishers.

36.   Neilson, K.M. and Friesel, R.E. Constitutive activation of fibroblast growth factor receptor-2 by a point mutation associated with Crouzon syndrome. *Journal of Biological Chemistry*, **1995**. 270, 26037-40.

37.   Jabs, E.W., Müller, U., Li, X., Ma, L., Luo, W., Haworth, I.S., Klisak, I., Sparkes, R., Warman, M.L., and Mulliken, J.B. A mutation in the homeodomain of the human MSX2 gene in a family affected with autosomal dominant craniosynostosis. *Cell*, **1993**. 75, 443-50.

38.   Jacob, S., Wu, C., Freeman, T.A., Koyama, E., and Kirschner, R.E. Expression of Indian Hedgehog, BMP-4 and Noggin in craniosynostosis induced by fetal constraint. *Annals of Plastic Surgery*, **2007**. 58, 215-21.

39. Oppenheimer, A.J., Rhee, S.T., Goldstein, S.A., and Buchman, S.R. Force-induced craniosynostosis in the murine sagittal suture. *Plastic and Reconstructive Surgery*, **2009**. 124, 1840-48.

40. Källén, K. Maternal smoking and craniosynostosis. *Teratology*, **1999**. 60, 146-50.

41. Honein, M.A. and Rasmussen, S.A. Further evidence for an association between maternal smoking and craniosynostosis. *Teratology*, **2000**. 62, 145-6.

42. Jentink, J., Loane, M.A., Dolk, H., Barisic, I., Garne, E., Morris, J.K., and de Jong-van den Berg, L.T. Valproic acid monotherapy in pregnancy and major congenital malformations. *New England Journal of Medicine*, **2010**. 362, 2185-93.

43. Olshan, A.F. and Faustman, E.M. Nitrosatable drug exposure during pregnancy and adverse pregnancy outcome. *International Journal of Epidemiology*, **1989**. 18, 891-99.

44. Rasmussen, S.A., Yazdy, M.M., Carmichael, S.L., Jamieson, D.J., Canfield, M.A., and Honein, M.A. Maternal thyroid disease as a risk factor for craniosynostosis. *Obstetrics & Gynecology*, **2007**. 110, 369-77.

45. Abramson, D.L., Janecka, I.P., and Mulliken, J.B. Abnormalities of the cranial base in synostotic frontal plagiocephaly. *Journal of Craniofacial Surgery*, **1996**. 7, 426-8.

46. Badve, C.A., Mallikarjunappa, M., Iyer, R.S., Ishak, G.E., and Khanna, P.C. Craniosynostosis: imaging review and primer on computed tomography. *Pediatric Radiology*, **2013**. 43, 728-42.

47.   Tartaglia, M., Bordoni, V., Velardi, F., Basile, R.T., Saulle, E., Tenconi, R., Di Rocco, C., and Battaglia, P.A. Fibroblast growth factor receptor mutational screening in newborns affected by metopic synostosis. *Child's Nervous System*, **1999**. 15, 389-94.

48.   Altobelli, D.E., Kikinis, R., Mulliken, J.B., Cline, H., Lorensen, W., and Jolesz, F. Computer-assisted three-dimensional planning in craniofacial surgery. *Plastic and Reconstructive Surgery*, **1993**. 92, 576-85.

49.   Stal, S., Chebret, L., and McElroy, C. The team approach in the management of congenital and acquired deformities. *Clinics in Plastic Surgery*, **1998**. 25, 485-91.

50.   Mehta, V.A., Bettegowda, C., Jallo, G.I., and Ahn, E.S. The evolution of surgical management for craniosynostosis. *Neurosurgical Focus*, **2010**. 29, E5.

51.   Baird, L.C., Gonda, D., Cohen, S.R., Evers, L.H., LeFloch, N., Levy, M.L., and Meltzer, H.S. Craniofacial reconstruction as a treatment for elevated intracranial pressure. *Child's Nervous System*, **2012**. 28, 411-18.

52.   Fearon, J.A., Munro, I.R., and Bruce, D. Observations on the use of rigid fixation for craniofacial deformities in infants and young children. *Plastic and Reconstructive Surgery*, **1995**. 95, 634-7.

53.   Berry-Candelario, J., Ridgway, E.B., Grondin, R.T., Rogers, G.F., and Proctor, M.R. Endoscope-assisted strip craniectomy and postoperative helmet therapy for treatment of craniosynostosis. *Neurosurgical Focus*, **2011**. 31, E5.

54.   Schaaf, H., Malik, C.Y., Streckbein, P., Pons-Kuehnemann, J., Howaldt, H.-P., and Wilbrand, J.-F. Three-dimensional photographic analysis of outcome after helmet treatment of a nonsynostotic cranial deformity. *Journal of Craniofacial Surgery*, **2010**. 21, 1677-82.

55.   Foster, K.A., Frim, D.M., and McKinnon, M. Recurrence of synostosis following surgical repair of craniosynostosis. *Plastic and Reconstructive Surgery*, **2008**. 121, 70-76.

56.   Williams, K.J., Cohen, S.R., Burstein, F.D., Hudgins, R., Boydston, W., and Simms, C. A longitudinal, statistical study of reoperation rates in craniosynostosis. *Plastic and Reconstructive Surgery*, **1997**. 100, 305-10.

57.   Ghali, G., Sinn, D.P., and Tantipasawasin, S. Management of nonsyndromic craniosynostosis. *Atlas of the Oral and Maxillofacial Surgery Clinics*, **2002**. 10, 1-41.

58.   Czerwinski, M., Hopper, R.A., Gruss, J., and Fearon, J.A. Major morbidity and mortality rates in craniofacial surgery: an analysis of 8101 major procedures. *Plastic and Reconstructive Surgery*, **2010**. 126, 181-86.

59.   Seruya, M., Oh, A.K., Boyajian, M.J., Posnick, J.C., Myseros, J.S., Yaun, A.L., and Keating, R.F. Long-term outcomes of primary craniofacial reconstruction for craniosynostosis: a 12-year experience. *Plastic and Reconstructive Surgery*, **2011**. 127, 2397-406.

60.   Siegel, M.I. and Mooney, M.P. Appropriate animal models for craniofacial biology. *The Cleft Palate-Craniofacial Journal*, **1990**. 27, 18-25.

61.   Grova, M., Lo, D.D., Montoro, D., Hyun, J.S., Chung, M.T., Wan, D.C., and Longaker, M.T. Animal Models of Cranial Suture Biology. *The Journal of Craniofacial Surgery*, **2012**. 23, 1954-58.

62.   Szpalski, C., Barr, J., Wetterau, M., Saadeh, P.B., and Warren, S.M. Cranial bone defects: current and future strategies. *Neurosurgical Focus*, **2010**. 29, E8.

63.   Shen, K., Krakora, S., Cunningham, M., Singh, M., Wang, X., Hu, F., Post, J., and Ehrlich, G. Medical treatment of craniosynostosis: recombinant Noggin inhibits coronal suture closure in the rat craniosynostosis model. *Orthodontics & Craniofacial Research*, **2009**. 12, 254-62.

64.   Heller, J.B., Gabbay, J.S., Wasson, K., Mitchell, S., Heller, M.M., Zuk, P., and Bradley, J.P. Cranial suture response to stress: expression patterns of Noggin and Runx2. *Plastic and Reconstructive Surgery*, **2007**. 119, 2037-45.

65.   Liu, J., Nam, H.K., Wang, E., and Hatch, N.E. Further Analysis of the Crouzon Mouse: Effects of the FGFR2C342Y Mutation Are Cranial Bone–Dependent. *Calcified Tissue International*, **2013**. 92, 451-66.

66.   Perlyn, C.A., DeLeon, V.B., Babbs, C., Govier, D., Burell, L., Darvann, T., Kreiborg, S., and Morriss-Kay, G. The craniofacial phenotype of the Crouzon mouse: analysis of a model for syndromic craniosynostosis using three-dimensional MicroCT. *The Cleft Palate-Craniofacial Journal*, **2006**. 43, 740-48.

67.   Perlyn, C.A., Morriss-Kay, G., Darvann, T., Tenenbaum, M., and Ornitz, D.M. A model for the pharmacological treatment of crouzon syndrome. *Neurosurgery*, **2006**. 59, 210-15.

68.   Mooney, M., Siegel, M.I., Burrows, A.M., Smith, T.D., Losken, H.W., Dechant, J., Cooper, G., Fellows-Mayle, W., Kapucu, M.R., and Kapucu, L.O. A rabbit model of human familial, nonsyndromic unicoronal suture synostosis II. Intracranial contents, intracranial volume, and intracranial pressure. *Child's Nervous System*, **1998**. 14, 247-55.

69.   Cray Jr, J., Burrows, A.M., Vecchione, L., Caccamese Jr, J.F., Losee, J.E., Moursi, A.M., Siegel, M.I., Cooper, G.M., and Mooney, M.P. Blocking bone morphogenetic protein function using in vivo noggin therapy does not rescue premature suture fusion in rabbits with delayed-onset craniosynostosis. *Plastic and Reconstructive Surgery*, **2011**. 127, 1163-72.

70.   Cooper, G.M., Curry, C., Barbano, T.E., Burrows, A.M., Vecchione, L., Caccamese, J.F., Norbutt, C.S., Costello, B.J., Losee, J.E., and Moursi, A.M. Noggin inhibits postoperative resynostosis in craniosynostotic rabbits. *Journal of Bone and Mineral Research*, **2007**. 22, 1046-54.

71.   Springer, I.N., Warnke, P.H., Terheyden, H., Açil, Y., Bülhoff, A., Kuchenbecker, S., Bolte, H., Russo, P.A., Vairaktaris, E.G., and Wiltfang, J. Craniectomy and noggin application in an infant model. *Journal of Cranio-Maxillofacial Surgery*, **2007**. 35, 177-84.

72.   Opperman, L.A., Adab, K., and Gakunga, P.T. Transforming growth factor-β2 and TGF-β3 regulate fetal rat cranial suture morphogenesis by regulating rates of cell proliferation and apoptosis. *Developmental Dynamics*, **2000**. 219, 237-47.

73.   Dwivedi, P., Lam, N., and Powell, B. Boning up on glypicans—opportunities for new insights into bone biology. *Cell Biochemistry and Function*, **2013**. 31, 91-114.

74.   Ai-Aql, Z., Alagl, A.S., Graves, D.T., Gerstenfeld, L.C., and Einhorn, T.A. Molecular mechanisms controlling bone formation during fracture healing and distraction osteogenesis. *Journal of Dental Research*, **2008**. 87, 107-18.

75.   Opperman, L.A., Nolen, A.A., and Ogle, R.C. TGF-β1, TGF-β2, and TGF-β3 Exhibit Distinct Patterns of Expression During Cranial Suture Formation and Obliteration In Vivo and In Vitro. *Journal of Bone and Mineral Research*, **1997**. 12, 301-10.

76.   Sanford, L.P., Ormsby, I., Gittenberger-de Groot, A.C., Sariola, H., Friedman, R., Boivin, G.P., Cardell, E.L., and Doetschman, T. TGF beta2 knockout mice have multiple developmental defects that are non-overlapping with other TGF beta knockout phenotypes. *Development*, **1997**. 124, 2659-70.

77.   Ito, Y., Yeo, J.Y., Chytil, A., Han, J., Bringas, P., Nakajima, A., Shuler, C.F., Moses, H.L., and Chai, Y. Conditional inactivation of Tgfbr2 in cranial neural crest causes cleft palate and calvaria defects. *Development*, **2003**. 130, 5269-80.

78.   Dwivedi, P., Grose, R., Hii, C., Filmus, J., Anderson, P., and Powell, B. Regulation of bone morphogenetic protein signalling and osteogenesis by glypicans in human cranial suture cells. *Bone*, **2011**. 48, S243.

79.   Wu, C.-J. and Lu, H.-K. Smad signal pathway in BMP-2-induced osteogenesis-a mini review. *Journal of Dental Sciences*, **2008**. 3, 13-21.

80.   Bragdon, B., Moseychuk, O., Saldanha, S., King, D., Julian, J., and Nohe, A. Bone morphogenetic proteins: a critical review. *Cellular Signalling*, **2011**. 23, 609-20.

81.   Warren, S.M., Brunet, L.J., Harland, R.M., Economides, A.N., and Longaker, M.T. The BMP antagonist noggin regulates cranial suture fusion. *Nature*, **2003**. 422, 625-29.

82.   Gazzerro, E., Pereira, R.C., Jorgetti, V., Olson, S., Economides, A.N., and Canalis, E. Skeletal overexpression of gremlin impairs bone formation and causes osteopenia. *Endocrinology*, **2005**. 146, 655-65.

83.   Filmus, J., Capurro, M., and Rast, J. Glypicans. *Genome biology*, **2008**. 9, 224.

84.   De Cat, B. and David, G. Developmental roles of the glypicans. in *Seminars in cell & developmental biology*. **2001**. Elsevier.

85.   Fico, A., Maina, F., and Dono, R. Fine-tuning of cell signaling by glypicans. *Cellular and Molecular Life Sciences*, **2011**. 68, 923-29.

86.   Kim, M.-S., Saunders, A.M., Hamaoka, B.Y., Beachy, P.A., and Leahy, D.J. Structure of the protein core of the glypican Dally-like and localization of a region important for hedgehog signaling. *Proceedings of the National Academy of Sciences*, **2011**. 108, 13112-17.

87.   Svensson, G., Awad, W., Håkansson, M., Mani, K., and Logan, D.T. Crystal Structure of N-Glycosylated Human Glypican-1 Core Protein structure of Two Loops Evolutionarily Conserved in Vertebrate Glypican-1. *Journal of Biological Chemistry*, **2012**. 287, 14040-51.

88.   Cooper, G.M., Usas, A., Olshanski, A., Mooney, M.P., Losee, J.E., and Huard, J. Ex vivo Noggin gene therapy inhibits bone formation in a mouse model of postoperative resynostosis. *Plastic and Reconstructive Surgery*, **2009**. 123, 94-103.

89.   Moioli, E.K., Clark, P.A., Xin, X., Lal, S., and Mao, J.J. Matrices and scaffolds for drug delivery in dental, oral and craniofacial tissue engineering. *Advanced Drug Delivery Reviews*, **2007**. 59, 308-24.

90.   Mooney, M.P., Losken, H.W., Moursi, A.M., Bradley, J., Azari, K., Acarturk, T.O., Cooper, G.M., Thompson, B., Opperman, L.A., and Siegel, M.I. Anti-TGF-β2 antibody therapy inhibits postoperative resynostosis in craniosynostotic rabbits. *Plastic and Reconstructive Surgery*, **2007**. 119, 1200-12.

91.   Lyn Chong, S., Mitchell, R., Moursi, A.M., Winnard, P., Wolfgang Losken, H., Bradley, J., Ozerdem, O.R., Azari, K., Acarturk, O., and Opperman, L.A. Rescue of coronal suture fusion using transforming growth factor-beta 3 (Tgf-β3) in rabbits with delayed-onset craniosynostosis. *The Anatomical Record Part A: Discoveries in Molecular, Cellular, and Evolutionary Biology*, **2003**. 274, 962-71.

92.   Frazier, B.C., Mooney, M.P., Losken, H.W., Barbano, T., Moursi, A., Siegel, M.I., and Richtsmeier, J.T. Comparison of craniofacial phenotype in craniosynostotic rabbits treated with anti-Tgf-β2 at suturectomy site. *The Cleft Palate-Craniofacial Journal*, **2008**. 45, 571-82.

93.   Gosain, A.K., Santoro, T.D., Song, L.-S., Capel, C.C., Sudhakar, P., and Matloub, H.S. Osteogenesis in calvarial defects: contribution of the dura, the pericranium, and the

surrounding bone in adult versus infant animals. *Plastic and Reconstructive Surgery*, **2003**. 112, 515-27.

94.   Mooney, M.P., Moursi, A.M., Opperman, L.A., and Siegel, M.I. Cytokine therapy for craniosynostosis. *Expert Opinion on Biological Therapy*, **2004**. 4, 279-99.

95.   Aw, M.S., Khalid, K.A., Gulati, K., Atkins, G.J., Pivonka, P., Findlay, D.M., and Losic, D. Characterization of drug-release kinetics in trabecular bone from titania nanotube implants. *International Journal of Nanomedicine*, **2012**. 7, 4883.

96.   Losic, D., Aw, M.S., Santos, A., Gulati, K., and Bariana, M. Titania nanotube arrays for local drug delivery: recent advances and perspectives. *Expert Opinion on Drug Delivery*, **2015**. 12, 103-27.

97.   Yamamoto, M., Tabata, Y., Hong, L., Miyamoto, S., Hashimoto, N., and Ikada, Y. Bone regeneration by transforming growth factor β1 released from a biodegradable hydrogel. *Journal of Controlled Release*, **2000**. 64, 133-42.

98.   Woo, E.J. Adverse events reported after the use of recombinant human bone morphogenetic protein 2. *Journal of Oral and Maxillofacial Surgery*, **2012**. 70, 765-7.

99.   Uludag, H., D'Augusta, D., Palmer, R., Timony, G., and Wozney, J. Characterization of rhBMP-2 pharmacokinetics implanted with biomaterial carriers in the rat ectopic model. *Journal of Biomedical Materials Research*, **1999**. 46, 193-202.

100. Lu, L., Stamatas, G.N., and Mikos, A.G. Controlled release of transforming growth factor β1 from biodegradable polymer microparticles. *Journal of Biomedical Materials Research*, **2000**. 50, 440-51.

101. Burdick, J.A., Mason, M.N., Hinman, A.D., Thorne, K., and Anseth, K.S. Delivery of osteoinductive growth factors from degradable PEG hydrogels influences osteoblast differentiation and mineralization. *Journal of Controlled Release*, **2002**. 83, 53-63.

102. Humber, C.C., Sándor, G., Davis, J.M., Peel, S.A., Brkovic, B.M., Kim, Y.D., Holmes, H.I., and Clokie, C.M. Bone healing with an in situ–formed bioresorbable polyethylene glycol hydrogel membrane in rabbit calvarial defects. *Oral Surgery, Oral Medicine, Oral Pathology, Oral Radiology, and Endodontology*, **2010**. 109, 372-84.

103. Lutolf, M. and Hubbell, J. Synthetic biomaterials as instructive extracellular microenvironments for morphogenesis in tissue engineering. *Nature Biotechnology*, **2005**. 23, 47-55.

104. Fournier, E., Passirani, C., Montero-Menei, C., and Benoit, J. Biocompatibility of implantable synthetic polymeric drug carriers: focus on brain biocompatibility. *Biomaterials*, **2003**. 24, 3311-31.

105. Cheng, I., Lin, Y.-C., Hwang, E., Huang, H.-T., Chang, W.-H., Liu, Y.-L., and Chao, C.-Y. Collagen VI protects against neuronal apoptosis elicited by ultraviolet irradiation via an Akt/phosphatidylinositol 3-kinase signaling pathway. *Neuroscience*, **2011**. 183, 178-88.

106. Hermann, C.D., Wilson, D.S., Lawrence, K.A., Ning, X., Olivares-Navarrete, R., Williams, J.K., Guldberg, R.E., Murthy, N., Schwartz, Z., and Boyan, B.D. Rapidly polymerizing

injectable click hydrogel therapy to delay bone growth in a murine re-synostosis model. *Biomaterials*, **2014**. 35, 9698-708.

107.   Losic, D. and Simovic, S. Self-ordered nanopore and nanotube platforms for drug delivery applications. *Expert Opinion on Drug delivery*, **2009**. 6, 1363-81.

108.   Gultepe, E., Nagesha, D., Sridhar, S., and Amiji, M. Nanoporous inorganic membranes or coatings for sustained drug delivery in implantable devices. *Advanced Drug Delivery reviews*, **2010**. 62, 305-15.

109.   Santos, A., Aw, M.S., Bariana, M., Kumeria, T., Wang, Y., and Losic, D. Drug-releasing implants: current progress, challenges and perspectives. *Journal of Materials Chemistry B*, **2014**. 2, 6157-82.

110.   Bariana, M., Aw, M.S., Moore, E., Voelcker, N.H., and Losic, D. Radiofrequency-triggered release for on-demand delivery of therapeutics from titania nanotube drug-eluting implants. *Nanomedicine*, **2014**. 9, 1263-75.

111.   Cölfen, H. and Mann, S. Higher-order organization by mesoscale self-assembly and transformation of hybrid nanostructures. *Angewandte Chemie International Edition*, **2003**. 42, 2350-65.

112.   Gomar-Nadal, E., Puigmartí-Luis, J., and Amabilino, D.B. Assembly of functional molecular nanostructures on surfaces. *Chemical Society Reviews*, **2008**. 37, 490-504.

113.   Masuda, H. and Fukuda, K. Ordered metal nanohole arrays made by a two-step replication of honeycomb structures of anodic alumina. *Science*, **1995**. 268, 1466-68.

114. Roy, P., Berger, S., and Schmuki, P. TiO$_2$ nanotubes: synthesis and applications. *Angewandte Chemie International Edition*, **2011**. 50, 2904-39.

115. Popat, K.C., Eltgroth, M., LaTempa, T.J., Grimes, C.A., and Desai, T.A. Titania Nanotubes: A Novel Platform for Drug-Eluting Coatings for Medical Implants? *Small*, **2007**. 3, 1878-81.

116. Grimes, C.A. Synthesis and application of highly ordered arrays of TiO$_2$ nanotubes. *Journal of Materials Chemistry*, **2007**. 17, 1451-57.

117. Macak, J., Tsuchiya, H., Ghicov, A., Yasuda, K., Hahn, R., Bauer, S., and Schmuki, P. TiO$_2$ nanotubes: self-organized electrochemical formation, properties and applications. *Current Opinion in Solid State and Materials Science*, **2007**. 11, 3-18.

118. Liu, Z., Hou, W., Pavaskar, P., Aykol, M., and Cronin, S.B. Plasmon resonant enhancement of photocatalytic water splitting under visible illumination. *Nano Letters*, **2011**. 11, 1111-16.

119. Chai, S., Zhao, G., Li, P., Lei, Y., Zhang, Y.-n., and Li, D. Novel sieve-like SnO$_2$/TiO$_2$ nanotubes with integrated photoelectrocatalysis: fabrication and application for efficient toxicity elimination of nitrophenol wastewater. *The Journal of Physical Chemistry C*, **2011**. 115, 18261-69.

120. Mor, G.K., Shankar, K., Paulose, M., Varghese, O.K., and Grimes, C.A. Enhanced photocleavage of water using titania nanotube arrays. *Nano Letters*, **2005**. 5, 191-95.

121.	Gong, J., Lai, Y., and Lin, C. Electrochemically multi-anodized TiO_2 nanotube arrays for enhancing hydrogen generation by photoelectrocatalytic water splitting. *Electrochimica Acta*, **2010**. 55, 4776-82.

122.	Jennings, J.R., Ghicov, A., Peter, L.M., Schmuki, P., and Walker, A.B. Dye-sensitized solar cells based on oriented TiO_2 nanotube arrays: transport, trapping, and transfer of electrons. *Journal of the American Chemical Society*, **2008**. 130, 13364-72.

123.	Zhu, K., Neale, N.R., Miedaner, A., and Frank, A.J. Enhanced charge-collection efficiencies and light scattering in dye-sensitized solar cells using oriented TiO_2 nanotubes arrays. *Nano Letters*, **2007**. 7, 69-74.

124.	Guo, W., Xue, X., Wang, S., Lin, C., and Wang, Z.L. An integrated power pack of dye-sensitized solar cell and Li battery based on double-sided TiO_2 nanotube arrays. *Nano Letters*, **2012**. 12, 2520-23.

125.	Wang, D.W., Fang, H.T., Li, F., Chen, Z.G., Zhong, Q.S., Lu, G.Q., and Cheng, H.M. Aligned titania nanotubes as an intercalation anode material for hybrid electrochemical energy storage. *Advanced Functional Materials*, **2008**. 18, 3787-93.

126.	Mun, K.-S., Alvarez, S.D., Choi, W.-Y., and Sailor, M.J. A stable, label-free optical interferometric biosensor based on TiO_2 nanotube arrays. *ACS Nano*, **2010**. 4, 2070-76.

127.	Gönüllü, Y., Rodríguez, G.C.M., Saruhan, B., and Ürgen, M. Improvement of gas sensing performance of TiO_2 towards NO_2 by nano-tubular structuring. *Sensors and Actuators B: Chemical*, **2012**. 169, 151-60.

128.   Liang, F., Luo, L.B., Tsang, C.K., Zheng, L., Cheng, H., and Li, Y.Y. TiO$_2$ nanotube-based field effect transistors and their application as humidity sensors. *Materials Research Bulletin*, **2012**. 47, 54-58.

129.   Yu, S., Peng, X., Cao, G., Zhou, M., Qiao, L., Yao, J., and He, H. Ni nanoparticles decorated titania nanotube arrays as efficient nonenzymatic glucose sensor. *Electrochimica Acta*, **2012**. 76, 512-17.

130.   Sharma, A. Anodizing titanium for space applications. *Thin Solid Films*, **1992**. 208, 48-54.

131.   Prida, V., Hernández-Vélez, M., Pirota, K., Menéndez, A., and Vázquez, M. Synthesis and magnetic properties of Ni nanocylinders in self-aligned and randomly disordered grown titania nanotubes. *Nanotechnology*, **2005**. 16, 2696-702.

132.   Wang, D., Liu, Y., Wang, C., Zhou, F., and Liu, W. Highly flexible coaxial nanohybrids made from porous TiO$_2$ nanotubes. *ACS Nano*, **2009**. 3, 1249-57.

133.   Lai, M., Cai, K., Zhao, L., Chen, X., Hou, Y., and Yang, Z. Surface functionalization of TiO$_2$ nanotubes with bone morphogenetic protein 2 and its synergistic effect on the differentiation of mesenchymal stem cells. *Biomacromolecules*, **2011**. 12, 1097-105.

134.   Aw, M.S., Gulati, K., and Losic, D. Controlling drug release from titania nanotube arrays using polymer nanocarriers and biopolymer coating. *Journal of Biomaterials and Nanobiotechnology*, **2011**. 2, 477-84.

135. Gulati, K., Ramakrishnan, S., Aw, M.S., Atkins, G.J., Findlay, D.M., and Losic, D. Biocompatible polymer coating of titania nanotube arrays for improved drug elution and osteoblast adhesion. *Acta Biomaterialia*, **2012**. 8, 449-56.

136. Sulka, G.D., Kapusta-Kołodziej, J., Brzózka, A., and Jaskuła, M. Anodic growth of TiO_2 nanopore arrays at various temperatures. *Electrochimica Acta*, **2013**. 104, 526-35.

137. Ou, H.H. and Lo, S.L. Review of titania nanotubes synthesized via the hydrothermal treatment: Fabrication, modification, and application. *Separation and Purification Technology*, **2007**. 58, 179-91.

138. Nakane, K., Shimada, N., Ogihara, T., Ogata, N., and Yamaguchi, S. Formation of TiO_2 nanotubes by thermal decomposition of poly (vinyl alcohol)-titanium alkoxide hybrid nanofibers. *Journal of Materials Science*, **2007**. 42, 4031-35.

139. Grimes, C.A. and Mor, G.K., Fabrication of TiO_2 nanotube arrays by electrochemical anodization: four synthesis generations, in TiO_2 Nanotube Arrays. **2009**, Springer. 1-66.

140. Mor, G.K., Varghese, O.K., Paulose, M., Shankar, K., and Grimes, C.A. A review on highly ordered, vertically oriented TiO_2 nanotube arrays: fabrication, material properties, and solar energy applications. *Solar Energy Materials and Solar Cells*, **2006**. 90, 2011-75.

141. Su, Z. and Zhou, W. Formation, morphology control and applications of anodic TiO_2 nanotube arrays. *Journal of Materials Chemistry*, **2011**. 21, 8955-70.

142. Ghicov, A. and Schmuki, P. Self-ordering electrochemistry: a review on growth and functionality of TiO_2 nanotubes and other self-aligned MOx structures. *Chemical Communications*, **2009**, 2791-808.

143. Yasuda, K., Macak, J.M., Berger, S., Ghicov, A., and Schmuki, P. Mechanistic aspects of the self-organization process for oxide nanotube formation on valve metals. *Journal of the Electrochemical Society*, **2007**. 154, 472-78.

144. Lee, W.-J., Alhoshan, M., and Smyrl, W.H. Titanium dioxide nanotube arrays fabricated by anodizing processes electrochemical properties. *Journal of the Electrochemical Society*, **2006**. 153, 499-505.

145. Zwilling, V., Darque-Ceretti, E., Boutry-Forveille, A., David, D., Perrin, M.Y., and Aucouturier, M. Structure and physicochemistry of anodic oxide films on titanium and TA6V alloy. *Surface and Interface Analysis*, **1999**. 27, 629-37.

146. Zwilling, V., Aucouturier, M., and Darque-Ceretti, E. Anodic oxidation of titanium and TA6V alloy in chromic media. An electrochemical approach. *Electrochimica Acta*, **1999**. 45, 921-2.

147. Gong, D., Grimes, C.A., Varghese, O.K., Hu, W., Singh, R., Chen, Z., and Dickey, E.C. Titanium oxide nanotube arrays prepared by anodic oxidation. *Journal of Materials Research*, **2001**. 16, 3331-34.

148. Macak, J.M., Sirotna, K., and Schmuki, P. Self-organized porous titanium oxide prepared in Na_2SO_4/NaF electrolytes. *Electrochimica Acta*, **2005**. 50, 3679-84.

149. Macak, J.M., Tsuchiya, H., and Schmuki, P. High-aspect-ratio TiO$_2$ nanotubes by anodization of titanium. *Angewandte Chemie International Edition*, **2005**. 44, 2100-102.

150. Albu, S.P., Ghicov, A., Macak, J.M., and Schmuki, P. 250 µm long anodic TiO$_2$ nanotubes with hexagonal self-ordering. *Physica Status Solidi (RRL)-Rapid Research Letters*, **2007**. 1, 65-7.

151. Paulose, M., Prakasam, H.E., Varghese, O.K., Peng, L., Popat, K.C., Mor, G.K., Desai, T.A., and Grimes, C.A. TiO$_2$ nanotube arrays of 1000 µm length by anodization of titanium foil: phenol red diffusion. *The Journal of Physical Chemistry C*, **2007**. 111, 14992-97.

152. Macak, J., Albu, S., Kim, D., Paramasivam, I., Aldabergerova, S., and Schmuki, P. Multilayer TiO$_2$–nanotube formation by two-step anodization. *Electrochemical and Solid-State Letters*, **2007**. 10, 28-31.

153. Prakasam, H.E., Shankar, K., Paulose, M., Varghese, O.K., and Grimes, C.A. A new benchmark for TiO$_2$ nanotube array growth by anodization. *The Journal of Physical Chemistry C*, **2007**. 111, 7235-41.

154. Paulose, M., Peng, L., Popat, K.C., Varghese, O.K., LaTempa, T.J., Bao, N., Desai, T.A., and Grimes, C.A. Fabrication of mechanically robust, large area, polycrystalline nanotubular/porous TiO$_2$ membranes. *Journal of Membrane Science*, **2008**. 319, 199-205.

155. Macak, J.M. and Schmuki, P. Anodic growth of self-organized anodic TiO$_2$ nanotubes in viscous electrolytes. *Electrochimica Acta*, **2006**. 52, 1258-64.

156. Kant, K. and Losic, D. A simple approach for synthesis of TiO_2 nanotubes with through-hole morphology. *Physica Status Solidi (RRL)-Rapid Research Letters*, **2009**. 3, 139-41.

157. Allam, N.K. and Grimes, C.A. Formation of vertically oriented TiO_2 nanotube arrays using a fluoride free HCl aqueous electrolyte. *The Journal of Physical Chemistry C*, **2007**. 111, 13028-32.

158. Hahn, R., Macak, J., and Schmuki, P. Rapid anodic growth of TiO_2 and WO_3 nanotubes in fluoride free electrolytes. *Electrochemistry Communications*, **2007**. 9, 947-52.

159. Wang, J. and Lin, Z. Anodic formation of ordered TiO_2 nanotube arrays: effects of electrolyte temperature and anodization potential. *The Journal of Physical Chemistry C*, **2009**. 113, 4026-30.

160. Kaneco, S., Chen, Y., Westerhoff, P., and Crittenden, J.C. Fabrication of uniform size titanium oxide nanotubes: Impact of current density and solution conditions. *Scripta Materialia*, **2007**. 56, 373-76.

161. Watcharenwong, A., Chanmanee, W., De Tacconi, N., Chenthamarakshan, C., Kajitvichyanukul, P., and Rajeshwar, K. Self-organized TiO_2 nanotube arrays by anodization of Ti substrate: effect of anodization time, voltage and medium composition on oxide morphology and photoelectrochemical response. *Journal of Materials Research*, **2007**. 22, 3186-95.

162. Regonini, D., Anodised TiO_2 nanotubes: voltage ramp influenceon the nano-structured oxide and investigation of phase changes promoted by thermal treatments. *Physica Status Solidi (A),* **2007**. 204, 1814-19.

163. Macak, J., Taveira, L., Tsuchiya, H., Sirotna, K., Macak, J., and Schmuki, P. Influence of different fluoride containing electrolytes on the formation of self-organized titania nanotubes by Ti anodization. *Journal of Electroceramics*, **2006**. 16, 29-34.

164. Macak, J.M., Tsuchiya, H., Taveira, L., Aldabergerova, S., and Schmuki, P. Smooth anodic TiO_2 nanotubes. *Angewandte Chemie International Edition*, **2005**. 44, 7463-65.

165. Sánchez-Tovar, R., Lee, K., García-Antón, J., and Schmuki, P. Formation of anodic TiO_2 nanotube or nanosponge morphology determined by the electrolyte hydrodynamic conditions. *Electrochemistry Communications*, **2013**. 26, 1-4.

166. So, S., Lee, K., and Schmuki, P. Ultrafast growth of highly ordered anodic TiO_2 nanotubes in lactic acid electrolytes. *Journal of the American Chemical Society*, **2012**. 134, 11316-18.

167. Clair, J.D.S. and DelPesco, T.W., Titanium chelate dispersions, **2004**, Google Patents.

168. Liu, Y. and Scheuer, C., Anodizing electrolytes for high voltage capacitor anodes, **2004**, Google Patents.

169. Banerjee, S., Misra, M., Mohapatra, S.K., Howard, C., Mohapatra, S.K., and Kamilla, S.K. Formation of chelating agent driven anodized TiO_2 nanotubular membrane and its photovoltaic application. *Nanotechnology*, **2010**. 21, 145201.

170. Yin, H., Liu, H., and Shen, W. The large diameter and fast growth of self-organized TiO_2 nanotube arrays achieved via electrochemical anodization. *Nanotechnology*, **2010**. 21, 035601.

171.   Sreekantan, S., Wei, L.C., and Lockman, Z. Extremely fast growth rate of TiO_2 nanotube arrays in electrochemical bath containing H2O2. *Journal of the Electrochemical Society*, **2011**. 158, 397-402.

172.   Bauer, S., Schmuki, P., von der Mark, K., and Park, J. Engineering biocompatible implant surfaces: Part I: Materials and surfaces. *Progress in Materials Science*, **2013**. 58, 261-326.

173.   Gulati, K., Aw, M.S., Findlay, D., and Losic, D. Local drug delivery to the bone by drug-releasing implants: perspectives of nano-engineered titania nanotube arrays. *Therapeutic Delivery*, **2012**. 3, 857-73.

174.   Aw, M.S., Kurian, M., and Losic, D. Non-eroding drug-releasing implants with ordered nanoporous and nanotubular structures: concepts for controlling drug release. *Biomaterials Science*, **2014**. 2, 10-34.

175.   Peng, L., Mendelsohn, A.D., LaTempa, T.J., Yoriya, S., Grimes, C.A., and Desai, T.A. Long-term small molecule and protein elution from TiO_2 nanotubes. *Nano Letters*, **2009**. 9, 1932-6.

176.   De Santo, I., Sanguigno, L., Causa, F., Monetta, T., and Netti, P.A. Exploring doxorubicin localization in eluting TiO_2 nanotube arrays through fluorescence correlation spectroscopy analysis. *Analyst*, **2012**. 137, 5076-81.

177.   Simovic, S., Losic, D., and Vasilev, K. Controlled drug release from porous materials by plasma polymer deposition. *Chemical Communication*. **2010**. 46, 1317-19.

178.   Vasilev, K., Poh, Z., Kant, K., Chan, J., Michelmore, A., and Losic, D. Tailoring the surface functionalities of titania nanotube arrays. *Biomaterials*, **2010**. 31, 532-40.

179.   Tejero, R., Anitua, E., and Orive, G. Toward the biomimetic implant surface: Biopolymers on titanium-based implants for bone regeneration. *Progress in Polymer Science*, **2014**. 39, 1406-47.

180.   Chen, X., Cai, K., Fang, J., Lai, M., Hou, Y., Li, J., Luo, Z., Hu, Y., and Tang, L. Fabrication of selenium-deposited and chitosan-coated titania nanotubes with anticancer and antibacterial properties. *Colloids and Surfaces B: Biointerfaces*, **2013**. 103, 149-57.

181.   SinnáAw, M. A multi-drug delivery system with sequential release using titania nanotube arrays. *Chemical Communications*, **2012**. 48, 3348-50.

182.   Cai, K., Jiang, F., Luo, Z., and Chen, X. Temperature-Responsive Controlled Drug Delivery System Based on Titanium Nanotubes. *Advanced Engineering Materials*, **2010**. 12, 565-70.

183.   Aw, M.S., Addai-Mensah, J., and Losic, D. Magnetic-responsive delivery of drug-carriers using titania nanotube arrays. *Journal of Materials Chemistry*, **2012**. 22, 6561-63.

184.   Shrestha, N.K., Macak, J.M., Schmidt-Stein, F., Hahn, R., Mierke, C.T., Fabry, B., and Schmuki, P. Magnetically Guided Titania Nanotubes for Site-Selective Photocatalysis and Drug Release. *Angewandte Chemie International Edition*, **2009**. 48, 969-72.

185.   Aw, M.S. and Losic, D. Ultrasound enhanced release of therapeutics from drug-releasing implants based on titania nanotube arrays. *International Journal of Pharmaceutics*, **2013**. 443, 154-62.

186.   Ketabchi, A., Komm, K., Miles-Rossouw, M., Cassani, D.A., and Variola, F. Nanoporous titanium surfaces for sustained elution of proteins and antibiotics. *PloS One*, **2014**. 9, 92080.

187.   Hu, Y., Cai, K., Luo, Z., Xu, D., Xie, D., Huang, Y., Yang, W., and Liu, P. TiO_2 nanotubes as drug nanoreservoirs for the regulation of mobility and differentiation of mesenchymal stem cells. *Acta Biomaterialia*, **2012**. 8, 439-48.

188.   Wei, H., Wu, S., Feng, Z., Zhou, W., Dong, Y., Wu, G., Bai, S., and Zhao, Y. Increased fibroblast functionality on CNN2-loaded titania nanotubes. *International Journal of Nanomedicine*, **2012**. 7, 1091.

189.   Sun, S., Yu, W., Zhang, Y., and Zhang, F. Increased preosteoblast adhesion and osteogenic gene expression on TiO_2 nanotubes modified with KRSR. *Journal of Materials Science: Materials in Medicine*, **2013**. 24, 1079-91.

190.   Harmankaya, N., Karlsson, J., Palmquist, A., Halvarsson, M., Igawa, K., Andersson, M., and Tengvall, P. Raloxifene and alendronate containing thin mesoporous titanium oxide films improve implant fixation to bone. *Acta Biomaterialia*, **2013**. 9, 7064-73.

191.   Koo, T.-H., Borah, J.S., Xing, Z.-C., Moon, S.-M., Jeong, Y., and Kang, I.-K. Immobilization of pamidronic acids on the nanotube surface of titanium discs and their interaction with bone cells. *Nanoscale Research Letters*, **2013**. 8, 1-9.

CHAPTER 3

FABRICATION AND CHARACTERISATION

OF TNT/Ti IMPLANTS

CHAPTER 3: Fabrication and Characterisation of TNT/Ti Implants

3.1. Introduction

As described in Chapter 2, the current goal of this craniosynostosis research project is to develop clinically viable cranial implants that can help prevent/delay bone re-fusion. Commonly used biomedical implantable devices are widely based on Titanium (Ti) and its alloys, due to its attractive properties such as fairly low modulus, high mechanical strength, easy processability, chemical inertness and corrosion resistance [1]. The native oxide layer on its surface provides Ti with excellent biocompatibility and appropriate integration, which is a prerequisite for biomedical implant success, particularly for hard tissue engineering applications such as dental implants, prosthetic devices, materials for craniofacial and maxillofacial reconstruction *etc*. [1-6]. Examples of various titanium implantable devices are depicted in **Figure 3.1**.

However, the current technology is limited by post-implantation infection and implant failure/rejection in majority of long-term (>10 years) cases [7-10]. With the advent of nanotechnology, nanotexturing of the implant surface has become a popular alternative to improve implant acceptance and integration [11-13]. Although there are a number of methods to fabricate nanoporous/nanotubular surfaces (as mentioned in Chapter 2, Section 2.4., p.41-46), electrochemical anodisation (EA) is the simplest, most inexpensive and highly scalable technique to grow Titania nanotubes (TNTs) on Ti surfaces. This method also provides a good control on the nanotube dimensions and arrangement [14, 15] and can be readily integrated into existing implant market for many anticipated applications [16-18].
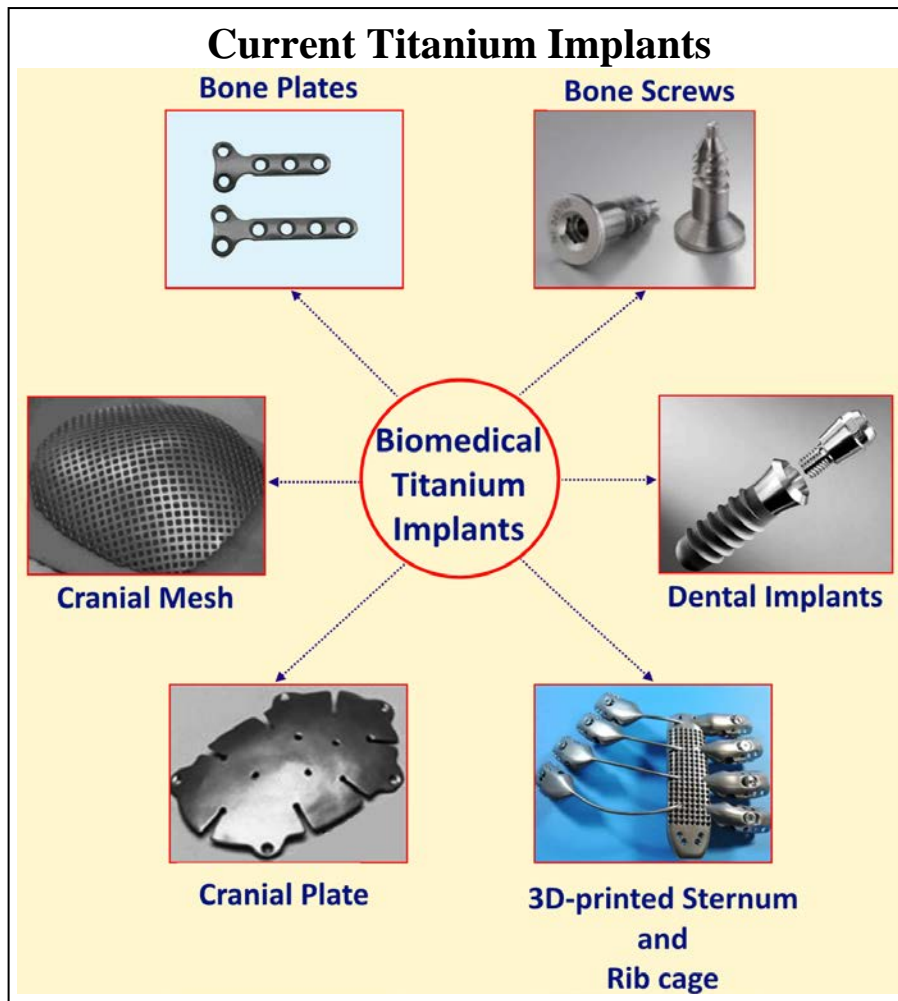
Figure 3.1. Various Titanium implants catering to different conditions in hard-tissue engineering.

The morphological characteristics of TNTs depend on many experimental conditions such as set-up configuration (two or three electrode), anodisation time, applied voltage, temperature, electrolyte composition and concentration, pH and Ti surface roughness [12]. Generally, TNT layers can be fabricated in either aqueous or non-aqueous electrolytes containing small amounts of fluoride ions (such as HF, NaF or NH_4F). While the duration, voltage, and fluoride concentration mainly control the nanotube length, diameter, and growth rate, the electrolyte characteristics, including solvent, polarity, water content, viscosity, organic additives *etc*. also effect the overall anodisation process and tube geometry [12, 16, 19]. The earlier generation of acidic, neutral and

alkaline aqueous electrolytes led to formation of non-uniform, disorganised and short nanotubular arrays, which were improved upon by anodisation in protic non-aqueous organic media such as ethylene glycol or glycerol. The latter conditions generated ordered arrays of TNTs with a smooth surface and very high aspect ratio [16, 20]. In order to obtain high quality and mechanically stable TNTs on Ti, aging of the organic electrolyte is often required [21, 22]. A recent study involving repeated anodisation of dummy Ti sheets in ethylene glycol electrolytes for up to 10 h generated a stable and mechanically robust anodic film [23]. Alternatively, addition of organic chelating agents, such as EDTA, glycolic and lactic acid (as described in Chapter 2, Section 2.4.4, p.47-49), can guide generation of ultrafast TNTs with intact structural and functional properties [24, 25].

This chapter concentrates on designing and fabricating the electrochemically anodised TNT/Ti cranial implants to be used as therapeutic-delivering interfaces for advanced craniosynostosis treatment. The specific aims of this study were: (i) to design and produce 3 mm circular discs via ultrasonic milling of Ti sheets, (ii) to configure the electrochemical set-up, optimise EA conditions and fabricate and characterise the TNT/Ti implants using ethylene glycol electrolyte (with and without lactic acid additive) and (iii) to modify the TNT/Ti implant by surface coating with biopolymers (Chitosan and Pluronic-F127) of varied thickness.

The first step in designing the cranial implants involved advanced ultrasonic milling to cut 3 mm circular Ti discs. This prompted the development of a smooth-edged TNT/Ti implant that fits into 3 mm defects during the future murine experiments. A precise design was needed to avoid tissue inflammation or unnecessary pressure on underlying dura. A laser cutting technique was also tested but the high heat produced during the process burnt the Ti surface, changing its roughness (data not included). The ultrasonically milled Ti discs were then anodised in either a traditional or a lactic acid-containing ethylene glycol electrolyte. These two electrolytes were explored and

compared to optimise the stability of TNT arrays, in order to avert undesired surface instabilities, cracks and delamination of the nanotube structure. The crystalline phase of LA-fabricated TNTs was examined by X-ray diffraction. Moreover, two different polymer modifications were also proposed: i) to improve the biocompatibility and modulate the implant interactions with the cell and *in vivo* environment and ii) to act as an barrier layer to inculcate slow and sustained release of the loaded therapeutics in the future studies. The surface morphology and wettability of polymer-coated and uncoated TNTs were characterised using scanning electron microscopy (SEM) and contact angle (CA) measurements, respectively.

3.2. Experimental section

3.2.1. Materials and chemicals

High purity titanium foil (99.6% of Ti) with a thickness of 0.20 mm, supplied by Nilaco (Japan), was used as substrate for the implant fabrication. Electrolytes used for EA: Ethylene glycol (99 vol %), ammonium fluoride (NH_4F) and DL-Lactic acid were obtained from Sigma–Aldrich (Australia). Two different polymers, low molecular weight chitosan with low degree of acetylation and Pluronic-F127 (PEO-PPO-PEO block copolymer) were also supplied by Sigma–Aldrich (Australia) and used as received. High-purity Milli-Q water, ultrapure grade (18.2 MΩ-cm) (pH = 6.5 ± 0.5) sieved through a 0.22 µm filter was used for all dilutions and solutions. All other reagents (ethanol, methanol, acetone, isopropanol) were purchased from Chem Supply (Australia) and used without further purification.

3.2.2. Aim I: Ti disc design and production

The Ti foils were annealed using XD-MZT multi-zones furnace at 450°C for 2 hours at a ramp rate of 30°C/min in air, prior to the processing. A state-of-art ultrasonic mill (DMG Ultrasonic 20 linear) at the Optonode of Australian national fabrication facility (ANFF) was used to precisely machine mechanically polished Ti strips into 3mm circular disc with uniform and smooth boundaries. The system involved kinematic superposition of the tool rotation with an additional oscillation, giving optimum control to cut the otherwise hard Ti metal. The high frequency and low amplitude vibrations from the tool were coupled with fine abrasive grains in the form of a slurry to selectively remove the desired Ti disc. The 3 mm disc was cleaned and degreased by successive sonication in acetone, ethanol and isopropanol, followed by rinsing with deionised water and drying with nitrogen gas.

3.2.3. Aim II: Fabrication of TNT/Ti implants

TNT arrays were fabricated on the Ti discs by simple two-step electrochemical anodisation in either traditional ethylene glycol or lactic acid containing organic electrolyte [24, 26]. An experimental set-up for TNT fabrication involved specially designed electrochemical cell with two-electrode configuration and computer controlled power supply (Agilent, USA) (**Figure 3.2**). The EA set-up essentially had the Ti disc (anode) contacted with an Aluminium back plate, securely pressed against the O-ring at the bottom of the cell, permitting the 3 mm circular area to be exposed to the anodisation electrolyte. The counter electrode was made of a coiled platinum wire which acted as cathode when connected to the voltage source. A temperature-controlled EA anodisation bath (MR Hie-Standard Thermostat, Heidolph, Germany) was used to maintain constant anodisation conditions.

Electrochemical Anodisation Set-up

Platinum Counter Electrode

$2H^+ + 2e^- \longrightarrow H_2$

Electrolyte

Power Supply

Titanium Working Electrode

$TiO_2 + 6F^- + 4H^+ \longrightarrow [TiF_6]^{2-} + 2H_2O$

Back Contact
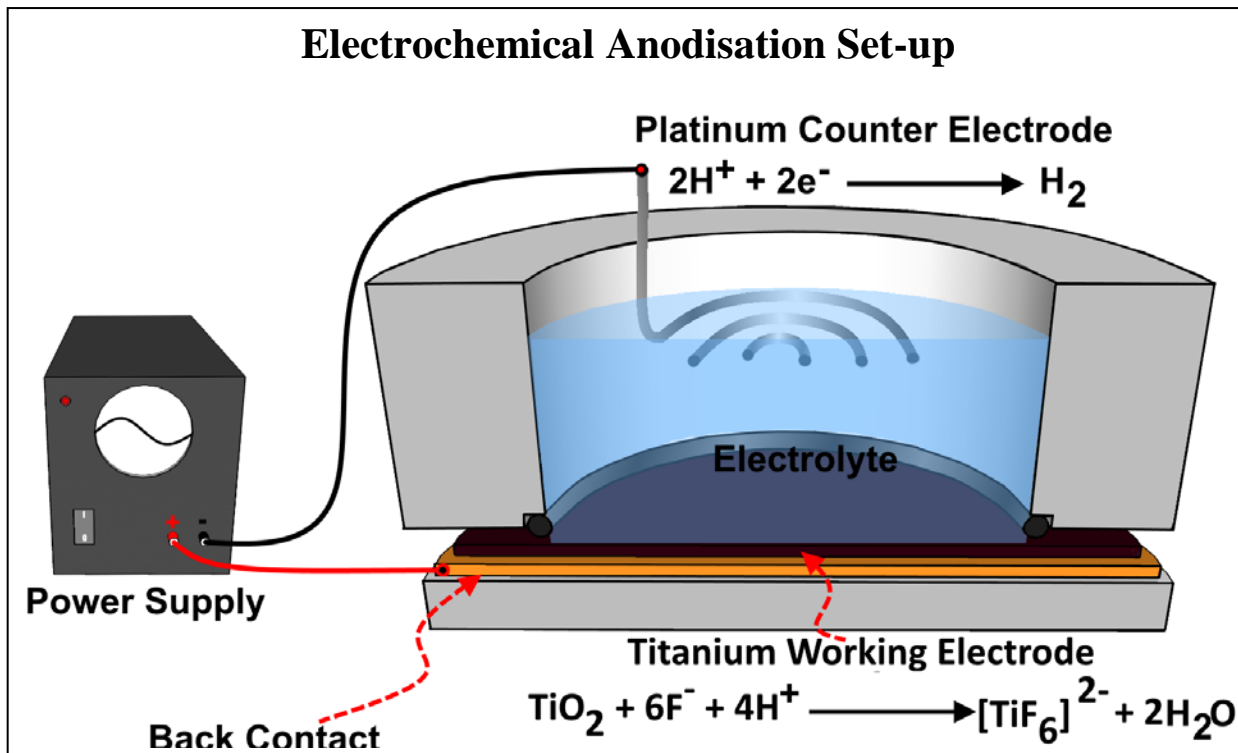
Figure 3.2. A schematic diagram showing the anodisation set-up with the electrochemical cell cut through into half for better visualisation.

The two-step anodisation approach leads to a better ordered TNT arrays with well-defined morphologies as schematically shown in **Figure 3.3**. For the traditional electrolyte (0.1 M NH$_4$F, 5 wt. % H$_2$O in EG) [13, 17, 27], the first anodisation was carried out at a constant voltage of 100 V applied for 2 h at room temperature (RT). This thick layer was then removed by sonication in methanol, resulting in underlying textured substrate with an arrangement of self-ordered dimple structures. In the second anodisation step, the etch pits on the titanium substrates acted as new growth points for a well-defined top layer anodised at 100 V for 1 h.
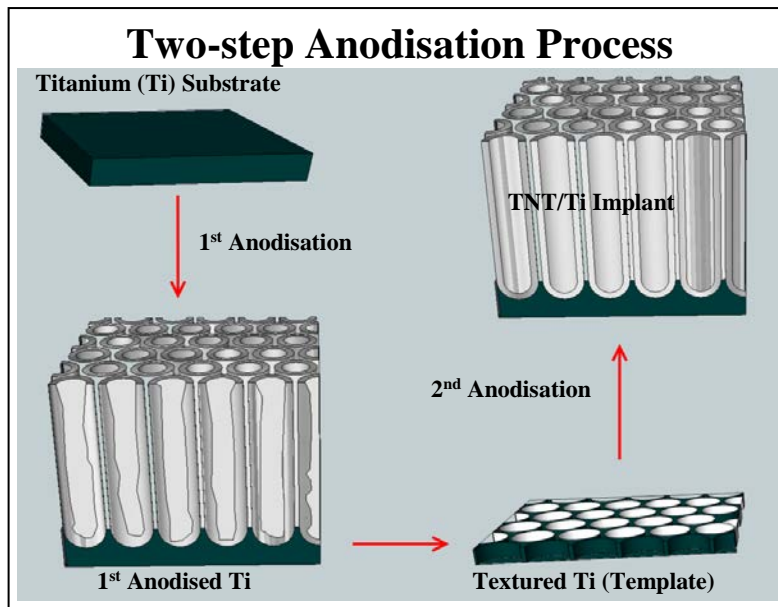
Figure 3.3. Scheme showing the two-step anodisation process.

For the lactic-acid containing electrolyte (1.5 M LA, 0.1 M NH_4F, 5 wt. % H_2O in EG) [24], the first anodisation was carried out at high temperature of electrolyte (60 °C) and 120 V for different times (3, 5, 10 and 30 min). Subsequently, the TNT layer was removed by sonication in methanol, leaving the nanotextured titanium surface for the second anodisation. The second anodisation was carried out under similar conditions to yield an ordered array of TNTs. Unlike the first anodised TNT layer, this second layer was rigid and stable enough for the proposed implant applications. The voltage–current–time parameters were adjusted and continuously monitored (Labview, National Instruments) during the anodisation process to ensure repeatability of the fabrication process. After anodisation, the implants were rinsed in deionised water and dried under nitrogen stream.

3.2.4. Aim III: Surface coating

Two polymers, chitosan (low molecular weight), and Pluronic-F127 (PEO-PPO-PEO block copolymer) were coated onto TNT/Ti implant discs. Polymer solutions of chitosan (1-2% (w/v), chitosan + 0.8 vol. % acetic acid in deionised water) and Pluronic-F127 (20% (w/v) in cold water) were prepared and spin-coated by pipetting a drop of the polymeric solutions (depending on the desired layer thickness) onto the TNT/Ti, followed by vacuum drying. The polymers were coated using a spin coater (WS-650 Lite, Laurell Technologies) programmed at 1500 rpm for 15 s.

3.3. Characterisation

3.3.1. Scanning electron microscopy (SEM)

Structural and morphological characterisation of the fabricated TNT/Ti implants was performed using a field-emission scanning electron microscope (SEM, FEI Quanta 450, Eindhoven, The Netherlands). The 3 mm TNT/Ti discs were mounted onto a holder with double-sided conductive tape and coated with a layer of 3 nm thick platinum using a vacuum evaporator. The top-view images were observed at normal incidence. The side view to measure the thickness of the nanotubes as well as polymer layers was acquired at 30° angle on mechanically scratched samples. The distances on the SEM image were determined using a measured click and drag line calculated by the SEM computer software based on the magnification of the image.

3.3.2. X-ray diffraction spectroscopy (XRD)

The crystal structure of annealed TNT/Ti implants was evaluated by X-ray diffraction (XRD) using a Rigaku Minflex 600 diffractometer with CoKα (40 kV, 15 mA) and a graphite monochromator. The samples were scanned between 20-80° (2θ) at the rate of $1.0°.min^{-1}$. The measurements were repeated on three TNT/Ti samples and showed similar spectra.

3.3.3. Contact angle measurements (CA)

The hydrophilicity/hydrophobicity of the titanium, uncoated and polymer-coated TNT/Ti discs, were measured using a sessile drop method on an optical contact angle measuring device (Attension, KSV instruments). A small amount of deionised water droplet (3 µl) was placed onto the sample surfaces to measure the dynamic CA. The value of contact angle for each substrate was the average value of 121 measurements over a time period of 5 ± 2.92 s, providing the degree of phase separation between the solid/liquid interface as well as the vapour/liquid interphase.

3.4. Results and discussion

3.4.1. Characterisation of prepared TNT/Ti implants

Figure 3.4 shows the digital image of Ti disc after ultrasonic milling and 2-step anodisation. The Ti sheet was drilled into a 3 mm disc attached with three petite hinges, after mechanical polishing. Before the anodisation, the hinges were clipped to obtain a circular Ti substrate. Formation of a yellowish-green layer indicates the successful TNT synthesis on the Ti surface which can be visually observed. The colour is directly related to the thickness of the nanotube layer, with the longer TNTs having a darker colour.
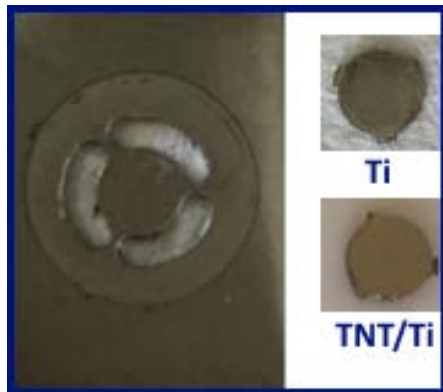
Figure 3.4. Image of ultrasonically milled Ti foil with the extracted Ti disc before and after anodisation (The tiny platform hinge help in handling the discs without hampering the nanotube layer).

3.4.1.1. TNTs prepared in traditional electrolyte

SEM analysis was carried out to examine the nanoarchitecture of TNTs fabricated by EA in traditional as well as lactic acid-containing electrolyte before and after polymer coating. An ethylene glycol (traditional) electrolyte containing fluorine ions is the most commonly used electrolyte to obtain high aspect ratio, highly ordered nanotubes with smooth surface [28-30]. **Figure 3.5** depicts the typical structure of TNTs fabricated in traditional electrolyte with **Figure 3.5a** showing the top surface with a thin porous oxide layer instead of a tubular structure. It is common to have a porous grassy layer on top from anodisation under mentioned conditions [29]. The thin porous layer was removed by sonication in isopropanol for 10 mins, unveiling the nanotubular structure underneath (**Figure 3.5b**). Loose pieces of leftover porous layer from the nanotube wall chemical dissolution (excessive etching at the top) in the electrolyte can be easily rinsed with deionised water. The nanotubes with opened pores featured an average diameter of 100 ± 20 nm (anodised at 100 V, RT). The cross-sectional micrograph (**Figure 3.5c**) confirms that

the prepared TNTs are vertically-aligned tubules with ~40 µm thickness (nanotube length for 1 h of anodisation). The bottom surface of the TNT layer detached from the nanotube substrate shows closed nanotubes (**Figure 3.5d**).
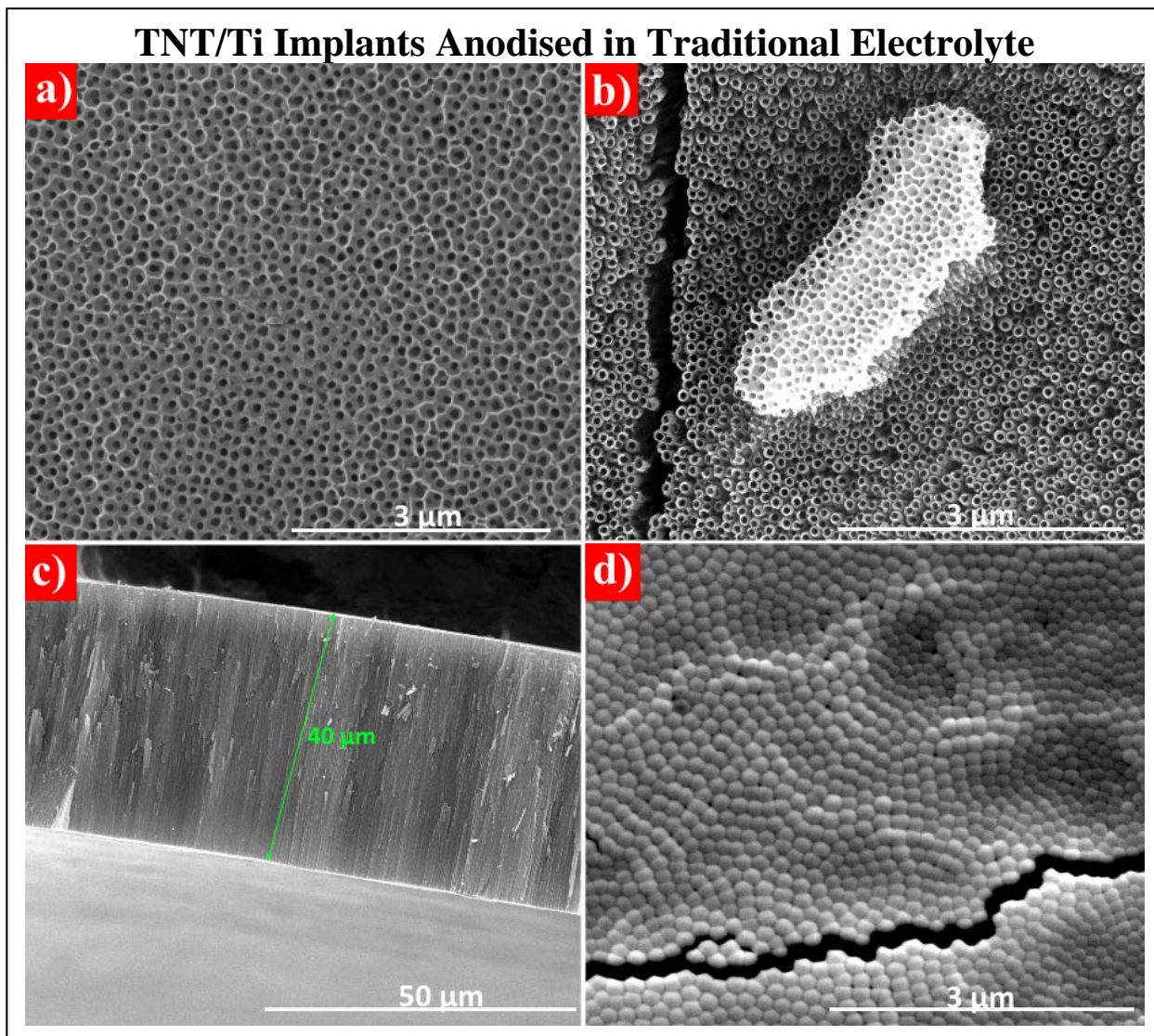
Figure 3.5. SEM images showing surface topography of a Ti disc anodised in a traditional electrolyte. (a-b) The top of nanotube surface showing nanoporous and nanotubular morphology obtained after removing of thin porous layer; (c) Cross-sectional image of nanotube layer showing

the total length of the fabricated TNTs; (d) The bottom surface showing the closed nanotube structures detached from underlying Ti substrate.

Visual as well as SEM assessments suggested that the nanotubes obtained from the traditional electrolyte were not mechanically stable and had several cracks, causing the TNT layer to delaminate from the Ti substrate. This can be attributed to the use of fresh electrolyte without aging, resulting in peeling of the TNT layer, even at short anodisation durations. Therefore, this approach was unsuitable for fabricating robust cranial TNT/Ti implants. The optimised electrolyte aging parameters were later published by our group in an incoherent study [23].

3.4.1.2. TNTs prepared in Lactic acid- containing electrolyte

To overcome the limitations of the traditional electrolyte, we adopted a recent approach that led to formation of highly adhesive and robust TNT layers at unprecedented growth rates (as described in section 2.3.7.4, p.47-49) [24]. SEM micrograph of the top surface of fabricated TNT/Ti implant in LA-containing electrolyte (anodised at 120 V, 60 $^{\circ}$C) confirms the formation of hexagonally arranged nanopores with average diameter of 120 ± 10 nm (**Figure 3.6a**). **Figure 3.6c-d** present the high-resolution partial top and cross-sectional images displaying hollow, tubular, densely packed TNT arrays with high degree of order. The image in **Figure 3.6d** depicts the high magnification image of TNT bottom and partial cross section of prepared TNT arrays.
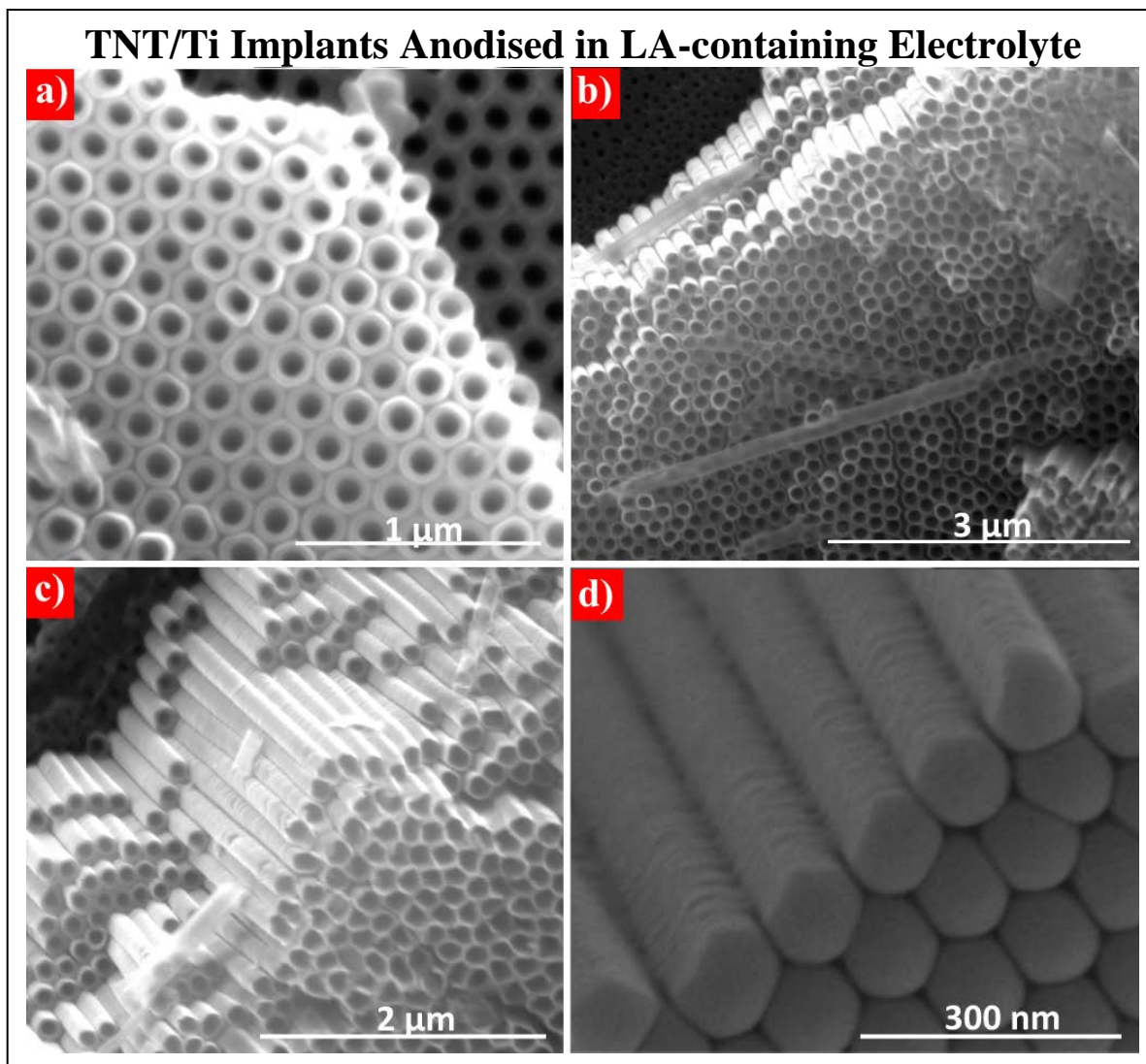
Figure 3.6. SEM images showing surface topography of a Ti disc anodised in a Lactic acid-containing electrolyte. (a) The top view with TNT pore diameter of 120 ± 10 nm, anodised at 120 V, 60 °C; (b-c) Partial top and cross-sectional view of the formed TNTs; (d) TNT bottom magnified at high resolution to show the layer arrangement and closed ends.

While the observation of TNT/Ti SEM images provided an indication of reproducibility and homogeneity of Titania nanotubes produced under specific electrolyte conditions, it also predicted different tube lengths synthesised at different anodisation times. **Figure 3.7a-c** displays the low magnification cross-sectional images of TNTs anodised in LA-containing electrolytes (120 V,

97

60 °C)   for 3, 5, 10 and 30 mins with layer thickness of approximately 17 µm, 35 µm, 55 µm and

80 µm, respectively.
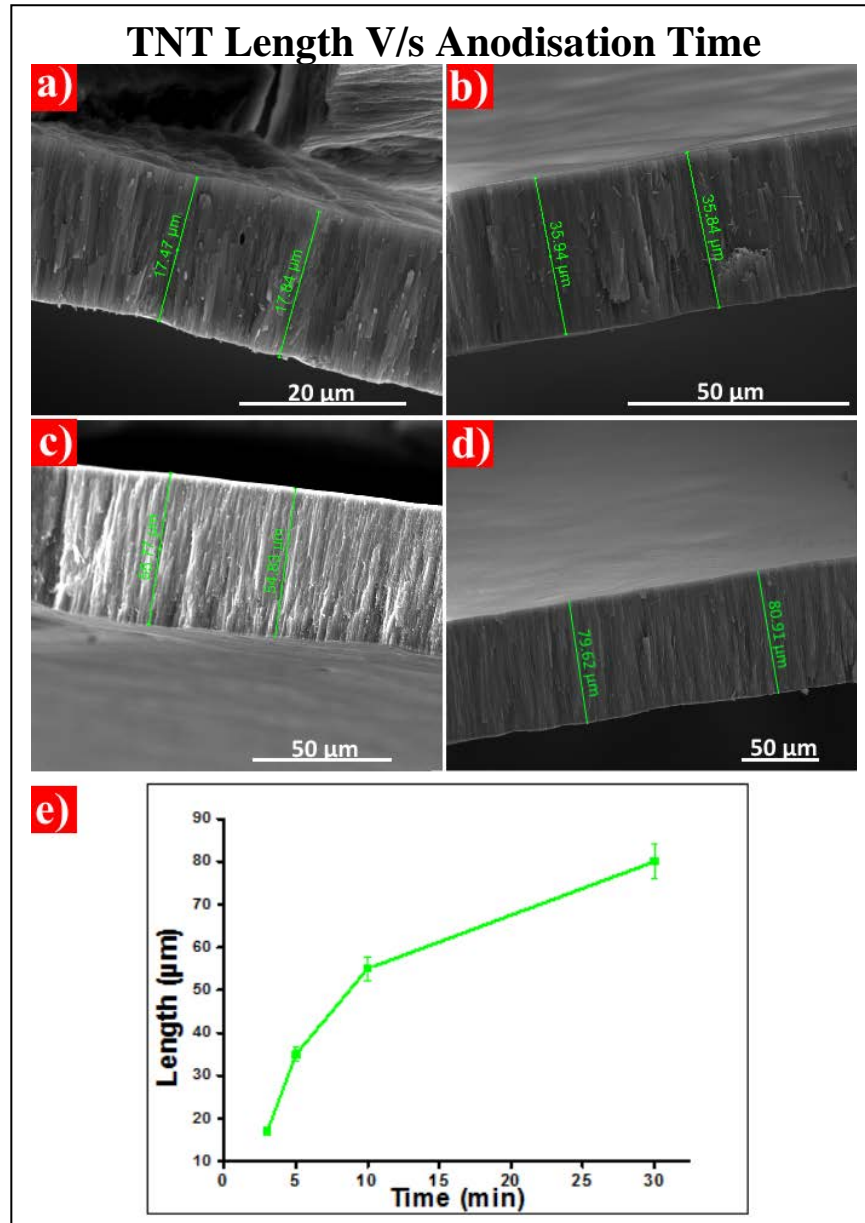
Figure 3.7. Average nanotube lengths at different anodisation times. SEM images of TNT cross-

sections with anodisation times (a) 3 min, (b) 5min, (c) 10 min and (d) 30 min which yielded

various nanotube lengths of 17 µm, 35 µm, 55 µm and 80 µm in that sequence; (e) Average

nanotube length v/s anodisation time curve for anodisation at 120 V, 60 °C. Error bars represent

mean ± SD for n = 3.

3.4.1.3. Comparison of TNTs prepared in traditional and Lactic acid- containing electrolyte
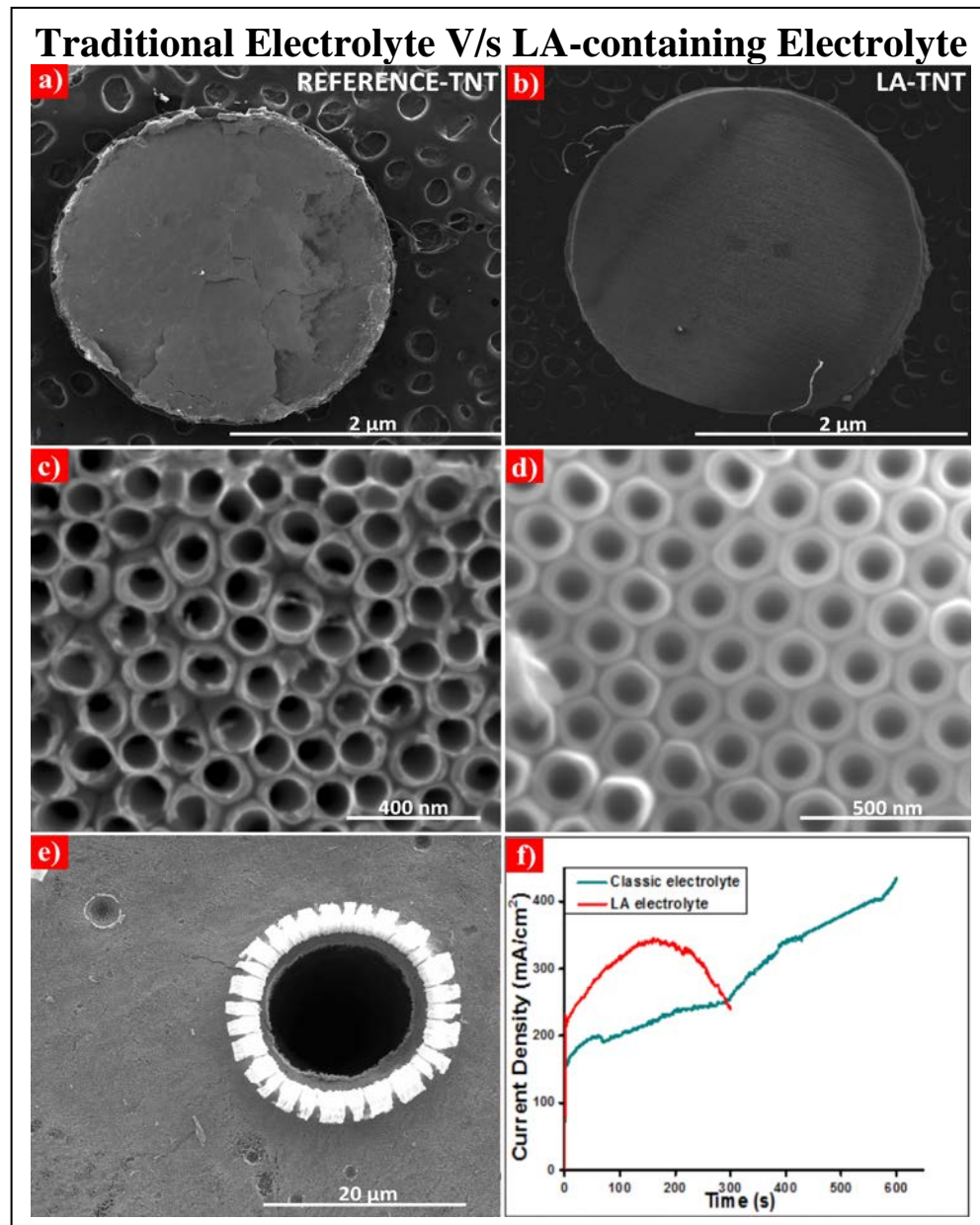
Figure 3.8. Morphological SEM characterisation of TNT implants fabricated under (a, c) traditional electrolyte (reference TNTs) and (b, d) Lactic acid-containing electrolyte; (e) A typical

breakdown morphology at 120 V and RT after 10 min of anodisation in traditional electrolyte. (f)

Representative curve for corresponding current density-time behaviours for anodisation at 120 V,

RT in traditional electrolyte along with bell shaped curve for TNTs anodised at 120 V, 60 °C in

LA electrolyte.

The TNT dimensions (pore diameter and nanotube length) can be altered by changing the

parameters of anodisation process such as anodisation voltage, time, temperature, pH and

additional species in the electrolytes. In **Figure 3.8** we have compared morphologies as well as the

current density-time curves for both LA electrolyte (at 60 °C, 120 V) and traditional electrolyte (at

RT, 100 and 120 V) conditions. **Figure 3.8a** and **c** show the TNT/Ti implant surface under

traditional conditions rendered a mechanically unstable layer with pore diameter 100 ± 20 nm,

while **Figure 3.8b** and **d** displayed well-adhered nanotube layer with pore diameters of

120 ± 10 nm.

Although different electrolyte conditions led to different nanotube dimensions, the voltage

plays a critical part in altering nanotube geometry. Generally, a higher applied voltage should give

a larger TNT diameter, but, in case of anodisation with traditional electrolyte at 120 V, a localised

breakdown of the oxide layer occurred due to sharp and continuous increase in current density

(**Figure 3.8e**).

In contrast, under the LA electrolyte shown in **Figure 3.8f**, current density dips after a few

minutes. This avoids the avalanche breakdown/burning of the sample, giving a thicker sample in

less time. Furthermore, under the LA conditions, the value of final current density is always lower

than under the traditional electrolyte conditions. Thus, the future studies in this project involve the

use of LA-containing electrolyte for anodisation (at 120 V, 5 mins) to obtain robust 35 µm thick TNT layer on Ti discs.

3.4.2. Crystal structure

Titania nanotube arrays are essentially a thin-film covering the Ti substrate which is relatable to the native oxide layer generally present on the metal surface. Hence, TNT phase transformation can be directly compared to the bulk material. XRD was used to assess the crystalline structure of the TNT/Ti implant prepared by electrochemical anodisation. The unannealed amorphous Ti substrate can be transitioned into an anatase configuration by annealing at 450 °C, and to a mixed anatase-rutile crystalline phase by heating at temperature of 550 °C and above [31]. In this study, the annealing of Ti disc in oxygen ambient at 450 °C pre-anodisation led to formation of vertically aligned nanotubes with anatase phase instead of an amorphous structure. This is in agreement with previous studies [32].
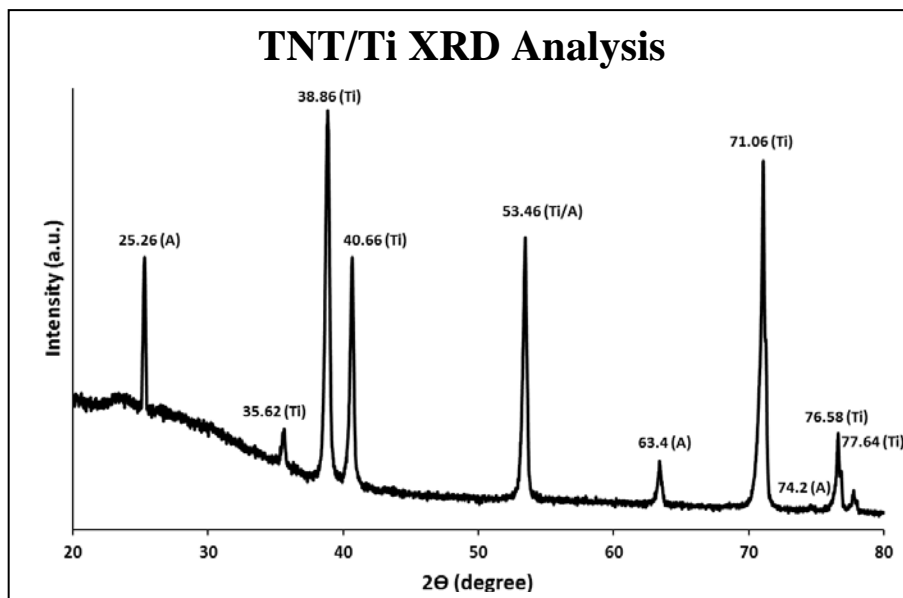
Figure 3.9. The XRD pattern of annealed TNT/Ti implant in the range of 20-80 °.

The XRD analysis of annealed TNTs can be seen in the **Figure 3.9**. The plot clearly shows a peak at 25.26° corresponding to anatase phase of titanium oxide. The other low intensity peaks at 38.0°, 53.40°, 63.4° and 74.2° also correspond to anatase structure, but are dwarfed or overlapped by the high intensity peaks at 38.8°, 40.6°, 53.4°, 71.5°, 76.6° and 77.6° form underlying Ti substrate [33, 34]. Inducing crystallinity to the TNTs alters their mechanical properties and subsequently their biological response to various bodily fluids and tissues.

3.4.3. Polymer surface coating

The TNT surfaces were coated with different polymers in order to improve its chemical and biological properties. Both chitosan and Pluronic-F127 are biodegradable polymers with low toxicity, high biocompatibility with cells and body fluids and weak immunogenic properties which makes them ideal for tissue engineering and drug delivery applications [35, 36]. These polymers were coated on to non-loaded TNT/Ti implants and characterised before being adopted for protein release and biofunctionlity studies *in vitro*, *ex vivo* and *in vivo*. Chitosan n(1-4,2-amino-2-deoxy-β-D-glucan) has a structure similar to hyaluronic acid, which is abundant in the ECM which makes the implant integration easier [37, 38].

    Figure 3.10 shows polymeric layers of chitosan of variable thickness, spin coated onto the TNT/Ti implants. SEM micrographs of the cross-section and top view (**Figure 3.10a-b**) of a polymer layer generated by 25 µl solution of 1% chitosan (1%-1cy) rendered a layer ~114 nm thin. Similarly, a 50 µl- 1% solution (1%-2cy) spin coated on the TNT surface gave an average thickness of 400 nm (**Figure 3.10c-d**). To produce a thicker layer as described for chitosan deposition by dip-coating [17], the solution concentration was increased to 2% (50 µl) (2%-2cy), to obtain a surface coating ~1 µm thick, evenly covering the nanopores (**Figure 3.10e-f**). These images are

colour-processed to discreetly highlight the ultra-thin film biopolymer coatings on the surface of TNT/Ti implant.
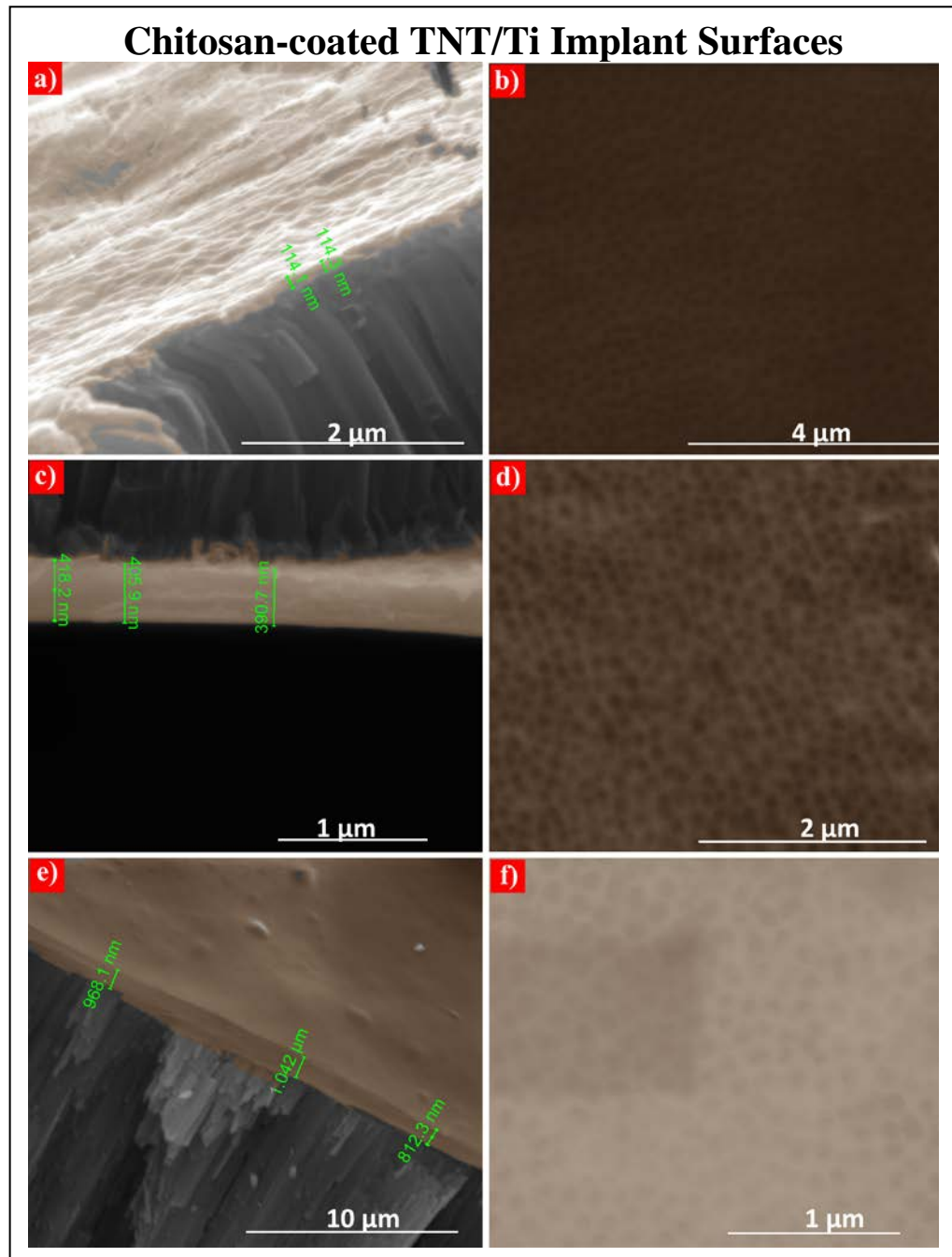
Figure 3.10. SEM images of chitosan thin film coated on the top of the TNT surface. The cross-sectional and corresponding top view of (a, b) 1%-25 µl (1%-1cy), (c, d) 1%-50 µl (1%-2cy) and

(e, f) 2%-50 µl (2%-2cy) spin-coated chitosan solutions (cy denotes the number of cycles of spin-coating).

Pluronic-F127 is a synthetic thermoreversible hydrogel comprising of amphiphilic copolymers consisting of units of polyethylene oxide (PEO) and polypropylene oxide (PPO). Modification of implant surface with Pluronic-F127 is an effective method to resist protein adsorption and bacterial adhesion [39, 40]. Corresponding cross-sectional and top-view image for the Pluronic-F127 coated on TNTs is presented in **Figure 3.11a-b** which helped determine the thickness of the polymeric film. The concentrated 20%-50 µl Pluronic-F127 solution produced a ~1 µm thick coating with micro- and nano-rough surface.
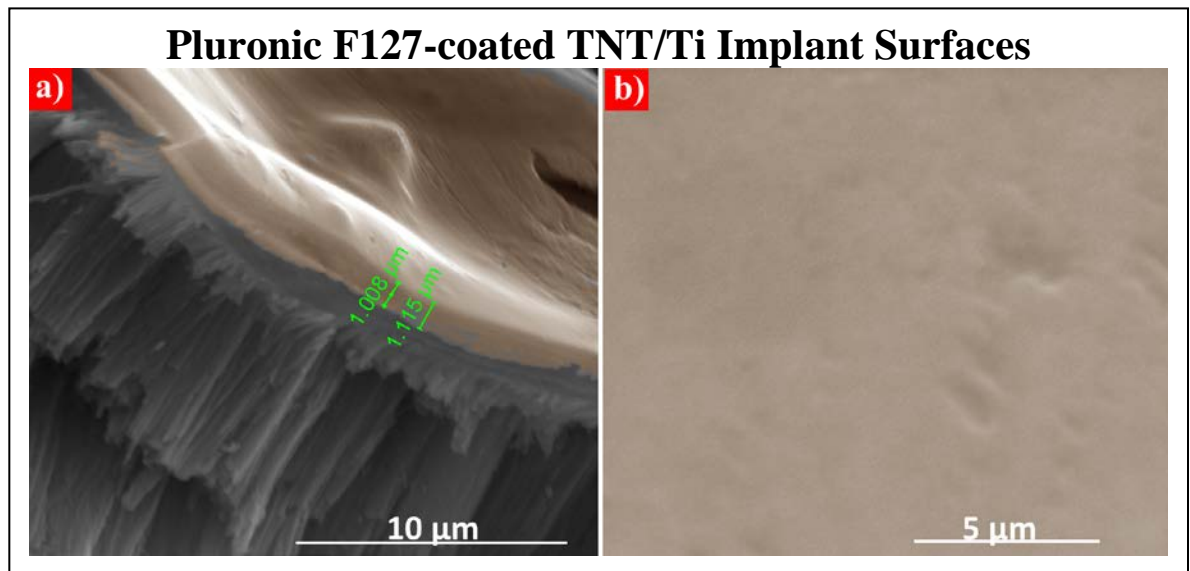
Figure 3.11. SEM images of Pluronic-F127 film coated on the top of the TNT surface. (a) Cross-sectional image and (b) Top view.

3.4.4. Surface wettability

The surface wettability (hydrophilicity/hydrophobicity) is crucial in determining the biological response to the implanted biomaterials. It affects the protein adsorption, platelet adhesion/activation and cell adhesion [14]. TNT/Ti implant surface wettability was therefore assessed by measuring the water contact angles (WCAs). High contact angles ($> 90^o$) are associated with hydrophobic surfaces with low surface energy and decreased water-material interaction. Whilst an increased surface energy and water-material interaction with low WCAs correlates to hydrophilic surfaces.

Table 3.1 summarises the WCAs for all the TNT/Ti implant surfaces used in this study. The pure titanium disc (before annealing) had a high WCA of $\sim95^o$ while after annealing the contact angle of Ti decreased to $\sim62^o$. The resulting images recorded from the video are shown in **Figure 3.12a-b**. There was minimal change in WCA by the end of the measurement. The anodised TNTs had a highly hydrophilic surface with initial WCA as 4° which decreased to a zero within a few seconds. **Figure 3.12c-d** shows a decrease in droplet height and contact angle with time (t=0 and t=f for initial and final measurement, respectively).

Sample	Contact Angle (^{o})
Ti unannealed	95.4±0.9
Ti annealed	61.7±1.0
TNT	4.0±0.6
TNT-CH	30.7±1.5
TNT-F127	31.4±3.5

Table 3.1. Average water contact angle (WCA) measurements for Ti and different TNT substrates.
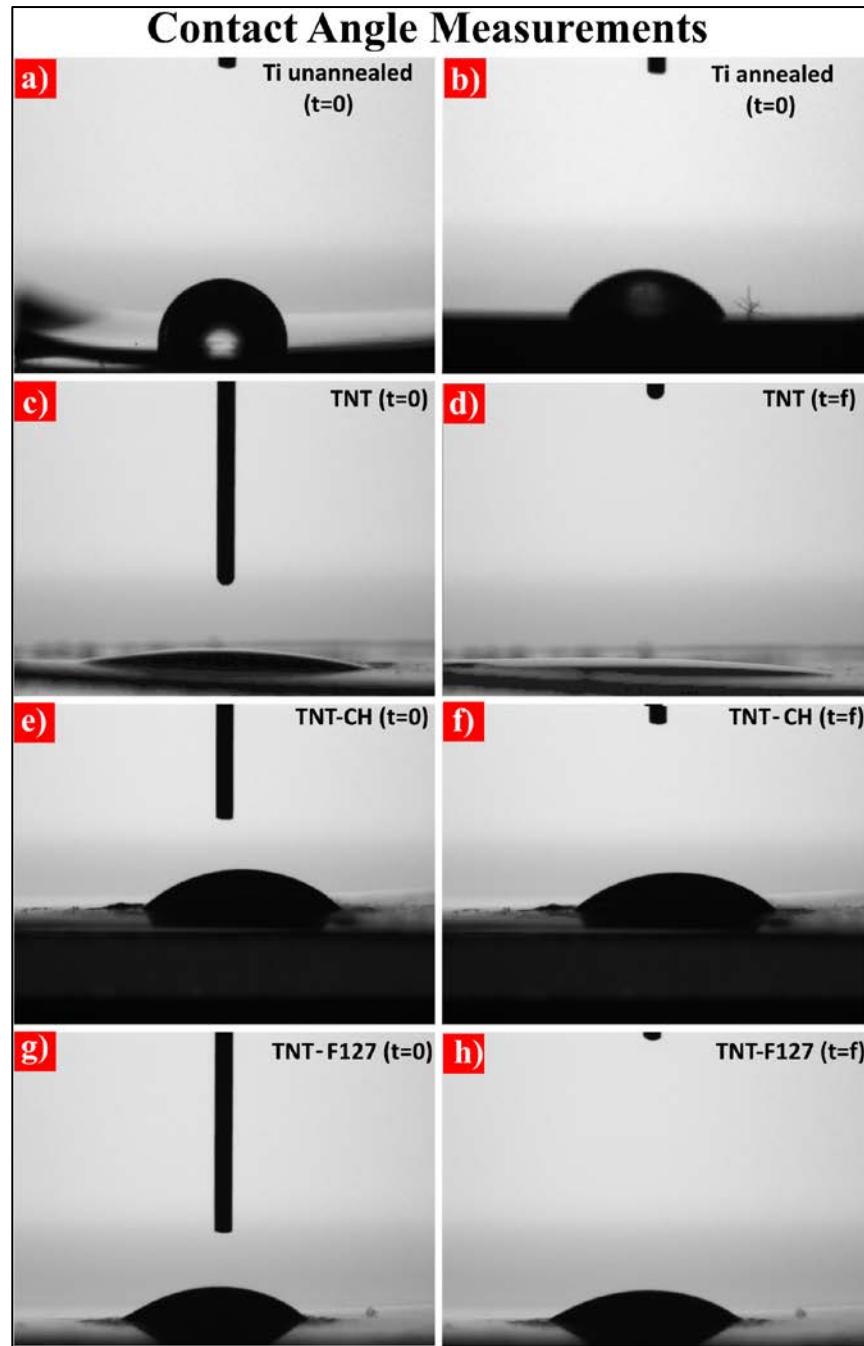
Figure 3.12. The contact angle (WCA) slides from the video for different implant surfaces. (Initial-WCA t=0 and final- WCA t=f at the end of the measurement).

The polymer surface modification by chitosan showed a drastic decline in contact angle ranging from 33º (at t=0) to 20º (at t=f) when compared to control Ti disc. This WCA with an

average of ~32º was still higher than uncoated TNT owing to the increment in carbon content. Similarly, the Pluronic-F127 modification gave a maximum (at t=0) and minimum (at t=f) CA of 38º and 23º approximately, averaging out to 31º. It was assumed that the large PPO chains deliver the slightly hydrophobic nature while PEO chains on both ends of the block copolymer contribute towards the hydrophilicity. The implant wettability is a considerable factor for its success and tissue integration.

3.5. Conclusions

This chapter demonstrates successful fabrication (by electrochemical anodisation) of TNT/Ti cranial implants to be used as an adjunctive molecular therapy for craniosynostosis treatment. An ultrasonic milling technique generated smooth-edged, 3 mm Ti discs which acted as the substrate for growing TNTs. Two different electrolytes (traditional ethylene glycol and lactic-acid (LA) containing ethylene glycol) were explored. The SEM results revealed that the LA containing electrolyte (at 120 V, 5 min, 60 ºC) led to ultrafast fabrication of large diameter, mechanically stable nanotubular implants (when compared to traditional electrolyte) and prevented the localised dielectric oxide breakdown at elevated voltages. This optimised method for generating TNTs with 120 ± 10 nm diameter and 35 µm thickness has been applied throughout the subsequent chapters of this thesis. The TNTs had an anatase crystalline structure, post-annealing, as analysed by X-ray diffraction. Furthermore, the TNT surfaces were successfully coated using biopolymers (chitosan and Pluronic-F127) to modulate the surface chemistry and control the subsequent protein release. Polymeric layers with varied thickness (100 nm to 1 µm) were produced consistently on the TNT surfaces. Their water contact angles were 30.71 ± 1.51º for TNT-CH and 31.36 ± 3.5º for TNT-F127 when compared with 4 ± 0.6º for uncoated TNTs. These results will assist in analysis and

interpretation of the implant interactions in cell culture and *in vivo* applications. The succeeding chapter optimises the *in vitro* release ability of TNT/Ti implants (polymer-coated and uncoated) for sustained delivery of bone inhibiting proteins (glypicans).

3.6. References

1.   Liu, X., Chu, P.K., and Ding, C. Surface modification of titanium, titanium alloys, and related materials for biomedical applications. *Materials Science and Engineering: R: Reports*, **2004**. 47, 49-121.

2.   Moioli, E.K., Clark, P.A., Xin, X., Lal, S., and Mao, J.J. Matrices and scaffolds for drug delivery in dental, oral and craniofacial tissue engineering. *Advanced Drug Delivery Reviews*, **2007**. 59, 308-24.

3.   Mendonça, G., Mendonça, D.B., Aragao, F.J., and Cooper, L.F. Advancing dental implant surface technology–from micron-to nanotopography. *Biomaterials*, **2008**. 29, 3822-35.

4.   Naidu, S.H., Kulkarni, N., and Saunders, M. Titanium basal joint arthroplasty: a finite element analysis and clinical study. *The Journal of Hand Surgery*, **2006**. 31, 760-65.

5.   Wang, K. The use of titanium for medical applications in the USA. *Materials Science and Engineering: A*, **1996**. 213, 134-37.

6.   Blake, G., MacFarlane, M., and Hinton, J. Titanium in reconstructive surgery of the skull and face. *British Journal of Plastic Surgery*, **1990**. 43, 528-35.

7.   Bishop, J.A., Palanca, A.A., Bellino, M.J., and Lowenberg, D.W. Assessment of compromised fracture healing. *Journal of the American Academy of Orthopaedic Surgeons*, **2012**. 20, 273-82.

8.   Darouiche, R.O. Treatment of infections associated with surgical implants. *New England Journal of Medicine*, **2004**. 350, 1422-29.

9.   Kurtz, S., Ong, K., Lau, E., Mowat, F., and Halpern, M. Projections of primary and revision hip and knee arthroplasty in the United States from 2005 to 2030. *The Journal of Bone & Joint Surgery American Volume*, **2007**. 89, 780-85.

10.   Landgraeber, S., Jäger, M., Jacobs, J.J., and Hallab, N.J. The pathology of orthopedic implant failure is mediated by innate immune system cytokines. *Mediators of Inflammation*, **2014**. 2014, 185150.

11.   Zhang, L. and Webster, T.J. Nanotechnology and nanomaterials: promises for improved tissue regeneration. *Nano Today*, **2009**. 4, 66-80.

12.   Losic, D. and Simovic, S. Self-ordered nanopore and nanotube platforms for drug delivery applications. *Expert Opinion on Drug Delivery*, **2009**. 6, 1363-81.

13.   Kumeria, T., Mon, H., Aw, M.S., Gulati, K., Santos, A., Griesser, H.J., and Losic, D. Advanced biopolymer-coated drug-releasing titania nanotubes (TNTs) implants with simultaneously enhanced osteoblast adhesion and antibacterial properties. *Colloids and Surfaces B: Biointerfaces*, **2015**. 130, 255-63.

14.   Macak, J., Tsuchiya, H., Ghicov, A., Yasuda, K., Hahn, R., Bauer, S., and Schmuki, P. TiO 2 nanotubes: self-organized electrochemical formation, properties and applications. *Current Opinion in Solid State and Materials Science*, **2007**. 11, 3-18.

15.   Sreekantan, S., Wei, L.C., and Lockman, Z. Extremely fast growth rate of TiO_2 nanotube arrays in electrochemical bath containing H_2O_2. *Journal of the Electrochemical Society*, **2011**. 158, 397-402.

16.   Losic, D., Aw, M.S., Santos, A., Gulati, K., and Bariana, M. Titania nanotube arrays for local drug delivery: recent advances and perspectives. *Expert Opinion on Drug Delivery*, **2015**. 12, 103-27.

17.   Gulati, K., Ramakrishnan, S., Aw, M.S., Atkins, G.J., Findlay, D.M., and Losic, D. Biocompatible polymer coating of titania nanotube arrays for improved drug elution and osteoblast adhesion. *Acta Biomaterialia*, **2012**. 8, 449-56.

18.   Popat, K.C., Eltgroth, M., LaTempa, T.J., Grimes, C.A., and Desai, T.A. Titania Nanotubes: A Novel Platform for Drug-Eluting Coatings for Medical Implants? *Small*, **2007**. 3, 1878-81.

19.   Roy, P., Berger, S., and Schmuki, P. TiO_2 nanotubes: synthesis and applications. *Angewandte Chemie International Edition*, **2011**. 50, 2904-39.

20.   Haring, A., Morris, A., and Hu, M. Controlling morphological parameters of anodized titania nanotubes for optimized solar energy applications. *Materials*, **2012**. 5, 1890-909.

21.   Zhu, W., Liu, X., Liu, H., Tong, D., Yang, J., and Peng, J. An efficient approach to control the morphology and the adhesion properties of anodized TiO_2 nanotube arrays for improved photoconversion efficiency. *Electrochimica Acta*, **2011**. 56, 2618-26.

22.   Jarosz, M., Pawlik, A., Kapusta-Kołodziej, J., Jaskuła, M., and Sulka, G.D. Effect of the previous usage of electrolyte on growth of anodic titanium dioxide (ATO) in a glycerol-based electrolyte. *Electrochimica Acta*, **2014**. 136, 412-21.

23.   Gulati, K., Santos, A., Findlay, D., and Losic, D. Optimizing Anodization Conditions for the Growth of Titania Nanotubes on Curved Surfaces. *The Journal of Physical Chemistry C*, **2015**. 119, 16033-45.

24.   So, S., Lee, K., and Schmuki, P. Ultrafast growth of highly ordered anodic TiO_2 nanotubes in lactic acid electrolytes. *Journal of the American Chemical Society*, **2012**. 134, 11316-8.

25.   Yin, H., Liu, H., and Shen, W. The large diameter and fast growth of self-organized TiO_2 nanotube arrays achieved via electrochemical anodization. *Nanotechnology*, **2010**. 21, 035601.

26.   Gulati, K., Aw, M.S., Findlay, D., and Losic, D. Local drug delivery to the bone by drug-releasing implants: perspectives of nano-engineered titania nanotube arrays. *Therapeutic Delivery*, **2012**. 3, 857-73.

27.   Aw, M.S., Kurian, M., and Losic, D. Non-eroding drug-releasing implants with ordered nanoporous and nanotubular structures: concepts for controlling drug release. *Biomaterials Science*, **2014**. 2, 10-34.

28.   Paulose, M., Peng, L., Popat, K.C., Varghese, O.K., LaTempa, T.J., Bao, N., Desai, T.A., and Grimes, C.A. Fabrication of mechanically robust, large area, polycrystalline nanotubular/porous TiO_2 membranes. *Journal of Membrane Science*, **2008**. 319, 199-205.

29.   Vasilev, K., Poh, Z., Kant, K., Chan, J., Michelmore, A., and Losic, D. Tailoring the surface functionalities of titania nanotube arrays. *Biomaterials*, **2010**. 31, 532-40.

30.   Paulose, M., Prakasam, H.E., Varghese, O.K., Peng, L., Popat, K.C., Mor, G.K., Desai, T.A., and Grimes, C.A. TiO_2 nanotube arrays of 1000 µm length by anodization of titanium foil: phenol red diffusion. *The Journal of Physical Chemistry C*, **2007**. 111, 14992-97.

31.   Varghese, O.K., Gong, D., Paulose, M., Grimes, C.A., and Dickey, E.C. Crystallization and high-temperature structural stability of titanium oxide nanotube arrays. *Journal of Materials Research*, **2003**. 18, 156-65.

32.   Park, J., Bauer, S., Schmuki, P., and von der Mark, K. Narrow window in nanoscale dependent activation of endothelial cell growth and differentiation on TiO_2 nanotube surfaces. *Nano Letters*, **2009**. 9, 3157-64.

33.   Su, Z., Zhang, L., Jiang, F., and Hong, M. Formation of crystalline TiO_2 by anodic oxidation of titanium. *Progress in Natural Science: Materials International*, **2013**. 23, 294-301.

34.   He, J., Zhou, W., Zhou, X., Zhong, X., Zhang, X., Wan, P., Zhu, B., and Chen, W. The anatase phase of nanotopography titania plays an important role on osteoblast cell morphology and proliferation. *Journal of Materials Science: Materials in Medicine*, **2008**. 19, 3465-72.

35.   Almeida, H., Amaral, M.H., Lobão, P., and Lobo, J.M.S. Pluronic® F-127 and pluronic lecithin organogel (PLO): main features and their applications in topical and transdermal administration of drugs. *Journal of Pharmacy and Pharmaceutical Sciences*, **2012**. 15, 592-605.

36.   Kung, S., Devlin, H., Fu, E., Ho, K.Y., Liang, S.Y., and Hsieh, Y.D. The osteoinductive effect of chitosan–collagen composites around pure titanium implant surfaces in rats. *Journal of Periodontal Research*, **2011**. 46, 126-33.

37.   Balasundaram, G. and Webster, T.J. An Overview of Nano-Polymers for Orthopedic Applications. *Macromolecular Bioscience*, **2007**. 7, 635-42.

38.   Bumgardner, J.D., Wiser, R., Gerard, P.D., Bergin, P., Chestnutt, B., Marini, M., Ramsey, V., Elder, S.H., and Gilbert, J.A. Chitosan: potential use as a bioactive coating for orthopaedic and craniofacial/dental implants. *Journal of Biomaterials Science, Polymer Edition*, **2003**. 14, 423-38.

39.   Escobar-Chávez, J.J., López-Cervantes, M., Naik, A., Kalia, Y., Quintanar-Guerrero, D., and Ganem-Quintanar, A. Applications of thermo-reversible pluronic F-127 gels in pharmaceutical formulations. *Journal of Pharmacy & Pharmaceutical Sciences*, **2006**. 9, 339-58.

40.   Diniz, I.M., Chen, C., Xu, X., Ansari, S., Zadeh, H.H., Marques, M.M., Shi, S., and Moshaverinia, A. Pluronic F-127 hydrogel as a promising scaffold for encapsulation of dental-derived mesenchymal stem cells. *Journal of Materials Science: Materials in Medicine*, **2015**. 26, 1-10.

CHAPTER 4

IN VITRO PROTEIN RELEASE STUDIES

FROM TNT/Ti IMPLANTS

CHAPTER 4: *In vitro* Protein Release Studies from TNT/Ti Implants

4.1. Introduction

The previous chapter has shown a simple and effective approach to fabricate TNT/Ti cranial implants. This chapter explores their feasibility *in vitro* as local therapeutic releasing systems for adjunctive surgical treatment in craniosynostosis management. The outcomes of high-risk cranial reconstruction surgery can be improved by developing an adjunctive molecular therapy involving localised and controlled delivery of bone antagonising proteins to delay/alter bone re-ossification [1-3]. Protein-delivery systems based on synthetic polymers (hydrogels and microspheres), collagenous materials and bulk titanium-fibre mesh have earlier been tested in animal models to inhibit bone re-formation at the craniectomy site [2, 4, 5]. Nonetheless, they lack therapeutic efficacy due to undesired pharmacokinetics and uncontrolled release patterns and adversely induced osteogenesis in some cases [4, 6, 7].

TNT-based platforms have been recognised as one of the most promising nanomaterials to overcome the limitations of conventional therapeutic-delivery systems [8]. Apart from intrinsic material properties such as high surface area, low immunogenicity, excellent chemical inertness and mechanical strength, TNTs have an ability to control and localise the release of active therapeutics over an affected site (mostly in bone-related pathologies *e.g.* inflammation, infection, cancer *etc*.) [8-11]. TNTs act as nanoreservoirs that can accommodate substantial amounts of bioactive agents and modulate their release over an extended duration [10, 12]. Previous studies have established the local drug delivering ability of TNTs with tailorable release patterns,

depending on the therapeutic requirements (refer to Chapter 2, Section 2.4.5, p.50-55). These included the slow and extended release of drugs, proteins, genes, RNAs *etc*., stimulated drug release using external sources (RF, magnetic field, ultrasound) and sequential release of multiple drugs and carriers for complex conditions [13-18]. Furthermore, the release characteristics have been modified by tailoring the nanotube dimensions (dependent on anodisation parameters) and surface chemistry [9, 11, 12]. The drug release mechanism from TNT arrays is elucidated by a diffusion-mediated process, thus the fabricated 120 ± 10 nm diameter TNTs alone cannot restrict/hinder the release of nanometeric protein molecules [11, 13]. However, incorporating a biopolymer coating onto the TNT surface has proven to be effective in improving the drug diffusion, wherein the polymer thickness, chemical properties and degradability modulate the release kinetics [9, 13, 19]. It was previously demonstrated that this strategy can avoid the initial uncontrolled release of active agents, thus providing proper kinetics and extended release of the molecules from the nanotubes, maximising their therapeutic effects [20, 21]. A slow and sustained release over a long duration (over several weeks) with zero-order kinetics is ideal for designing advanced implantable delivery systems [22, 23].

The TNT/Ti delivery system is a promising tool to control the protein release dynamics whilst protecting the loaded sensitive molecules against protein unfolding, deactivation or precipitation [11, 12, 24]. Proteins are generally high molecular weight, hydrophilic macromolecules with intrinsic physical and chemical lability/instability in most conditions, which makes them difficult to administer than conventional low molecular weight robust drugs [25]. This chapter optimises the delivery performance of TNT/Ti implants for controlled release of two types of proteins, Fluorescein isothiocyanate-labelled Bovine Serum Albumin (FITC-BSA) and Glypicans (GPC1 and GPC3). FITC-BSA formed an ideal control because it a widely used protein that does not cause

any immunogenic response or therapeutic action *in vivo* [26]. Moreover, the fluorescent labelling aids towards easy and sensitive quantification and analysis of the released BSA [27]. On the other hand, Glypicans (heparan sulfate proteoglycans) can have an inhibitory (bone antagonising) effect on the BMP2 bioactivity. Thus, a controlled delivery of GPC1/GPC3 form proposed TNT-based implants is likely to prevent BMP2-mediated bone formation and hence sutural fusion [28, 29].

The main focus of this chapter was to evaluate the *in vitro* release characteristics of the model proteins from the nano-engineered Ti implants, before adapting the system for murine studies. The specific aims of this study were (i) to measure the physical characteristics (hydrodynamic diameter and charge) of model proteins, (ii) to establish the release characteristics of control protein by exploring the effects of loading techniques (in vacuum or air) and different biopolymer coatings and (iii) to establish release profiles for GPC1 and GPC3 entrapped within polymer-coated and uncoated TNTs at room temperature and 37 °C, and mathematically model their kinetics.

It is important to assess the physiochemical properties of the model proteins since they influence the diffusion process and overall release pharmacokinetics. A stable hydrodynamic diameter in physiological buffer (as excipient) would affirm their structural integrity and monodispersity (minimal aggregation) and render them as suitable candidates for prolonged release applications [30, 31]. Moreover, a better loading would lead to higher encapsulation and retention of proteins and possibly prolonged release periods and improved shelf-life [30, 31]. The concept of biopolymer coating over the TNTs that further improves the overall release efficiency is depicted in **Figure 4.1**. After optimising the release parameters, this approach was extended to study the release and pharmacokinetic properties of glypicans loaded within the nanotubes at room and physiological temperatures (to simulate *in vivo* release conditions). If successful, this *in vitro*

delivery system can provide opportunities for an *in vivo* preclinical investigation in a murine model to prevent cranial bone growth.
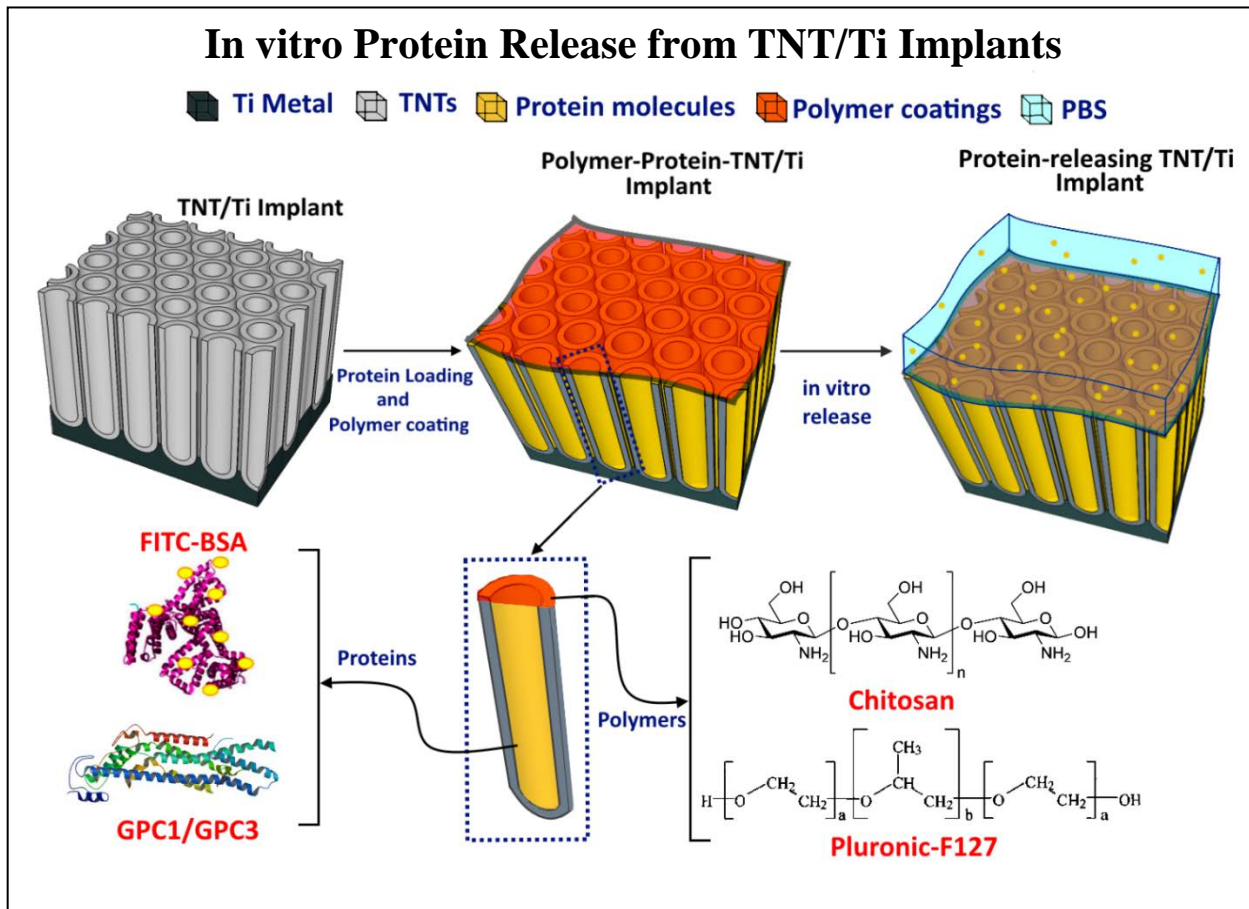
Figure 4.1. Scheme of local protein delivery system, consisting of TNT/Ti implants coated with biopolymer to achieve an extended release. The lower part shows the core structure of model proteins and the chemical structures of the two biopolymers used for coating the implant surface.

4.2. Experimental section

4.2.1. Materials and chemicals

High purity titanium foil (99.6% of Ti) with a thickness of 0.20 mm, supplied by Nilaco (Japan), was used as a substrate for the fabrication of the implants. The chemicals for electrolyte preparation and polymer surface coatings as well as analytical grade reagents have been previously listed (Chapter 3, Section 3.2.1, p.88). The model proteins, recombinant human glypicans (GPC3 and GPC1) were obtained from R&D systems (USA) and FITC-Labelled Bovine serum albumin (BSA) (control protein) was supplied by Sigma–Aldrich (Australia). The 10X phosphate buffered saline (PBS) at pH 7.4 from HyClone, Fisher Scientific (USA) was used to reconstitute the model proteins at 100 µg/ml. High-purity Milli-Q water was utilised throughout this study for dilutions and washing.

4.2.2. Fabrication/characterisation of TNT/Ti implants

TNT/Ti implants were prepared by simple two-step electrochemical anodisation of titanium foil in lactic acid containing organic electrolyte (as described in Chapter 3 Section 3.2.3, p. 91), whilst the detailed specifics of this work are described in the upcoming sub-sections. However, the surface and morphological characterisation of the prepared TNT/Ti implants has briefly been restated in this Chapter.

4.2.3. Protein size measurements

The average hydrodynamic diameter and zeta potential of the model and control proteins before loading were determined by laser light scattering using a monochromatic laser ray diffusion counter, Zetasizer Nano ZS at 25 °C and analysed using Dispersion Technology Software (Malvern Instruments Ltd., UK). A He-Ne laser beam, with the angle of measurement set as 90°, was used to carry out size measurements before and after analysing the zeta potential to equilibrate the samples and check for protein agglomeration.

A diffusion barrier technique was used to isolate a small protein volume from the electrodes that generally denature the protein samples. Briefly, the folded capillary cell was filled with 700 µl of PBS (pH 7.4) and put into the Zetasizer for 2-3 minutes to allow the temperature to equilibrate. The cell was then removed and 50 µl of the protein sample was pipetted directly into the bottom of the cell (*i.e.* U- bend where the mobility measurement is made) using a gel loading tip. After the sample was loaded, the size and zeta potential measurements were collected using standard methods. ExPASy bioinformatics resource portal (ProtParam) provided access to scientific databases and software tools to confirm the protein characteristics.

4.2.4. Protein loading and surface coating

The TNT/Ti discs were employed as nanoreservoirs and loaded with the model proteins via a simple lyophilisation method [32]. The discs were rinsed with water and ethanol to facilitate the penetration of the loading solution and allowed to air dry. The FITC-Labelled BSA was tested for different loading concentrations and techniques (vacuum-drying and air-drying). Briefly, a 10 µl concentrated solution of FITC-Labelled BSA (100 µg/ml in sterile PBS) was pipetted onto each

surface and gently spread to ensure even coverage. Half of the samples were allowed to dry for 2 h under vacuum (created using a vacuum pump attached to a desiccator to obtain high pressure-low vacuum conditions for solvent evaporation) and the other half in the air at room temperature. The loading procedure was repeated on the dried samples until an appropriate amount of protein was present inside the TNT pores. These samples were denoted as TNT/BSA and loaded with a test amount of 5 µg and 10 µg to check the release. The BSA-loaded implant surfaces were then spin-coated with Chitosan (1-2%) and Pluronic-F127 (20%) polymeric solutions at varied concentrations to obtain different thickness of layers on the TNT surfaces to prolong the release. The details of polymeric surface coating were described in in Chapter 3 (Section 3.2.4, p.92)

The TNT/Ti implants were filled with GPC1 and GPC3 using vacuum drying technique (based on better loading efficiency obtained by preliminary control FITC-BSA study). A test amount of 5 µg/sample (10 µl drop of 100 µg/ml GPCs in sterile PBS repeated 5 times) was optimised for all *in vitro* glypican release studies. These loading amounts were selected on the basis of previous cell and animal studies, suggesting that a few nanograms of bone antagonising proteins can have profound inhibitory effects on the BMP2 pathway [33-35]. Then, the implants were gently wiped to remove any surface accumulated protein and coated with a 2%-50 µl of chitosan solution. All experiments were performed in triplicates.

4.2.5. Protein quantification and release studies

To characterise the *in vitro* release profile, the protein-loaded TNT/Ti samples were immersed in 500 µl of PBS at room temperature in capped eppendorf tubes. The amount of eluted protein was measured periodically at various time points (for up to a month) by removing 200 µl of the aliquot, replacing it with fresh PBS each time (to maintain the sink conditions) and analysing it by using a

photoluminescence spectrophotometer (Fluoromax 4, Horiba Jobin Yvon- Edison, USA). The FITC-Labelled BSA released from the TNTs was analysed directly, wherein intensities of fluorescent peaks (emission wavelength- λ_{em}= 516 nm and excitation wavelength- λ_{ex} = 435 nm) were converted to corresponding concentrations by using a calibration curve.

To measure the amount of released glypicans (GPCs), a FluoroProfile® Protein Quantification Kit (from Sigma–Aldrich, USA) was used to label the proteins and to obtain a fluorescent signal. This involved preparation of a working reagent from the kit by mixing water/sample buffer, Flouroprofile fluorescent reagent and quantification buffer in an 8:1:1 ratio. Equal volumes (100 μl) of working reagent and the released aliquot from the TNTs were mixed together and incubated for at least 30 min prior to measurement of the fluorescent signal (at λ_{em}= 620 nm and λ_{ex} = 510 nm). A blank was also prepared by adding equal volumes of working reagent and buffer to subtract the background attenuation. Since the fluorescence intensity is directly proportional to protein concentration, the released protein concentrations were calculated against the standard protein (BSA from the kit) calibration curve. The glypican release was carried out at both room temperature and 37 °C (simulating the conditions in a murine model).

Prior to the initial release experiments, the quantification of proteins loaded within the TNTs was performed by ultrasonically stimulating the loaded samples in PBS overnight to induce active release. The amount of protein in the eluate was confirmed using photoluminescence spectrophotometer against the standardised calibration curve. Since the existing standard colorimetric measurements (such as BCA test) weren't sensitive enough, this technique provided a simple and quick alternative method to analyse micro to nanograms amount of loaded proteins. This was a less accurate but more viable approach when compared to standard thermogravimetric

analysis (TGA). The average of loading values was used to determine the TNT loading efficiency as follows:

$$\text{Loading Efficiency \%} = \frac{\text{Protein amount in the eluate}}{\text{Initial amount of Protein loaded}} \times 100$$

4.2.6. Error analysis

The experiments in this study were conducted in triplicate and variations in estimated data were analysed. The standard deviations associated with the experimentally measured and processed data were represented using error bars (set at 95% confidence interval of the mean) while plotting the drug release curves.

4.3. Results and discussion

4.3.1. Structural characterisation of TNT/Ti implants

Chapter 3 (Sections 3.4.1.2, p.96-98 and 3.4.3, p.102-104) show the detailed SEM micrographs of uncoated and polymer-coated TNT implant surfaces with hexagonally aligned tubular structures with lengths of ~35 µm and constant pore diameters of 120 ± 10 nm. The highly-ordered and well-defined nanotubular structures with closed bottoms are ideal nanoreservoirs for protein loading which deem these implants suitable for implantable delivery applications. It is worth mentioning that these nanotubular layers can be grown easily and reproducibly onto different medical grade Titanium implants (*i.e.* plates, screws, stents, pins, rods, mails, pines and wires) [10]. The representative morphology of the TNT/Ti implants characterised by SEM are summarised in **Figure 4.2**.
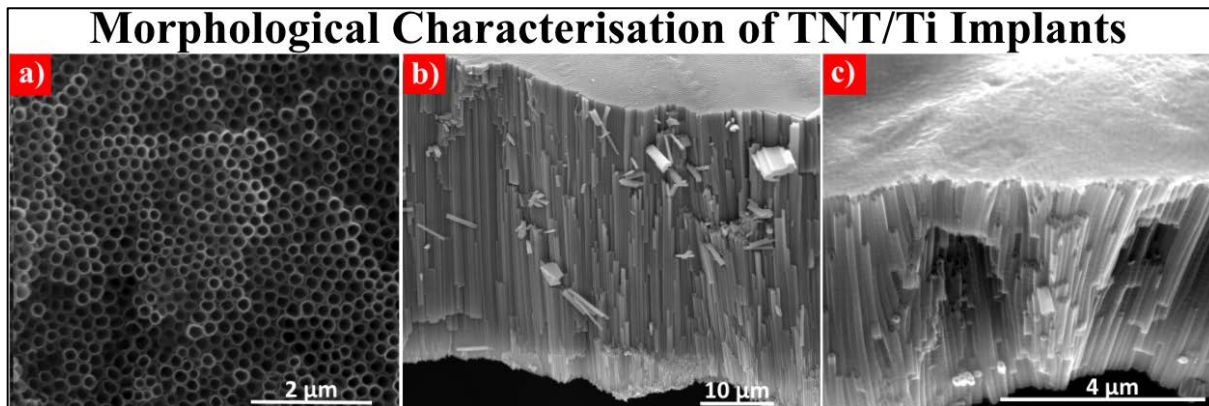
Figure 4.2. SEM images of TNT grown on Ti discs using the anodisation technique (prepared in LA electrolyte, 120 V, 5 min). (a) The top surface showing the nanotubes with consistent pore diameter (120 ± 10 nm), (b) the cross-section showing densely packed nanotube arrays along the whole length (~35 µm) and (c) the partial top and cross-sectional view of chitosan-coated TNTs showing closed pores on the top (The TNTs were scratched and broken off the substrate to obtain better images).

4.3.2. Characterisation of model proteins (Aim I)

The physical characteristics of the model proteins used in this study are outlined in **Table 4.1**. The average sizes (hydrodynamic diameter) of FITC-Labelled BSA, GPC1 and GPC3, calculated by dynamic light scattering were 7.5 ± 0.2, 8.7 ± 0.1 and 10.1 ± 0.1 nm respectively (**Figure 4.3**). The corresponding zeta potential (ζ) measurements showed negatively charged values for all three proteins with the net charges of -13.6 ± 1.6 mV (FITC-BSA) , -9.8 ± 3.6 mV (GPC1) and -12.5 ± 2.2 mV (GPC3) at pH 7.4. These values were consistent with the theoretical isoelectric points of the model proteins calculated using the ExPASy bioinformatics resource portal (ProtParam). The size measurements that were repeated after the charge determination showed no significant changes

in the protein diameters, confirming the stability and preservation of the protein structure due to the use of diffusion barrier technique.
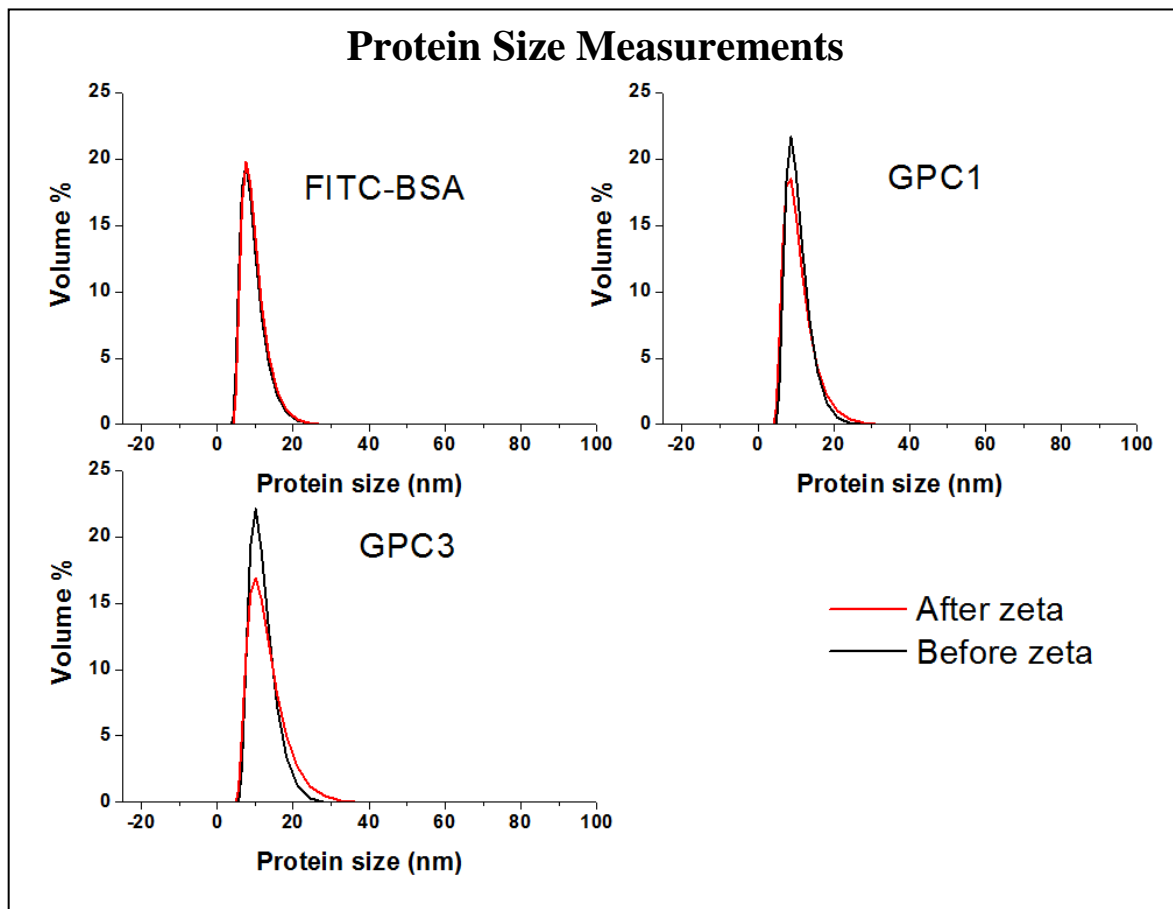
Figure 4.3. Volume distribution curve showing the size of the model proteins, FITC-Labelled BSA, GPC1 and GPC3, before and after zeta potential measurements (using diffusion barrier method) by Zetasizer Nano ZS.

Protein	Size (nm) ± SD	ζ (mV) at pH = 7.2 ± SD	Isoelectric point (pI) [a]	Molecular wt. (kDa) [b]
FITC-BSA	7.5 ± 0.2	-13.6 ± 1.6	4.7	67.0
GPC 1	8.7 ± 0.1	-9.8 ± 3.6	6.5	56.8
GPC3	10.1 ± 0.1	-12.5 ± 2.2	5.9	61.6

Table 4.1. Physical characteristics of the proteins to be loaded into TNT/Ti implants from 5 separate measurements.

a- Isoelectric point theoretically determined by the software- ExPASy bioinformatics resource portal (ProtParam).

b- Molecular weight as supplied by the manufacturer and confirmed by ProtParam.

4.3.3. *In vitro* release studies (Aims II and III)

Three different sets of experimental data for protein molecules diffusing out of TNT/Ti implants were collected and compared, evaluating the effects of: (i) loading/drying techniques, (ii) different polymer coatings on TNT surfaces for control protein (Aim II) and (iii) temperature on the release characteristics of glypicans (GPC1 and GPC3) (Aim III). The preliminary testing was performed on the control FITC-BSA protein to establish ideal parameters (loading and polymer coating thickness) for glypican release.

4.3.3.1. Influence of loading/drying method on drug release

Cumulative release profiles for the control protein (FITC-BSA) loaded into TNTs and dried under air or vacuum conditions are presented in **Figure 4.4**. The release data were divided into two phases; firstly an initial rapid elution of the molecules (burst release) for 6 h with 35-70% release, followed by a prolonged, slower elution phase (sustained release) that lasted up to 21 days, depending on the amount of the loaded protein and the drying method. This biphasic release profile is characteristic for diffusion-controlled release kinetics from nanoporous structures [10]. The high amount of instantaneous burst release indicates the elution of protein molecules from the surface layer, owing to large concentration gradient at the nanopore (120 ± 10 nm diameter)-PBS interface and weak physical containment of proteins.

A considerable difference in overall release profile of air- and vacuum-loaded FITC-BSA was observed, due to the difference in loading efficiency % in between the two methods. The vacuum drying technique for loading was more efficient (~ 90% loading efficiency) than simple air drying (based on capillary force dependent filling), showing a more gradual elution curve. This is supported by the notion that under vacuum drying, the proteins were trapped deeper inside the nanotubular channels, and therefore needed a longer time to diffuse. Nearly all curves plateaued to a receding line towards the end of the release at 4, 13, 11 and 21 days for 5 and 10 µg air- and vacuum-loaded samples, respectively. As expected, a higher loading amount led to a longer and sustained release from the nanotubes (with variable rates of elution).

Influence of Loading Method on FITC-BSA Release
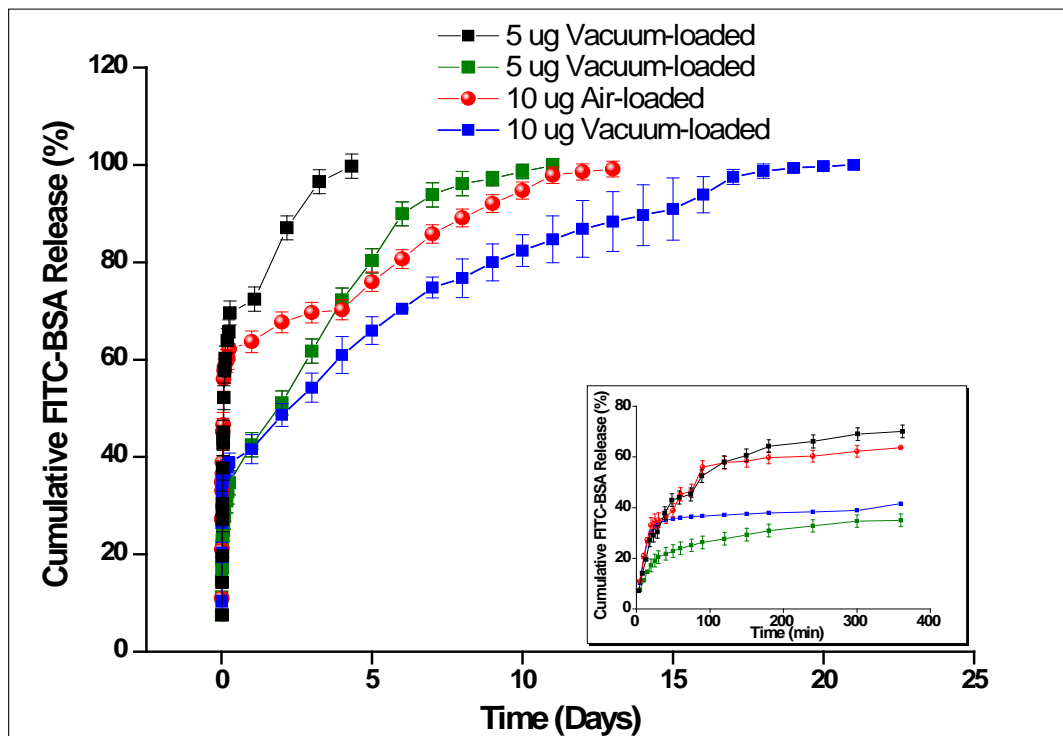
Figure 4.4. Protein release profile from TNT/Ti implants prepared in LA electrolyte (120 V, 5 min) loaded with 5 and 10 µg of FITC-BSA, dried under different loading conditions (air and vacuum). The inset depicts the rapid burst release in the first 6 h. Error bars represent mean ± SD for n = 3.

The corresponding release characteristics extracted from the release graphs in **Figure 4.4** and loading efficiencies (estimated by fluorescence spectroscopy) are listed in **Table 4.2**, to show release efficiency in terms of protein release % at various time points (1 h, 6 h, 24 h, 7 days, 14 days and 21 days). Throughout the experiments the burst release (t_B) was calculated at 6 h for all cases, while the midpoint signifying the elution of half the amount of loaded protein (t_{50}) from the TNT nanopores was recorded at less than a day for air-loaded samples and 1-3 days for vacuum-

loaded samples, respectively. Nevertheless, the vacuum loading method improved the release efficiency and extended the release period.

TNT samples	Release efficiency (%)					Release duration (h/d)			Loading Efficiency (%)
	6 h	1 d	7 d	14 d	21 d	t_B (h)	t_{50} (h/d)	t_{100} (d)	
5 µg vacuum-loaded	34.9	42.5	93.8	100.0	100	6	1.2 d	11 d	86 ± 4
10 µg vacuum-loaded	41.6	43.3	74.8	89.6	100	6	2.3 d	21 d	89 ± 3
5 µg air-loaded	69.7	72.5	100.0	100.0	100	6	1.2 h	4 d	57 ± 3
10 µg air-loaded	63.7	67.6	85.8	100.0	100	6	1.4 h	13 d	64 ± 2

Table 4.2. Release parameters of the *in vitro* studies of FITC-BSA eluted from TNTs loaded and dried under different conditions.

4.3.3.2. Influence of biopolymer surface coating

Having established an efficient loading technique to maximise the loading efficiency and to extend the protein release, the FITC-BSA loaded nanotubes were further coated with two different biopolymers of varying thickness to modulate the release characteristics. Comparative biphasic protein release profiles from TNTs with and without polymer films (Chitosan and Pluronic-F127) are presented in **Figure 4.5**. Results show that cumulative burst release (**Figure 4.5a**) in comparison with uncoated TNTs (36%) was suppressed to 15-34% when the loaded implants were

covered with polymeric films. The different thickness of the coated polymeric films have been described previously (Chapter 3, Section 3.4.3, p.102-104).

The polymer coating also significantly extended the overall protein release duration to up to 30 days for the thickest chitosan coating (**Figure 4.5b**). In this scenario, the release kinetics was not only diffusion-driven, but was also controlled by the transport of protein molecules through the polymer matrix and the rate of degradation of the polymeric film [9, 20, 36, 37].

Previously, a detailed study from our group investigated the *in situ* degradation of chitosan coating on TNT/Ti implants which led to formation of microscale tubular mesh (chitosan microtubules) upon immersion in physiological PBS buffer for up to 5 weeks [38]. This can justify the slow and favourable release kinetics and the chitosan thickness dependent extended release. Furthermore, the electrostatic attraction between the positively-charged amino groups in chitosan and the negatively charged proteins, can alter and impede the migration of the protein molecules out of the nanotubes [20, 38].

Influence of Polymer Coating on FITC-BSA Release
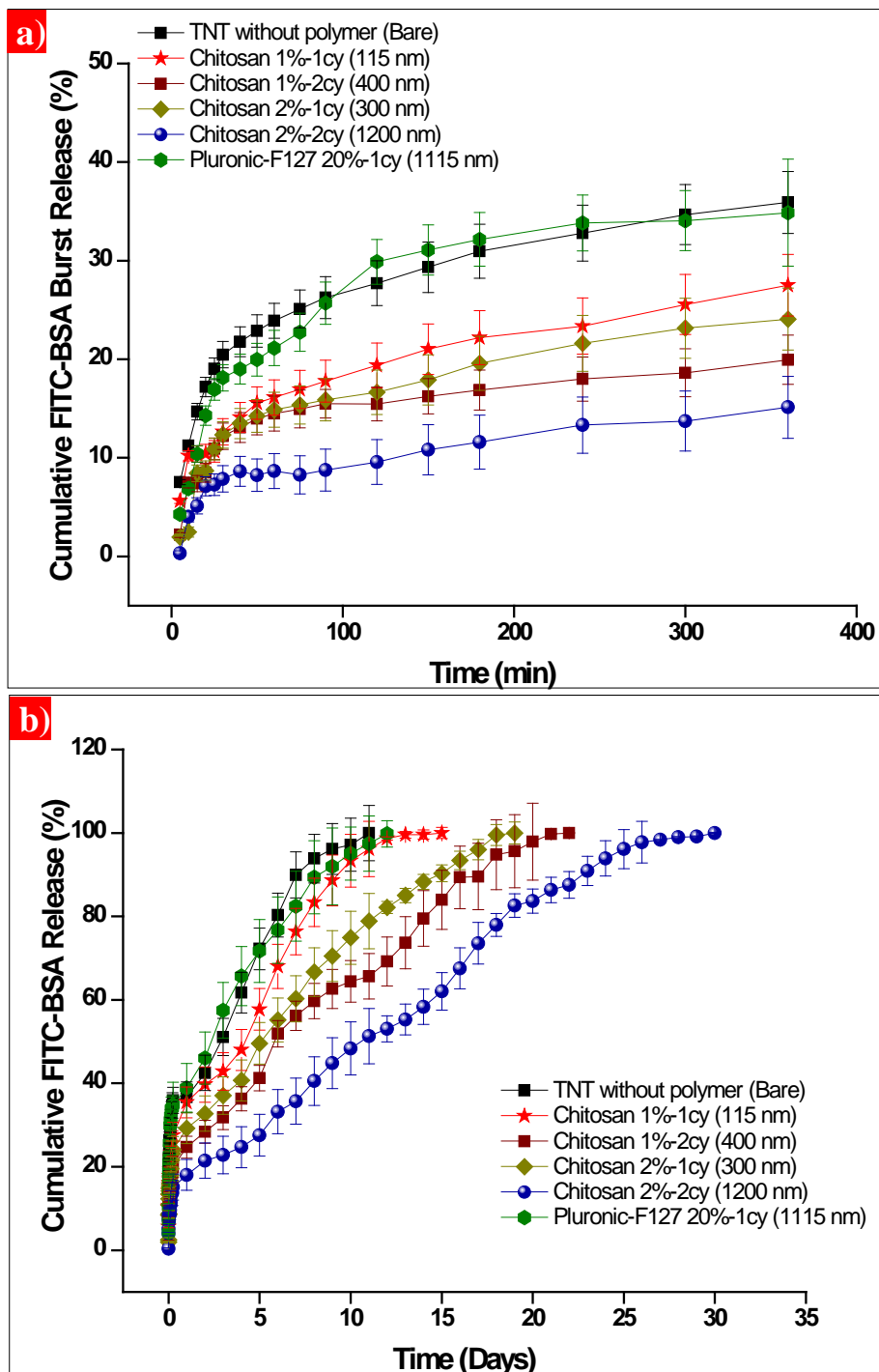
Figure 4.5. Comparative protein release graphs of control FITC-BSA from TNT/Ti implants

(prepared in LA electrolyte, 120 V, 5 min) with and without polymer-coating showing (a) the

rapid initial burst release and (b) overall sustained release. Chitosan (1200, 400, 300 and 115 nm

thick) and Pluronic-F127 (1115 nm thick) biopolymers spin coated onto the TNT/Ti surfaces, evenly covering the nanopores were tested for the release studies. Error bars represent mean ± SD for n = 3.

A thin Pluronic-F127 layer coated to cover the open ends of TNT implants was also tested for the release study, but it failed to inhibit the burst release, and the overall release lasted for 12 days (similar to uncoated TNTs). This could be attributed to the thermoreversible sol-gel behaviour of Pluronic-F127 which at temperatures higher than 23 °C, transforms into a semi-permeable gel, thus permitting the unhindered diffusion of protein molecules through it [39].

Table 4.3 summarises the release parameters of FITC-BSA from polymer-coated TNTs in comparison with the bare TNTs. A promising highlight was the substantial reduction of burst release from 35.91% of bare (uncoated) TNT to 15.1%, 19.94%, 24.04% and 27.50% for 1200, 400, 300 and 115 nm thick chitosan coating, respectively. This enormous plummet can help eliminate the initial uncontrolled release from surface of the TNT implants and fine-tune the release behaviour of polymer-coated TNTs by controlling the polymer thickness. This is particularly relevant to design therapeutic delivery systems requiring flexibility with desired release kinetics, time, and dosage for specific applications, such as short-term inflammation suppression, moderate-term antibacterial action, or long-term delivery of growth factors/inhibitors in fracture healing, bone cancer and potentially craniosynostosis [9].

TNT samples	Release efficiency (%)						Release duration (h/d)		
	6h	1 d	7 d	14 d	21 d	30 d	t_B (h)	t_{50} (h/d)	t_{100} (d)
Bare TNTs	35.9	36.7	89.9	100.0	100.0	100.0	6	2.8 d	11 d
Chitosan-coated TNTs (1%- 25 µl/1 cy)	27.5	35.4	76.4	99.6	100.0	100.0	6	4.2 d	15 d
Chitosan-coated TNTs (1%- 50 µl/2 cy)	19.9	24.7	56.2	79.5	99.7	100.0	6	5.9 d	22 d
Chitosan-coated TNTs (2%- 25 µl/1 cy)	24.0	29.2	60.2	88.3	100.0	100.0	6	5.3 d	19 d
Chitosan-coated TNTs (2%- 50 µl/2 cy)	15.1	18.0	35.7	58.3	86.3	100.0	6	10.1 d	30 d
Pluronic-F127-coated TNTs (2%- 50 µl/2 cy)	34.9	38.9	82.5	100.0	100.0	100.0	6	2.7 d	12 d

Table 4.3. Release parameters of the *in vitro* studies of FITC-BSA eluted from uncoated and polymer (Chitosan and Pluronic-F127) -coated Titania nanotubes (TNTs).

4.3.3.3 Glypican release study and influence of temperature

The size of FITC-labelled BSA (66kDa) is similar to that of glypicans that are responsible for co-regulating skull growth [40], hence this aforementioned approach can be extended for craniosynostosis therapy. The release kinetics of bone inhibiting glypicans, GPC1 and GPC3 with and without 2% chitosan coating were tested at room temperature and 37 °C (to mimic the *in vivo* environment). **Figure 4.6** highlights comparative glypican release characteristics showing the

biphasic diffusion of model proteins at room temperature. The release process lasted for 9 and 11 days for GPC1 and GPC3, with 41% and 46% of initial burst release (graph inset) from the uncoated nanotubular surfaces. Corresponding cumulative amounts of protein released in nanograms are shown on the right hand-side y-axis. This non-salient difference in the GPC1 and GPC3 release duration is due to the slightly larger hydrodynamic diameter of GPC3 which improves its retention within the nanotubes and retards its diffusion.

Glypican Release at Room Temperature
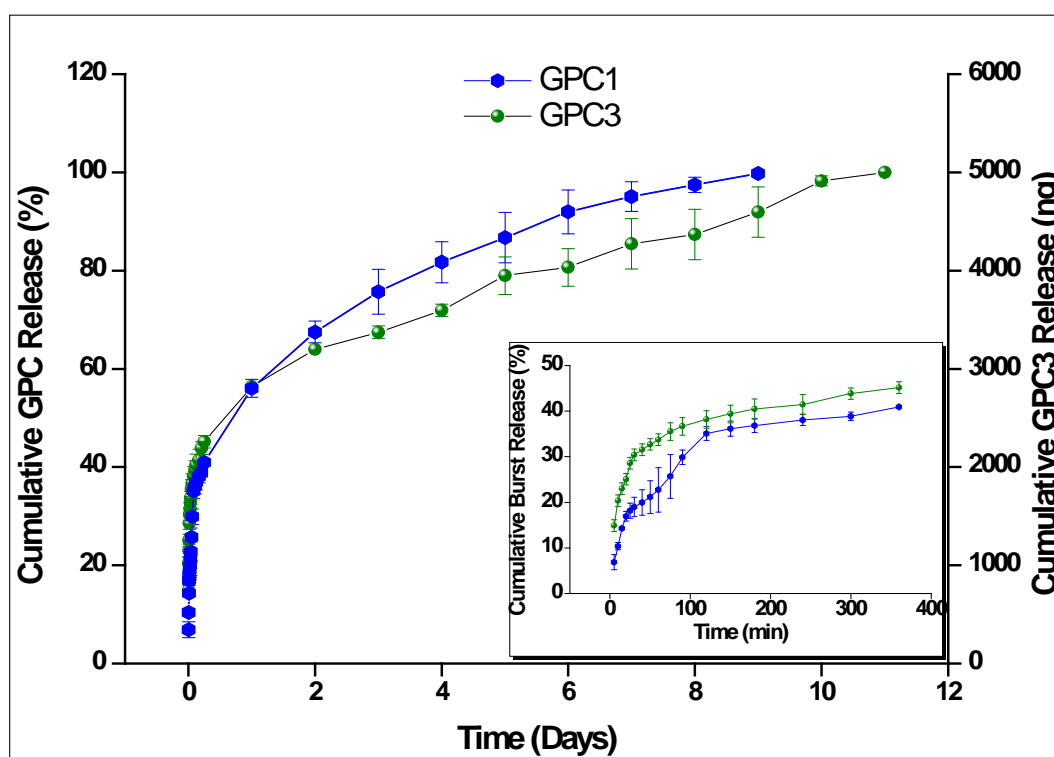
Figure 4.6. Protein release profiles from TNT/Ti implants prepared in LA electrolyte (120 V, 5 min) and loaded with 5 µg of GPC1 and GPC3 at room temperature (RT). The inset depicts the rapid burst release in the first 6 h. Error bars represent mean ± SD for n = 3.

Since 2%-2 cy chitosan-coated TNTs performed significantly better than the other coated and uncoated nanotubes, these implants were chosen for further glypican release studies. Comparative release curves of GPC1 and GPC3 loaded into TNTs with and without chitosan coating at 37 °C are presented in **Figure 4.7a-b**. It was re-established that polymer coating over protein-loaded TNTs provided a lower burst and longer release time. **Table 4.4** summarises the release parameters from chitosan-coated and uncoated TNTs at both RT and 37 °C, with considerably extended glypican release (GPC1- 14 days and GPC3- 16 days) as a result of polymer coating when compared with uncoated TNTs (GPC1- 4 days and GPC3- 5 days).

The release pattern from uncoated TNTs were shortened when the temperature was changed from RT to 37 °C (**Table 4.4**), implying that the release of assemblies of proteins loaded within TNTs were accelerated at physiological temperature due to an increase in amount of energy available for diffusion [41]. Moreover, temperature change might have also affected the rate of chitosan degradation [38]. At 37 °C, the burst release ranged from 63-64% for uncoated TNTs to 36-37% for chitosan-coated samples (which is considerably higher than that obtained for control FITC-BSA at RT). Therefore, these results show that sustained release of proteins form nanotubular therapeutic implants is impacted by the surface chemistry as well as the release temperature. Other parameters such as pore-diameter, nanotube length, surface wettability, loading amount *etc*. can further influence the *in vitro* release characteristics [10, 42].

Glypican Release at Physiological Temperature
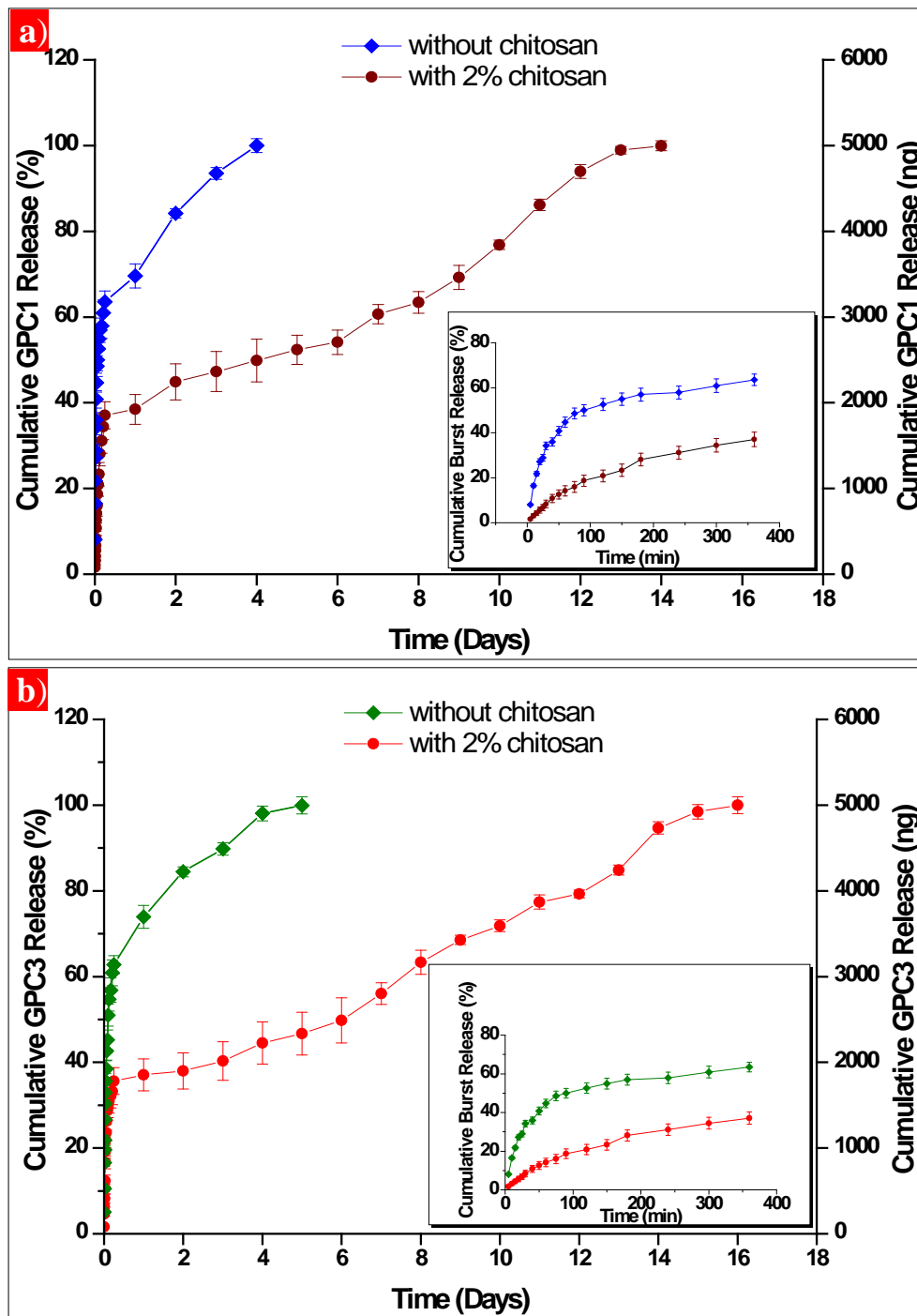
Figure 4.7. Protein release profiles from TNT/Ti implants prepared in LA electrolyte (120 V, 5 min) and loaded with 5 µg of (a) GPC1 and (b) GPC3 at physiological temperature (37 °C). The inset depicts the rapid burst release in the first 6 h. Error bars represent mean ± SD for n = 3.

TNT samples	Release efficiency (%)				Release duration (h/d)		
	6 h	1 d	7 d	14 d	t_B (h)	t_{50} (h/d)	t_{100} (d)
TNTs with GPC1 at RT	40.9	56.0	95.1	100.0	6	0.9 d	9 d
TNTs with GPC3 at RT	45.9	56.6	85.4	100.0	6	0.6 d	11 d
TNTs with GPC1 at 37°C	63.5	69.6	100.0	100.0	6	1.5 h	4 d
TNTs with GPC3 at 37°C	62.7	73.9	100.0	100.0	6	2.5 h	5 d
Chitosan-coated TNTs with GPC1 at 37°C	37.1	38.5	60.7	100.0	6	4 d	14 d
Chitosan-coated TNTs with GPC3 at 37°C	35.6	37.1	56.0	94.7	6	6 d	16 d

Table 4.4. Release parameters of the *in vitro* studies of GPCs eluted from uncoated and Chitosan-coated Titania nanotubes (TNTs) at room and physiological temperature.

The actual concentration of glypicans released from the nanotubular system at physiological temperature on any given day is presented in **Figure 4.8**. The maximum absolute values measured in the experiments (during sustained release periods) are within the adequate range (50-250 ng/ml) for clinical applications (therapeutic window); this scenario is in tandem with previous cell studies showing regulatory effects of glypicans on BMP pathway [33].

Glypican Release Concentrations
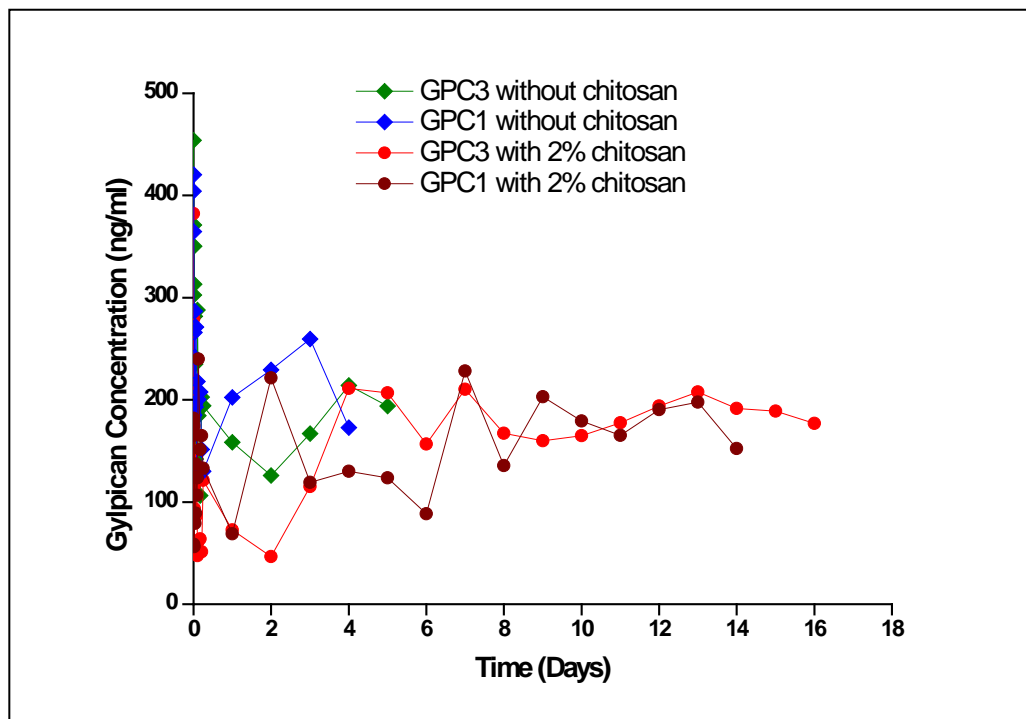
Figure 4.8. Glypican release concentrations (in nanograms) from TNT/Ti implants prepared in LA electrolyte (120 V, 5 min) and loaded with 5 µg of GPC1 and GPC3 at physiological temperature (37 °C).

4.4. Mathematical modelling of glypican release kinetics (Aim III)

The release of drug molecules form the TNTs in most cases can be essentially considered as a diffusion-controlled process, based on one-dimensional Fick's first law, from a non-degradable/ non-eroding drug-carrier system [43, 44]. Aforementioned release systems also involved mass transfer of therapeutics from a high concentration region (protein-loaded nanotubes) to a low concentration region (PBS). The chitosan coating further complexed the release kinetics of the TNT-based reservoir system by delaying the glypican release (based on polymer degradation) [45].

As observed from the *in vitro* drug release curves (**Figure 4.5** and **4.6**), the biphasic release profiles (*i.e.* burst + sustained) can be fitted onto different drug release models to analyse the GPC1/GPC3 transport mathematically. The following analysis models can be used to predict the release behaviour and performance of our implantable delivery system:

Zero-order Model: $F = M_t/M_f = K_o t$

First-order Model: $\log F = K_1 t$

Higuchi Model: $F = K_H t^{1/2}$

Korsmeyer-Peppas Model: $F = K_P t^n$

where, F is the fraction of drug release given by the ratio of the drug amount released at time t (M_t) to the final amount of drug released (M_f), n is the exponent of diffusion that can be linked to the drug transport mechanism, while K_o, K_1, K_H and K_P are the kinetic constants for zero-order, first-order, Higuchi and Korsmeyer-Peppas models, respectively. **Tables 4.5** and **4.6** summarise the values of kinetic constants, co-relation factors (R^2) and diffusion exponents obtained from fitting the *in vitro* data to the investigated kinetic models. The analytical computation of n can help characterise the release mechanisms. For a cylinder, with $n \leq 0.45$, the release mechanism is Fickian diffusion, with $0.45 < n < 0.89$, release is governed by non-Fickian or anomalous diffusion and with $n = 0.89$, case II drug transport takes place leading to zero order release [43, 46-48].

Sample Name	Zero-Order model				First-Order model			
	Burst release		Sustained release		Burst release		Sustained release	
	$K_0 \, min^{-1}$	R^2	$K_0 \, min^{-1}$	R^2	$K_0 \, min^{-1}$	R^2	$K_0 \, min^{-1}$	R^2
TNTs with GPC1 at RT	0.0009	0.79	3E-05	0.97	0.0016	0.61	2E-05	0.54
TNTs with GPC3 at RT	0.0007	0.71	3E-05	0.99	0.0009	0.57	2E-05	0.67
TNTs with GPC1 at 37°C	0.0013	0.69	7E-05	0.97	0.0015	0.47	4E-05	0.65
TNTs with GPC3 at 37°C	0.0015	0.71	5E-05	0.96	0.002	0.54	2E-05	0.54
Chitosan-coated TNTs with GPC1 at 37°C	0.001	0.83	3E-05	0.96	0.003	0.66	2E-05	0.57
Chitosan-coated TNTs with GPC3 at 37°C	0.0009	0.84	3E-05	0.98	0.0034	0.48	2E-05	0.79

Table 4.5. Comparison of release constants and co-relation factors for burst and sustained release obtained by fitting the *in vitro* release data to zero-order and first order model.

The burst release data fits well to both Higuchi (diffusion limited process) and Korsmeyer-Peppas (estimated mechanism of diffusion) models for all the glypican-loaded samples. The initial burst release is caused by fast diffusion of the molecules at the solid-liquid interface at the surface layer. This is supported by the exponent of diffusion value (n greater than 0.5 but less than 0.89) form the Korsmeyer-Peppas model suggesting that the proteins undergo anomalous transport in which both the concentration gradient and polymer degradation (for chitosan-coated TNTs) are governing the diffusion mechanism [23, 48]. However, the high n values (close to 0.89) for chitosan-coated TNTs roughly describe the case II drug transport mechanism that engenders to a zero-order release kinetics [47].

Beyond the burst release, the diffusion of drug molecules represent a slow and steady fashion which fits to the zero-order release model. As the protein amount decreases over time, the concentration gradient plummets, thus declining the release rate before plateauing. However, the sustained release data correlates well (based on R^2 values) to Higuchi and Korsmeyer-Peppas model (with the diffusion exponent less than 0.5), indicating Fickian diffusion controlled release

during this period (first 60% of sustained release) [23, 48]. The therapeutic dosage following a zero ordered profile is the most desirable therapy mechanism, where release occurs at constant rate independent of the time and concentration [22, 23].

Sample Name	Higuchi model				Korsmeyer – Peppas model					
	Burst release		Sustained release		Burst release			Sustained release		
	$K_H min^{-1}$	R^2	$K_H min^{-1}$	R^2	$K_P min^{-n}$	n	R^2	$K_p min^{-n}$	n	R^2
TNTs with GPC1 at RT	0.0204	0.92	0.0089	0.99	0.260	0.564	0.97	0.275	0.284	0.98
TNTs with GPC3 at RT	0.0156	0.97	0.0086	0.97	0.374	0.588	0.96	0.410	0.201	0.97
TNTs with GPC1 at 37ºC	0.0303	0.96	0.0119	0.99	0.256	0.561	0.94	0.364	0.269	0.99
TNTs with GPC3 at 37ºC	0.034	0.94	0.0870	0.99	0.196	0.661	0.95	0.527	0.178	0.99
Chitosan-coated TNTs with GPC1 at 37ºC	0.022	0.99	0.0094	0.98	0.097	0.870	0.99	0.322	0.224	0.98
Chitosan-coated TNTs with GPC3 at 37ºC	0.0207	0.90	0.0090	0.93	0.104	0.863	0.97	0.234	0.301	0.99

Table 4.6. Comparison of release constants and co-relation factors for burst and sustained release obtained by fitting the in vitro release data to Higuchi and Korsmeyer-Peppas model.

Although the theoretical predictions for the drug release profiles is comparable with our experimental data, these models are limited by certain assumptions to stimulate the ideal drug transport state (*i.e.* pseudo-steady state, one-dimensional flow, phase uniformity, perfect sink conditions, continuous motion, constant diffusion coefficient, no interaction between the drug and

matrix, high length to thickness ration of the system, short times/small portions of the release curves *etc*.) [22]. These factors may impact the rational design of therapeutic-releasing platforms.

The achieved kinetic properties of the proteins released from nanoengineered implants over the period of weeks show promise to be translated into clinically viable therapy. However, for a long-term osteogenic inhibition, the amount of proteins loaded within the bone implants should be substantially increased leading to a sustained release over months. Upscaling to bigger animal models and children would also involve larger implantable discs, containing more proteins and prolonged clinical efficacy

4.5. Conclusions

This study demonstrates the ability of designed TNT/Ti cranial implants for controlled and long-term elution of bone-inhibiting proteins for advanced craniosynostosis therapy. The results reiterate that electrochemically anodised TNTs of controlled dimensions can be successfully fabricated on Ti discs and surface coated with desired polymers. The study specifically shows the loading and release kinetics of three model proteins, including FITC-BSA, GPC1 and GPC3. Before loading the TNT/Ti based delivery system, the model proteins were characterised to analyse their interfacial properties (size and charge) with all three proteins elucidating homogeneously dispersed, negatively charged molecules in the size range of 7.5-10.1 nm.

Different strategies were explored to control and modulate the protein loading and release efficiencies, including variable loading/drying techniques (in air and vacuum) and biopolymer coating of different thickness. The vacuum drying led to a better loading efficiency (86-89%), compared to the air-loaded samples (57-64%) and delayed the release of control proteins from

uncoated-TNTs for up to 21 days. The *in vitro* protein release studies revealed a biphasic release profile with initial burst for 6h, followed by a slower sustained release. The biopolymer coatings, Chitosan (1200, 400, 300 and 115 nm thick) and Pluronic-F127 (1115 nm thick) on the top of the protein-loaded TNT platforms altered the release behaviour and delayed the release by limiting the diffusion (based on the polymer degradation). The chitosan layers impeded the elution and sustained the release for 15-30 days while the Pluronic-F127 layer did not have any significant effects on the release duration (12 days), compared with uncoated TNTs (11 days).

Subsequently, the optimised parameters were applied to establish the release characteristics of GPC1 and GPC3 eluted form uncoated and chitosan-coated TNTs at room and physiological temperatures. The release rate was accelerated at 37 °C due to increase in diffusion energy, with the duration of elution lasting to 4-5 days (as compared to 9-11 days at RT) for uncoated and 14-16 days for chitosan-coated TNTs. Nonetheless, these results consolidated the importance of polymer coating to improve the release behaviour and obtain favourable kinetics.

Finally, valid mathematical models were fitted to the experimental data, providing evidence that the burst release (from polymer-coated samples) and overall sustained release followed a zero-order release profile. The values of diffusion coefficient (n) further elucidated that for most samples, the burst release showed an anomalous diffusion, immediately followed by a Fickian diffusion before plateauing to a uniform release curve. Thus, variable release rates can be achieved by simply modifying the implant characteristics for an optimum dosage within the therapeutic window and required timeframe. However, TNT/Ti implants can only be viable for adjunctive craniosynostosis therapy, if the *in vitro* results can be translated into successful delivery of glypicans *in vivo* (in a pathological murine model) at the surgical site to prohibit new bone

formation. The next chapter elucidates a pre-*in vivo* cell study to evaluate the biological response at TNT-cell interface of (human) suture mesenchymal cells and to establish the basic groundwork for craniofacial implantation.

4.6. References

1.   Cooper, G.M., Usas, A., Olshanski, A., Mooney, M.P., Losee, J.E., and Huard, J. Ex vivo Noggin gene therapy inhibits bone formation in a mouse model of postoperative resynostosis. *Plastic and Reconstructive Surgery*, **2009**. 123, 94-103.

2.   Moioli, E.K., Clark, P.A., Xin, X., Lal, S., and Mao, J.J. Matrices and scaffolds for drug delivery in dental, oral and craniofacial tissue engineering. *Advanced Drug Delivery Reviews*, **2007**. 59, 308-24.

3.   Wilkie, A.O. Craniosynostosis: genes and mechanisms. *Human Molecular Genetics*, **1997**. 6, 1647-56.

4.   Springer, I.N., Warnke, P.H., Terheyden, H., Açil, Y., Bülhoff, A., Kuchenbecker, S., Bolte, H., Russo, P.A., Vairaktaris, E.G., and Wiltfang, J. Craniectomy and noggin application in an infant model. *Journal of Cranio-Maxillofacial Surgery*, **2007**. 35, 177-84.

5.   Uludag, H., D'Augusta, D., Palmer, R., Timony, G., and Wozney, J. Characterization of rhBMP-2 pharmacokinetics implanted with biomaterial carriers in the rat ectopic model. *Journal of Biomedical Materials Research*, **1999**. 46, 193-202.

6.   Mooney, M.P., Moursi, A.M., Opperman, L.A., and Siegel, M.I. Cytokine therapy for craniosynostosis. *Expert Opinion on Biological Therapy*, **2004**. 4, 279-99.

7.   Yamamoto, M., Tabata, Y., Hong, L., Miyamoto, S., Hashimoto, N., and Ikada, Y. Bone regeneration by transforming growth factor β1 released from a biodegradable hydrogel. *Journal of Controlled Release*, **2000**. 64, 133-42.

8.   Santos, A., Aw, M.S., Bariana, M., Kumeria, T., Wang, Y., and Losic, D. Drug-releasing implants: current progress, challenges and perspectives. *Journal of Materials Chemistry B*, **2014**. 2, 6157-82.

9.   Aw, M.S., Gulati, K., and Losic, D. Controlling drug release from titania nanotube arrays using polymer nanocarriers and biopolymer coating. *Journal of Biomaterials and Nanobiotechnology*, **2011**. 2, 477.

10.   Losic, D. and Simovic, S. Self-ordered nanopore and nanotube platforms for drug delivery applications. *Expert Opinion on Drug Delivery*, **2009**. 6, 1363-81.

11.   Peng, L., Mendelsohn, A.D., LaTempa, T.J., Yoriya, S., Grimes, C.A., and Desai, T.A. Long-term small molecule and protein elution from TiO_2 nanotubes. *Nano Letters*, **2009**. 9, 1932-36.

12.   Ketabchi, A., Komm, K., Miles-Rossouw, M., Cassani, D.A., and Variola, F. Nanoporous titanium surfaces for sustained elution of proteins and antibiotics. *PloS One*, **2014**. 9, 92080.

13.   Aw, M.S., Kurian, M., and Losic, D. Non-eroding drug-releasing implants with ordered nanoporous and nanotubular structures: concepts for controlling drug release. *Biomaterials Science*, **2014**. 2, 10-34.

14.   Aw, M.S., Addai-Mensah, J., and Losic, D. Magnetic-responsive delivery of drug-carriers using titania nanotube arrays. *Journal of Materials Chemistry*, **2012**. 22, 6561-63.

15.   Aw, M.S. and Losic, D. Ultrasound enhanced release of therapeutics from drug-releasing implants based on titania nanotube arrays. *International Journal of Pharmaceutics*, **2013**. 443, 154-62.

16.   Bariana, M., Aw, M.S., Moore, E., Voelcker, N.H., and Losic, D. Radiofrequency-triggered release for on-demand delivery of therapeutics from titania nanotube drug-eluting implants. *Nanomedicine*, **2014**. 9, 1263-75.

17.   Gulati, K., Aw, M.S., Findlay, D., and Losic, D. Local drug delivery to the bone by drug-releasing implants: perspectives of nano-engineered titania nanotube arrays. *Therapeutic Delivery*, **2012**. 3, 857-73.

18.   Gulati, K., Kogawa, M., Maher, S., Atkins, G., Findlay, D., and Losic, D., Titania Nanotubes for Local Drug Delivery from Implant Surfaces, in *Electrochemically Engineered Nanoporous Materials*. **2015**, Springer. p. 307-55.

19.   Aw, M.S., Simovic, S., Addai-Mensah, J., and Losic, D. Polymeric micelles in porous and nanotubular implants as a new system for extended delivery of poorly soluble drugs. *Journal of Materials Chemistry*, **2011**. 21, 7082-89.

20.   Gulati, K., Ramakrishnan, S., Aw, M.S., Atkins, G.J., Findlay, D.M., and Losic, D. Biocompatible polymer coating of titania nanotube arrays for improved drug elution and osteoblast adhesion. *Acta Biomaterialia*, **2012**. 8, 449-56.

21. Kumeria, T., Mon, H., Aw, M.S., Gulati, K., Santos, A., Griesser, H.J., and Losic, D. Advanced biopolymer-coated drug-releasing titania nanotubes (TNTs) implants with simultaneously enhanced osteoblast adhesion and antibacterial properties. *Colloids and Surfaces B: Biointerfaces*, **2015**. 130, 255-63.

22. Grassi, M. and Grassi, G. Mathematical modelling and controlled drug delivery: matrix systems. *Current Drug Delivery*, **2005**. 2, 97-116.

23. Brophy, M.R. and Deasy, P. Application of the Higuchi model for drug release from dispersed matrices to particles of general shape. *International Journal of Pharmaceutics*, **1987**. 37, 41-7.

24. Crommelin, D.J., Formulation of biotech products, including biopharmaceutical considerations, in *Pharmaceutical Biotechnology*. **2013**, Springer. p. 69-99.

25. Davis, S.S. Meeting the Challenges of Viable Delivery Systems for Peptide and Protein Pharmaceuticals. *American Pharmaceutical Review*, **2002**. 5, 29-36.

26. Fu, H., Rahaman, M.N., Brown, R.F., and Day, D.E. Evaluation of BSA protein release from hollow hydroxyapatite microspheres into PEG hydrogel. *Materials Science and Engineering: C*, **2013**. 33, 2245-50.

27. Wischke, C. and Borchert, H.H. Fluorescein isothiocyanate labelled bovine serum albumin (FITC-BSA) as a model protein drug: opportunities and drawbacks. *Die Pharmazie-An International Journal of Pharmaceutical Sciences*, **2006**. 61, 770-74.

28.   Dwivedi, P.P., Grose, R.H., Filmus, J., Hii, C.S., Xian, C.J., Anderson, P.J., and Powell, B.C. Regulation of bone morphogenetic protein signalling and cranial osteogenesis by Gpc1 and Gpc3. *Bone*, **2013**. 55, 367-76.

29.   Dwivedi, P., Lam, N., and Powell, B. Boning up on glypicans—opportunities for new insights into bone biology. *Cell Biochemistry and Function*, **2013**. 31, 91-114.

30.   Solaro, R., Chiellini, F., and Battisti, A. Targeted delivery of protein drugs by nanocarriers. *Materials*, **2010**. 3, 1928-80.

31.   Mitragotri, S., Burke, P.A., and Langer, R. Overcoming the challenges in administering biopharmaceuticals: formulation and delivery strategies. *Nature reviews Drug Discovery*, **2014**. 13, 655-72.

32.   Popat, K.C., Eltgroth, M., LaTempa, T.J., Grimes, C.A., and Desai, T.A. Titania Nanotubes: A Novel Platform for Drug-Eluting Coatings for Medical Implants? *Small*, **2007**. 3, 1878-81.

33.   Dwivedi, P., Grose, R., Hii, C., Filmus, J., Anderson, P., and Powell, B. Regulation of bone morphogenetic protein signalling and osteogenesis by glypicans in human cranial suture cells. *Bone*, **2011**. 48, 243.

34.   Shen, K., Krakora, S., Cunningham, M., Singh, M., Wang, X., Hu, F., Post, J., and Ehrlich, G. Medical treatment of craniosynostosis: recombinant Noggin inhibits coronal suture closure in the rat craniosynostosis model. *Orthodontics & Craniofacial Research*, **2009**. 12, 254-62.

35.   Cooper, G.M., Curry, C., Barbano, T.E., Burrows, A.M., Vecchione, L., Caccamese, J.F., Norbutt, C.S., Costello, B.J., Losee, J.E., and Moursi, A.M. Noggin inhibits postoperative resynostosis in craniosynostotic rabbits. *Journal of Bone and Mineral Research*, **2007**. 22, 1046-54.

36.   Polishchuk, A.Y., Zimina, L., Kosenko, R.Y., Iordanskii, A., and Zaikov, G. Diffusion-activation laws for drug release from polymer matrices. *Polymer Degradation and Stability*, **1991**. 31, 247-54.

37.   Agnihotri, S.A., Mallikarjuna, N.N., and Aminabhavi, T.M. Recent advances on chitosan-based micro-and nanoparticles in drug delivery. *Journal of Controlled Release*, **2004**. 100, 5-28.

38.   Gulati, K., Johnson, L., Karunagaran, R., Findlay, D., and Losic, D. In-situ transformation of chitosan films into microtubular structures on the surface of nano-engineered titanium implants. *Biomacromolecules*, **2016**. 17, 1261-71.

39.   El-Kamel, A. In vitro and in vivo evaluation of Pluronic F127-based ocular delivery system for timolol maleate. *International Journal of Pharmaceutics*, **2002**. 241, 47-55.

40.   Coussens, A.K., Wilkinson, C.R., Hughes, I.P., Morris, C.P., Van Daal, A., Anderson, P.J., and Powell, B.C. Unravelling the molecular control of calvarial suture fusion in children with craniosynostosis. *BMC Genomics*, **2007**. 8, 458.

41.   Ford, J.L., Mitchell, K., Rowe, P., Armstrong, D.J., Elliott, P.N., Rostron, C., and Hogan, J.E. Mathematical modelling of drug release from hydroxypropylmethylcellulose matrices: effect of temperature. *International Journal of Pharmaceutics*, **1991**. 71, 95-104.

42. Losic, D., Aw, M.S., Santos, A., Gulati, K., and Bariana, M. Titania nanotube arrays for local drug delivery: recent advances and perspectives. *Expert Opinion on Drug Delivery*, **2015**. 12, 103-27.

43. Gulati, K., Kant, K., Findlay, D., and Losic, D. Periodically tailored titania nanotubes for enhanced drug loading and releasing performances. *Journal of Materials Chemistry B*, **2015**. 3, 2553-59.

44. Ritger, P.L. and Peppas, N.A. A simple equation for description of solute release I. Fickian and non-Fickian release from non-swellable devices in the form of slabs, spheres, cylinders or discs. *Journal of Controlled Release*, **1987**. 5, 23-36.

45. Ritger, P.L. and Peppas, N.A. A simple equation for description of solute release II. Fickian and anomalous release from swellable devices. *Journal of Controlled Release*, **1987**. 5, 37-42.

46. Kumeria, T., Bariana, M., Altalhi, T., Kurkuri, M., Gibson, C.T., Yang, W., and Losic, D. Graphene oxide decorated diatom silica particles as new nano-hybrids: towards smart natural drug microcarriers. *Journal of Materials Chemistry B*, **2013**. 1, 6302-11.

47. Dash, S., Murthy, P.N., Nath, L., and Chowdhury, P. Kinetic modeling on drug release from controlled drug delivery systems. *Acta Poloniae Pharmaceutica*, **2010**. 67, 217-23.

48. Korsmeyer, R.W., Gurny, R., Doelker, E., Buri, P., and Peppas, N.A. Mechanisms of solute release from porous hydrophilic polymers. *International Journal of Pharmaceutics*, **1983**. 15, 25-35.

CHAPTER 5

BIOLOGICAL RESPONSE OF HUMAN SUTURE MESENCHYMAL CELLS TO TITANIA NANOTUBE-BASED IMPLANTS FOR ADVANCED CRANIOSYNOSTOSIS THERAPY

Statement of Authorship

Title of Paper	
Publication Status	☑ Published ☐ Accepted for Publication ☐ Submitted for Publication ☐ Unpublished and Unsubmitted work written in manuscript style
Publication Details	Colloids and Surfaces B: Biointerfaces, 2017, 150, 59-67.

Principal Author

Name of Principal Author (Candidate)	Manpreet Bariana
Contribution to the Paper	Under supervision of P. Dwivedi, S. Ranjitkar, J.A. Kaidonis, D. Losic and P.J. Anderson, I developed, designed, and performed the experiments, interpreted and processed the data and wrote the manuscript for submission.
Overall percentage (%)	80
Certification:	This paper reports on original research I conducted during the period of my Higher Degree by Research candidature and is not subject to any obligations or contractual agreements with a third party that would constrain its inclusion in this thesis. I am the primary author of this paper.
Signature		Date	21/7/2016

Co-Author Contributions

By signing the Statement of Authorship, each author certifies that:

    i.   the candidate's stated contribution to the publication is accurate (as detailed above);

    ii.   permission is granted for the candidate in include the publication in the thesis; and

    iii.   the sum of all co-author contributions is equal to 100% less the candidate's stated contribution.

Name of Co-Author	Prem Dwivedi
Contribution to the Paper	I helped the candidate with the tissue and cell culture experiments, including the MTT assay, cell adhesion and proliferation studies. I give consent for Manpreet Bariana to present this paper for examination towards the Doctorate of philosophy
Signature		Date	21/7/2016

Name of Co-Author	Sarbin Ranjitkar		
Contribution to the Paper	I acted as secondary supervisor for the candidate and aided in statistical analysis, editing and evaluation of manuscript for submission. I give consent for Manpreet Bariana to present this paper for examination towards the Doctorate of philosophy.		
Signature		Date	21/7/2016

Name of Co-Author	John Kaidonis		
Contribution to the Paper	I acted as secondary supervisor for the candidate and aided in development and design of the experiments and evaluation of manuscript for submission. I give consent for Manpreet Bariana to present this paper for examination towards the Doctorate of philosophy.		
Signature		Date	21/7/2016

Name of Co-Author	Dusan Losic		
Contribution to the Paper	I acted as secondary supervisor for the candidate and aided in nanoengineered implant fabrication and evaluation of manuscript for submission. I give consent for Manpreet Bariana to present this paper for examination towards the Doctorate of philosophy.		
Signature		Date	21/7/2016

Name of Co-Author	Peter J. Anderson		
Contribution to the Paper	I acted as primary supervisor of the candidate and aided in evaluation of experimental design and manuscript for submission. I give consent for Manpreet Bariana to present this paper for examination towards the Doctorate of philosophy.		
Signature		Date	21/7/2016

Biological response of human suture mesenchymal cells to Titania nanotube-based implants for advanced craniosynostosis therapy

Manpreet Bariana[1]*, Prem Dwivedi[2], Sarbin Ranjitkar[1], John A. Kaidonis[1], Dusan Losic[3]*, Peter J. Anderson[1,4]*

[1]School of Dentistry, The University of Adelaide, Adelaide, SA 5005, Australia

[2]Women's and Children's Hospital, 72 King William St, Adelaide, SA 5006, Australia

[3]School of Chemical Engineering, The University of Adelaide, Adelaide, SA 5005, Australia

[4]Australian Craniofacial Unit, 72 King William St, Adelaide, SA 5006, Australia

Abstract

Titania nanotubes (TNTs) engineered on titanium (Ti) surfaces (*i.e.* TNT/Ti) and loaded with specific drugs have been recognised as a promising solution for localised therapeutic delivery to address several medical problems not feasible with conventional drug administration. We propose the use of TNT/Ti protein-releasing implants to treat paediatric craniofacial abnormality in craniosynostosis caused by premature fusion of cranial sutures. In this study, we have analysed the biological response of human suture mesenchymal cells (SMCs), extracted from two different patients undergoing craniofacial reconstruction surgery, at the TNT/Ti implant surface. The

experimental groups included large-diameter TNT/Ti implants, with and without biopolymer surface coating (Chitosan and Pluronic-F127) while the controls comprised of flat Ti disc and tissue culture plastic. The non-loaded implant surfaces and the cellular interactions at the implant-cell interface were characterised using scanning electron microscopy (SEM). The SMC adhesion, viability and proliferation were determined by MTT assay and manual cell counting at day 1 and day 3 of cell incubation. SEM showed significant reduction in initial attachment and adhesion of SMCs at TNT-cell biointerface compared with the control Ti discs. Subsequent cell proliferation results also revealed a decrease in the number of viable cells on the TNT surfaces. The nanotopography and structural features along with the surface chemistry dictated the cellular response, with nanotubular surfaces (with and without polymer coating) impeding cell adhesion and proliferation. Our findings hold promise for the use of TNT-based cranial implants as a delivery system to prevent sutural bone growth for advanced craniosynostosis therapy.

KEYWORDS: Craniosynostosis; protein-releasing implants; Titania nanotubes; cranial implants; human suture mesenchymal cells; cellular response

1. Introduction

Craniosynostosis is a paediatric craniofacial abnormality caused by premature fusion of cranial sutures [1]. It is a largely unknown but fairly common pathology occurring in approximately 1 in 2500 live births [1]. The early suture closure (**Fig. 1**) can be associated with morphologic abnormalities such as dysmorphic head and asymmetric facial features, causing raised intracranial pressure and impaired cerebral blood flow leading to significant morbidity [2-4]. The conventional management of this disease relies on invasive surgical reconstruction of the cranial vault. Although the prematurely fused bones are excised and reshaped to increase the intracranial volume, patients

often require repetitive interventions as the brain grows [5, 6]. Depending on the severity and cause,

patients can have single or multiple fused sutures [7].
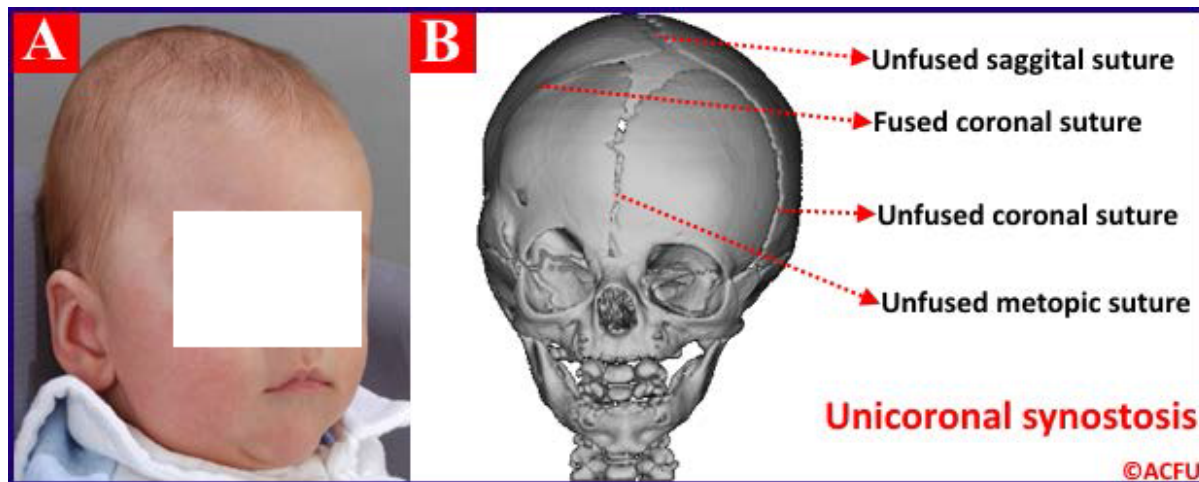
Fig. 1. A digital (A) and radiological (B) image of an infant skull with unicoronal synostosis (i.e. suture fusion on the right side) before undergoing a cranial vault reconstruction surgery at the Australian Craniofacial Unit (ACFU).

The suture pathophysiology is related to abnormal proliferation and differentiation of cells at the

osteogenic fronts within a growing skull [8]. The current goal of craniosynostosis research is to

design therapeutic implants that can alter/delay premature suture fusion by altering the events at

the cellular level, thus avoiding the multiple operations.

Medical implants made from Titanium (Ti) and its alloys have extensively been explored for use

in orthopaedic, dental and craniofacial applications by virtue of their bioinertness and

biocompatibility [9, 10]. Moreover, numerous surface modifications and micro- and nano-

structuring techniques have been explored in the last two decades to avoid post-implantation

infection and implant rejection [11, 12]. Previous studies have confirmed the relevance of both

chemical and structural modification of Ti implants at micro and nano scales to modulate the

cellular response and bioactivity [13-16]. One of the simplest and most efficient approaches to generate nanostructured surfaces is to electrochemically anodise Ti to grow an oxide layer with Titania nanotubes (TNTs) [17, 18]. The concept of TNT/Ti drug-releasing implants has been established as a superior localised therapeutic-delivery platform in treating bone-related diseases due to their outstanding chemical and mechanical properties as well as easily tuneable dimensions and loading capacity [11, 12, 16, 19]. These implants have been successfully applied for slow and extended release of therapeutics with varied chemistries and solubilities, triggered on-demand release of externally stimulated payloads and sequential release of multiple drugs and carriers [20-23]. Numerous studies have demonstrated the capabilities of TNTs to release substantial amount of drugs (antibiotic, anticancer, antibacterial), proteins, genes and RNAs catering to bone-implant challenges [12, 19, 24]. Extending this approach to craniosynostosis therapy, TNT/Ti cranial implants present a promising platform for localised delivery of proteins (bone antagonists), prohibiting sutural bone formation in a murine model.

The TNT/Ti implants are polymer-coated (with Chitosan and Pluronic-F127) in order to modulate the implant interactions and extend the release of loaded proteins *in vivo*. Both Chitosan and Pluronic-F127 are biodegradable polymers with low toxicity, high biocompatibility and weak immunogenic properties which make them ideal for tissue engineering and drug delivery applications [25, 26].

For successful clinical implantation and optimal functioning of the TNT/Ti implant, it is essential to understand the events at suture cell-biomaterial interface. Human primary suture cells or suture mesenchymal cells (SMCs) are a complex population derived from bone-forming tissues of the skull calvarial plates. The tissue complex comprises of cells at different stages of differentiation

including mesenchymal cells, osteoprogenitor cells, preosteoblasts, osteoblasts, osteocytes and cells from other developmental lineages [8, 27]. Previous research based on an *in vitro* model of explant human calvarial suture tissue culture has identified the cellular mechanisms involved in abnormal bone growth during suture morphogenesis [27-29]. Experimental evidence shows that the cranial osteoblasts potentially de-differentiate into pre-osteoblastic cells when cultivated in the absence of osteogenic cues, making them ideal candidates for studying cell behaviour at the TNT/Ti implant surface [30]. In addition, they are likely to behave as stem cells cultured on TNTs [31, 32].

Owing to their nanotopographical surface features (closely mimicking the natural extracellular matrix/ bone morphology), TNT/Ti implants are known to modulate and control cell behaviour and surface interaction. In addition to nanoscale surface morphology, the cell adhesion and subsequent proliferation, migration and differentiation are highly dependent on TNT porosity and pore dimensions. The surface roughness, chemistry, wettability, charge and the crystal phase also affect cell physiology. TNTs with variable dimensions and surface properties have been shown to influence the behaviour of a variety of cell types cultured on the surface, *e.g.* osteoblasts, fibroblasts, chondrocytes, myocytes, keratinocytes, endothelial cells and mesenchymal stem cells (MSCs). However, the cellular response of different cell types to similar TNT morphologies (diameters) is conflicting [13, 14, 31-35].

The events succeeding an *ex vivo*/clinical implantation involve the immediate adsorption of extracellular matrix (ECM) proteins (vitronectin and fibronectin) from the media or the body serum onto the implant surface. The protein adsorption and subsequent unfolding expose the functional groups and provide anchorage sites to the surrounding cell surface receptors (integrins), which

cluster to form a focal adhesion complex, thereby controlling cell adhesion, spreading and function [34-36].

The response of different phenotypic cell lines to the TNTs with variable topographical characteristics (diameters) is not universal. In some studies, 30 nm TNTs show good MSC adhesion, while in others 70-100 nm TNT surfaces promote elongation and expression of osteogenic differentiation markers [37]. Comparisons also indicate that 15 nm diameter TNTs promote MSC activity, integrin clustering and focal formation while 100 nm TNTs impair cell functions and induce cell death [31]. Furthermore, 30-100 nm [15], 50 nm [38] and 70 nm [38, 39] TNTs are known to significantly enhance osteoblast cell growth and function, contradicting the findings of impaired osteoblastic function when the nanotube diameter is larger than 50 nm [31].

Considering all the ambiguities about the varied cellular behaviour on TNTs, our aim was to evaluate the *in vitro* performance of large-diameter TNT/Ti implants on the adhesion, proliferation, viability and morphology of human suture mesenchymal cells. Since the TNT/Ti implants show promise in treating paediatric craniofacial abnormality (*i.e.* craniosynostosis), the SMCs (primary cells) extracted from affected patients undergoing *craniectomy* gives this novel study an opportunity to improve existing knowledge. Our specific objectives were (i) to fabricate TNT/Ti implants and to investigate the initial human SMC interaction at the implant surfaces, (ii) to compare the human SMC behavior (adhesion, spreading and proliferation) within and between the polymer-coated (with Chitosan and Pluronic-F127) and uncoated TNT surfaces (*i.e.* three experimental groups), including Ti disc and polystyrene tissue culture plastic (*i.e.* two control groups) and (iii) to investigate the effects of surface chemistry and wettability on human SMC viability between the polymer-coated and uncoated TNT/Ti implants. The concept of extracting

suture tissue from craniosynostosis patients and culturing SMCs on TNT/Ti implants is schematically summarised in **Fig. 2.**
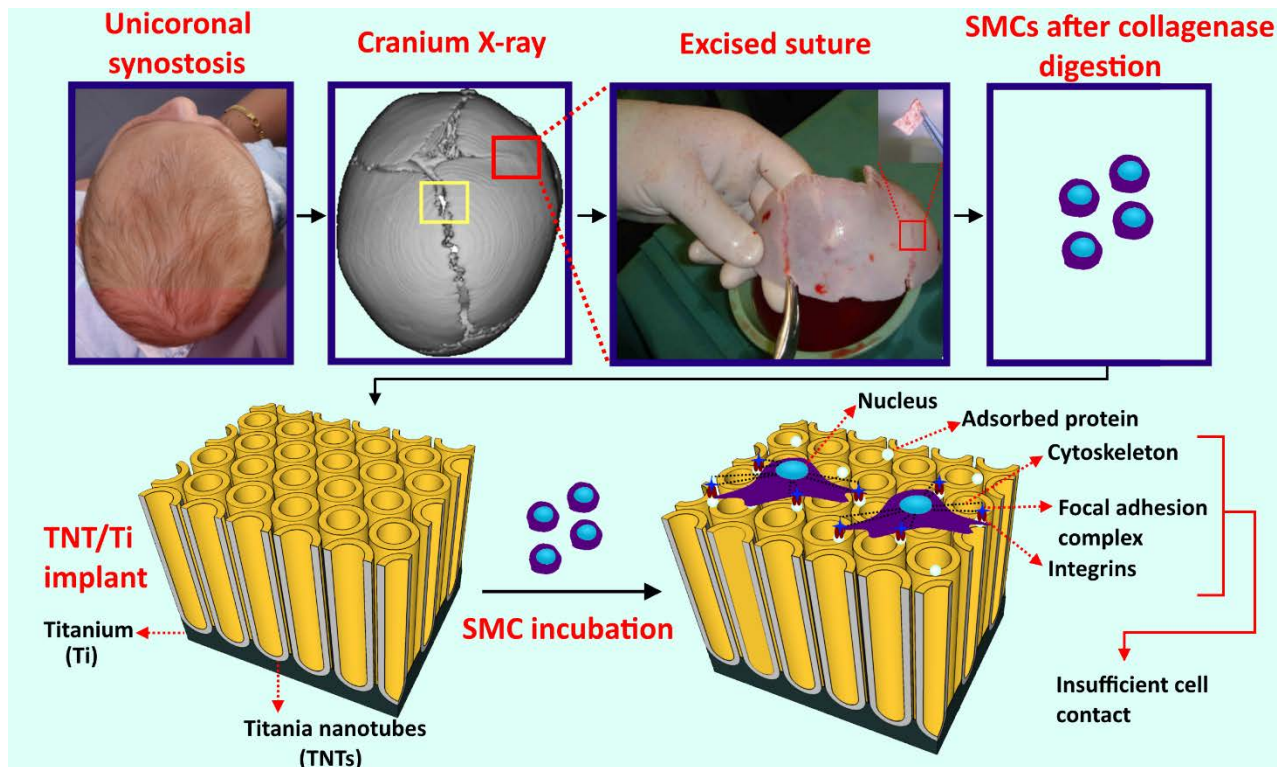
Fig. 2. *Schematic diagram summarising the excision of human calvarial suture tissue and extraction of suture mesenchymal cells (SMCs) from a patient undergoing craniofacial reconstruction surgery at ACFU. The lower part of the scheme shows the TNT/Ti implant with SMCs cultured on the top. It further depicts the cell-biomaterial interface with protein adsorption, integrin clustering, focal contact formation and initial cell adhesion.*

The initial SMC attachment and morphology at the cell-implant bio-interface (on experimental and control surfaces) were analysed using scanning electron microscopy (SEM) while the subsequent adhesion and proliferative activities were evaluated by measuring the number of attached cells, using MTT assay and manual cell counting at day 1 and day 3 of cell incubation. The final SMC response and viability were determined by combined assessment of the surface topography and

chemistry using the above mentioned analysis tools. The null hypotheses were that the SMC behavioral response to the experimental groups would be similar to the control groups, and that the nanotopography and surface chemistry would have no significant effects on their number and viability.

2. Materials and methods

2.1. Fabrication of TNT/Ti implants

The Ti foil was mechanically polished and cleaned by sonication, followed by ultrasonic milling to obtain 3 mm circular discs. TNT arrays were fabricated on the Ti discs by simple two-step electrochemical anodisation in lactic acid containing organic electrolyte [40] (**Supplementary Information – Sections 1-2**).

2.2. Surface coating of TNT/Ti implants

Polymer solutions of chitosan (2% (w/v) chitosan + 0.8 vol.% acetic acid in deionised water) and Pluronic-F127 (20% (w/v) in cold water) were prepared and spin-coated at 1500 rpm for 15 s onto the TNT/Ti, followed by vacuum drying.

2.3. Surface characterisation

A field-emission scanning electron microscope (SEM, FEI Quanta 450, The Netherlands) was used to characterise the TNT structure, and to measure of the thickness of the nanotube and polymer layers. The contact angles of the TNT/Ti implants were measured at the initial (t=0) and the final time points (t=f; f=5.00 ± 2.92 s) using a sessile drop method on an optical contact angle measuring device (Attension, KSV Instruments, Australia).

2.4 Human suture samples and primary cell culture

Human calvarial suture tissues were excised from two patients undergoing corrective craniosynostosis surgery at the Australian Craniofacial Unit, Adelaide. Consent was provided by the parent/guardian, in accordance with the guidelines of the Research Ethics Committee of the Women's and Children's Health Network, Adelaide, South Australia (HREC# 1033/10/2014). Briefly, the suture tissues (suture mesenchyme plus 3 mm of bone on either side for unfused coronal sutures, or fused bony plate plus 3 mm of bone on either side for fused coronal/sagittal sutures) were dissected from the patients' skulls. After removing the overlying pericranium, primary cells were obtained by collagenase digestion and explant culture using a previously described method [8, 30] (**Supplementary Information – Section 4**).

2.5. MTT cell proliferation assay

Four human primary suture cell lines (from fused and unfused sutures of both patients) were used to optimise the MTT assay with different cell numbers (10^4, 2×10^4 and 5×10^4 cells/well) and time points (day 1 and day 3). Cell adhesion (after day 1) and proliferation (after day 3) were assessed using the commercially available MTT assay kit (Promega CellTiter 96® Non-Radioactive Cell Proliferation Assay), by applying modified Mosmann method [41]. Before seeding the cells onto the implant surfaces, the 3 mm discs (positive control Ti, Titania nanotubes (TNTs), chitosan-coated TNTs and Pluronic-F127-coated TNTs) were plated in a 96-well plate and effectively sterilised under ultraviolet light for 30 min (**Supplementary Information – Section 3**). The cells with a density of 2×10^4 cells/well (in 100 µl of DMEM medium) were incubated with sterilised implants in culture plates for 24 and 72 h. After the respective co-incubation, 15 µl of the dye solution was added to each well as per manufacturer's directions. The plates were further incubated

for 4 h at 37 $^{\circ}$C in 5% CO_2 environment, and 100 µl of solubilisation/stop solution was added to dissolve the formazan crystals. The absorbance of the resulting purple solution was measured at a wavelength of 590 nm using a UV–Vis spectrophotometer. Variations in cell activity resulted in changes in the amounts of formazan formed, reflecting on the interactions at the cell-implant interface. Cells cultured on tissue culture plastic were used as a negative control in each experiment. All measurements were done in triplicate in two independent experiments.

2.6. Cell viability

In a separate parallel set of experiments, the number of cells adhering and proliferating on the implant surfaces were quantified by trypsinising and manually counting them using a haematocytomter. Similar layout as the MTT studies was used with fused and unfused cells from both the patients. Each treatment was carried out in triplicate and identical experiment was repeated twice at two different time points (24 and 72 h).

2.7. Characterisation of cell morphology on implants

SEM analyses were conducted to study the morphology of human suture cells cultured on both the control and experimental surfaces. After a culture time of 24 h, the surfaces were washed with PBS to remove the extra medium and the non-adherent cells. The implants with attached cells were immersed in glutaraldehyde/paraformaldehyde solution to fix the cells. The cells were then washed by dipping the implants in PBS buffer for 5 min, and then by sequentially dehydrating in ethanol (70% and 90% EtOH for 15 min each followed by two 15 min washes in 100% EtOH). After the samples were immersed in hexamethyldisilazane (HMDS):100% EtOH (1:1) solution for 10 min

and then twice in 100% HMDS for 10 min, they were air-dried and mounted on SEM holders to be sputter coated with 3 nm platinum layer.

2.8. Statistical analysis

One-way repeated measures ANOVA (with Bonferroni post-hoc tests) was used to analyse the effects of implants surfaces (control and experimental groups) on the absorbance and cell number values over time (IBM SPSS statistics 22, IBM Corporation, USA). Statistical significance was set at the 0.05 probability level.

3. Results and discussion

3.1. Structural characterisation of TNT/Ti Implants

The surface and morphology of the fabricated TNT/Ti implants characterised by SEM are depicted in **Fig. 3A**. For this study, nanotubes with large diameters (120 ± 10 nm) and 35 µm lengths were utilised to minimise cell adhesion and proliferation. Although, a Ti disc was used as a model implant, this technique can easily and reproducibly be translated onto medical grade Ti plates and screws.
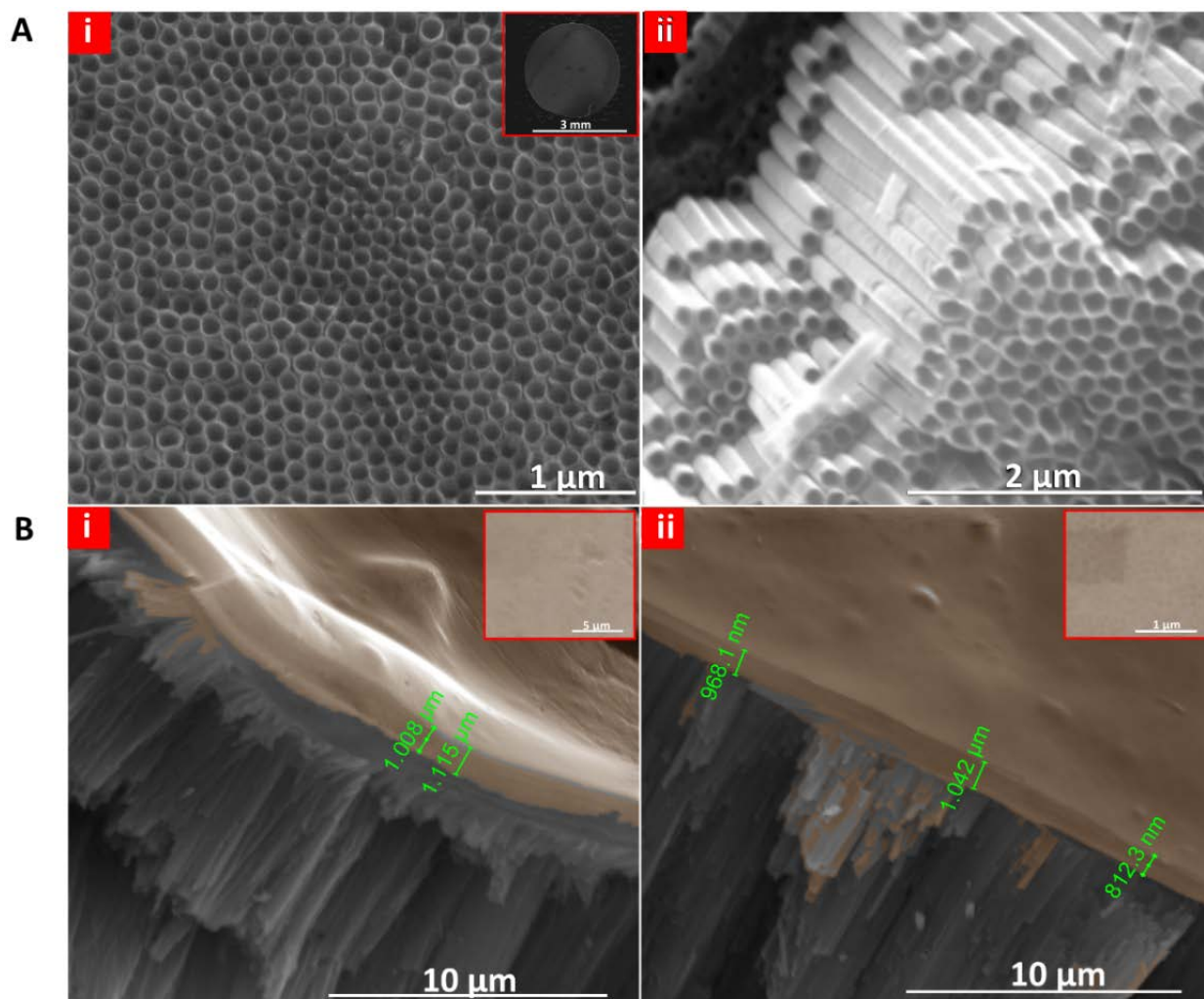
Fig. 3. SEM images of TNT/Ti implants fabricated by electrochemical anodisation of Ti in NH₄F/ethylene glycol/LA electrolyte at 120 V for 5 min. (A) Uncoated TNT/Ti substrates, (i) the top view showing the nanoporous structure and surface topography with 120 ± 10 nm pore diameter (inset: the 3mm TNT/Ti implant) and (ii) high resolution cross-sectional view of TNT arrays showing vertically aligned, self-assembled nanotubes; (B) Angled cross-sectional images of TNTs spin-coated with biopolymers showing (i) the Pluronic-F127 layer (prepared from 20% solution) and (ii) the Chitosan layer (prepared from 2% solution) layer (the insets show the respective top views).

Fig. 3B shows the surfaces of polymeric layers of Pluronic-F127 and Chitosan spin-coated onto the TNT/Ti, reflecting on the effects of surface chemistry on cellular behaviour. The 2% chitosan solution and the 20% Pluronic-F127 solution both rendered a surface coating ˜1 μm thick, evenly covering the nanopores.

Chitosan n(1-4,2-amino-2-deoxy-β-D-glucan) is a biopolymer that promotes implant integration due to its structural similarity to hyaluronic acid present in the ECM [42, 43]. Pluronic-F127 is a hydrogel comprising of amphiphilic copolymers of ethylene oxide and propylene oxide units. Modification of implant surface with Pluronic-F127 is an effective method to resist protein adsorption and bacterial adhesion [44, 45].

The surface wettability (hydrophilicity/hydrophobicity) affects the protein adsorption as well as cell adhesion [46]. **Table 1** summarises the water contact angles (WCAs) for all the implant surfaces used in this study. The pure titanium disc (before annealing) had a high WCA of ˜95° while annealing decreased the contact angle to ˜62°. The anodised TNTs had a highly hydrophilic surface with initial WCA of 4°, decreasing to a zero within a few seconds.

Sample	Contact Angle (°)
Ti unannealed	95.41 ± 0.91
Ti annealed	61.73 ± 1.00
TNT	4.00 ± 0.60
TNT-CH	30.71 ± 1.51
TNT-F127	31.36 ± 3.50

Table 1. Average (mean ± SD) water contact angle (WCA) measurements for Ti and different TNT/Ti substrates.

Chitosan-coated TNT surfaces showed a drastic decline in hydrophilicity owing to the increment in carbon content, with an initial WCA of 33° (at t=0) and the final WCA of 20° (at t=f). Similarly, for the Pluronic-F127 modification, the WCA declined from 38° (at t=0) to 23° (at t=f) approximately. We are assuming that the large polypropylene chains led to the observed decrease in wettability. The corresponding video images at the initial measurement (t=0) and the final measurement (t=f; f=5.00 ± 2.92 s) are shown in **Fig. S1** (**Supplementary Information- Section 5**).

3.2. SMC adhesion and morphology

SMC adhesion at the SMC-implant interface is affected by implant surface properties and topography. Possible mechanisms of cell attachment may include surface charge-dependent electrostatic physiochemical linkages, or protein-mediated attractive and repulsive forces [47-49]. **Fig. 4** presents the low and high magnification SEM images of cell adhesion and morphology after 1 day of incubation on flat Ti disc, TNT/Ti (with 120 nm diameter), Chitosan-coated TNT (TNT-CH) and Pluronic-F127-coated TNT (TNT-F127).

In the control Ti (**Fig. 4A-i**), many round protein aggregates were visible on the surface along with an even distribution of a large number of SMCs. The positively-charged protein molecules acted as pre-existing interfacial anchorage sites on the negatively-charged Ti, accessible to integrins for successful cell attachment. The corresponding high-resolution inset consolidates the findings, showing isolated, spread-out and flattened cells due to high protein adsorption. In contrast, uncoated (**Fig. 4A-ii**) and polymer-coated nanotubular surfaces (**Fig. 4B**) displayed less protein aggregates and hence less initial cellular attachment. These results support the notion that a cellular body identifies an implant surface via protein organisation and quantity [33, 37, 49].
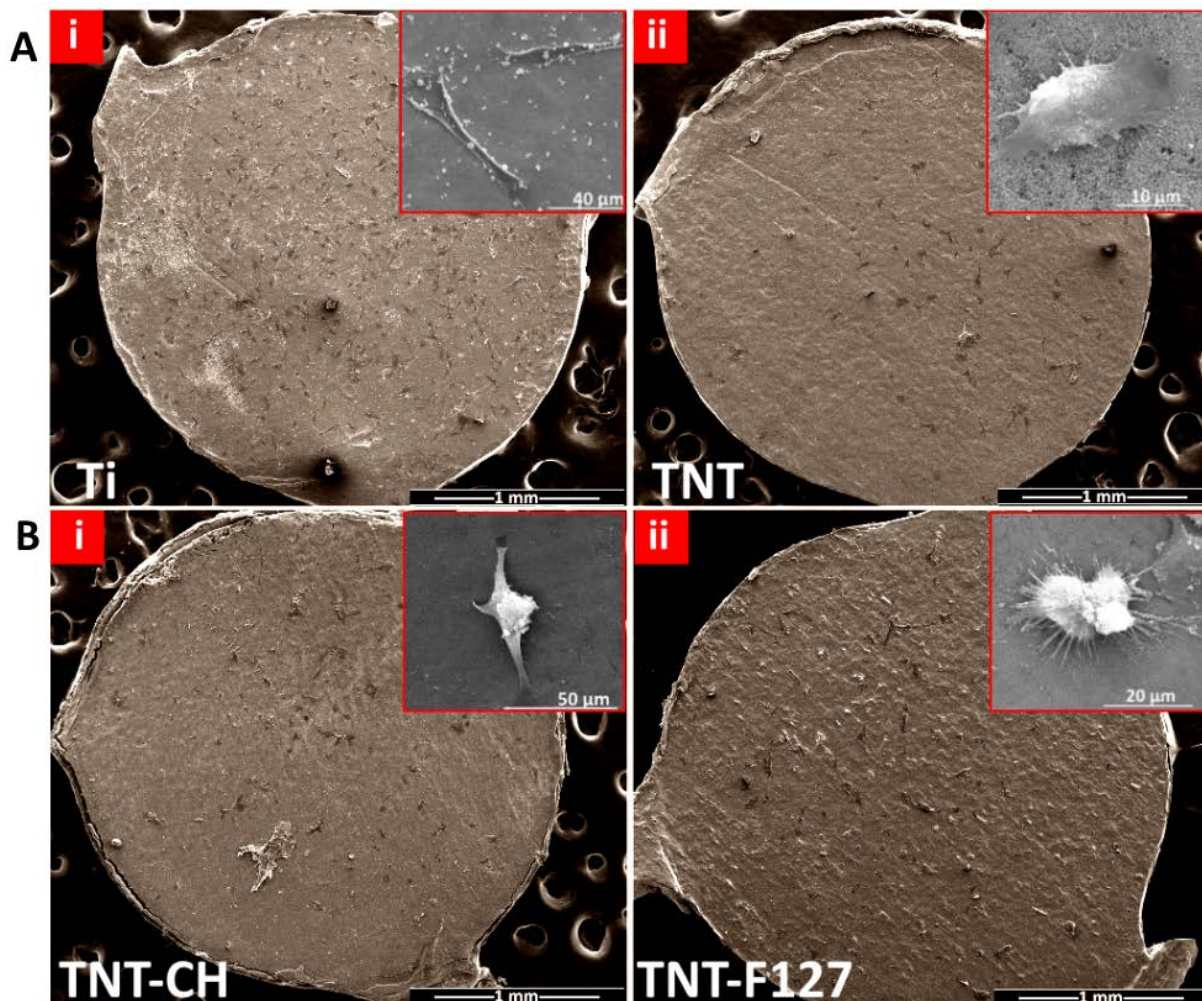
Fig. 4. *SEM images for SMC attachment after 24 h of incubation on different implant surface. (A) The low and high resolution (inset) images on (i) Flat Ti disc and (ii) TNT/Ti (with 120 nm diameter); (B) The low and high resolution (inset) images of TNTs coated with (i) Chitosan (TNT-CH) and (ii) Pluronic-F127 (TNT-F127). All TNTs used were prepared under the same conditions.*

Cell interaction (adhesion and spreading) on the implant surface is mediated by integrin clustering into focal adhesion complexes which activate intracellular signalling and cytoskeletal reorganisation [13, 31]. Significantly lower cell density on TNTs is a diameter-dependent phenomenon as proposed earlier. For nanotopography to guide cell adhesion, the ideal feature size

(nanotube diameter) should be ~15 nm which is comparable to the 10 nm integrin extracellular domain [13]. Hence, for our TNT/Ti implant (**Fig. 4A-ii**, inset), the large nanotube diameter led to limited cell adhesion and inadequate flattening and cytoskeletal elongation (due to unstable focal contacts), with prominent filopodia and lamellipodia extensions [13, 31-33].

Our results further elucidate that a thin layer of positively charged chitosan shows reduction in initial cell attachment (**Fig. 4B-i**), which could be due to the decrease in hydrophilicity (compared with uncoated TNT/Ti) and affinity towards incoming protein molecules. The low density of free amino groups (low degree of acetylation) also minimalise the chances of electrostatic adhesion onto the surface [48, 50, 51]. The resulting high resolution inset shows cells with rounded nuclei and flattened but stretched lamellipodia. These morphological changes can be attributed to electrostatic adhesion of cells but with insufficient focal contact formation, which could cause cytoskeletal stress leading to impaired spread and improper reorganisation with unstable extensions.

Similarly, Pluronic-F127-coated implant surfaces have low cell numbers because the non-ionic amphiphilic copolymer hinders initial protein adsorption (**Fig. 4B-ii**) [44, 45]. The cells have hemispheroidal shape with microspikes (short transparent tubular filopodia) causing minimal spreading. Overall, these results confirm that nanotopographical cues and surface chemistry influence the morphology of adherent cells. The succeeding cellular events such as proliferation, differentiation and even apoptosis intricately depend on aforementioned parameters [13, 31, 32, 34, 52, 53].

The lack of adherence to the TNT surfaces due to low integrin clustering may ultimately result in cell apoptosis (anoikis). This anchorage-dependent phenomenon is driven by the cytoskeletal stress

and the cell phenotype [54]. **Fig. S2 (Supplementary Information- Section 6)** shows the typical cell features observed in the SEM imaging studies conducted in the absence of an osteogenic media at different passage numbers.

As a part of separate study, a more in-depth analysis of effects of different polymer-coated and uncoated implant surfaces on the cytoskeletal reorganisation and cell spreading has been performed in murine osteoblasts, using Phaloidin-DAPI staining and confocal microscopy. **Fig. S3 (Supplementary Information- Section 7)** shows the preliminary results from these studies which are in agreement with the above mentioned SMC interactions (adhesion and spreading) with different implant surfaces including, control flat Ti disc, TNT/Ti (with 120 nm diameter) and TNTs coated with Chitosan (TNT-CH).

3.3. SMC proliferation

Cell adhesion on the implant surface does not assure cell viability and functionality. In order to assess the combined effects of SMC proliferation and metabolic activity, MTT assay was used. MTT dye is taken up by functional cells and reduced by a mitochondrial reaction to formazan, which colours the cytoplasm violet (the colour intensity/absorbance being proportional to number of live cells). Initially, the MTT kit was tested for optimisation with different cell numbers (10^4, 2×10^4 and 5×10^4 cells/well) and 2×10^4 cells/well was chosen as standard for all the experiments (data not shown). Histograms showing absorbance of active cells adhered to the different implant surfaces after day 1 and day 3 of the culture are summed up in **Fig 5**. The SMCs from both the craniosynostosis patients (extracted from fused and unfused sutural regions) showed similar responses on the test implant surfaces, indicating that both the nanotube diameter and surface chemistry play a role in deciding the cell fate.
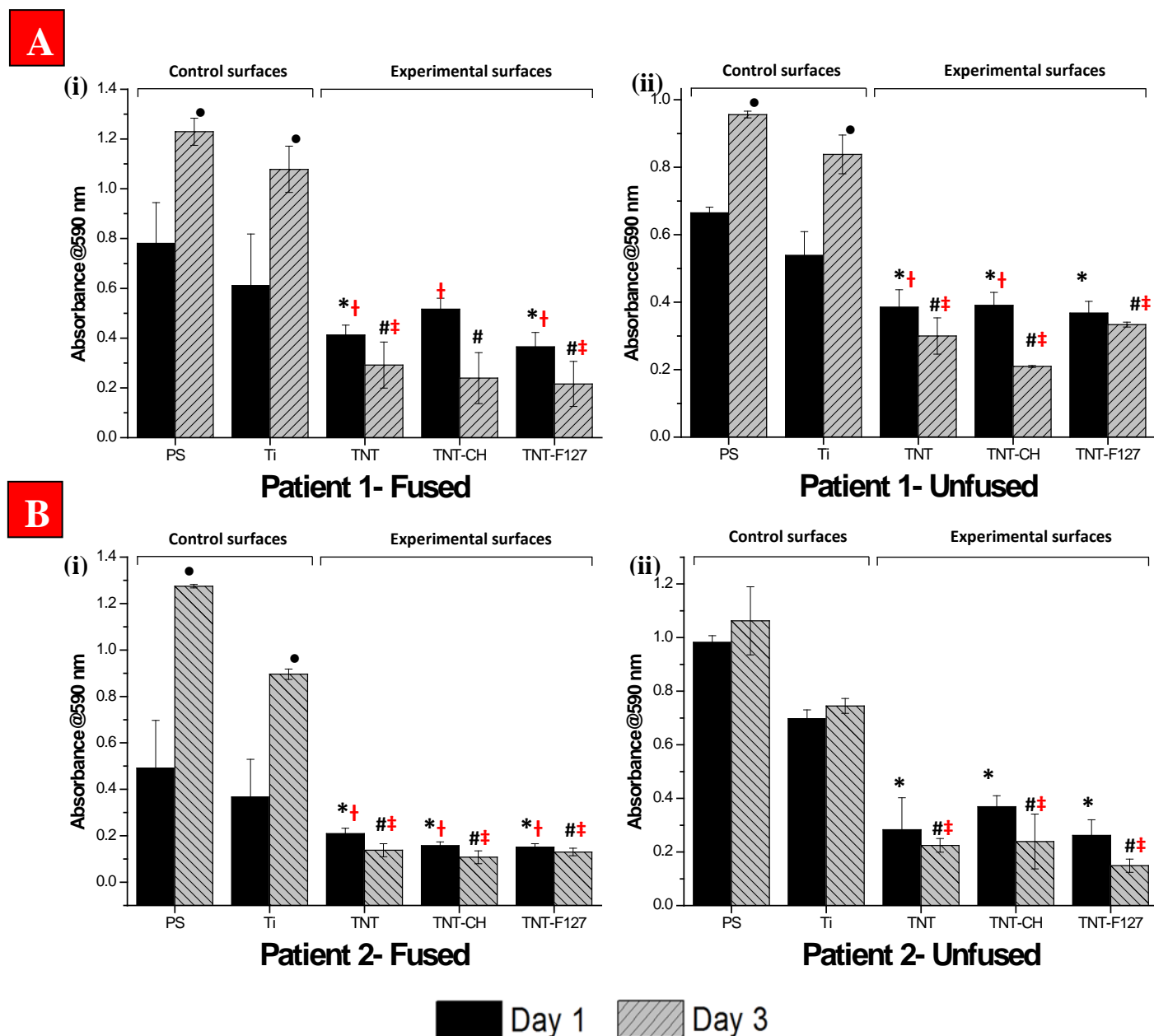
Fig. 5 MTT assay data showing the absorbance of the reaction product of MTT solution for SMCs cultured on Polystyrene (PS), flat Ti disc, Titania nanotube (TNT/Ti), Chitosan-coated TNT (TNT-CH) and Pluronic-F127- coated TNT (TNT-F127) on day 1 and 3 for (A) Patient 1- (i) fused and (ii) unfused sutures and (B) Patient 2- (i) fused and (ii) unfused sutures. The statistical symbols depict-*: significant difference between the control and experimental surfaces on day 1, #: significant difference between the control and experimental surfaces on day 3, †: non-significant difference within the experimental surfaces on day 1, ‡:

non-significant difference within the experimental surfaces on day 3 and •: significant difference within the group on day 1 and 3.

Fig. 5A and B show good SMC viability on control Ti surfaces (similar to polystyrene tissue culture plastic- PS) on day 1 and better proliferation on day 3 for both the patients (fused and unfused sutures). In contrast, the uncoated and polymer-coated nanotubular surfaces led to significant decreases in healthy and viable cells on day 1, and further overall decrease in their proliferative ability on day 3, suggesting a large number of SMCs would have undergone apoptosis/anoikis.

One-way repeated measures ANOVA showed a significant effect of nanotopography (nanotube diameter) and surface chemistry (polymer coatings) on the absorbance value obtained by MTT assay between control and experimental groups, thus defying our null hypothesis. Post-hoc tests showed significantly less SMC adhesion and proliferation in TNT, TNT-CH and TNT-F127 compared with either control Ti and PS group ($p < 0.05$ for each comparison). There was no significant difference between the same experimental groups on different days, indicating that the initial cell adhesion governs subsequent cellular behaviour ($p > 0.05$ for each comparison).

3.4. Cell viability

Fig. 6 shows the SMC adhesion on day 1 and its proliferation on day 3 when cultured on different implants surfaces. As expected, PS supported highest cell adhesion and proliferation which was comparable to that of control Ti ($p > 0.05$). The trends of the cells adherence and proliferation as functions of incubation time were similar to those observed in the MTT proliferative assay (**Fig. 5**), with a sharp significant decreases in cell number on the uncoated and polymer-coated nanotubular implants ($p < 0.05$).
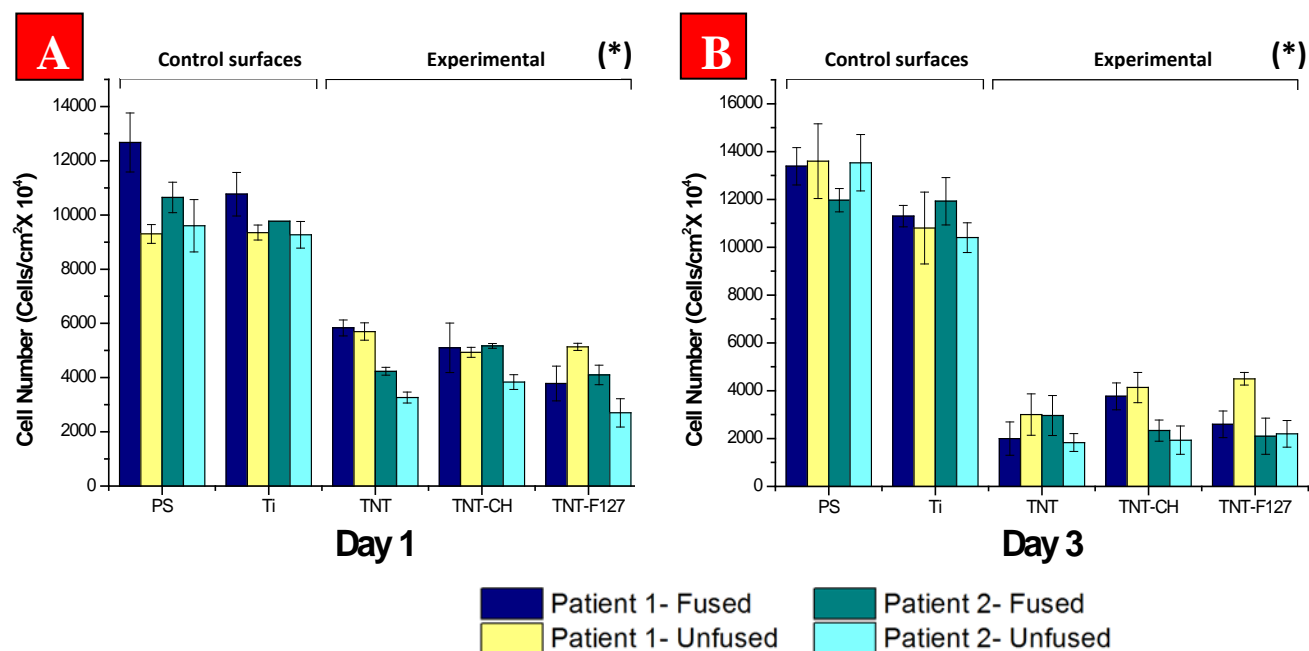
Fig. 6. The cell counting studies showing (A) SMC adhesion (day 1) and (B) proliferation (day 3) on Polystyrene (PS), flat Ti disc, Titania nanotube (TNT/Ti), Chitosan-coated nanotube (TNT-CH) and Pluronic-F127-coated nanotubes (TNT-F127) based implants. There were significant (*) differences in cell number between the control and experimental surfaces with cultured suture cell derived from both the patients (fused and unfused sutures)

The cells from Patient 2 (both from fused and unfused sutures) reached confluency faster than those from Patient 1. The individual variations observed in the rate of proliferation in between the cell lines (data not shown) could be attributed to patient factors such as the severity/ syndrome of craniosynostosis, gender, age *etc*.

4. Conclusion

We evaluated the influence of surface topography and surface modification of electrochemically anodised TNTs/Ti implants on behavioral response of human suture mesenchymal cells extracted from two craniosynostosis patients undergoing a cranial reconstruction surgery. The experimental

data indicated that the nanotubular topography (large diameter) of anodised TNT surfaces led to overall reduction in cell adhesion and proliferation. A decrease in cell viability/number was observed due to insufficient focal contact formation and intergrin clustering on the large pore diameters on the top. Moreover, a thin coating on TNT/Ti implant surface using two different biopolymers (Chitosan and Pluronic-F127) also affected the cell behavior negatively, indicating the impact of surface chemistry on SMC viability. Both polymeric coatings impeded cell growth and activity by hindering initial protein adsorption, indicating that cell fate (morphology and function) can be modulated by controlling the implant topography and chemistry. Low cell adhesion and proliferation render this TNT-based implant suitable as a delivery system to reduce sutural bone growth as part of advanced craniosynostosis therapy. The polymeric coatings not only modulate the implant interactions with the cell environment but can also act as a biodegradable barrier to inculcate slow and sustained release of the loaded therapeutics. Future studies will involve a wide range of experiments, incorporating in vitro, pre-in vivo and in vivo studies (in wildtype and pathological murine model) to test the protein delivery potential of TNT/Ti implants for cranial bone inhibitory applications. If successful, the proposed therapy with TNT/Ti implants could significantly improve the quality of life of affected children by reducing the need for several surgical interventions and associated morbidity.

Acknowledgments

Appendix A. Supplementary data

The Supporting Information file provides specific details on the Materials and methods section, the contact angle images, SEM images showing various SMC features and an additional study involving confocal characterisation of murine osteoblasts on various implant surfaces.

References

1.   Wilkie, A.O., *Epidemiology and genetics of craniosynostosis.* American Journal of Medical Genetics, 2000. **90**(1): p. 82-83.

2.   Cunningham, M.L. and C.L. Heike, *Evaluation of the infant with an abnormal skull shape.* Current Opinion in Pediatrics, 2007. **19**(6): p. 645-651.

3.   Morriss-Kay, G.M. and A.O. Wilkie, *Growth of the normal skull vault and its alteration in craniosynostosis: insights from human genetics and experimental studies.* Journal of Anatomy, 2005. **207**(5): p. 637-653.

4.   Gosain, A.K., J.G. McCarthy, and J.H. Wisoff, *Morbidity associated with increased intracranial pressure in Apert and Pfeiffer syndromes: the need for long-term evaluation.* Plastic and Reconstructive Surgery, 1996. **97**(2): p. 292-301.

5.   Panchal, J. and V. Uttchin, *Management of craniosynostosis.* Plastic and Reconstructive Surgery, 2003. **111**(6): p. 2032-2048.

6.   Foster, K.A., D.M. Frim, and M. McKinnon, *Recurrence of synostosis following surgical repair of craniosynostosis.* Plastic and Reconstructive Surgery, 2008. **121**(3): p. 70e-76e.

7.   Kimonis, V., et al. *Genetics of craniosynostosis.* in *Seminars in pediatric neurology.* Elsevier, 2007. **14**(3): p. 150-161.

8.   Coussens, A.K., et al., *Identification of genes differentially expressed by prematurely fused human sutures using a novel in vivo–in vitro approach.* Differentiation, 2008. **76**(5): p. 531-545.

9.   Eufinger, H. and M. Wehmöller, *Individual prefabricated titanium implants in reconstructive craniofacial surgery: clinical and technical aspects of the first 22 cases.* Plastic and Reconstructive Surgery, 1998. **102**(2): p. 300-308.

10.   Moioli, E.K., et al., *Matrices and scaffolds for drug delivery in dental, oral and craniofacial tissue engineering.* Advanced Drug Delivery Reviews, 2007. **59**(4): p. 308-324.

11.   Losic, D., et al., *Titania nanotube arrays for local drug delivery: recent advances and perspectives.* Expert Opinion on Drug Delivery, 2015. **12**(1): p. 103-127.

12.   Santos, A., et al., *Drug-releasing implants: current progress, challenges and perspectives.* Journal of Materials Chemistry B, 2014. **2**(37): p. 6157-6182.

13.   Park, J., et al., *Narrow window in nanoscale dependent activation of endothelial cell growth and differentiation on TiO_2 nanotube surfaces.* Nano Letters, 2009. **9**(9): p. 3157-3164.

14.   He, J., et al., *The anatase phase of nanotopography titania plays an important role on osteoblast cell morphology and proliferation.* Journal of Materials Science: Materials in Medicine, 2008. **19**(11): p. 3465-3472.

15. Brammer, K.S., et al., *Improved bone-forming functionality on diameter-controlled TiO$_2$ nanotube surface.* Acta Biomaterialia, 2009. **5**(8): p. 3215-3223.

16. Gulati, K., et al., *Biocompatible polymer coating of titania nanotube arrays for improved drug elution and osteoblast adhesion.* Acta Biomaterialia, 2012. **8**(1): p. 449-456.

17. Huang, Q., et al., *Reduced platelet adhesion and improved corrosion resistance of superhydrophobic TiO$_2$-nanotube-coated 316L stainless steel.* Colloids and Surfaces B: Biointerfaces, 2015. **125**: p. 134-141.

18. Losic, D. and S. Simovic, *Self-ordered nanopore and nanotube platforms for drug delivery applications.* Expert Opinion on Drug Delivery, 2009. **6**(12): p. 1363-1381.

19. Gulati, K., et al., *Local drug delivery to the bone by drug-releasing implants: perspectives of nano-engineered titania nanotube arrays.* Therapeutic Delivery, 2012. **3**(7): p. 857-873.

20. Bariana, M., et al., *Radiofrequency-triggered release for on-demand delivery of therapeutics from titania nanotube drug-eluting implants.* Nanomedicine, 2014. **9**(8): p. 1263-1275.

21. Aw, M.S., J. Addai-Mensah, and D. Losic, *Magnetic-responsive delivery of drug-carriers using titania nanotube arrays.* Journal of Materials Chemistry, 2012. **22**(14): p. 6561-6563.

22. Aw, M.S. and D. Losic, *Ultrasound enhanced release of therapeutics from drug-releasing implants based on titania nanotube arrays.* International Journal of Pharmaceutics, 2013. **443**(1): p. 154-162.

23. SinnáAw, M., *A multi-drug delivery system with sequential release using titania nanotube arrays.* Chemical Communications, 2012. **48**(27): p. 3348-3350.

24. Gulati, K., et al., *Titania nanotubes for local drug delivery from implant surfaces*, in *Electrochemically Engineered Nanoporous Materials*. 2015, Springer. p. 307-355.

25.   Almeida, H., et al., *Pluronic® F-127 and pluronic lecithin organogel (PLO): main features and their applications in topical and transdermal administration of drugs.* Journal of Pharmacy and Pharmaceutical Sciences, 2012. **15**(4): p. 592-605.

26.   Kung, S., et al., *The osteoinductive effect of chitosan–collagen composites around pure titanium implant surfaces in rats.* Journal of Periodontal Research, 2011. **46**(1): p. 126-133.

27.   Coussens, A.K., et al., *In vitro differentiation of human calvarial suture derived cells with and without dexamethasone does not induce in vivo-like expression.* Journal of Cellular Physiology, 2009. **218**(1): p. 183-191.

28.   Coussens, A.K., et al., *Unravelling the molecular control of calvarial suture fusion in children with craniosynostosis.* BMC Genomics, 2007. **8**(1): p. 458.

29.   Dwivedi, P., et al., *Regulation of bone morphogenetic protein signalling and osteogenesis by glypicans in human cranial suture cells.* Bone, 2011. **48**: p. S243.

30.   de Pollack, C., et al., *Increased bone formation and osteoblastic cell phenotype in premature cranial suture ossification (craniosynostosis).* Journal of Bone and Mineral Research, 1996. **11**(3): p. 401-407.

31.   Park, J., et al., *TiO$_2$ nanotube surfaces: 15 nm—an optimal length scale of surface topography for cell adhesion and differentiation.* Small, 2009. **5**(6): p. 666-671.

32.   Park, J., et al., *Nanosize and vitality: TiO$_2$ nanotube diameter directs cell fate.* Nano Letters, 2007. **7**(6): p. 1686-1691.

33.   Tan, A., et al., *Review of titania nanotubes: fabrication and cellular response.* Ceramics International, 2012. **38**(6): p. 4421-4435.

34.   Brammer, K.S., C.J. Frandsen, and S. Jin, *TiO₂ nanotubes for bone regeneration.* Trends in Biotechnology, 2012. **30**(6): p. 315-322.

35.   Bacakova, L., et al., *Modulation of cell adhesion, proliferation and differentiation on materials designed for body implants.* Biotechnology Advances, 2011. **29**(6): p. 739-767.

36.   Anselme, K., *Osteoblast adhesion on biomaterials.* Biomaterials, 2000. **21**(7): p. 667-681.

37.   Oh, S., et al., *Stem cell fate dictated solely by altered nanotube dimension.* Proceedings of the National Academy of Sciences, 2009. **106**(7): p. 2130-2135.

38.   Das, K., S. Bose, and A. Bandyopadhyay, *TiO₂ nanotubes on Ti: influence of nanoscale morphology on bone cell–materials interaction.* Journal of Biomedical Materials Research Part A, 2009. **90**(1): p. 225-237.

39.   Oh, S., et al., *Significantly accelerated osteoblast cell growth on aligned TiO₂ nanotubes.* Journal of Biomedical Materials Research Part A, 2006. **78**(1): p. 97-103.

40.   So, S., K. Lee, and P. Schmuki, *Ultrafast growth of highly ordered anodic TiO₂ nanotubes in lactic acid electrolytes.* Journal of the American Chemical Society, 2012. **134**(28): p. 11316-11318.

41.   Mosmann, T., *Rapid colorimetric assay for cellular growth and survival: application to proliferation and cytotoxicity assays.* Journal of Immunological Methods, 1983. **65**(1): p. 55-63.

42.   Balasundaram, G. and T.J. Webster, *An overview of nano-polymers for orthopedic applications.* Macromolecular Bioscience, 2007. **7**(5): p. 635-642.

43.   Bumgardner, J.D., et al., *Chitosan: potential use as a bioactive coating for orthopaedic and craniofacial/dental implants.* Journal of Biomaterials Science, Polymer Edition, 2003. **14**(5): p. 423-438.

44.   Escobar-Chávez, J.J., et al., *Applications of thermo-reversible pluronic F-127 gels in pharmaceutical formulations.* Journal of Pharmacy & Pharmaceutical Sciences, 2006. **9**(3): p. 339-58.

45.   Diniz, I.M., et al., *Pluronic F-127 hydrogel as a promising scaffold for encapsulation of dental-derived mesenchymal stem cells.* Journal of Materials Science: Materials in Medicine, 2015. **26**(3): p. 1-10.

46.   Macak, J., et al., *TiO$_2$ nanotubes: self-organized electrochemical formation, properties and applications.* Current Opinion in Solid State and Materials Science, 2007. **11**(1): p. 3-18.

47.   Lavenus, S., et al., *Cell interaction with nanopatterned surface of implants.* Nanomedicine, 2010. **5**(6): p. 937-947.

48.   Kabaso, D., et al., *Mechanics and electrostatics of the interactions between osteoblasts and titanium surface.* Computer Methods in Biomechanics and Biomedical Engineering, 2011. **14**(05): p. 469-482.

49.   Minagar, S., et al., *Cell response of anodized nanotubes on titanium and titanium alloys.* Journal of Biomedical Materials Research Part A, 2013. **101**(9): p. 2726-2739.

50.   Yuan, Y., et al., *Mechanical property, degradation rate, and bone cell growth of chitosan coated titanium influenced by degree of deacetylation of chitosan.* Journal of Biomedical Materials Research Part B: Applied Biomaterials, 2008. **86**(1): p. 245-252.

51.   Shokuhfar, T., *Recent progress toward surface modification of bone/dental implants with titanium and zirconia dioxide nanotubes.* Journal of Nanotechnology and Smart Materials, 2014. **1**: p. 1-14.

52.   Bauer, S., et al., *Improved attachment of mesenchymal stem cells on super-hydrophobic TiO$_2$ nanotubes.* Acta Biomaterialia, 2008. **4**(5): p. 1576-1582.

53.   Brammer, K.S., et al., *Comparative cell behavior on carbon-coated TiO$_2$ nanotube surfaces for osteoblasts vs. osteo-progenitor cells.* Acta Biomaterialia, 2011. **7**(6): p. 2697-2703.

54.   Nikkhah, M., et al., *Engineering microscale topographies to control the cell–substrate interface.* Biomaterials, 2012. **33**(21): p. 5230-5246.

Supplementary Information

Materials and Methods

1) Materials

Titanium foil (99.6 % of Ti) with a thickness of 0.20 mm (Nilaco, Japan) was used as the implant substrate. Ethylene glycol, ammonium fluoride (NH_4F) and DL-Lactic acid were supplied by Sigma–Aldrich (Sydney, Australia). High-purity Milli-Q water, ultrapure grade (18.2 MΩ), was used for all the dilution and washing steps. Two different polymers, including chitosan (low molecular weight, low degree of acetylation) and Pluronic-F127 (PEO-PPO-PEO block copolymer), were obtained from Sigma–Aldrich (Australia) for surface coating on implants.

2) Fabrication of TNT/Ti implants

TNTs/Ti implants were fabricated from Ti discs by a two-step anodisation process using a specially designed electrochemical cell and computer-controlled power supply (Agilent, USA). Briefly, the discs were degreased by sonication in acetone, ethanol and isopropanol, followed by rinsing with Milli-Q water and drying with nitrogen gas. The first anodisation was carried out in ammonium fluoride/ethylene glycol/lactic acid electrolyte (5 % Milli-Q water, 0.1 M NH_4F and 1.5 M $C_3H_6O_3$ in $C_2H_4(OH)_2$) in a temperature-controlled bath at 60 ^{o}C and 120 V for 5 min. Subsequently, the deposited TNT layer was delaminated and the second anodisation was carried out under similar conditions at 120 V to yield a vertically aligned array of TNTs. The anodisation parameters were adjusted and continuously monitored (Labview, National Instruments) during the fabrication process to assure repeatability. All experiments were conducted using the TNT/Ti implants prepared under same conditions.

3) Sterilisation of TNT/Ti implants

The fabricated implants (each sample in triplicate) were placed individually in the wells of a 96-well plate, followed by UV irradiation for 30 min before culturing the cells onto their surfaces as described in our earlier work (16, 24). The UV-sterilisation method provided effective cleaning by decreasing the hydrocarbon contamination (from the anodization), without altering or damaging the TNT surface structure (as in case of high-temperature autoclaving) [1-3]. This method was deemed suitable for the present study since the nanotubes were empty (did not contain active protein) and the photocatalytic degradation of protein molecules was irrelevant. For separate release studies involving protein-loaded TNTs, a low-temperature hydrogen peroxide gas plasma technology has been deemed suitable.

4) Human suture mesenchymal cell (SMC) culture

The dissected suture samples from the two patients were minced into 1 mm fragments and incubated in 0.25% collagenase for 2 h at 37°C, followed by centrifugation and washing with PBS. Cells were then plated in 12-well plates containing minimal medium consisting of high glucose, Dulbecco's modified essential medium (DMEM, Invitrogen Life Technologies, MD, USA), supplemented with L-Glutamine (584 mg/l), 10% foetal bovine serum (Invitrogen, Carlsbad, CA, USA), 1% antibiotics (penicillin 100 IU/ml), Streptomycin (100 μg/ml) and 1% antibiotic:antimycotic (Sigma-Aldrich, MI, USA) and were incubated at 37 °C in a humidified atmosphere with 5% CO_2 in air. Upon confluence, cells were plated into T25 flasks and were used between P3 and P7.

Results

5) Water Contact angle (WCA) measurements

The surface wettability of different substrates (Ti unannealed, Ti annealed, TNT, TNT-CH and TNT-F127) was estimated using contact angle analysis. The corresponding images to the data presented in **Table 1**, recorded from the video at the initial measurement (t=0) and the final measurement (t=f), are shown in **Fig. S1.** The value of contact angle for each substrate was calculated as the average value of 121 measurements over a period of 5.00 ± 2.92 s. The images show a decrease in droplet height and contact angle with time for the nanotubular implants (with and without polymer). The control Ti surfaces showed minimal changes in droplet height, hence the final images (t=f) are not shown.
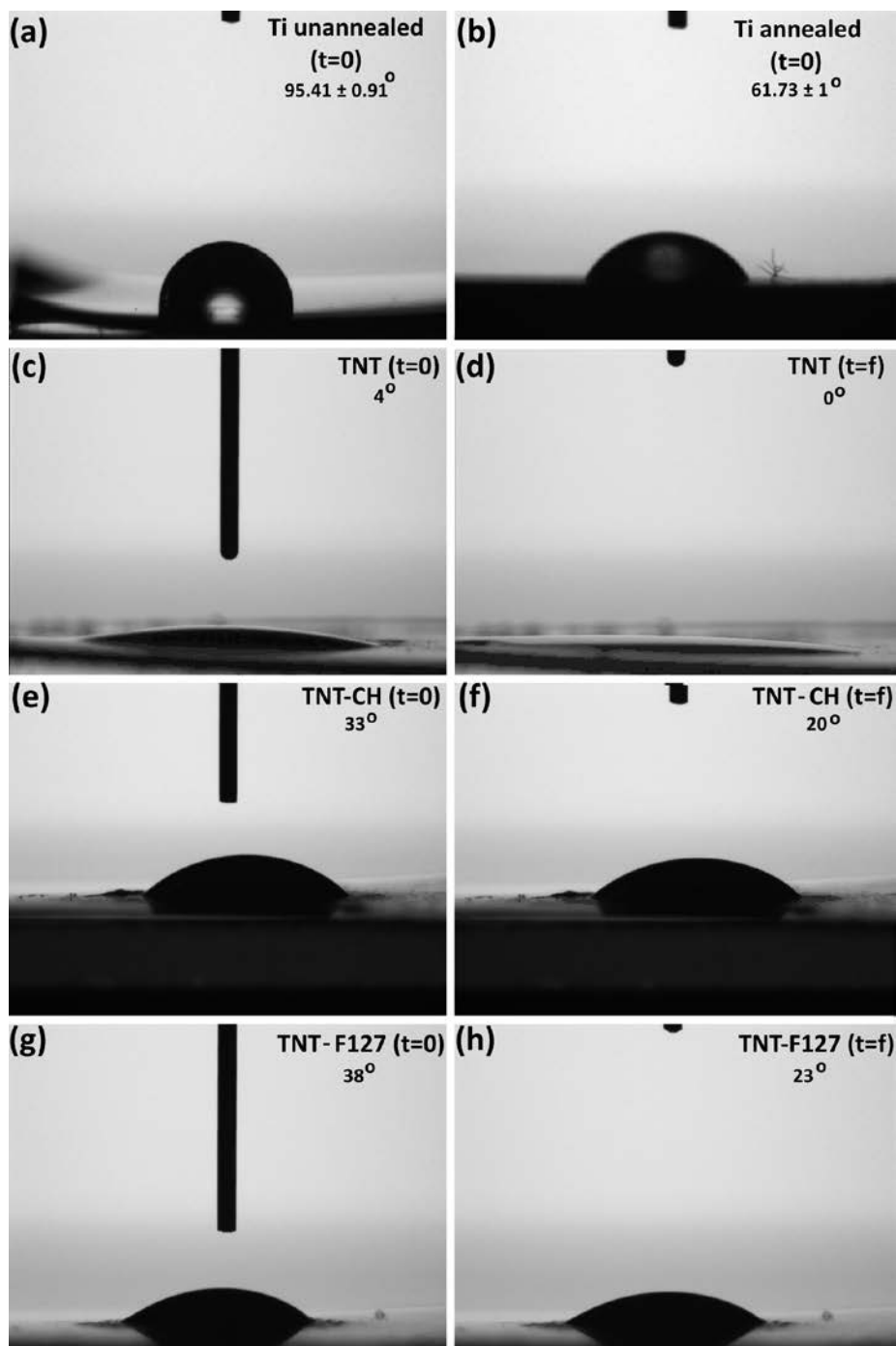
Fig. S1. The water contact angle (WCA) slides from the video for different implant surfaces. (t=0 – initial WCA and t=f (5.00 ± 2.92 s) - final WCA at the end of the measurement. (a)Ti unannealed (95.41 ± 0.91), (b) Ti annealed (61.73 ± 1), (c,d) TNT (4 ± 0.6), (e,f) TNT-CH (30.71 ± 1.51) and (g,h) TNT-F127(31.36 ± 3.5).

5) SEM-based SMC characterisation

Since the SMCs were extracted from the fused and unfused calvarial sutures of two different craniosynostosis patients, the tissue milieu was a heterogeneous mixture of bone cells at different levels of differentiation. The SEM micrographs revealed that the cultured cells included osteoprogenitor cells as well as pre-osteoblasts and osteoblasts. **Fig. S2** shows the characteristic cell features common to the three repeated sets of imaging studies done in the absence of an osteogenic media at different passage numbers.
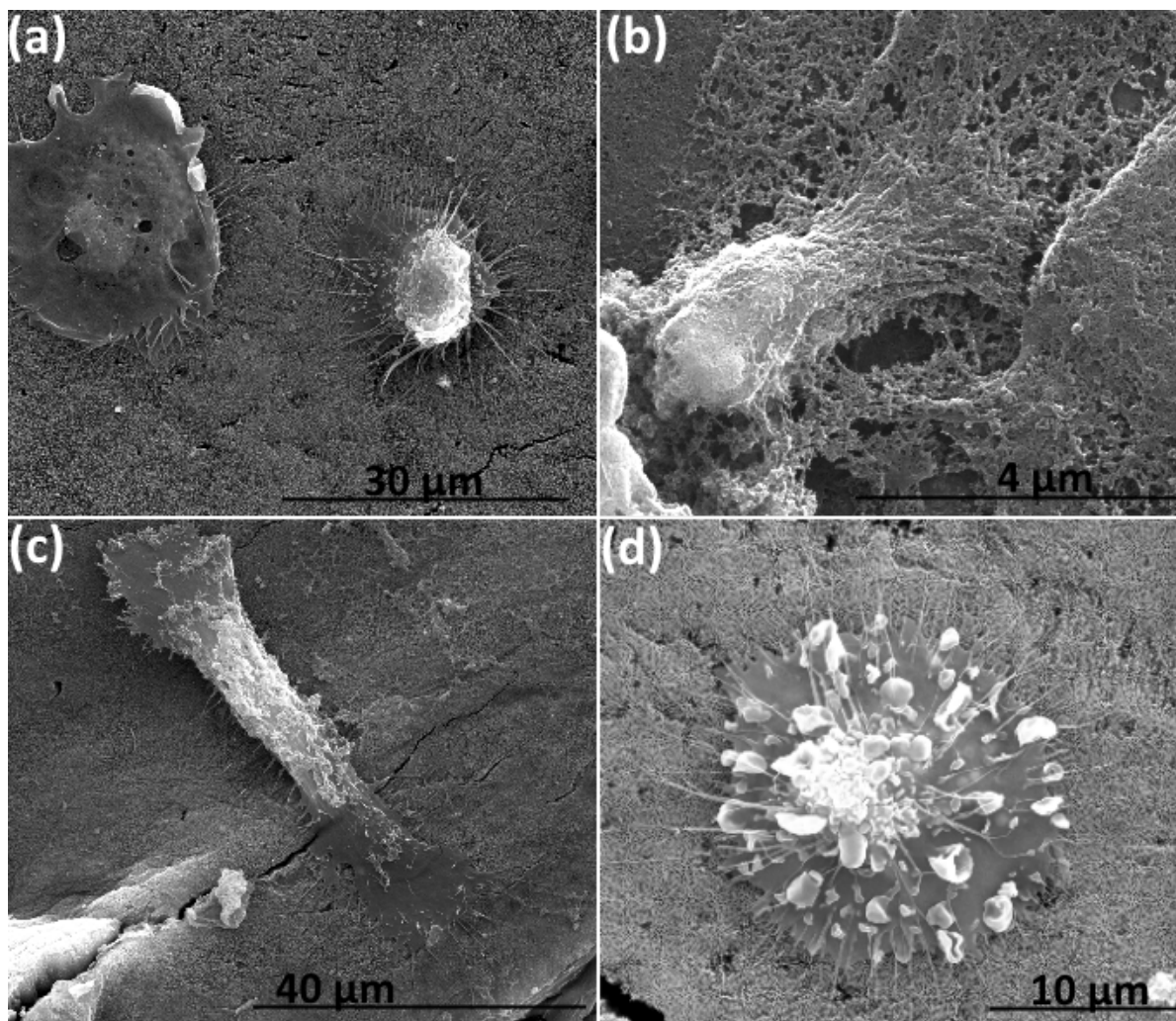
Fig. S2. SEM micrographs of cultured SMCS on TNT/Ti implants (prepared under the same conditions). (a) A typical example of SMC culture showing a flattened osteoprogenitor cell and the transformed pre-osteoblast with protrusions from the cellular body, (b) A cell secreting ECM, (c) An extended cell nucleus with high cytoskeletal stress which might undergo differentiation or anoikis depending on the presence or absence of an osteogenic media and (d) A typical apoptotic cell on TNT surface.

Additional study

7) Osteoblast morphology characterisation by confocal microscopy

Osteoblast cell morphology was assessed by using a previously described method [4]. It involved incubation of the cells on various implant surfaces [including control flat Ti disc, TNT/Ti (with 120 nm diameter) and TNTs coated with Chitosan (TNT-CH)] for 24 h, prior to fixing the osteoblasts (in 4% paraformaldehyde/PBS, 20 min) and blocking the samples with goat serum (2.5% in PBS for 1 h). This was followed by permeabilisation with Triton X-100 (0.5 % in PBS) for 5 min and labelling with Phalloidin-TRITC (10µg/ml in PBS) at room temperature in the dark for 1 h. Then the cells were thoroughly washed with PBS and incubated with DAPI (4′,6-diamidine-2′-phenylindoledihydrochloride) (1 µg/ml in methanol) for 10 min. The samples were washed in PBS, mounted in glycerol (50 % in PBS) and examined by confocal microscopy. The images showed cellular actin filament networks stained with phalloidin (red) and nuclei stained with DAPI (blue). **Fig. S3** shows variations in osteoblast morphology in relation to attachment and spreading according to the surface property and topography of TNT/Ti implants. These trends are similar to those shown by SMCs in our current study, with control Ti surface promoting enhanced cell adhesion and flattening and the uncoated and chitosan-coated TNT/Ti surfaces displaying impaired cell attachment and limited spreading.
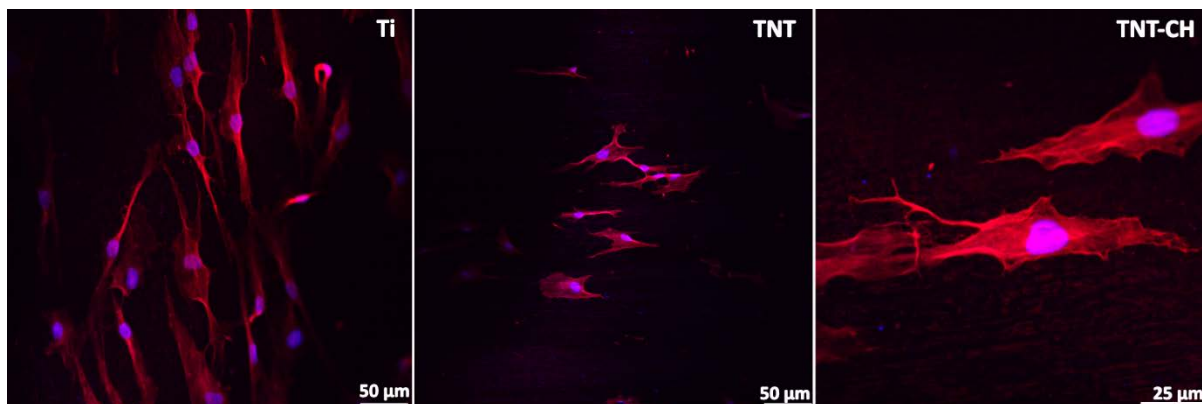
Fig. S3 *Confocal microscopy images showing the variations in the osteoblast morphology relating to attachment and spreading on different implant surface; Ti = Titanium surface, TNT = Titania nanotubes and TNT-CH = Chitosan-coated Titania nanotubes [Phalloidin (red, cytoskeleton) and DAPI (blue, nuclei) stained].*

Additional references

1.   I. Junkar, et al., Influence of various sterilization procedures on TiO_2 nanotubes used for biomedical devices. *Bioelectrochem*. **109**, 2016, 79-86.

2.   L. Zhao, et al., The role of sterilization in the cytocompatibility of titania nanotubes. *Biomaterials*. **31**(8), 2010, 2055-2063.

3.   W. Att, et al., The effect of UV-photofunctionalization on the time-related bioactivity of titanium and chromium–cobalt alloys. *Biomaterials*. 2009. **30**(26), 2009, 4268-4276.

4.   G.J. Atkins, et al., The induction of a catabolic phenotype in human primary osteoblasts and osteocytes by polyethylene particles. *Biomaterials*. **30**(22), 2009, 3672-3681.

CHAPTER 6

GLYPICAN-BASED DRUG RELEASING TITANIA IMPLANTS TO REGULATE BMP2 BIOACTIVITY AS A POTENTIAL APPROACH FOR CRANIOSYNOSTOSIS THERAPY

This chapter is based on the following article submitted to Nanomedicine: Nanotechnology, Biology and Medicine:

Manpreet Bariana, Prem Dwivedi, Sarbin Ranjitkar, John A. Kaidonis, Dusan Losic, Peter J. Anderson, " Glypican-based drug releasing titania implants to regulate BMP2 bioactivity as a potential approach for craniosynostosis therapy".

Statement of Authorship

Title of Paper	Glypican-based drug releasing titania implants to regulate BMP2 bioactivity as a potential approach for craniosynostosis therapy.
Publication Status	☐ Published ☐ Accepted for Publication ☑ Submitted for Publication ☐ Unpublished and Unsubmitted work written in manuscript style
Publication Details	Nanomedicine: Nanotechnology, Biology and Medicine (submitted November, 2016)

Principal Author

Name of Principal Author (Candidate)	Manpreet Bariana		
Contribution to the Paper	Under supervision of P. Dwivedi, S. Ranjitkar, J.A. Kaidonis, D. Losic and P.J. Anderson, I developed, designed, and performed the experiments, interpreted and processed the data and wrote the manuscript for submission.		
Overall percentage (%)	80		
Certification:	This paper reports on original research I conducted during the period of my Higher Degree by Research candidature and is not subject to any obligations or contractual agreements with a third party that would constrain its inclusion in this thesis. I am the primary author of this paper.		
Signature		Date	21/11/2016

Co-Author Contributions

By signing the Statement of Authorship, each author certifies that:

    I.   the candidate's stated contribution to the publication is accurate (as detailed above);

    II.   permission is granted for the candidate in include the publication in the thesis; and

    III.   the sum of all co-author contributions is equal to 100% less the candidate's stated contribution.

Name of Co-Author	Prem Dwivedi		
Contribution to the Paper	I helped the candidate with the cell culture experiments, including transfection and DLR assay. I give consent for Manpreet Bariana to present this paper for examination towards the Doctorate of philosophy		
Signature		Date	21/11/2016

CHAPTER 6: M. Bariana, P. Dwivedi, S. Ranjitkar, J. Kaidonis, D. Losic, P.J. Anderson , "Glypican-based drug releasing titania implants to regulate BMP2 bioactivity as a potential approach for craniosynostosis therapy", Nanomedicine: Nanotechnology, Biology and Medicine, 2016 (Under review)

Name of Co-Author	Sarbin Ranjitkar		
Contribution to the Paper	I acted as secondary supervisor for the candidate and aided in statistical analysis, editing and evaluation of manuscript for submission. I give consent for Manpreet Bariana to present this paper for examination towards the Doctorate of philosophy.		
Signature		Date	21/11/2016

Name of Co-Author	John Kaidonis		
Contribution to the Paper	I acted as secondary supervisor for the candidate and aided in development and design of the experiments and evaluation of manuscript for submission. I give consent for Manpreet Bariana to present this paper for examination towards the Doctorate of philosophy.		
Signature		Date	21/11/2016

Name of Co-Author	Dusan Losic		
Contribution to the Paper	I acted as secondary supervisor for the candidate and aided in nanoengineered implant fabrication and evaluation of manuscript for submission. I give consent for Manpreet Bariana to present this paper for examination towards the Doctorate of philosophy.		
Signature		Date	21/11/2016

Name of Co-Author	Peter J. Anderson		
Contribution to the Paper	I acted as primary supervisor of the candidate and aided in evaluation of experimental design and manuscript for submission. I give consent for Manpreet Bariana to present this paper for examination towards the Doctorate of philosophy.		
Signature		Date	21/11/2016

Glypican-based drug releasing titania implants to regulate BMP2 bioactivity as a potential approach for craniosynostosis therapy

Manpreet Bariana, MTech[a], Prem Dwivedi, PhD[b], Sarbin Ranjitkar, PhD[a], John A. Kaidonis, PhD[a*], Dusan Losic, PhD[c]*, Peter J. Anderson, DSc,[a,b,d]*

- a- School of Dentistry, The University of Adelaide, Adelaide, SA 5005, Australia

  E-mail: manpreet.bariana@adelaide.edu.au; sarbin.ranjitkar@adelaide.edu.au; john.kaidonis@adelaide.edu.au

- b- Women's and Children's Hospital, 72 King William St, Adelaide, SA 5006, Australia

  E-mail: prem.dwivedi@adelaide.edu.au

- c- School of Chemical Engineering, The University of Adelaide, Adelaide, SA 5005, Australia

  E-mail: dusan.losic@adelaide.edu.au

  Telephone: +61 8 8313 4648

- d- Australian Craniofacial Unit, 72 King William St, Adelaide, SA 5006, Australia

  E-mail: haemro2@hotmail.com

  Telephone: +61 8 8161 7235; Fax: +61 8 8161 7080

Abstract word count: 146

Complete manuscript word count: 4419

Number of references: 60

Number of figures/tables: 6

Abstract

Advances in molecular biology and nanomedicine based therapies hold promise to obviate the need of multiple surgical interventions (associated with current management) in craniosynostosis by preventing bone re-ossification. One such adjunctive therapy involves application of glypicans 1 and 3 (GPC1 and GPC3) that are BMP inhibitors implicated in downregulating the BMP2 activity in prematurely fusing sutures. Electrochemically anodized Titania nanotube (TNT) arrays have been recognized as a promising localized, long-term drug delivery platform for bone-related therapies. This study presents the application of nanoengineered TNT/Ti implants loaded with recombinant glypicans towards targeting craniofacial disorders. By using Dual luciferase Reporter assay, we tested the biofunctionality of eluted glypicans from the TNT/Ti implants for BMP2 bioactivity regulation in C2C12 murine myoblast cell line. BMP2 activity was inhibited significantly for up to 15 days by the glypicans released from polymer-coated TNT/Ti implants, indicating their potential application in adjunctive craniosynostosis treatment.

Keywords: craniosynostosis, titania nanotubes, bone morphogenetic proteins, glypicans, drug delivery systems

Background

Craniosynostosis is a developmental disorder, characterized by pathologic premature fusion of cranial sutures in around 1 in 2500 live births.[1,2] Cessation of skull growth at the obliterated suture can be associated with severe sequelae, including raised intracranial pressure, impaired cerebral blood flow, airway obstruction, impaired hearing and vision, abnormal head shape, asymmetric facial features *etc*.[1-3] The current treatment involves complex cranial vault remodeling surgery, which may require repetitive interventions to accommodate the growing brain.[4,5] The potential morbidity and complications associated with the current management necessitate the development of a non-surgical, adjunctive molecular therapy to regulate cranial bone growth.

Although the exact pathophysiology of suture obliteration remains unclear, advancements in molecular biology and availability of gene analysis tools and genetically-engineered animal models have unraveled the underlying molecular control mechanisms of suture morphogenesis and pathogenesis.[6-8] Members of the transforming growth factor-beta (TGF-beta) superfamily, including bone morphogenetic proteins (BMPs), are potent bone inducers and mutations in BMP signaling pathway (in perisutural region) have been associated with craniosynostosis.[9-11] Thus, it is likely that the osteogenic BMP pathway can be manipulated to treat craniofacial anomalies. BMP activity is stringently controlled via a complex interplay of intracellular and extracellular regulatory molecules. Bone antagonising proteins, such as glypicans (GPCs) and noggin, can act as potential therapeutic agents for controlling the rate of bone growth, by downregulating the BMP osteogenic activity.[3,12,13] Noggin has been found to inhibit BMP-dependent bone formation in different animal models, but its effects were short-term and restricted to initial phases of bone healing.[14,15] This has led to exploration of other bone antagonizing proteins including, glypicans (a six membered family of heparan sulphate

proteoglycans). Glypicans (GPC1 and GPC3) have been mechanistically linked to sequester the BMP2 ligands or directly bind to the receptors, thereby inhibiting BMP2-mediated bone mineralization.[3,13,16,17] In skull sutures, GPC1/GPC3 expression in mesenchymal cells controls the BMP2 activity and the GPC1-GPC3-BMP axis synergistically regulates skull growth.[3] Therefore, controlled local delivery of GPCs over the operative site may help improve the surgical outcomes.

A major challenge in developing the glypican-based adjuvant therapy is to provide a long-term sustained delivery of these bioactive proteins at the site of administration in optimal concentrations.[12,15] Localized and temporally controlled release of these proteins are limited by their large molecular size and short half-lives.[12] So far, the localized administration of the therapeutic proteins into the craniofacial regions has been explored either directly using a carrier (polymer-based microspheres, hydrogels, and implants, lipid nanoparticles, ceramics, titanium fiber-mesh or porous glass) or indirectly using gene based therapies (both viral and non-viral vectors).[15,18] Nonetheless, they lack therapeutic efficacy due to undesired pharmacokinetics and uncontrolled release patterns, and/or are too complex to formulate.[12,18] Some of the collagen-based vehicles have also been shown to promote osteogenesis in rat cranial defects, making them unsuitable for bone inhibiting applications.[19]

Localized drug delivery systems (LDDSs) based on nanoengineered titanium (Ti) implants have recently emerged as a promising strategy to treat complex bone pathologies.[20-22] These drug-releasing implants made of Titania nanotubes (TNTs) fabricated on Ti surface by a simple, self-ordering electrochemical process have several advantages over conventional delivery systems, including outstanding structural properties, excellent biocompatibility, high *in vivo* chemical stability, tailorable drug loading, controllable therapy-specific release characteristics (*i.e.* slow and extended, delayed, multi-drug or externally triggered release) and

easy surgical implantation.[23-30] Furthermore, TNTs can be fabricated on any 3D non-planar or curved Ti surfaces, making them easily adaptable to current implant technology.[31]

While the drug delivery potential of these TNT on Ti implants (TNT/Ti implants) has been extensively explored for local delivery of antibiotic, anti-inflammatory, chemotherapeutic, anabolic and antiresorptive agents in orthopedic applications and bone therapies (*e.g.* bone repair, infections, bone cancer, osteomyelitis, *etc*.), it has yet not been considered for treatment of craniofacial and cytoskeletal disorders (via protein delivery).[21,32-37] Proteins are generally high molecular weight, hydrophilic macromolecules with intrinsic physical and chemical lability/instability in most conditions, which makes them difficult to administer than conventional low molecular weight robust drugs.[38] Only a handful of studies on TNT-based protein delivery exist in the literature that controlled the protein release dynamics whilst protecting the loaded sensitive molecules against protein unfolding, deactivation or precipitation.[39-42] The aforementioned properties and applications of TNT-based implants make them suitable candidates to be tested for glypican encapsulation and localized delivery. However, simple physical entrapment of the molecules within the nanotubes may lead to a high initial burst and shorter release periods. To overcome this, biopolymer coatings (chitosan or PLGA) have been proposed to extend the duration of drug elution.[29,33]

Application of nanoengineered TNT/Ti-based drug eluting implants towards developing a molecular adjuvant to existing surgical techniques in craniosynostosis therapy will require a wide range of *in vitro* and *in vivo* studies. In this paper, we present (i) an improved fabrication design to modify the TNT/Ti implants for bone-inhibiting protein delivery applications, (ii) first *in vitro* study using murine C2C12 cell line to evaluate the effectiveness of chitosan-coated TNT/Ti implants for localized release of recombinant glypicans (rGPC1 and rGPC3) either independently or synergistically (rGPC1+3) in phosphate buffer (PBS, pH 7.4) and (iii) second

in vitro study to assess the functionality of the released exogenous recombinant glypicans for BMP2 bioactivity regulation in C2C12 cells.

It was hypothesized that recombinant glypicans (bone antagonising proteins) released from TNT/Ti implants would downregulate the BMP2 osteogenic activity throughout the release duration. The electrochemically prepared TNT/Ti implants were loaded with the model proteins (experimental- rGPC1, rGPC3 and rGPC1+3, and control- FITC-BSA) and surface-coated with chitosan to extend the release duration. The released proteins from the implants were quantified spectrophotometrically and tested in easily transfected C2C12 murine myoblast cell line to modulate BMP2 signaling. A genetic reporter assay (Dual luciferase reporter assay) involving an experimental plasmid construct (consisting of BMP2-reponsive element fused experimental reporter) and a control reporter plasmid vector was used to evaluate the protein bioactivity.[43] The released recombinant glypicans were expected to suppress the luciferase activity (measured via luminometer) in the transfected C2C12 cells. In absence of inhibitory molecules, these cells can undergo BMP2-mediated differentiation in an osteogenic medium and mimic ectopic bone formation.[44,45] The schematic of GPC release from TNTs and BMP2 signaling/inhibition in transfected C2C12 cells is shown in **Figure 1**.
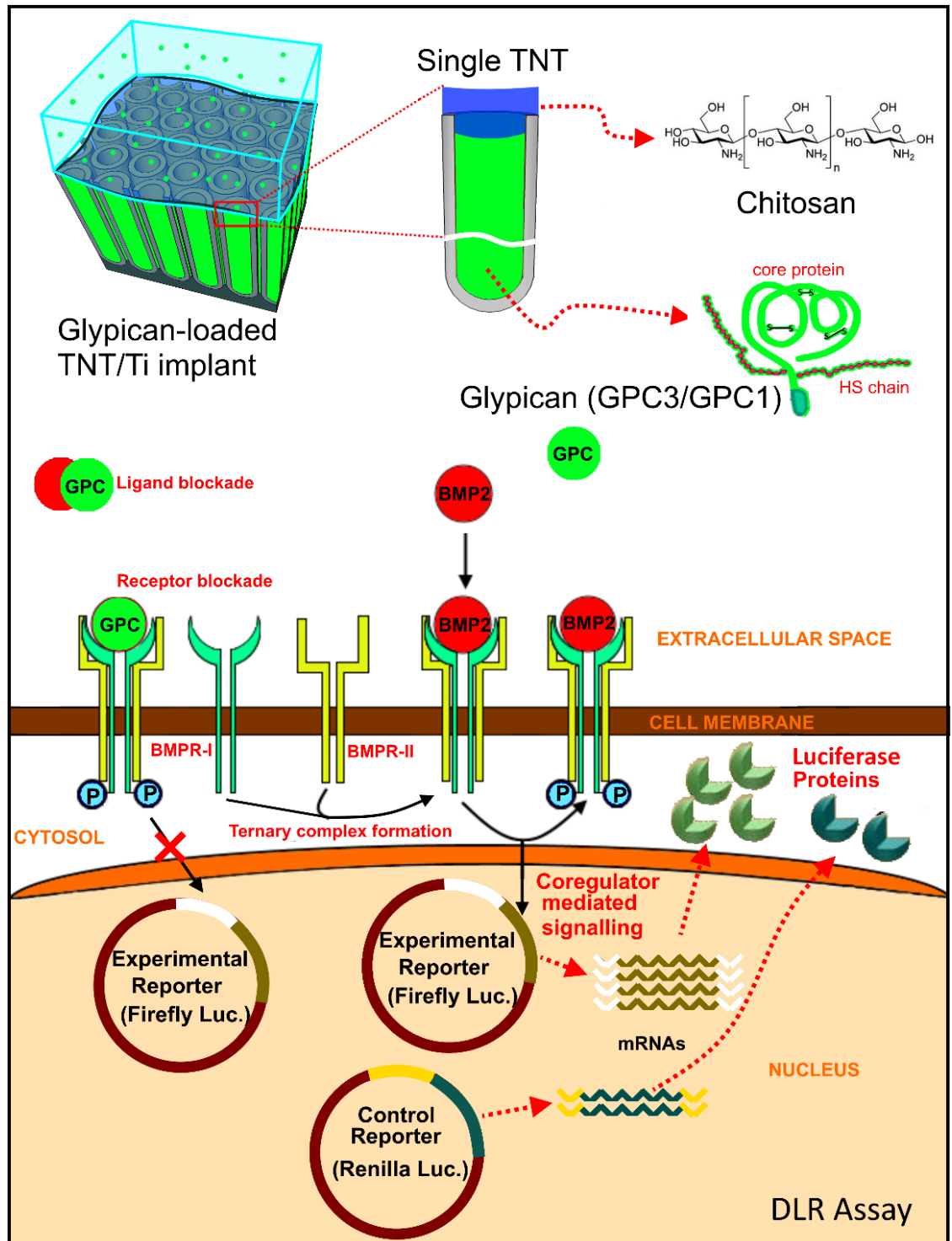
Figure 1. Schematic showing the release of glypican (GPC)- based protein therapeutics from

chitosan-coated TNT/Ti implants, and their impact on the BMP signaling cellular pathway

involving glypican-mediated inhibition detected by Dual luciferase reporter (DLR) assay (in C2C12 cells transfected with BMP-responsive and control luciferase constructs).

Methods

TNT Fabrication

The Titanium foil (Nilaco, Japan) was mechanically polished and cleaned by sonication and cut in 3 mm circular discs via ultrasonic milling (using DMG Ultrasonic 20 linear). TNT arrays were fabricated by modified two-step electrochemical anodization in lactic acid containing organic electrolyte (comprising of Ethylene glycol, ammonium fluoride and DL-Lactic acid (Sigma-Aldrich, Australia).[46] The first anodization was carried out in a temperature-controlled bath at 60 $^{\circ}$C and 120 V for 5 min. Subsequently, the deposited TNT layer was removed by sonication in methanol and the second anodization was carried out under similar conditions to obtain TNT/Ti implants. The voltage-current-time parameters were continually recorded (Labview, National Instruments) during the anodization to ensure repeatability and reproducibility of the fabrication method. For morphological characterization, a field-emission scanning electron microscope (SEM, FEI Quanta 450, The Netherlands) was used and the thickness of the nanotubes was measured at an angle from SEM cross-sections.

Protein loading and *in vitro* release

TNT/Ti implants were loaded with recombinant glypicans [rGPC1, rGPC3, rGPC1+3 (1:1)], obtained from R&D systems (USA) and FITC-Labelled BSA (as control) from Sigma–Aldrich (Australia) using vacuum drying technique. A 10 µl drop of respective protein was pipetted onto each surface and gently spread to ensure even coverage. The surfaces were then allowed to dry under vacuum at room temperature for 2 h. After drying, the loading step was repeated

on dried samples until an appropriate amount of protein was present in the TNT pores (5 µg/sample). The protein-loaded implant surfaces were then coated with chitosan (Sigma–Aldrich, Australia), to prolong the release. Polymer solution of chitosan (2% (w/v), chitosan + 0.8 vol. % acetic acid in deionized water) was spin-coated onto the protein-loaded TNT surfaces at 1500 rpm for 15 s and the layers were also vacuum dried for 2 h. TNTs without any protein served as a negative control in each experiment.

To check the *in vitro* release profile, these samples were then immersed in 500 µl of PBS at room temperature in capped eppendorf tubes. The amount of eluted protein was measured at day 1, 8 and 15 by removing the buffer with protein and replacing it with fresh PBS each time. The FITC-Labelled BSA released from the TNTs was analyzed directly by using a fluorimeter (λ_{em}= 516 nm and λ_{ex} = 435 nm). To measure the amount of released glypicans (GPCs), a FluoroProfile® Protein Quantification Kit (Sigma–Aldrich, USA) was employed to label the proteins and obtain a fluorescent signal (λ_{em}= 620 nm and λ_{ex} = 510 nm). Since the fluorescence intensity is directly proportional to protein concentration, the unknown released protein concentrations were calculated against the calibration curve. Rest of the protein solutions of known concentrations were stored for the cell studies while the release continued.

Cell culture and plating

C2C12 murine myoblast cells (obtained from Prof. Murray Whitelaw, School of Biomedical Sciences, the University of Adelaide, South Australia) were maintained in T75 cm^2 flask containing minimal medium consisting of high glucose, Dulbecco's modified essential medium (DMEM, Invitrogen, USA), supplemented with L-Glutamine (584 mg/l), 10% fetal bovine serum (Invitrogen, USA), 1% antibiotics (penicillin 100 IU/ml), Streptomycin (100 µg/ml) and

1% antibiotic:antimycotic (Sigma-Aldrich, USA) and were incubated at 37 °C in a humidified

incubator with 5% CO_2 in air. The confluent cells were then trypsinized by adding 2 ml

of warm 1X Trypsin-EDTA (Sigma-Aldrich, USA) and incubated for a minute to detach them

from the plate bottom. Then, they were suspended in fresh media, transferred into a tube and

centrifuged at 1200 rpm for 5 min and the pellet was resuspended in fresh media. The cells were

stained with trypan blue and manually counted using a haematocytomter and plated in a 24-

well plate at the density of 10,000 cells/well and grown in 400 µl of minimal medium.

Cell transfection and treatment

 Transfection-grade plasmids were prepared, purified (using Qiagen Plasmid midi kit, USA)

and their integrity was confirmed by 1% agarose gel electrophoresis (data not shown). To

generate BMP reporter cells, C2C12 cells were transiently transfected with *pID183-Luc* (Firefly

Luc.) and control plasmid, *pRLTK-Luc* (Renilla Luc.). Briefly, C2C12 cells (10,000 cells/well)

were seeded in a 24-cell plate and were allowed to attach overnight. After 24 h they were

transfected using two different transfection agents, Fugene HD and DNA (2:1, 4:1) and

Lipofectamine 3000 (both obtained from ThermoFisher, USA), to test BMP2 activity. The

Fugene HD and DNA (2:1) ratio was selected for transfection after carrying out a test BMP2

reporter assay in C2C12 cells. For each transfection, 1 µl of 200ng of the BMP responsive

promoter luciferase construct *pID183-Luc* (5.78kb) was mixed with 23 µl of DMEM medium

in an eppendorf tube together with 1 µl of 50ng of *pRLTK-Luc* construct (4.05 kb). In all

transfections, the final amount of DNA was kept constant by addition of the appropriate empty

vector plasmid.

In another tube, 0.5 µl of Fugene HD was diluted to 25 µl in DMEM medium and mixed

with 25 µl of diluted DNA plasmids. After incubation for 30-45 min at room temperature for

DNA-Fugene HD complex formation, the complex was aliquoted into each well of a 24-well plate and incubated at 37 °C. The next day the media was replaced with 400 µl serum-free medium containing BMP2 (100ng/well) on one half and no BMP2 on the other, along with the proteins (rGPC1, rGPC3, rGPC1+3 and FITC-BSA) released from Titania nanotube implants (diluted from the original concentration to 40 ng/well) and negative control (chitosan-coated TNTs). The pristine form of recombinant GPCs (control, day 0) was initially tested to confirm the BMP2 regulation.

Cell lysis and Dual luciferase Reporter (DLR) Assay

The Dual luciferase activity in cell lysates was determined by the DLR assay kit (Dual-Luciferase® Reporter Assay System - Promega) employing the manufacturer's protocol, using a luminometer model TD 20/20 (Turner Design Instruments, Sunnyvale, CA).[47] Initially, the media from cells cultured for 24 h in the presence of specific inhibitors was discarded followed by washing with sterile PBS. 100 µl of 1X Passive lysis buffer (PLB) was added into each well and a lysate was obtained by incubating the plates at 37 °C for 20-30 min. The lysis was observed under optical microscope and the lysate was frozen at -20 °C for minimum of 24 h. This was followed by pre-dispensing 25 µl of Luciferase Assay Reagent II (LAR II) reagent into the desired wells. Then, 20 µl of PLB lysate/well was transferred into the luminometer wells containing LAR II and mixed by pipetting up and down 2-3 times. The firefly luciferase activity was measured by initiating the luminometer for first reading. This was followed by automated injection of 25 µl of Stop & Glo® Reagent, initiating a reading for the Renilla luciferase activity. This cycle was repeated for all the wells in the plate. The results were expressed as relative luciferase unit (RLU), which is the ratio of firefly and Renilla Luciferase activity, to eliminate variations in luciferase expression between different sets. All assays were

performed in triplicate and repeated at 3 different time points corresponding to day 1, 8 and 15 of TNT-protein release.

Unpaired t-tests and One-way ANOVA were conducted to validate the transfection efficiency and to check for significant changes in luciferase expressions within different groups on each day. Multiple comparison tests/longitudinal analysis were not performed as the transiently transfected cells could show varied degree of rBMP2 cell receptors (induced rBMP2 binding and activity) at different time points.

Results

Fabrication and characterization of TNT/Ti implants

The morphology of the prepared TNT/Ti implants before and after coating with chitosan was characterized by FE-SEM and is summarized in **Figure 2**. The images of the top surface of uncoated TNT/Ti samples show the upper (open) ends of TNTs with an average diameter of 120 ± 10 nm (Figure 2A). A typical cross-sectional image of the free-standing nanotubes, removed from the Ti substrate (for imaging purposes only), is presented in Figure 2B. The total thickness/length of the layer was approximately 35 µm, which can be varied by changing the anodization time to optimize the protein loading capacity. Figure 2C presents the lower (closed) end of densely packed arrays of TNTs.

The color-processed images highlighting the chitosan spin-coated on the top of protein-loaded TNT surface are depicted in Figure 2D-F. The polymer forms a thin layer completely covering the nanopores to provide a barrier to diffusion of the loaded protein molecules during release (Figure 2D). The cross-sectional images at high and low magnifications are presented in Figure 2E-F. These images display vertically aligned, highly ordered, and densely packed arrays of TNTs with an estimated 1 µm thick chitosan coating on the top. The polymer layer

thickness can be manipulated by controlling the chitosan concentration and spin-coating parameters.
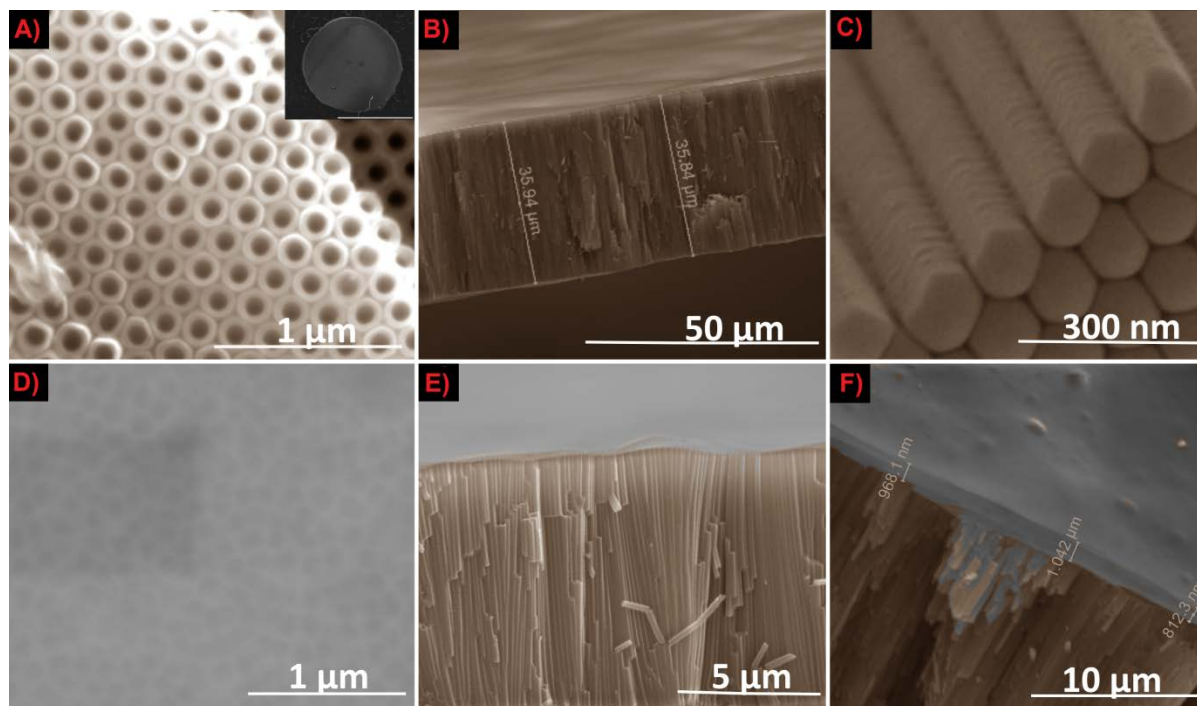
Figure 2. SEM images of TNT/Ti fabricated by electrochemical anodization of Ti in Lactic acid electrolyte at 120 V for 5mins. The top panel shows the uncoated TNT/Ti substrates with (A) the TNT surface having an open nanotubular structure (inset: the TNT/Ti implantable disc, scale: 2 mm), the angled cross-section showing (B) straight, high-aspect ratio TNTs across the whole length and (C) the closed bottom surface. The bottom panel displays the top (D) and (E-F) angled cross-sectional images of spin-coated chitosan layer covering the nanopores along with the polymer layer thickness (~1 µm).

Protein release studies

The protein release profiles for recombinant glypicans (rGPC1, rGPC3 and rGPC1+3) and the control protein (FITC-BSA) loaded into chitosan-coated TNT/Ti implants was established using a fluorescent spectrophotometer. **Figure 3** shows the comparative protein release biphasic

pattern including, the burst phase over first 6 h and a subsequent slower overall release. **Table 1** lists the corresponding release characteristics extracted from these profiles, summarizing the release efficiency (protein release %) at different time points (6 h, 24 h, 7 d and 14 d) and the total duration of the release for different samples. The burst release (t_B) was calculated at 6 h for all cases, while the midpoint signifying the elution of half the amount of loaded protein (t_{50}) from the TNT nanopores was recorded at less than a day for uncoated samples and 3-6 d for chitosan-coated samples, respectively. The glypican release period from uncoated TNT/Ti implants was short (4-5 d), hence the samples were excluded from the cell study experiments (graphs not shown).
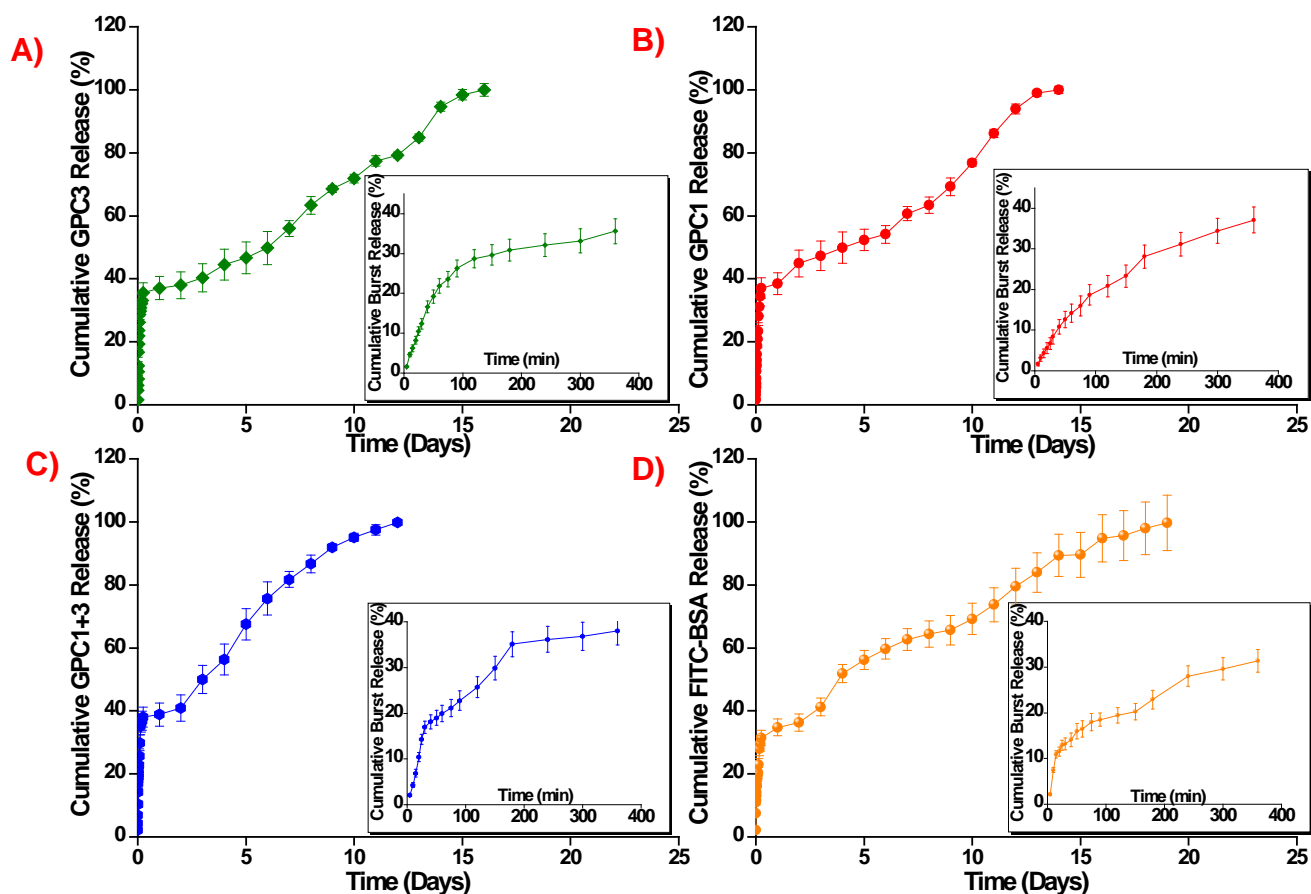
Figure 3. The cumulative protein release profiles for (A-D) rGPC3, rGPC1, rGPC1+3 and FITC-BSA eluted from chitosan-coated TNT/Ti implants. The TNT fabrication and protein

loading (in vacuum) were carried out under same experimental conditions. Error bars represent mean ± SD for n = 3.

The chitosan coating suppressed the initial burst release caused due to high concentration across large-diameter uncoated pores (from 63% to 31%) and significantly improved the release pattern. Furthermore, the biopolymer coating provided an extended release of the protein molecules by acting as a physical barrier, isolating the proteins from the bulk solution. Figure 3A-D show the sustained elution of rGPC3, rGPC1, rGPC1+3 and FITC-BSA from chitosan-coated TNTs, lasting for 16, 14, 12 and 19 d, respectively. The insets represent the corresponding burst release profiles. The protein release profiles describe the case II drug transport (Korsmeyer-Peppas model) that engenders to zero-order release kinetics. A zero-ordered diffusion profile is significant to maintain the constant drug dosages within the therapeutic window.[48]

TNT/Ti samples	Release efficiency (%)				Release duration (h/d)		
	6h	1d	7d	14d	t_B (h)	t_{50} (h/d)	t_{100} (d)
Chitosan-coated TNTs with rGPC1	37.08	38.46	60.67	100	6	4d	14d
Chitosan-coated TNTs with rGPC3	35.61	37.07	56.01	94.66	6	6d	16d
Chitosan-coated TNTs with rGPC1+3	38.05	38.86	81.72	100	6	3d	12d
Chitosan-coated TNTs with FITC-BSA	31.38	34.78	62.63	89.35	6	3.8d	19d
Uncoated TNTs with rGPC1	63.52	69.57	100	100	6	1.5 h	4d
Uncoated TNTs with rGPC3	62.72	73.93	100	100	6	2.5 h	5d

Table 1. Release characteristics (mean cumulative release percentage at different time points and release durations) of the *in vitro* studies of rGPC1, rGPC3, rGPC1+3 and control protein

eluted from uncoated and chitosan-coated Titania nanotubes (TNTs) at physiological temperature.

Transfection and BMP2 activity in C2C12 cell line

Murine myoblast C2C12 cells transfected using two different commercial formulations showed no significant cell death when observed by light microscopy. The luciferase expressions from DLR assays induced via rBMP2 addition and compared to the basal transfection formulations (effect of rBMP2 on *pID183-Luc* construct in C2C12 cells), assessed separately for Fugene HD (4:1), Fugene HD (2:1) and Lipofectamine 3000 (1.5 µm) using unpaired t-tests are summarized in **Figure 4** and showed successful transfection. Both Fugene HD and plasmid DNA ratios (4:1 and 2:1) yielded similar transfection efficiencies measured via luciferase activity (50-70% increase in induction), while Lipofectamine 3000 was comparatively less efficient. The basal expressions showing vehicle treatment (no rBMP2) were measured to get rid of background attenuation. The 2:1 ratio formulation was used for transfecting cells to test the glypican activity, as it promoted maximal luciferase output with minimal input.
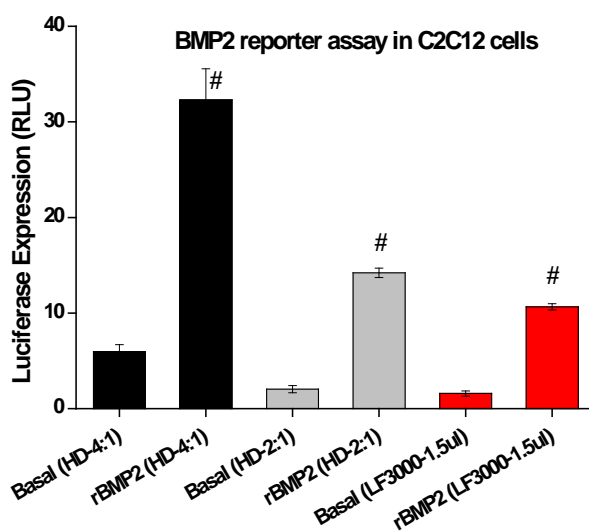
Figure 4. Functional analysis of transfected BMP2-responsive promoter in C2C12 cells with Fugene HD (4:1), Fugene HD (2:1) and Lipofectamine 3000 (1.5 µl). Statistically significant

differences are denoted by # ($p \leq 0.05$) between basal luciferase expressions versus expressions induced by rBMP2 (separately for Fugene HD (4:1), Fugene HD (2:1) and Lipofectamine 3000 (1.5 µm)) using unpaired t-tests. These observations reflect successful transfection and BMP2 pathway activation. Error bars represent ± SD for n = 3 (technical replicates); RLU: relative light unit.

Biological activity of the administered proteins released from TNTs

The effect of released exogenous glypicans from the proposed TNT/Ti protein-delivery system on BMP2 osteogenic activity was investigated in transiently transfected C2C12 cells. This was verified using DLR assay by co-incubating the recombinant proteins released from TNTs at day 1, 8 and 15, and assessing their ability to block the action of rBMP2 in C2C12 cells. One-way ANOVA was used to test for significant differences in luciferase activities of rBMP2 proteins and other groups (including rBMP2 + GPC1; rBMP2 + GPC3 and rBMP2 + GPC 1+3 at day 0 in addition to rBMP2 + Released BSA and rBMP2 + TNT + chitosan at days 1, 8 and 15). **Figure 5** confirms the biological activity of released glypicans elucidated by repression in rBMP2 activity. Figure 5A shows blockage of ~50% rBMP2 activity by 100 ng/ml of pristine rGPC1, rGPC3 and rGPC1+3 added from the stock solution (control, day 0) with statistically significant differences in luciferase activities between rBMP2 and other groups ($p \leq 0.01$). This was followed by testing the *in vitro* cumulative protein release amounts (collected and measured spectrophotometrically) in the cell experiments. The rGPC1 and rGPC3 released from TNTs showed similar bioactivity on day 1 (Figure 5B) and reduced the rBMP2 activity by ~40-50%. Exposure of the cloned cells to the released glypicans (rGPC1 and rGPC3) on day 8 showed a 65-75% inhibition in rBMP2 activity (Figure 5C), which reiterates the functionality of the released proteins. At both days 1 and 8, significant differences were noted in luciferase activities

between rBMP2 and glypican treated groups ($p \leq 0.05$ and $p \leq 0.001$ respectively). However, there were borderline significant differences in luciferase expression between rBMP2 and other groups ($p \leq 0.06$) at day 15 (Figure 5D). Moreover, the synergistic incubation of the two glypicans (rGPC1+3) did not show enhanced repression potential when compared with individual proteins, contrary to the earlier findings.[3] The positive (rBMP2 + Released BSA) and the negative (TNTs without any therapeutic agent) control groups did not have any significant inhibitory effects on the BMP2 signaling pathway. All the cells were incubated with an initial 100ng/ml of stimulatory rBMP2 which showed significant increase in BMP signaling relative to basal luciferase activity.
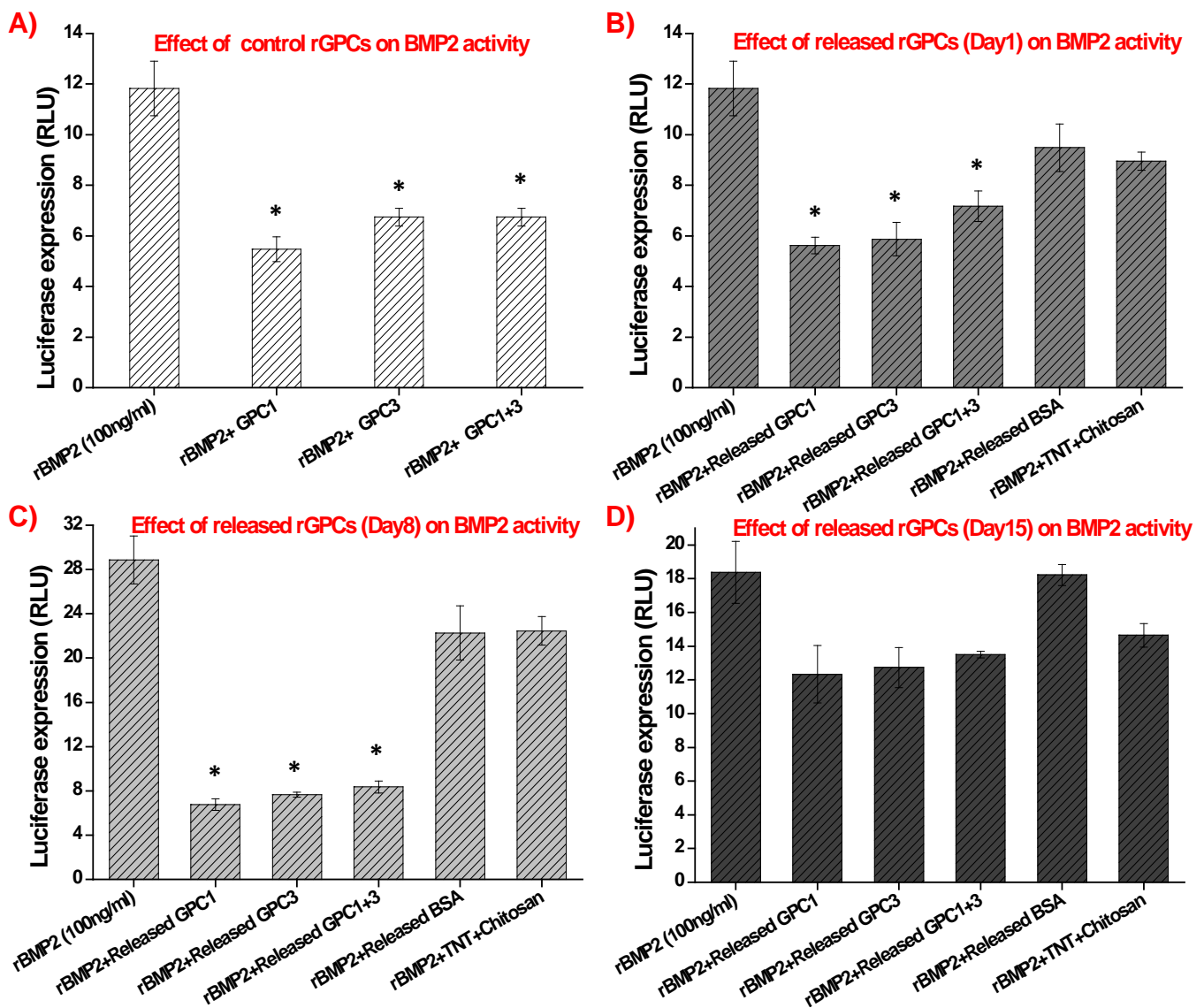
Figure 5. The inhibitory effects of rGPC1, rGPC3 and rGPC1+3 released from proposed TNT-based cranial implants on BMP2 signaling in murine C2C12 cells. The FITC-BSA-loaded and non-loaded TNT/Ti discs acted as positive and negative controls, respectively. Cells were co-transfected with a BMP-responsive luciferase reporter, a control luciferase vector for inducing transfection and the subsequently treated with 100ng/ml of BMP2 and 100ng/ml of (A) control recombinant glypicans (day 0, added from the stock solution), (B) released proteins on day 1, (C) released proteins on day 8 and (D) released proteins on day 15. Luciferase expression was assayed 24 h post-treatment. The statistical significant difference compared to BMP2 treatment is denoted by * ($p \leq 0.01$ for day 0, $p \leq 0.05$ for day 1 and $p \leq 0.001$ for day 8). Error bars represent mean $\pm$ SD for n = 3; RLU: relative light unit.

Discussion

Craniosynostosis, the premature fusion of cranial sutures in children, has been associated with mutations in the bone morphogenetic protein (BMP) signaling pathway.[49,50] Recent progress in molecular biology has highlighted the regulatory effects of BMP2 antagonists, including glypicans (GPC1 and GPC3), on suture morphogenesis and cellular functions.[3,6,7] Despite the research and development, there still remains a need to develop a viable sustained protein delivery system that can localize glypican release at the sutural site. This study demonstrates the potential of using electrochemically engineered TNTs fabricated on Ti surfaces (TNT/Ti implants) as localized protein-delivery implants for bone-inhibitory craniofacial applications.

Our modified fabrication method (involving the addition of lactic acid) overcomes the synthesis limitations of traditional electrolyte which required optimised ageing (to increase the Ti ion concentration) and longer anodization periods to obtain stable nanotubes.[31] The anodization conditions that we used led to formation of highly adhesive, high quality and robust

TNT layers (without any cracks) at unprecedented growth rates, suitable for cranial applications (Figure 2A-C). Moreover, our fabrication method produced large diameter nanotubes (> 100 nm) which can be used in bone cell inhibition, further consolidating our work.[51] Although a Ti disc was used as a model substrate, these nanotubes can be reproducibly fabricated on existing Ti-based cranial implants, thus ensuring easy integration into clinical practice.

Our results support and complement previous reports that have established different polymer-based surface modification techniques to achieve sustained and extended release of active molecules from TNTs, including plasma polymerization (to reduce the nanopore diameter) and dip-coating to completely or partially close the open top of the nanotubes. The plasma deposition required a complex high-vacuum set-up, while the simpler dip-coating method rendered inaccurate thickness with a micro-rough surface.[33,52,53] To address these drawbacks, a spin-coating approach was applied to deposit chitosan layer to cover the protein-loaded TNT/Ti implant surfaces, owing to its simplicity and repeatability (Figure 2D-F). Chitosan was chosen because it is a highly biocompatible and biodegradable polymer, well explored in several orthopedic applications.[54]

The present *in vitro* study elucidated the controlled and sustained delivery (for up to 16 d) of sensitive bone-antagonising protein molecules (glypicans) from polymer-coated TNTs, with a zero-ordered release profile (Figure 3 and Table 1). FITC-BSA was used as a control because of its similarity in physical attributes (molecular weight, hydrodynamic volume and charge) with the glypicans. Moreover, fluorescent labelling aided towards easy and sensitive quantification and analysis of the released BSA.[55] These results were in line with the findings from other works, thus re-establishing the success of TNT/Ti implants as promising delivery platforms.[40,42,56]

The native glypicans have shown to block the BMP2 inductive activity, thereby hindering suture cell differentiation into osteoblasts [3,13] Herein, murine myoblast cell line, C2C12, was explored to study the inhibitory effects of exogenous glypicans released from TNT/Ti implants due to their ease of transfection. Moreover, BMP2 can stimulate osteoblastic differentiation in C2C12 cells (instead of forming multinucleated myotubes upon serum starvation), making these cells relevant to the current application.[17,57-60]

The strategy employed here involved C2C12 cells transiently transfected with a plasmid construct consisting of a BMP2 specific regulatory element (promotor) fused with a firefly luciferase reporter gene (*pID183-Luc*). A Renilla luciferase (*pRLTK-Luc)* containing control plasmid was also co-transfected to provide reference to compare results, and reduce error due to experimental variations such as transfection and cell handling. Cell function studies conducted using DLR assay helped evaluate cell responses to BMP2 responsive luciferase reporter construct. On activation of the BMP2 signaling pathway, the active regions of the plasmid transcribed mRNAs to translate into active luciferase proteins. The amount of firefly luciferase was dependent on the activity of the BMP2 regulatory element while production of the Renilla luciferase was independent of experimental promoter. This quantitative bioassay is a quick and sensitive method to measure BMP2 bioactivity as compared to the standard ALP activity assay.[43] The assay results elucidated that the released recombinant glypicans maintained their bioactivity and downregulated the BMP2 induction (luciferase expression) in transfected C2C12 cells, throughout the release period, thus confirming the proposed hypothesis. Loading TNTs with higher amount of glypicans (> 5 µg) and using more frequent buffer aliquoting may further extend the release of active proteins.

Further studies are needed for *in vivo* evaluation of the glypican-loaded TNT/Ti systems implanted in wildtype and Crouzon mice (with craniosynostosis). These results are likely to

form a valuable platform for future animal and human trials in developing an adjunctive molecular treatment for craniosynostosis.

Acknowledgements

References

1. Wilkie AO. Craniosynostosis: genes and mechanisms. *Hum Mol Genet* 1997;**6**:1647-1656

2. Wilkie AO. Epidemiology and genetics of craniosynostosis. *Am J Med Genet* 2000;**90**:82-83.

3. Dwivedi P, Grose R, Hii C, Filmus J, Anderson P and Powell B. Regulation of bone morphogenetic protein signalling and osteogenesis by glypicans in human cranial suture cells. *Bone* 2011;**48**: 243-254.

4. Foster KA, Frim DM and McKinnon M. Recurrence of synostosis following surgical repair of craniosynostosis. *Plast Reconstr Surg* 2008;**121**:70-76.

5. Panchal J and Uttchin V. Management of craniosynostosis. *Plast Reconstr Surg* 2003;**111**:2032-2048.

6. Coussens AK, Hughes IP, Wilkinson CR, Morris CP, Anderson PJ, Powell BC, et al. Identification of genes differentially expressed by prematurely fused human sutures using a novel in vivo–in vitro approach. *Differentiation* 2008;**76**:531-545.

7. Coussens AK, Wilkinson CR, Hughes IP, Morris CP, Van Daal A, Anderson PJ, et al. Unravelling the molecular control of calvarial suture fusion in children with craniosynostosis. *BMC Genomics* 2007;**8**:458-483.

8. Grova M, Lo DD, Montoro D, Hyun JS, Chung MT, Wan DC, et al. Animal Models of Cranial Suture Biology. *J Craniofac Surg* 2012;**23**:1954-1958.

9. Wu C-J and Lu H-K. Smad signal pathway in BMP-2-induced osteogenesis-a mini review. *J Dent Sci* 2008;**3**:13-21.

10. Marie PJ, Debiais F and Hay E. Regulation of human cranial osteoblast phenotype by FGF-2, FGFR-2 and BMP-2 signaling. *Histol Histopathol* 2002;**17**:877-85.

11. Maxson R and Ishii M. The Bmp pathway in skull vault development. *Front Oral Biol* 2008;**12**:197-208.

12. Mooney MP, Moursi AM, Opperman LA and Siegel MI. Cytokine therapy for craniosynostosis. *Expert Opin Biol Ther* 2004;**4**:279-299.

13. Dwivedi P, Lam N and Powell B. Boning up on glypicans—opportunities for new insights into bone biology. *Cell Biochem Funct* 2013;**31**:91-114.

14. Cray Jr J, Burrows AM, Vecchione L, Caccamese Jr JF, Losee JE, Moursi AM, et al. Blocking bone morphogenetic protein function using in vivo noggin therapy does not rescue premature suture fusion in rabbits with delayed-onset craniosynostosis. *Plast Reconstr Surg* 2011;**127**:1163-1172.

15. Springer IN, Warnke PH, Terheyden H, Açil Y, Bülhoff A, Kuchenbecker S, et al. Craniectomy and noggin application in an infant model. *J Craniomaxillofac Surg* 2007;**35**:177-184.

16. Cooper GM, Curry C, Barbano TE, Burrows AM, Vecchione L, Caccamese JF, et al. Noggin inhibits postoperative resynostosis in craniosynostotic rabbits. *J Bone Miner Res* 2007;**22**:1046-1054.

17. Jiao X, Billings PC, O'Connell MP, Kaplan FS, Shore EM and Glaser DL. Heparan sulfate proteoglycans (HSPGs) modulate BMP2 osteogenic bioactivity in C2C12 cells. *J Biol Chem* 2007;**282**:1080-1086.

18. Moioli EK, Clark PA, Xin X, Lal S and Mao JJ. Matrices and scaffolds for drug delivery in dental, oral and craniofacial tissue engineering. *Adv Drug Deliv Rev* 2007;**59**:308-324.

19. Yamamoto M, Tabata Y, Hong L, Miyamoto S, Hashimoto N and Ikada Y. Bone regeneration by transforming growth factor β1 released from a biodegradable hydrogel. *J Control Release* 2000;**64**:133-142.

20. Aw MS, Khalid KA, Gulati K, Atkins GJ, Pivonka P, Findlay DM, et al. Characterization of drug-release kinetics in trabecular bone from titania nanotube implants. *Int J Nanomedicine* 2012;**7**:4883-4892.

21. Gulati K, Aw MS and Losic D. Drug-eluting Ti wires with titania nanotube arrays for bone fixation and reduced bone infection. *Nanoscale Res Lett* 2011;**6**:1-6.

22. Yang L and Webster TJ. Nanotechnology controlled drug delivery for treating bone diseases. *Expert Opin Drug Deliv* 2009;**6**:851-864.

23. Losic D, Aw MS, Santos A, Gulati K and Bariana M. Titania nanotube arrays for local drug delivery: recent advances and perspectives. *Expert Opin Drug Deliv* 2015;**12**:103-127.

24. Aw MS, Kurian M and Losic D. Non-eroding drug-releasing implants with ordered nanoporous and nanotubular structures: concepts for controlling drug release. *Biomater Sci* 2014;**2**:10-34.

25. Santos A, Aw MS, Bariana M, Kumeria T, Wang Y and Losic D. Drug-releasing implants: current progress, challenges and perspectives. *J Mater Chem B* 2014;**2**:6157-6182.

26. Shrestha NK, Macak JM, Schmidt-Stein F, Hahn R, Mierke CT, Fabry B, et al. Magnetically Guided Titania Nanotubes for Site-Selective Photocatalysis and Drug Release. *Angew Chem Int Ed* 2009;**48**:969-972.

27. Wang Q, Huang J-Y, Li H-Q, Chen Z, Zhao AZ-J, Wang Y, et al. TiO(2) nanotube platforms for smart drug delivery: a review. *Int J Nanomedicine* 2016;**11**:4819-4834.

28. Xu J, Zhou X, Gao Z, Song YY and Schmuki P. Visible-Light-Triggered Drug Release from TiO$_2$ Nanotube Arrays: A Controllable Antibacterial Platform. *Angew Chem* 2016;**128**:603-607.

29. Song Y-Y, Schmidt-Stein F, Bauer S and Schmuki P. Amphiphilic TiO$_2$ nanotube arrays: an actively controllable drug delivery system. *J Am Chem Soc* 2009;**131**:4230-4232.

30. Roy P, Berger S and Schmuki P. TiO$_2$ nanotubes: synthesis and applications. *Angew Chem Int Ed* 2011;**50**:2904-2939.

31. Gulati K, Santos A, Findlay D and Losic D. Optimizing Anodization Conditions for the Growth of Titania Nanotubes on Curved Surfaces. *J Phys Chem C* 2015;**119**:16033-16045.

32. Losic D and Simovic S. Self-ordered nanopore and nanotube platforms for drug delivery applications. *Expert Opin Drug Deliv* 2009;**6**:1363-1381.

33. Gulati K, Ramakrishnan S, Aw MS, Atkins GJ, Findlay DM and Losic D. Biocompatible polymer coating of titania nanotube arrays for improved drug elution and osteoblast adhesion. *Acta Biomater* 2012;**8**:449-456.

34. Kumeria T, Mon H, Aw MS, Gulati K, Santos A, Griesser HJ, et al. Advanced biopolymer-coated drug-releasing titania nanotubes (TNTs) implants with simultaneously enhanced osteoblast adhesion and antibacterial properties. Colloids Surf, B 2015;**130**:255-263.

35. Shokuhfar T, Sinha-Ray S, Sukotjo C and Yarin AL. Intercalation of anti-inflammatory drug molecules within TiO 2 nanotubes. *RSC Adv* 2013;**3**:17380-17386.

36. Liang K, Li X and Tay BK. 2011. Large diameter TiO$_2$ nanotube fabrication for bone morphogenetic protein delivery *Nanoelectronics Conference (INEC), 2011 IEEE 4th International*, IEEE, p.1-2.

37. Lai S, Zhang W, Liu F, Wu C, Zeng D, Sun Y, et al. TiO$_2$ nanotubes as animal drug delivery system and in vitro controlled release. *J Nanosci Nanotechno* 2013;**13**:91-97

38. Davis SS. Meeting the Challenges of Viable Delivery Systems for Peptide and Protein Pharmaceuticals. *Am Pharama Rev*. p.1-7.

39.   Crommelin DJ. 2013. Formulation of biotech products, including biopharmaceutical considerations *Pharmaceutical Biotechnology*. Springer; p.69-99.

40. Peng L, Mendelsohn AD, LaTempa TJ, Yoriya S, Grimes CA and Desai TA. Long-term small molecule and protein elution from TiO$_2$ nanotubes. *Nano Lett* 2009;**9**:1932-1936.

41. Ketabchi A, Komm K, Miles-Rossouw M, Cassani DA and Variola F. Nanoporous titanium surfaces for sustained elution of proteins and antibiotics. *PloS One* 2014;**9**: 92080-92089.

42. Popat KC, Eltgroth M, LaTempa TJ, Grimes CA and Desai TA. Titania Nanotubes: A Novel Platform for Drug-Eluting Coatings for Medical Implants? *Small* 2007;**3**:1878-1881.

43. Zilberberg L, ten Dijke P, Sakai LY and Rifkin DB. A rapid and sensitive bioassay to measure bone morphogenetic protein activity. *BMC Cell Biol* 2007;**8**:41-47.

44.   Katagiri T, Yamaguchi A, Komaki M, Abe E, Takahashi N, Ikeda T, et al. Bone morphogenetic protein-2 converts the differentiation pathway of C2C12 myoblasts into the osteoblast lineage. *J Cell Biol* 1994;**127**:1755-1766.

45. Nishimura R, Kato Y, Chen D, Harris SE, Mundy GR and Yoneda T. Smad5 and DPC4 are key molecules in mediating BMP-2-induced osteoblastic differentiation of the pluripotent mesenchymal precursor cell line C2C12. *J Biol Chem* 1998;**273**:1872-1879.

46. So S, Lee K and Schmuki P. Ultrafast growth of highly ordered anodic TiO_2 nanotubes in lactic acid electrolytes. *J Am Chem Soc* 2012;**134**:11316-11318.

47. Dwivedi PP, Hii CS, Ferrante A, Tan J, Der CJ, Omdahl JL, et al. Role of MAP Kinases in the 1, 25-Dihydroxyvitamin D3-induced Transactivation of the Rat Cytochrome P450C24 (CYP24) Promoter specific functions for ERK1/ERK2 and ERK5. *J Biol Chem* 2002;**277**:29643-29653.

48. Grassi M and Grassi G. Mathematical modelling and controlled drug delivery: matrix systems. *Curr Drug Deliv* 2005;**2**:97-116.

49. Dwivedi PP, Anderson PJ and Powell BC. Development of an efficient, non-viral transfection method for studying gene function and bone growth in human primary cranial suture mesenchymal cells reveals that the cells respond to BMP2 and BMP3. *BMC Biotechnol* 2012;**12**:45-54.

50. Warren SM, Brunet LJ, Harland RM, Economides AN and Longaker MT. The BMP antagonist noggin regulates cranial suture fusion. *Nature* 2003;**422**:625-629.

51. Park J, Bauer S, Schlegel KA, Neukam FW, von der Mark K and Schmuki P. TiO_2 nanotube surfaces: 15 nm—an optimal length scale of surface topography for cell adhesion and differentiation. *Small* 2009;**5**:666-671.

52. Aw MS, Simovic S, Addai-Mensah J and Losic D. Polymeric micelles in porous and nanotubular implants as a new system for extended delivery of poorly soluble drugs. *J Mater Chem* 2011;**21**:7082-7089.

53. Simovic S, Losic D and Vasilev K. Controlled drug release from porous materials by plasma polymer deposition. *Chem Commun* 2010;**46**:1317-1319.

54. Balasundaram G and Webster TJ. An Overview of Nano-Polymers for Orthopedic Applications. *Macromol Biosci* 2007;**7**:635-642.

55. Wischke C and Borchert H-H. Fluorescein isothiocyanate labelled bovine serum albumin (FITC-BSA) as a model protein drug: opportunities and drawbacks. - *Int JPharma Sci* 2006;**61**:770-774.

56. Gulati K, Kogawa M, Maher S, Atkins G, Findlay D and Losic D. 2015. Titania Nanotubes for Local Drug Delivery from Implant Surfaces *Electrochemically Engineered Nanoporous Materials*, Springer; p.307-355.

57. Gallea S, Lallemand F, Atfi A, Rawadi G, Ramez V, Spinella-Jaegle S, et al. Activation of mitogen-activated protein kinase cascades is involved in regulation of bone morphogenetic protein-2-induced osteoblast differentiation in pluripotent C2C12 cells. *Bone* 2001;**28**:491-498.

58. Nojima J, Kanomata K, Takada Y, Fukuda T, Kokabu S, Ohte S, et al. Dual roles of smad proteins in the conversion from myoblasts to osteoblastic cells by bone morphogenetic proteins. *J Biol Chem*2010;**285**:15577-15586.

59. Nakashima A, Katagiri T and Tamura M. Cross-talk between Wnt and bone morphogenetic protein 2 (BMP-2) signaling in differentiation pathway of C2C12 myoblasts. *J Biol Chem* 2005;**280**:37660-37668.

60. Cordonnier T, Langonné A, Sohier J, Layrolle P, Rosset P, Sensébé L, et al. Consistent osteoblastic differentiation of human mesenchymal stem cells with bone morphogenetic protein 4 and low serum. *Tissue Eng Part C Methods* 2010;**17**:249-259.

CHAPTER 7 & 8

IN VIVO EXPERIMENTAL PROTOCOL

In vivo experimental protocol

A. Materials

The chemicals used in implant fabrication have been described in detailed in Chapter 3 (Section 3.2.1, p.88). Reagents pertaining animal experiments involved Ketamine hydrochloride (Ceva Animal Health Pty Ltd, Australia), Xylazine (Troy Laboratories Pty Ltd, Australia), Buprenorphine (Reckitt Benckiser Healthcare, UK), Lacrilube (Allergan, USA) 70% Ethanol (Chem Supply, Australia), sterile saline buffer (InterPharma Pty Ltd, Australia), Formalin (Orion Laboratories Pty Ltd, Australia), PBS (HyClone, USA), medical Carbon dioxide gas (BOC, Australia), EDTA, KOH and Tris-HCl buffer (Chem Supply, Australia). The equipment to assist the surgery included, a weighing scale (A&D, Australia), alcohol swabs (Briemarpak, Australia), surgical scissors, sterile disposable scalpel blade, scalpel handle (ProSciTech Pty Ltd, Australia), biopsy puncture (3 mm diameter, Stiefel Laboratories, Melbourne, VIC), forceps, needles (18, 25 and 27 gauge) and syringes (1 and 5 ml) (BD, Singapore).

B. TNT/Ti implant fabrication and sterilisation

All TNT/Ti implants were fabricated using the standardised anodisation protocol described in Chapter 3 (Section 3.2.3, p.91). The model proteins (5 µg/sample), GPC3 and BSA, were loaded within the nanotubular implants using a vacuum drying technique. Half the samples were surface coated with 2% chitosan solution and the rest remained uncoated. The specific details of protein loading and polymer coating have already been described and optimised in Chapter 4 (Section 4.2.4, p.120). Prior to the animal experiments, the protein-loaded implants were

sterilised using low-temperature hydrogen peroxide gas plasma (STERRAD® 100 NX™ System, Advanced sterilisation Products, Irvine, CA, USA).

C. Animals

All animal experiments were conducted under the approval of Animal Ethics Committees of the University of Adelaide and the Women's and Children's Hospital, Adelaide. They complied with strict adherence to the Australian code for the care and use of animals for scientific purposes. Wildtype (C57Bl/6 mixed background) and genetically modified Crouzon (Fgfr2$^{c342y/+}$, C57Bl/6 mixed background) mice were obtained from an ongoing breeding colony of craniosynostotic mice housed at the animal care facility at Women's and Children's Hospital (CERT-2114 and CERT-2115). Prior to the surgery, all mice were managed using the existing protocol (AE884/6/15) in a light- and temperature-controlled, pathogen-free environment with unrestricted access to water and food.

D. Experimental and study groups

The murine experiments were subdivided into two broad categories: (i) to investigate the Ti/TNT implant biocompatibility (implanted both subcutaneously and adjacent to the exposed dura) (**Chapter 7**), and (ii) then to evaluate the ability of glypican-releasing Ti/TNT implants in preventing bone-regrowth within a critical-sized defect (**Chapter 8**). For the first set of study, which was to establish tissue compatibility, the wildtype mice were randomly assigned to two different groups involving: (i) placement of Ti/TNT implants subcutaneously (n = 5) and (ii) placement of Ti/TNT vehicle control within the craniectomy (critical-sized) defect. The implants were surface-coated with biopolymers, Chitosan and Pluronic-F127 to assess the

localised reactions or undue adverse effects due to the implantation (n = 9, 3 in each subgroup with uncoated, Chitosan-coated and Pluronic-F127-coated TNTs).

The second set of studies involved both wildtype (WT) and Crouzon (CZ) mice randomised into 3 treatment groups: (i) craniectomy with no treatment, which served as the surgical control group (n=6 for CZ and n=6 for WT), (ii) craniectomy with non-specific, bovine serum albumin (BSA) loaded TNT/Ti implant (sub-grouped into chitosan-coated and uncoated), which served as the protein control groups (n= 5 in both subgroups for WT), (iii) Craniectomy with GPC3 loaded TNT/Ti implants (sub-grouped into chitosan-coated and uncoated), which served as the experimental groups (n=8 for WT, n=12 in both subgroups for CZ).

E. Surgical model

Mice were anaesthetised by injecting a mixture of 100 mg/kg Ketamine hydrochloride and 10 mg/kg Xylazine via intraperitoneal route, followed by a subcutaneous injection of 0.05mg/kg of the analgesic, Buprenorphine. Once the mice was unresponsive to paw-pinching, their eyes were protected by lacrilube to prevent corneal damage. The hair on the scalp were disinfected using 70 % ethanol and a C-shaped incision was made on the skin over the parietal bone. The skin flap was gently lifted to expose the cranium and sutures underneath. The subcutaneous TNT/Ti implants were carefully placed in the pocket between the skull and the skin, and the wound was closed with resorbable sutures.

For craniectomy studies, the musculature and the periosteum were reflected and 3 mm circular critical-sized defects were created, lateral to the left coronal suture, to act as implantation sites. This was biologically consistent and comparable to human surgical process where the whole sutural region is removed along with strips from the adjoining bones, to present

a homogenous cell population during the wound healing. All defects were carefully generated under lighted magnifying lamp using a fine biopsy puncture, to take out the disc of skull bone, ensuring that the underlying dura was not damaged. This is critical as damaging the dura might impair the healing of the overlying bone. A continuous saline buffer irrigation was maintained to avoid excessive dryness of the cranium during surgery. Meticulous care was also taken to prevent damage to the underlying vascularisation in order to avoid exsanguination. Intra-operative images illustrating the ability to create a critical-sized defect at appropriate location is presented in **Figure A**.
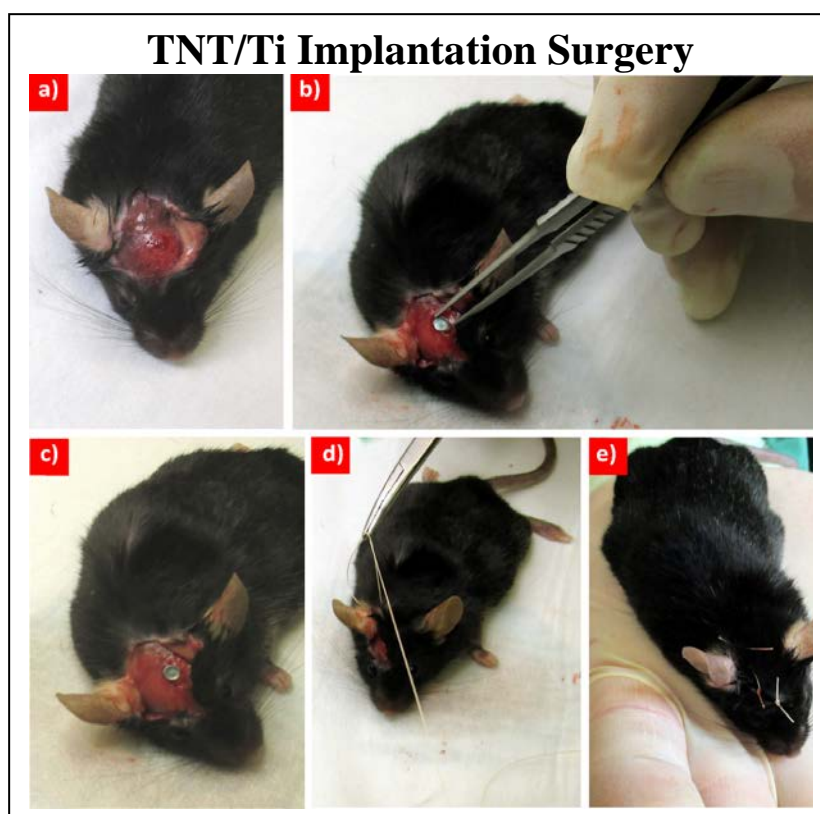
Figure A. Skull defect implantation of TNT/Ti disc in Fgfr2 strain wildtype mice. a) a 3 mm critical-sized defect (CSD) in the mice skull with removed periosteum; b) defect filled with the TNT/Ti implant (protein-loaded or non-loaded); c) the implant sitting precisely on top of the CSD; d) incision closed with resorbable suture; e) post-operative care.

The defects were either left empty (to act as sham controls) or filled with protein-loaded 3 mm TNT/Ti implants (with nanotubular surfaces against dura), with assigned therapeutic interventions as mentioned in Section D. The protein dosages were chosen based on the previous *in vitro* studies (**Chapter 4** and **6**). The surgical sites were then sutured and the mice were allowed to recover on a heat pad/incubator or held in the palm of hand to establish rhythmic breathing, before being transferred into individual husbandry cages. Post-operative analgesia via subcutaneous administration was provided by injecting 0.25 % Marcaine at the end of the surgery and 0.05mg/kg Buprenorphine, 8 h post-operatively.

All the mice were kept under observation to look for skin reaction over the implant, weight loss or distress, twice a day for 10 days post-operation, then weekly up to 3 months. Crouzon mice also needed mushy food after surgery and a weekly teeth trim. At 12 weeks after successful surgery, the mice were euthanised via asphyxiation using carbon dioxide (at flow rate of 0.5%, until the breathing movements ceased). The animal skulls were dissected and the scalp was incised from the canthi of the eyes down to the parietal bones and occiput of the cranium. The TNT/Ti implants were retrieved for morphological characterisation with SEM. Changes in defect area/width and bone volume were assessed using micro-CT scanning, followed by histological evaluations to observe any adverse tissue/skin reactions and/or new bone induction for both set of studies.

F. Scanning electron microscopy/EDAX analysis

The morphological characterisation of the post-operative TNT/Ti implant surface was performed using a field-emission scanning electron microscope (SEM, FEI Quanta 450, Eindhoven, The Netherlands). The 3 mm TNT/Ti discs were fixed in 10 % neutral buffered formalin overnight, mounted onto a holder with double-sided conductive tape and coated with

a layer of 3 nm thick platinum before being imaged. The system was equipped with energy dispersive X-ray Spectrometry (EDS) software that enabled surface composition (elemental) of peculiar samples to be analysed. EDS was further coupled with a CPS (Counts per Second) mapping smart feature that provided a visual representation (map) of the X-ray count rate at every pixel in the dataset. The mapped surface (different areas of interest) with the brightest pixels indicated the highest count areas, and dark or black areas indicate little or no X-ray counts. This showed the chemical/elemental distribution of aggregates across the TNT/Ti surface.

G. Micro-computed (micro-CT) analysis

At the end of the 3 months study, the skulls of the euthanised mice were dissected from the soft tissue, cleared with 1 % KOH for skeletonisation, stored in 10 % neutral buffered formalin and imaged using micro-CT to determine bone-regrowth within the therapeutically intervened defects, in comparison to the control defects. The micro-CT images were acquired using a small animal, high-resolution scanner, Skyscan 1076 (Bruker-micro-CT, Kontich, Belgium). Briefly, the micro-CT scanner was operated at source parameters: 50 kV, 110 µA with a rotation step of 0.6, 0.5 mm Al filter, scanning width of 35 mm and imaging time of 48 min, to obtain an image resolution of 8.7 µm.

The cross-sectional slices were reconstructed using the Skyscan NRecon software package (version 1.6.9., Bruker) with a ring artefact correction of 15, beam hardening correction of 30%, smoothing of 1 pixel, misalignment correction <10 and thresholding limits ranging from 0 to 0.11. The obtained bitmap (BMP) files were realigned using the Data viewer software (version 1.5.1, Bruker) and the coronal sections were saved as datasets. The files were then imported into CTan software (version v.1.14, Bruker) for 2D and 3D morphometric analysis. From the

entire data set, a circular region of interest (ROI), with a diameter of 3 mm and a height of 100 scan slices (including the whole defect area with the newly formed bone inside), was selected for analysis. The ROI was set where the original defect was located, since the margins were visually recognisable. By auto-interpolation between layers, ROI became the volume-of-interest (VOI) which formed the essential basis for all quantitative analysis. Parameters measured were total volume (TV), bone volume (BV) and bone surface area (BS) for each VOI. The defect was identified and visualised with the aid of 3D reconstruction software package, Avizo 9.0 (Visualisation Sciences Group, Massachusetts, USA), which volume rendered the BMPs (resized into half using TCONV software, v.1.0, Bruker) to obtain a 3D image.

H. Histological analysis

For histological examination, all the cranial specimens were decalcified by submersion in 10% EDTA in 0.1 M Tris Buffer (pH 7.4) plus 7% sucrose for up to 4 weeks at room temperature and embedded in paraffin wax. The sections were then cut into 7 μm thick serial sections of sagittal slices using a rotary microtome (Leica Microsystems GmbH, Germany). They were cut parallel to the surface of the defect, with an intention to observe the new bone formation from the defect boundary to the centre of the defect. The slices were floated on water bath and mounted onto APES-coated slides which were dried overnight on slide warmer (Fisher) at 37°C. After an incubation at 60°C for 16 h, selected slides for each sample were deparaffinised in xylene and then rehydrated through a graded series of alcohol solutions and distilled water. The sections were then stained using haematoxylin and eosin (H&E), Movat Pentachrome (MOV), Periodic Acid-Schiff (PAS), Alcian Blue and/or Picro-Sirius Red (SR) and mounted in Depex (Sigma-Aldrich). An immunohistochemical Tartrate-Resistant Acid Phosphatase (TRAP) Staining was also performed on selective slides. The elaborate staining protocols (from

ihcworld.com, americanmastertech.com or sigmaaldrich.com) and the specific reagents are described in Appendix A. The slides were imaged using bright field microscope (Carl Zeiss Jena, Germany) equipped with a DFC480 digital camera (Leica Microsystems, Germany). A dark field microscope (Leica MZ16FA Stereo Microscope) with a polarisation filter was also used to analyse selective Picro-Sirius Red slides.

I. Statistical analysis

Statistical analyses were conducted using the SPSS statistics 22 software (IBM Corporation, USA). The first set of univariate tests (using one-way repeated measures ANOVA, Bonferroni adjustments) was performed for the tissue response studies (**Chapter 7**) to determine whether there were associations between the 'outcomes' (changes in BV and BS) and 'variables' (effect of uncoated and polymer coated TNTs). The second set of univariate tests (using one-way repeated measures ANOVA, Bonferroni adjustments) was constructed to test the 'outcomes' (changes in BV and BS) with the 'variables' (treatment groups) and any interactions between them, for both CZ and WT mice (**Chapter 8**). Shapiro-Wilk test of normality was performed to check the normality of the data distribution. A two-way ANOVA was also constructed to test the associations in between 'outcomes' from different genotypes (CZ and WT) (**Chapter 8**). Statistical significance was set at the 0.05 probability level.

CHAPTER 7

ASSESSMENT OF *IN VIVO* TISSUE

RESPONSE TO TNT/Ti IMPLANTS

CHAPTER 7: Assessment of *In Vivo* Tissue Response to TNT/Ti Implants

7.1. Introduction

The development of an optimal biointerface between the cranial bone and the biomaterial is essential for the success of titanium implants [103, 251, 252]. The biocompatibility of the implant surface is governed by its favorable interaction with the living tissues and/or the cellular environment, adjacent to the placement site [253, 254]. Ideally, the response to implant can be determined on the basis of three critical factors, including (i) tissue reaction – absence of chronic, persistent acute inflammation, inflammatory exudates, neutrophil and macrophage influx; (ii) fibrous capsule formation – absence of excessive fibrous tissues aggregates around the material post-implantation, along with collagen fibers (immature type III or type I) and glycosaminogylcans (GAGs); (iii) mechanical stability and implant safety in the physiological milieu – excellent wear and corrosion resistance, an elastic modulus comparable to the bone and optimal surface characteristics [252, 254-257]. Furthermore, for craniosynostosis application, the implant material should neither induce excessive bone formation nor cause undesired bone resorption (osteolysis).

Rigorous *in vivo* and *in vitro* studies (mimicking the physiological environment) have been integral to assess the ability of implantable biomaterials in generating an appropriate host tissue response [254, 257-259]. Previously, Chapter 5 described the preliminary *in vitro* testing of the proposed TNT/Ti cranial implants in order to minimise the animal numbers in *in vivo* studies. The cytocompatibility and biological response, in terms of cell morphology, viability and biofunctionlity (adhesion and proliferation) of human suture cells on TNT/Ti surface, render these

implants suitable for craniosynostosis applications. Furthermore, the alteration of TNT/Ti surface properties, including topography, chemistry, wettability and energy, tend to impact the cellular response near the local tissue.

Although, the *in vitro* data can reflect the material response in physiological conditions, its extrapolation and translation into *in vivo* situations can be challenging. This chapter focuses on assessing the *in vivo* biocompatibility of TNT/Ti implants in the animal model (Fgfr2 wildtype mice), prior to exploring their glypican delivering efficacy. Currently, the calvarial bone critical-sized defect (CSD) murine model is the most commonly used animal model in cranial development and bone regeneration studies [17, 260, 261]. A CSD refers to the smallest size intraosseous wound that will not heal during the lifetime of the animal, without any therapeutic invention [17, 262, 263]. It forms an ideal model to study the TNT/Ti implant biocompatibility and subsequent bio-functionality by providing a reproducible, non-load bearing and quantifiable orthotopic site for assessing changes in cranial bone regeneration.

In this chapter, a wildtype murine model was used: (i) to evaluate the biocompatibility of TNT/Ti implants (polymer-coated and uncoated) inserted either subcutaneously or within the CSD, by histologically assessing the adjacent tissue (skin and bone) response, (ii) to investigate undesired/excessive bone or cartilage formation inside the CSD, by quantification via micro-CT imaging and (iii) to characterise the TNT/Ti discs retrieved at the end of the study, by SEM analysis.

Scanning electron microscopy (SEM) coupled with energy dispersive X-ray spectrometry (EDS) was used to surface analyse the recovered TNT/Ti implants, post-operatively (Aim III). Digital photographs were taken to record each step during and after the surgery. For TNT/Ti

implants to conform to the biocompatibility requirements, two main analytical techniques were used, including histology and micro-CT scanning. Histologic observations (Aim I) were directed to evaluate the cellular organisation, extracellular matrix components (adverse inflammatory reactions and/or abnormal fibrous tissue formation) and mineralisation (if any) around the implant. The initial histological analysis was performed using H&E stained sections at 12 weeks after implantation to obtain full cellular details wherein, the cell nuclei appeared blue and the collagen fibers appeared pale pink [264]. This was followed by Alcian blue staining to identify the presence of any cartilage corresponding to endochondral ossification (encompassing chrondogenesis) [34]. Alcian blue stains the tissue proteoglycans blue/magenta to purple, and helps to distinguish chorondocytes from osteogenic cells [264]. Micro-CT imaging (Aim II) further examined the morphologic changes (volume and spatial density of bone regrowth) within the critical-sized defect at the end of the 12 week implantation study. This imaging modality used X-ray radiations to generate numerous projections of the mineralized bone (with hydroxyapatite). These projections were later processed and converted in high resolution 3D images of the mice skulls.

7.2. Materials and methods

A common materials and methods protocol for all *in vivo* studies has been described in experimental section preceding this Chapter (p.214-221). Briefly, the wildtype mice were implanted with sterilised TNT/Ti implants and divided into four sub-groups, including subcutaneously implanted TNT/Ti discs (SC, n=5), and uncoated (TNT, n=3), chitosan-coated (TNT-CH, n=3) and Pluronic-F127-coated TNT/Ti discs inserted within the CSD (TNT-F127, n=3). A flowchart relating to experimental layout with different implanted groups is shown in **Figure 7.1**. All the animals underwent surgery under general anesthesia (Xylazine and Ketamine),

along with analgesia (Buprenorphine). At doses specified earlier (Section E, p.216), these agents provided anesthesia for up to 45 min. The subcutaneous insertion under the incised skin flap took approximately 15 min while the cranial surgery lasted approximately 30 min. All mice were kept under regular daily observation for 3 months with ad-libitum supply of food and water. The mice were then euthanised by CO_2 asphyxiation and the harvested skulls (implantation sites) were evaluated via histology and micro-CT. The retrieved TNT-Ti implants from all sub-groups were visually assessed and surface analysed using SEM.
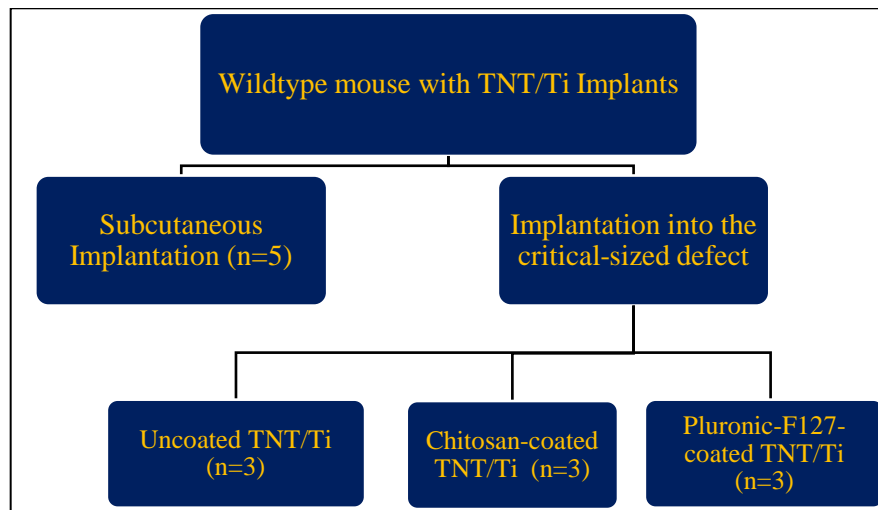
Figure 7.1. Flowchart displaying the experimental layout for evaluating tissue response to TNT/Ti implants.

7.3. Results and discussion

7.3.1. Visual assessment and implant surface characterisation

Most mice tolerated the surgical procedure well, without any intra-operative complications. A low 5% mortality rate occurred during the procedure from complications with the surgery or operative hemorrhage. Mice that had post-op hemorrhage were excluded from the further analysis. Rest of the healthy mice were euthanised 12 weeks post-implantation and the skulls were harvested. No wound dehiscence was observed in any specimen. **Figure 7.2** sums up the post-mortem characterisation of TNTs implanted subcutaneously, as well as uncoated and polymer-coated TNTs implanted within the CSD. Upon general observation at necropsy, the tissue around the implant showed no evident lesions, inflammation, infection or purulence. The implants were either attached to the skin or the periosteum over the defect and were often surrounded by a thin layer of fibrous tissue. The surface morphology of the retrieved implant were evaluated by SEM imaging. When the superficial layer of soft tissues was removed, the top surface of most implants were clearly visible. The nanotube layer was stable and did not delaminate. The subcutaneous TNT/Ti disc (SC, **Figure 7.2a**) showed an intact nanotube layer, with visible open pores underneath a thin discontinuous fibrous tissue. The surface of uncoated TNT/Ti implants inserted in the defect (TNT, **Figure7.2b**) was relatively clear, with an ordered array of nanotubes, open at the top. The chitosan-coated TNT/Ti discs (TNT-CH, **Figure 7.2c**) also exhibited open nanotube structure, with a fully degraded polymer layer by the end of the study. However, the Pluronic-F127-coated implants (TNT-F127, **Figure 7.2d**) showed a complex surface topography, with a dense fibrous tissue capsule completely blocking the nanopores.
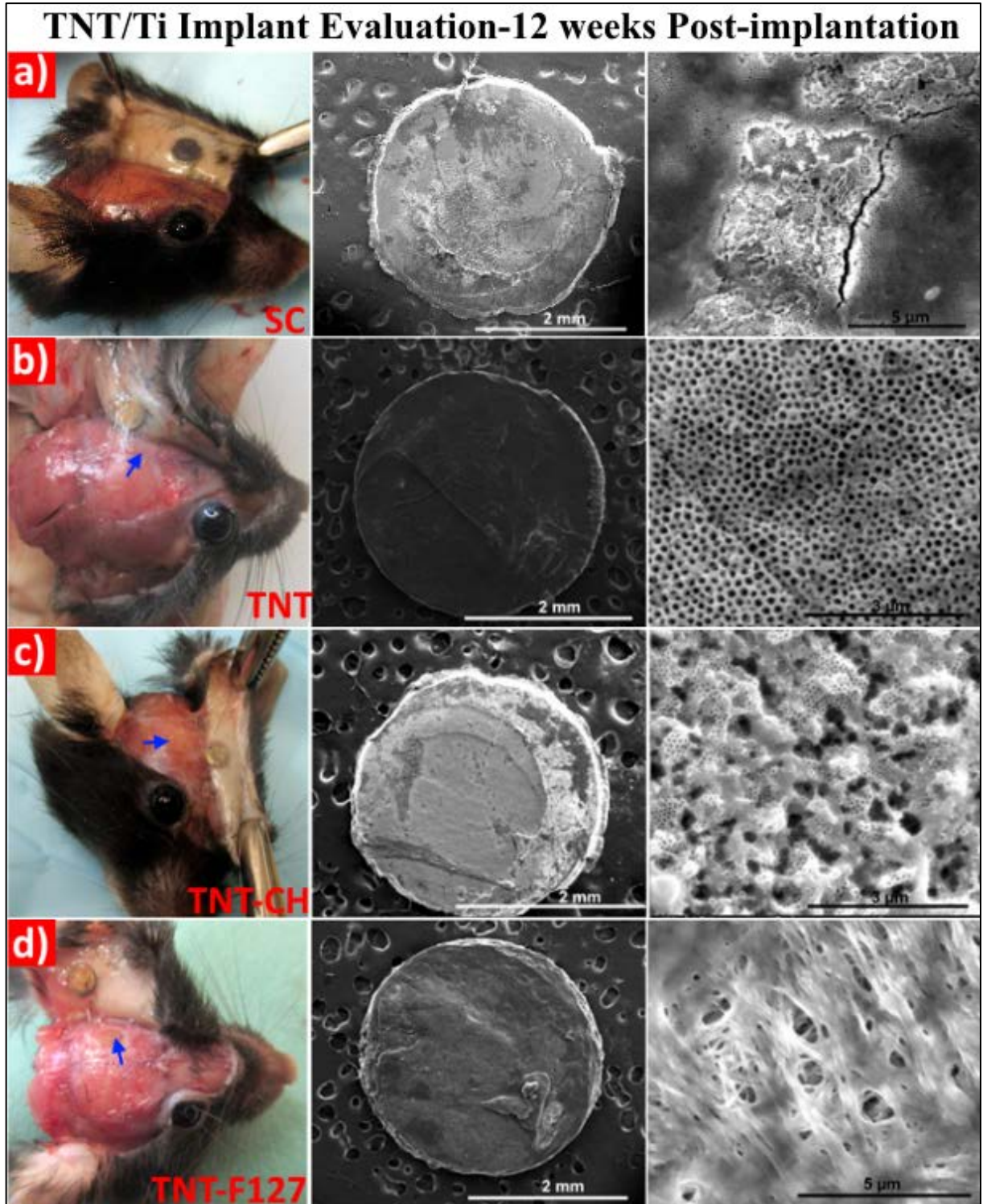
Figure 7.2. The representative images of TNT/Ti implantation in various sub-groups corresponding to (a) subcutaneous insertion (SC) and placement within the CSD for (b) uncoated

(TNT), (c) chitosan-coated (TNT-CH) and (d) Pluronic-F127-coated (TNT-F127) discs. The blue

arrows mark the implantation site (defect).

To investigate the peculiar surface characteristics of Pluronic-F127-coated TNTs, elemental

composition analysis and mapping by Energy Dispersive Spectroscopy (EDS) was performed. This

allowed identification of particular elements and their relative proportions in the layer covering the

TNT-F127 surface. **Figure 7.3a** presents the X-ray spectrum generated from the scan area of the

corresponding SEM (**Figure 7.2d**).
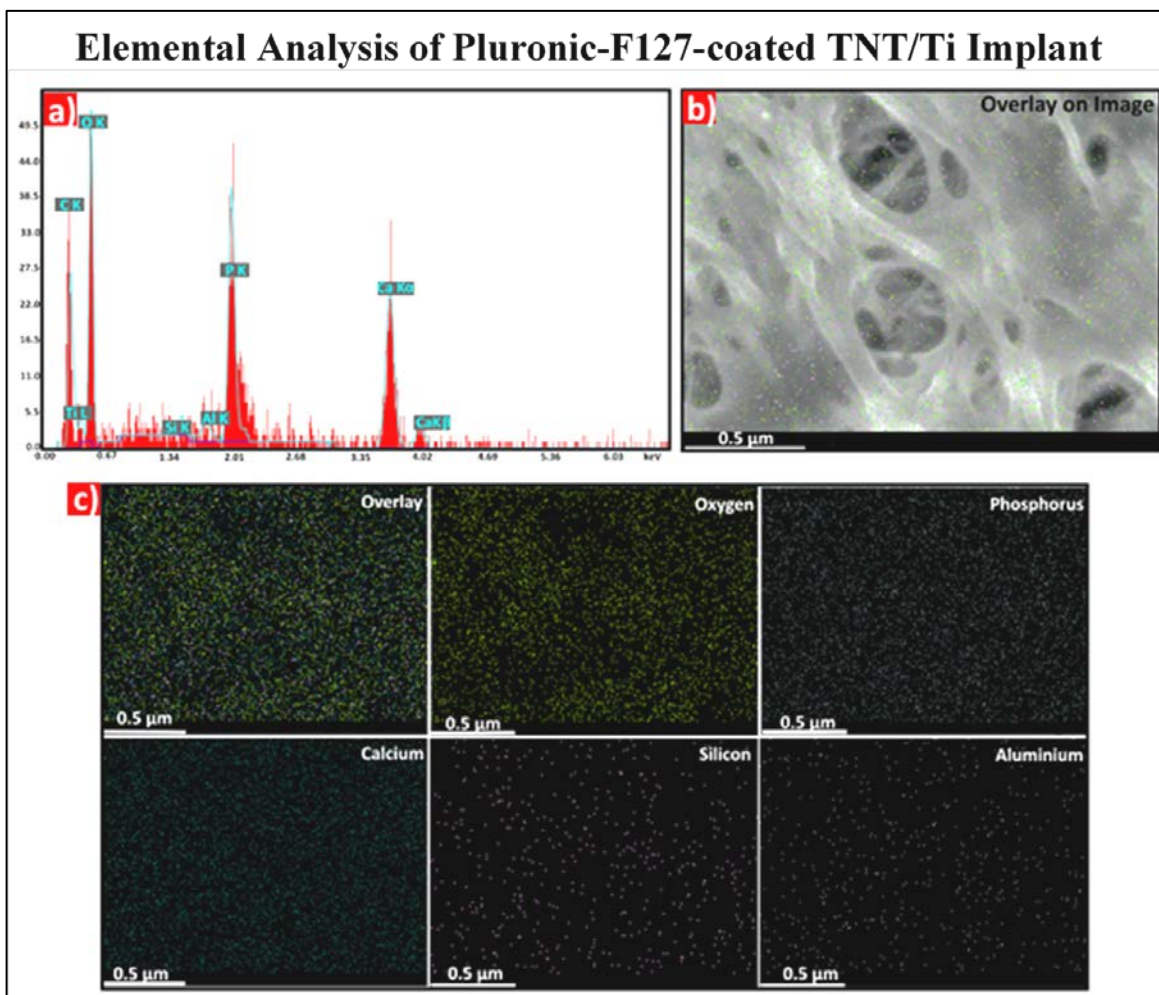
Figure 7.3. SEM-EDS-CPS characterisation of the materials deposited onto the Pluronic-F127-

coated TNT/Ti implants. a) The EDS spectrum showing the major and minor elements present at

the surface, b) and c) elemental mapping and distribution overlaying the implant surface.

The surface elements comprised mainly of carbon, oxygen, phosphorus and calcium, along with trace amounts of titanium (from the substrate underneath), silicon and aluminum. This indicated the deposition of bone-inducing hydroxyapatite onto the surface that was undesirable for current application. The elemental mapping in area of interest is presented in **Figure 7.3b-c**, showing the distribution of various elements across the surface.

7.3.2. Morphological assessment of the skull

The influence of TNT/Ti implants on *in vivo* bone regrowth was also evaluated within the critical sized calvarial defects in Fgfr2 wildtype mice. After 12 weeks of implantation, the morphology of newly formed bone in harvested samples was reconstructed using micro-CT imaging. For craniosynostosis application, minimal natural bone growth within the CSD is desirable. The representative digital and micro-CT images from each group (SC, TNT, TNT-CH and TNT-F127) are shown in **Figure 7.4**. The results demonstrated no marked difference on SC samples (**Figure 7.4a**), while the TNT and TNT-CH skulls (**Figure 7.4b-c**) showed minor new bone formation from the periphery of the defect (pre-existing bone edge). On the other hand, TNT-F127 skulls (**Figure 7.4d**) exhibited almost filled defect with substantial amount of newly formed bone, thicker at the edge and thinner at the centre of defect. This observation was consistent with the SEM results, confirming the bone-inducing properties of Pluronic-F127-coated TNT/Ti implants.
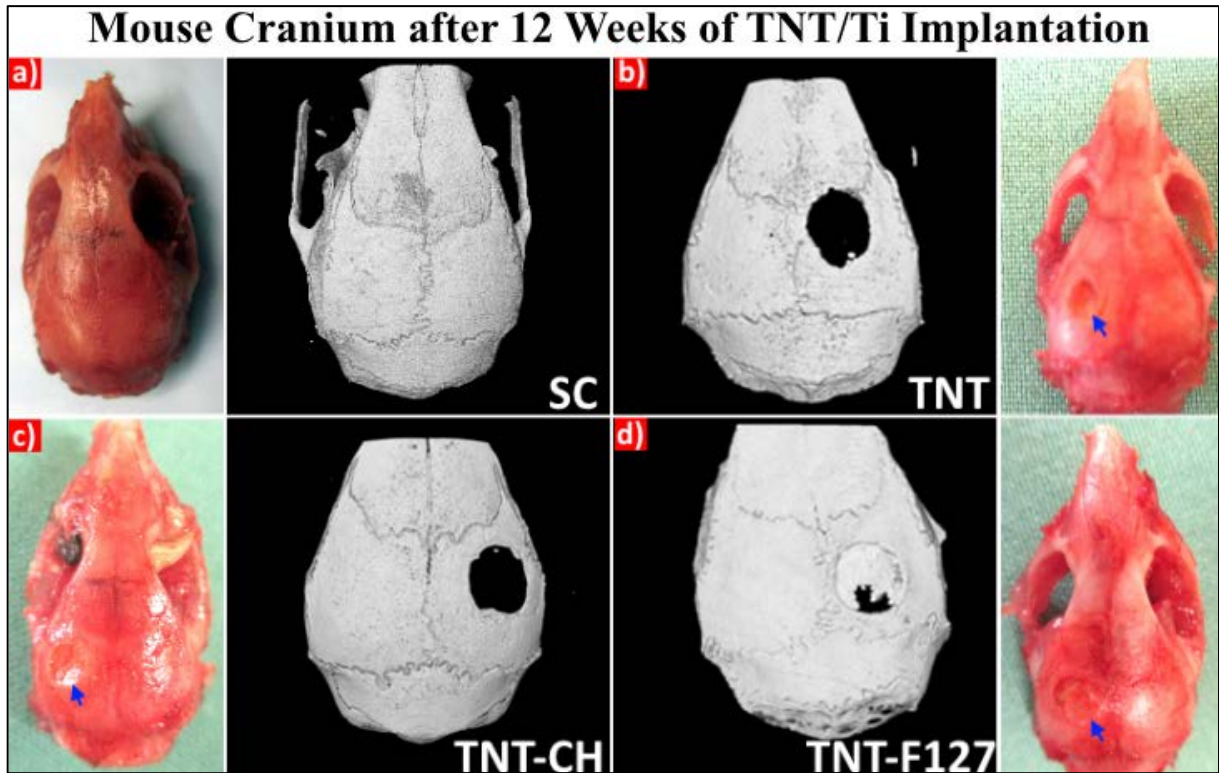
Figure 7.4. The digital and reconstructed micro-CT images of mice cranium, 12 weeks after implantation, showing the impact of different TNT/Ti implants. a) Subcutaneous implant (n=5); new bone formation within the 3 mm CSD for (b) uncoated (TNT), (c) Chitosan-coated (TNT-CH) and (d) Pluronic-F127-coated (TNT-F127) discs (n=3 in each group). The blue arrows on digital photographs mark the implantation (defect) site for visual observations.

The structural assessment was followed by the quantitative volumetric analysis using CT analysis software (CTan). The bone regrowth within the 3 mm defect (volume of interest) was quantified in terms of new bone volume (BV) and bone surface area (BS), represented in **Figure 7.4**. Bone volume, an indicator of relative amount of newly formed bone, was significantly higher ($p < 0.05$) for TNT-F127 coated TNT/Ti group when compared to all the other groups. The BV quantified in **Figure 7.5a** was in the following order: control (0.38 ± 0.07 mm^3) < uncoated TNT

$(0.34 \pm 0.05 \text{ mm}^3) <$ TNT-CH $(0.38 \pm 0.04 \text{ mm}^3) <$ TNT-F127 $(0.75 \pm 0.14 \text{ mm}^3)$. Bone surface area (**Figure 7.5b**) showed almost similar trend in this order: control $(9.65 \pm 1.14 \text{ mm}^2) <$ TNT-CH $(10.89 \pm 1.15 \text{ mm}^2) <$ uncoated TNT $(12.18 \pm 0.71 \text{ mm}^2) <$ TNT-F127 $(23.20 \pm 2.46 \text{ mm}^2)$. The Shapiro-Wilk test of normality was non-significant for all the variables within each group. The pairwise comparisons (univariate analysis, ANOVA) between the groups and the dependent variables (BV and BS) showed that the changes in quantitative indices of uncoated and Chitosan-coated TNTs were non-significant when compared to the control sample (without any implant). These results reinforced the previous findings from this study, wherein TNT and TNT-CH implants did not induce unnecessary bone healing (osteoinduction) or bone resorption (osteolysis). The TNT-F127 samples were excluded from the proposed release studies (Chapter 8) to ensure experimental accuracy, since it yielded significantly higher bone regeneration than all other groups.
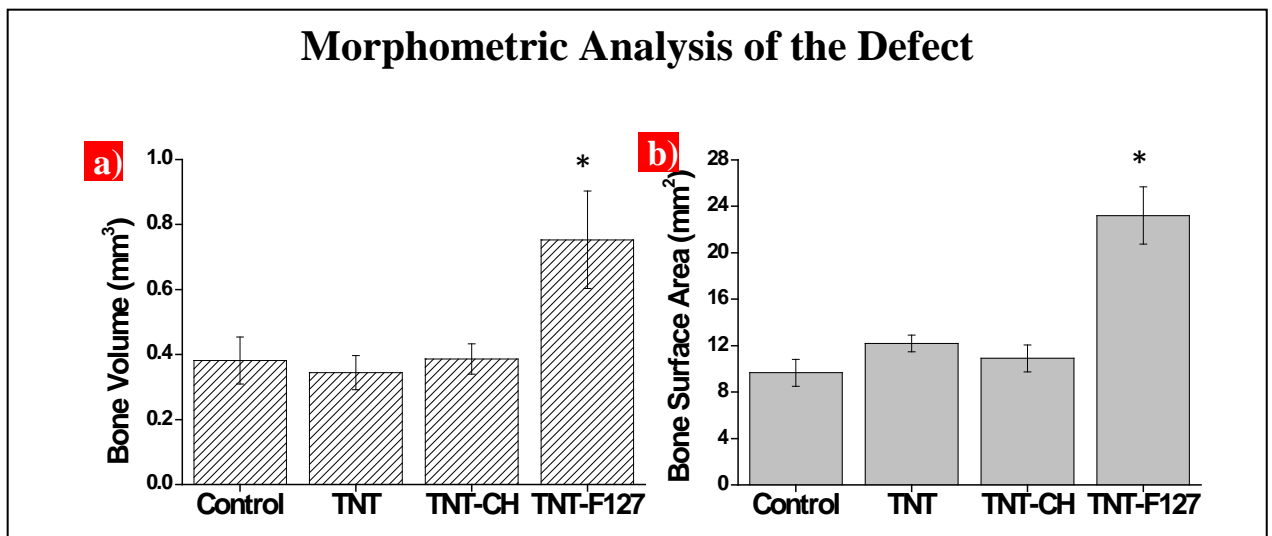
Figure 7.5. Quantitative micro-CT analyses using CTan software showing a) new bone volume (BV) and b) bone surface area (BS) in wildtype mice at 12 weeks post-operation. The Pluronic-F127 coated implant surface induced significantly more bone than rest of the groups (*p<0.05).

7.3.3. Histological analysis of implant biocompatibility

Micro-CT measurements provided information about the amount of new bone formation within the defect area, but lacked information about the non-mineralised tissues and cellular response. The assessment of implant biocompatibility was made by observing the tissue response around the implantation site. The H&E stained sections of skin (over the implant) and the bone (around the defect site) permitted identification of different cell types localised in the soft and hard tissues of interest. **Figure 7.6** shows the microanatomy and cellular structure of the skin covering the subcutaneous implants.
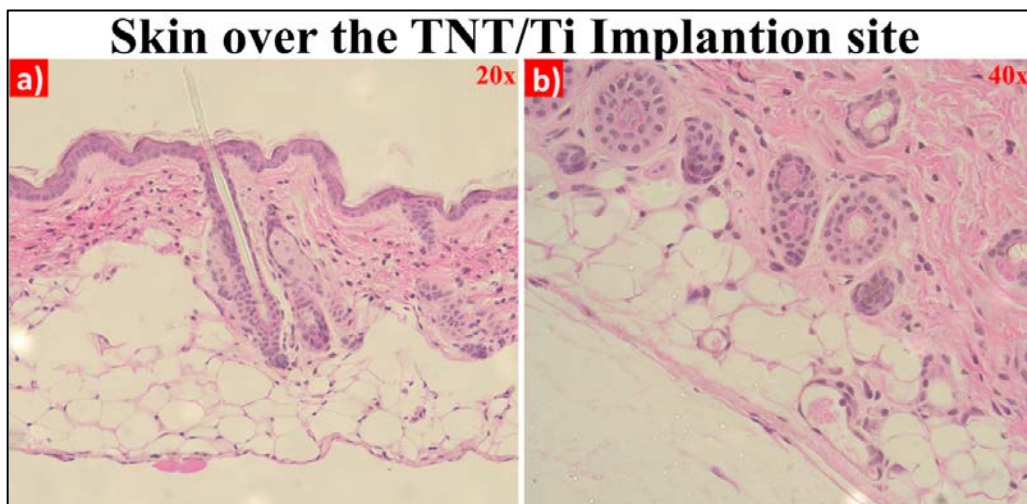
Figure 7.6. Histological analysis of skin over the subcutaneously implanted TNT/Ti discs at a) low and b) high magnification.

The 20× micrograph shows a thin epidermis (formed of 2-3 cell layers), the dermis (formed of dense connective tissue) and the hair follicles associated with the sebaceous glands. The 40× magnification depicts the details of hair follicles and the adipose tissue layer underneath. There

was no discernable difference (in comparison with the normal tissue), adverse reaction or inflammation within the skin layers, establishing the TNT/Ti implant inertness.

The H&E bone histology of the cranial defect, implanted with uncoated and polymer-coated TNT/Ti implants are shown in **Figures 7.7** and **7.8**, respectively. For all the groups, there was no necrosis, lipoma formation or subdural hematoma. Furthermore, there were no signs of chronic inflammation, *i.e.* no observable influx of macrophages, giant bodies or neutrophils. The new bone, within the defect, was presented as a compact structure (in dark pink) while the connective tissue was observed as a loosely bound network of fibroblasts and collagen (in a pale pink). The bone cells (osteocytes and osteoblasts) were present within or at the bone surface. The multinucleated osteoclasts were absent at the implant proximity.
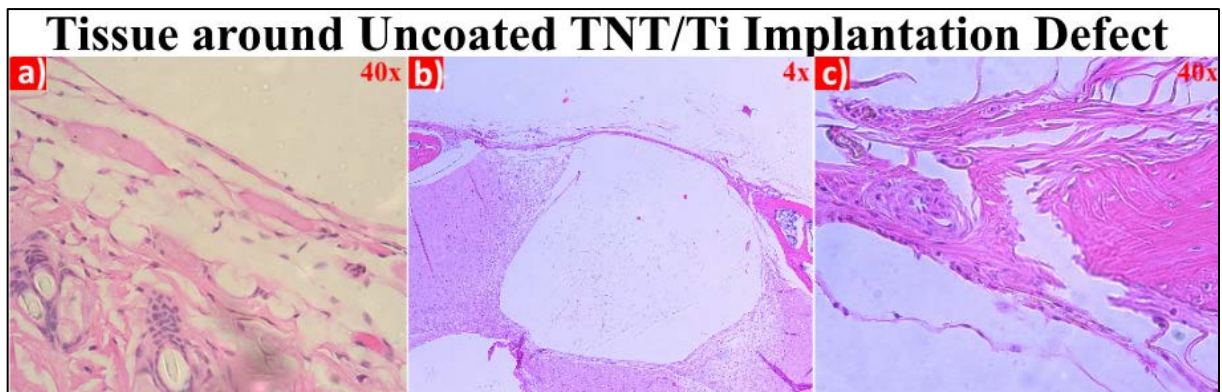
Figure 7.7. Histological evaluation of the tissue around the uncoated TNT/Ti implant site. Representative histology images of a) normal skin over the implant, b) the defect at low magnification (4×) and c) the defect edge at high magnification (40×).

In the micrographs corresponding to the group with uncoated TNT/Ti implants (TNT), the skin cells were healthy and normal **(Figure 7.7a)** and no mineralised bone was observed in the empty cranial defect. Instead, a thin layer of immature fibrous tissue coverage was found over the dura

(**Figure 7.7b**). At 40× resolution at the edge of the defect some fibroblasts and collagen fibers were present along with small amount of bone tissue. In the TNT-CH group, most of the new bone emanated from the margins of the defects and an immature but thick and loose fibrous connective tissue lined the top of the dura (**Figure 7.8a**). The high resolution images (**Figure 7.8b-c**) showed the fibrous layer that was almost acellular around the edge.

Histological evidence further supported the radiographic findings, indicating that the TNT-F127 group showed nearly complete osseous closure of the defect, with a thin layer of newly formed bone along the dural surface. A thick, firm and aligned fibrous tissue layer with tightly packed collagen fibers was also observed over the newly formed bone (**Figure 7.8d-f**). Few solitary bony islands scattered on the dura infiltrated the fibrous tissue network. These observations are based on many histological sections and the extent of bony repair was slightly variable within the sub-groups.
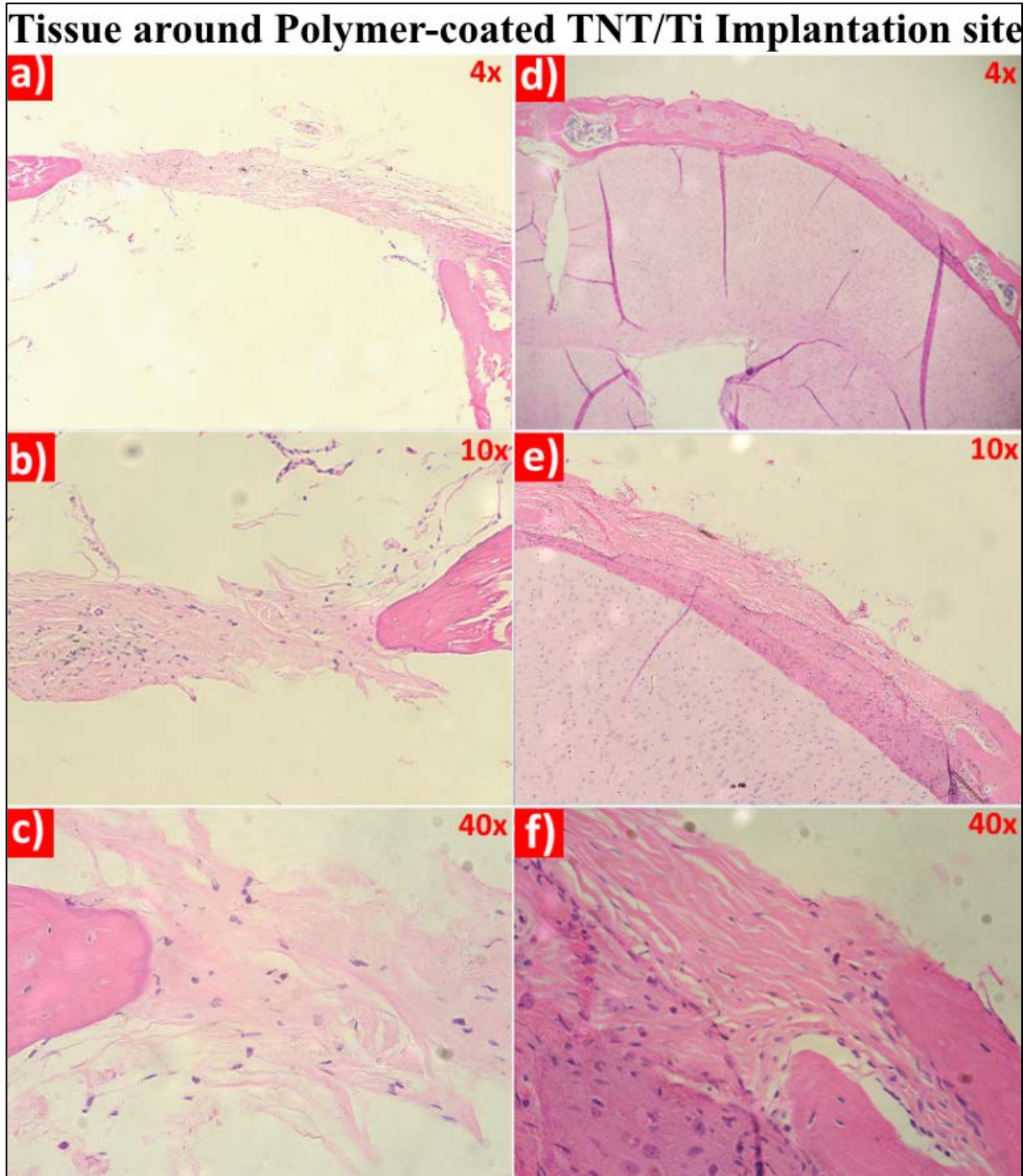
Figure 7.8. Histological evaluation of the tissue around the polymer-coating TNT/Ti implant site. Representative low and high magnification histology images of a-c) chitosan-coated implant (TNT-CH) and b) Pluronic-F127-coated implant (TNT-F127).

In order to confirm the mechanism of ossification during new bone formation within the defect, Alcian blue labelling was performed. This was to eliminate the possibility of progenitor cell differentiation into chrondogenic cell line, leading to cartilage formation instead of direct ossification. **Figure 7.9** clearly showed the absence of any bright blue regions or large cells, corresponding to cartilage or cartilage forming cells (chorondocytes or chrondoblasts), indicating intramembranous ossification.
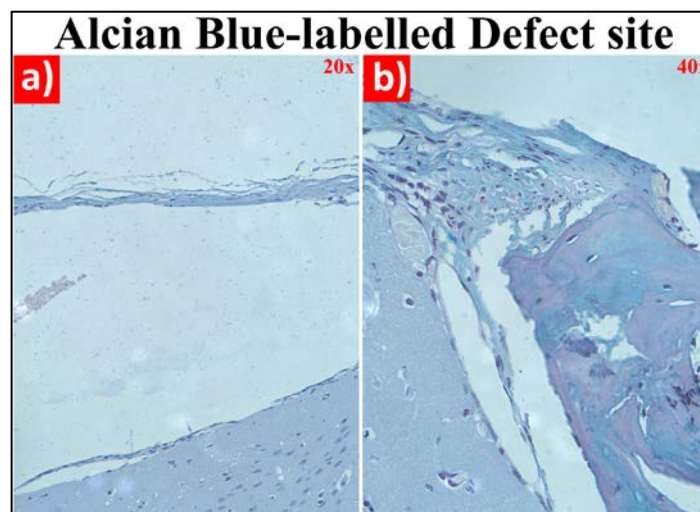
Figure 7.9. Alcian blue staining showing absence of chrondoblasts and cartilage in the fibrous tissue a) over dura and b) at the defect edge.

7.4. Conclusion

This study assessed the biocompatibility of the TNT/Ti cranial implants, implanted subcutaneously and within a surgically created critical-sized defect (CSD, 3 mm in diameter). The implants were sub-grouped into four categories: subcutaneous TNT/Ti (SC); uncoated TNT/Ti (TNTs), Chitosan-coated TNT/Ti (TNT-CH) and Pluronic-F127-coated TNT/Ti (TNT-F127), inserted within the defect. Overall, the necropsy results indicated no adverse skin or bone tissue response to the

TNT/Ti discs (absence of inflammation, necrosis, infection or large cells such as neutrophils, macrophages *etc*.). Visual analysis showed a thin fibrous tissue layer covering TNT/Ti implant surface that was attached to the skin flap or the periosteum over the defect. Specific morphological analysis of the retrieved implants using scanning electron microscopy showed a well-adhered nanotube layer on the Ti disc, with partially open nanopores for the subcutaneously implanted samples. The TNT and TNT-CH samples exhibited fully open nanotubular structure, with obvious polymer degradation in the latter case. However, the TNT-F127 sample showed the complete blockage of nanotube by a dense fibrous tissue layer. EDS-CPS mapping elementally identified the layer to be associated with deposited hydroxyapatite. These results were consistent with the micro-CT and histological analysis of the harvested skulls. The H&E labelling showed no abnormal effect on the tissue morphology in SC mice. Furthermore, the uncoated TNT samples produced radiologically quantifiable bone growth along the defect edges. This was reconfirmed by histological images showing minor peripheral bone formation with a thin immature fibrous tissue over the defect. Similarly, the TNT-CH group showed a relatively thicker, non-mineralised fibrous layer within the defect with slight bone growth at the margins. The TNT-F127 group showed prominent osteogenesis with thin new bone across majority of the defect. Thick, mature and highly organised collagen fibers were also aligned over the newly formed bone, directing bone thickening. Furthermore, Alcian blue staining showed no cells with chrondogenic descent or signs of cartilage during bone formation. The TNT/Ti implant biocompatibility was a pre-requisite for long term implantation and future *in vivo* therapeutic intervention studies.

7.5. References

1.   Brunette, D.M., Tengvall, P., Textor, M., and Thomsen, P., *Titanium in medicine: material science, surface science, engineering, biological responses and medical applications*. **2012**: Springer Science & Business Media.

2.   Moioli, E.K., Clark, P.A., Xin, X., Lal, S., and Mao, J.J. Matrices and scaffolds for drug delivery in dental, oral and craniofacial tissue engineering. *Advanced Drug Delivery Reviews*, **2007**. 59, 308-24.

3.   Schmidt, C., Ignatius, A.A., and Claes, L.E. Proliferation and differentiation parameters of human osteoblasts on titanium and steel surfaces. *Journal of Biomedical Materials Research*, **2001**. 54, 209-15.

4.   Bjursten, L.M., Rasmusson, L., Oh, S., Smith, G.C., Brammer, K.S., and Jin, S. Titanium dioxide nanotubes enhance bone bonding in vivo. *Journal of Biomedical Materials Research Part A*, **2010**. 92, 1218-24.

5.   Pearce, A., Richards, R., Milz, S., Schneider, E., and Pearce, S. Animal models for implant biomaterial research in bone: a review. *European Cells & Materials*, **2007**. 13, 1-10.

6.   Marchant, R., Hiltner, A., Hamlin, C., Rabinovitch, A., Slobodkin, R., and Anderson, J.M. In vivo biocompatibility studies. I. The cage implant system and a biodegradable hydrogel. *Journal of Biomedical Materials Research*, **1983**. 17, 301-25.

7.   Kasemo, B. Biocompatibility of titanium implants: surface science aspects. *The Journal of Prosthetic Dentistry*, **1983**. 49, 832-37.

8. Singhatanadgit, W. Biological responses to new advanced surface modifications of endosseous medical implants. *Bone and Tissue Regeneration Insights*, **2009**. 2, 1-11.

9. Kikuchi, M., Itoh, S., Ichinose, S., Shinomiya, K., and Tanaka, J. Self-organization mechanism in a bone-like hydroxyapatite/collagen nanocomposite synthesized in vitro and its biological reaction in vivo. *Biomaterials*, **2001**. 22, 1705-11.

10. Bansiddhi, A., Sargeant, T., Stupp, S., and Dunand, D. Porous NiTi for bone implants: a review. *Acta Biomaterialia*, **2008**. 4, 773-82.

11. Cooper, G.M., Mooney, M.P., Gosain, A.K., Campbell, P.G., Losee, J.E., and Huard, J. Testing the "critical-size" in calvarial bone defects: revisiting the concept of a critical-sized defect (CSD). *Plastic and Reconstructive Surgery*, **2010**. 125, 1685-92.

12. Ye, J.-H., Xu, Y.-J., Gao, J., Yan, S.-G., Zhao, J., Tu, Q., Zhang, J., Duan, X.-J., Sommer, C.A., and Mostoslavsky, G. Critical-size calvarial bone defects healing in a mouse model with silk scaffolds and SATB2-modified iPSCs. *Biomaterials*, **2011**. 32, 5065-76.

13. Lee, J.Y., Musgrave, D., Pelinkovic, D., Fukushima, K., Cummins, J., Usas, A., Robbins, P., Fu, F.H., and Huard, J. Effect of bone morphogenetic protein-2-expressing muscle-derived cells on healing of critical-sized bone defects in mice. *The Journal of Bone & Joint Surgery*, **2001**. 83, 1032-39.

14. SCHMITZ, J.P. and Hollinger, J.O. The critical size defect as an experimental model for craniomandibulofacial nonunions. *Clinical Orthopaedics and Related Research*, **1986**. 205, 299-308.

15.   Spicer, P.P., Kretlow, J.D., Young, S., Jansen, J.A., Kasper, F.K., and Mikos, A.G. Evaluation of bone regeneration using the rat critical size calvarial defect. *Nature Protocols*, **2012**. 7, 1918-29.

16.   Rentsch, C., Schneiders, W., Manthey, S., Rentsch, B., and Rammelt, S. Comprehensive histological evaluation of bone implants. *Biomatter*, **2014**. 4, 27993.

17.   Dimitriou, R., Tsiridis, E., and Giannoudis, P.V. Current concepts of molecular aspects of bone healing. *Injury*, **2005**. 36, 1392-404.

CHAPTER 8

IN VIVO PROTEIN RELEASE STUDIES OF IMPLANTABLE TNT/Ti DELIVERY SYSTEM TO STOP BONE RE-GROWTH

CHAPTER 8: *In vivo* Protein Release Studies of Implantable TNT/Ti Delivery System to Inhibit Cranial Defect Healing

8.1. Introduction

A major challenge of craniofacial research is to reduce the frequency and severity of complications associated with secondary surgery due to post-operative bone-reossification after primary cranial vault reconstruction [1]. The desire for developing adjunctive methods to treat craniosynostosis has triggered extensive research in the molecular and cranial biology to unravel the mechanisms underlying normal and pathological bone growth events [2-4]. Furthermore, advancements in genetic microarray mapping techniques, and the availability of clinically relevant, genetically-modified animal models, have contributed towards understanding the roles of genes and growth factors in the aetiopathology of syndromic craniosynostosis [2, 5-9]. The well-established Crouzon mouse model displays phenotypic characteristics and cellular complexities that are similar to Crouzon syndrome in humans (associated with Fgfr2$^{c342y/+}$ mutation) [10, 11]. These genetically heterozygous mutant mice have dome-shaped rounded skulls, wide set and proptotic eyes, underdeveloped maxilla, relatively protruded mandibles and prematurely fused coronal sutures (unilateral and/or bilateral synostosis) in the majority (90%) of cases. The sagittal and lambdoid suture obliteration has also been reported in 70% and 30-40% of mice, respectively, depending on the severity of the syndrome [11-13]. A critical-sized defect (CSD) in Crouzon mouse cranium can be used to study and quantify the post-operative bone healing in a craniosynostosis model.

The role of bone morphogenetic protein 2 (BMP2) signalling, which occurs downstream to the Fgfr2 pathway, is well established in normal bone induction and suture fusion (refer to Chapter 2, Section 2.3.4, p.28-32). The perturbation of BMP2 pathway via delivery of BMP2 antagonising molecules (including glypicans, noggin *etc.*) can inhibit bone formation and improve treatment outcomes [14-19]. Although noggin has previously been shown to inhibit BMP-dependent bone formation in different animal models, its effects were short-term and restricted to initial phases of bone healing (refer to Chapter 2, Section 2.3.5, p.35-36). Recently, an elaborate micro-array study showed decreased expressions of glypican 1 and glypican 3 (GPC1 and GPC3) in the sutural region during premature suture fusion in affected children, implicating their involvement in regulating suture patency and osteogenesis [2, 18]. These observations imply that controlled delivery of these proteoglycans at the craniectomy sites in optimal concentrations may lead to an effective therapeutic intervention. However, the lack of clinically viable delivery system to target the bone-forming mechanisms in perisutural area with desirable pharmacokinetics and release pattern still remains a challenge. Since bone formation is a continuous process, a localised delivery platform providing a slow and prolonged application of the glypicans is necessary to observe discernible effects. Moreover, the protein concentration is critical in craniofacial delivery as the heterogeneous suture cells can respond paradoxically to the same biomolecule at different concentrations [20]. Chapters 4 and 6 have demonstrated the *in vitro* ability of protein-loaded Titania nanotubular implants (TNT/Ti discs) to provide a sustained delivery of GPC1 and GPC3 over a period of 2 weeks, depending on the amount of loaded protein. The released glypicans also suppressed the BMP2 activity in transfected C2C12 cells, confirming successful delivery of potent bioactive molecules from the nanoengineered implants. These nanotubular implants showed promise and improvement in terms of release rate and duration over previously researched craniofacial delivery methods

(such as gene transfer technology, direct application of the protein, absorbable collagen sponges and hydrogels *etc*.) [21, 22].

The overall objective of this chapter was to test the *in vivo* efficacy of chitosan-coated and uncoated TNT/Ti implants as delivery platforms capable of localising and releasing the biologically active model proteins (control-BSA and experimental-GPC3) within the murine cranial defects. As described earlier (refer to Chapter 3, Section 3.4.3, p.102 and Chapter 4, Section 4.3.3.2, p.129-133), the biopolymer (chitosan) coating should reduce the initial burst and provide sustained release over a few weeks. The specific aims were (i) to evaluate the effects of BSA (protein control) and rGPC3 (experimental) released from TNT/Ti implants on bone re-growth within the defect site in a **wildtype** mice model, (ii) to assess the bone-antagonising effect of GPC3 released from TNT/Ti implants (chitosan-coated and uncoated) in a **Crouzon** mice model (Fgfr2$^{c342y/+}$ mutated) and to compare it with the wildtype mice, and (iii) to investigate degradation of chitosan film covering the TNT/Ti surface due to the exposure to the physiological milieu and fluids in the cranium of the mice, at 1, 2, 5 and 12 weeks post-operation.

Intra- and post-operative digital photographs were obtained for visual analysis of the cranial defects. Scanning electron microscopy (SEM) was used to observe the chitosan degradation on implants retrieved at different time points (1, 2, 5 and 12 weeks post-operation). High-resolution micro-CT was employed to analyse the amount of bone regenerated within the cranial defect sites at 12 weeks of implantation. The 3D data reconstruction helped calculate the bone volume (BV) and surface area (BS) in relation to the non-mineralised medullary space within the defect site (volume of interest). Qualitative histological analysis of the craniectomy sites using H&E, Periodic Acid-Schiff (PAS), Movat Pentachrome, Picro-Sirius Red and TRAP staining showed

the variance in new bone regeneration, defect width and fibrous tissue accumulation between different groups (refer to Appendix A).

8.2. Materials and methods

A detailed protocol for the *in vivo* studies has been described in the common experimental section (p.214-221). Briefly, the ability of Ti/TNT implants to release therapeutic concentrations of active BSA and/or GPC3 was investigated using a 3 mm critical-sized defect (CSD) lateral to the left coronal suture, in both wildtype (WT) and Crouzon (CZ) mice. The creation of CSD in a Crouzon model, along with placement of the implant is shown in **Figure 8.1**. The mice were implanted with sterilised protein-loaded TNT/Ti implants under general anaesthetic (Xylazine and Ketamine) and analgesic (Buprenorphine) agents as described earlier (Section E, p.216)

Figure 8.1. TNT/Ti implant disc placement within the 3 mm critical-sized defect (CSD) in a Crouzon mouse.

This animal models were divided into two sets involving, the wildtype and Crouzon mice. A flowchart relating to experimental layout with different treatment groups (therapeutic interventions) is shown in **Figure 8.2**. The original defects (control, day 0) on the day of the surgery were also analysed as a baseline in both the models. All the animals used were adults

of 3 months of age at the time of surgery, except wildtype control mice that were older adults of 4 months. The effect of sex on the bone healing was not analysed, but an equal male to female ratio was maintained throughout the groups.
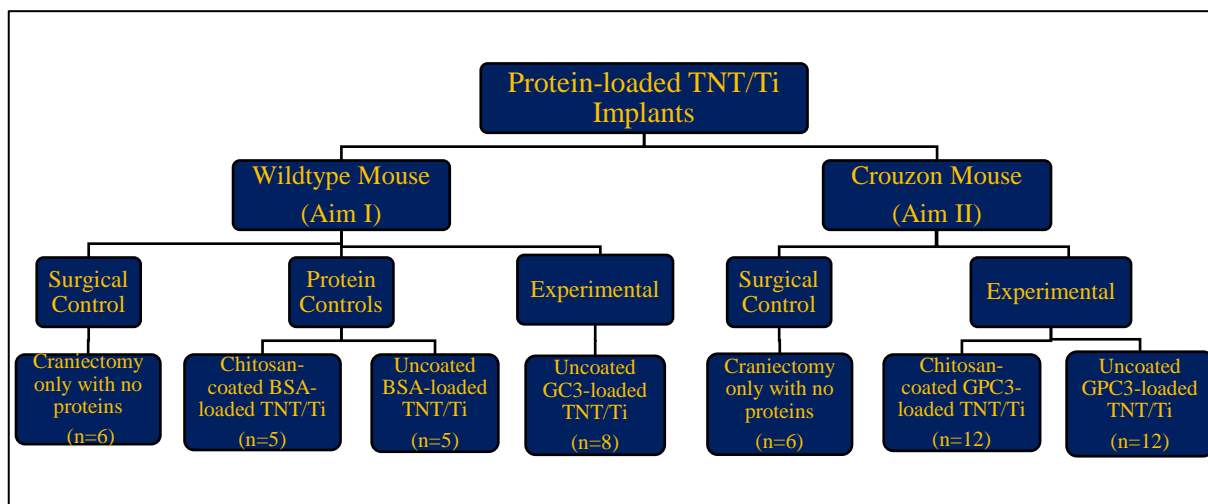
Figure 8.2. Flowchart explaining the experimental layout with different treatment groups. The protein controls were preliminarily tested just in wildtype mice, to establish that the inert BSA did not cause any bone inhibition and the implants did not induce any adverse bone resorption. The surgical control and uncoated (without any polymer coating) GPC3-treated implantation sites were directly compared between the genotypes as a part of Aim II. Aim III related to the chitosan degradation process is not included in this flowchart.

All mice were kept under daily observation and provided with regular food and water up to 3 months to encourage full recovery. The Crouzon mice required special access to ground and mushy food and weekly tooth trimming due to mandibular prognathism. All mice were humanely euthanised by CO_2 asphyxiation at 90 days and the skulls were collected and deskinned for further analysis (Section E, p.218).

The quantitative volumetric analysis was performed using micro-CT and related software (Section G, p.219). The qualitative histological investigations with H&E showed the newly-

formed bone (pink) and fibrous tissue (pale pink) in different groups. A Movat Pentachrome staining helped differentiate new and old bone sections with collagen (light yellow), elastin (black), muscle (red), mucin (blue to green) and fibrin (intense red) that were labelled differently in the tissue sections. A Periodic Acid-Schiff (PAS) staining was also performed to observe secreted mucins and glycogen (red/purple), followed by Picro-Sirius Red staining in selected samples to identify collagen type I (thick large bundles in red) and type III (thin bundles in red) fibres under a bright field microscope. Sirius red sections were also analysed under polarised light to visualise a fibre thickness-dependent colour change (from green to yellow to orange to red with increasing thickness). A Tartrate-resistant acid phosphatase (TRAP) marker was further used to observe any bone resorption around the delaminated TNTs in the defects, marked by presence of osteoclasts (in red) [23-25]. The retrieved TNT/Ti implant surfaces were analysed using SEM.

8.3. Results and discussion

8.3.1. TNT/Ti implant analysis

8.3.1.1. Surface analysis

Surface characteristics of a representative uncoated TNT/Ti implant retrieved after the release study (12 weeks post-implantation) are shown in **Figure 8.3**. The digital and SEM image of the implanted disc (**Figure 8.3a-b)** depicted a well adherent TNT layer on the underlying Ti. A high-resolution SEM (**Figure 8.3a-b**) confirmed the unique geometry of TNTs with ordered arrays of open-pored structures (120 ± 10 nm in diameter).
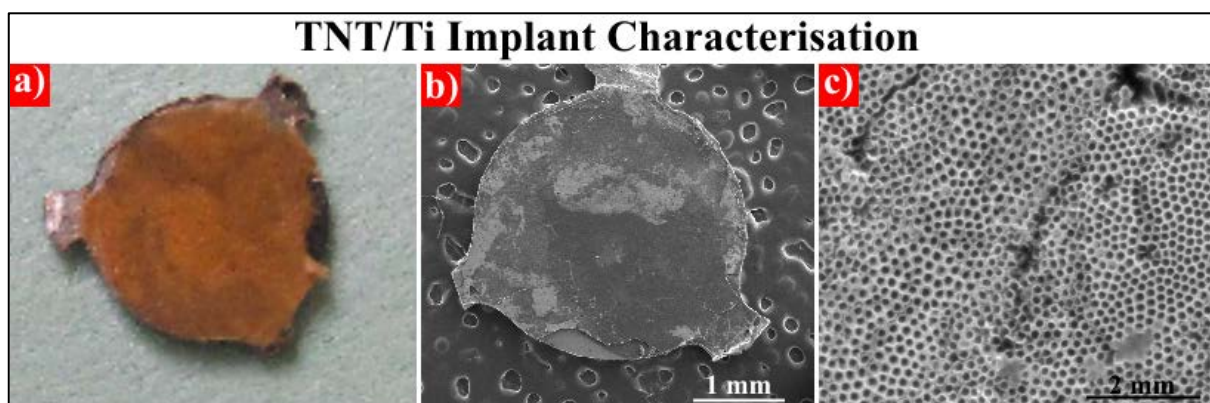
Figure 8.3. The surface characterisation of representative TNT/Ti implant (without polymer coating) retrieved after the *in vivo* release study showing (a) digital photograph of the implanted disc and (b-c) scanning electron microscope image of the TNT surface.

In uncoated TNT/Ti implants, the model proteins were released into the CSD and the perisutural region by passive diffusive transport based on the concentration gradient in the cranial environment (extracellular matrix and interstitial fluids) [26]. However, for chitosan-coated TNT/Ti implants (polymer thickness ~1 µm; refer to Chapter 3, Section 3.4.3, p.102-103) and Chapter 4, Section 4.3.3.2, p.129-133), the release kinetics of the protein encapsulated inside the nanotubes also depended on *in vivo* polymer degradation and transformation.

The chitosan films undergo enzymatic hydrolysis in the presence of several proteases, mainly lysozymes (present in body fluids) [27]. The SEM images of chitosan films (coating the TNT surface) after 1, 2, 5 and 12 weeks of implantation (**Figure 8.4**) clearly show the dissolution of chitosan coating over time and its transformation into a microscale mesh. The partially open pores (with patches of undissolved polymer) were responsible for slow release of the therapeutic proteins. The rate of *in vivo* chitosan degradation was much slower than that previously observed in an *in vitro* study (degradation in PBS) [28].
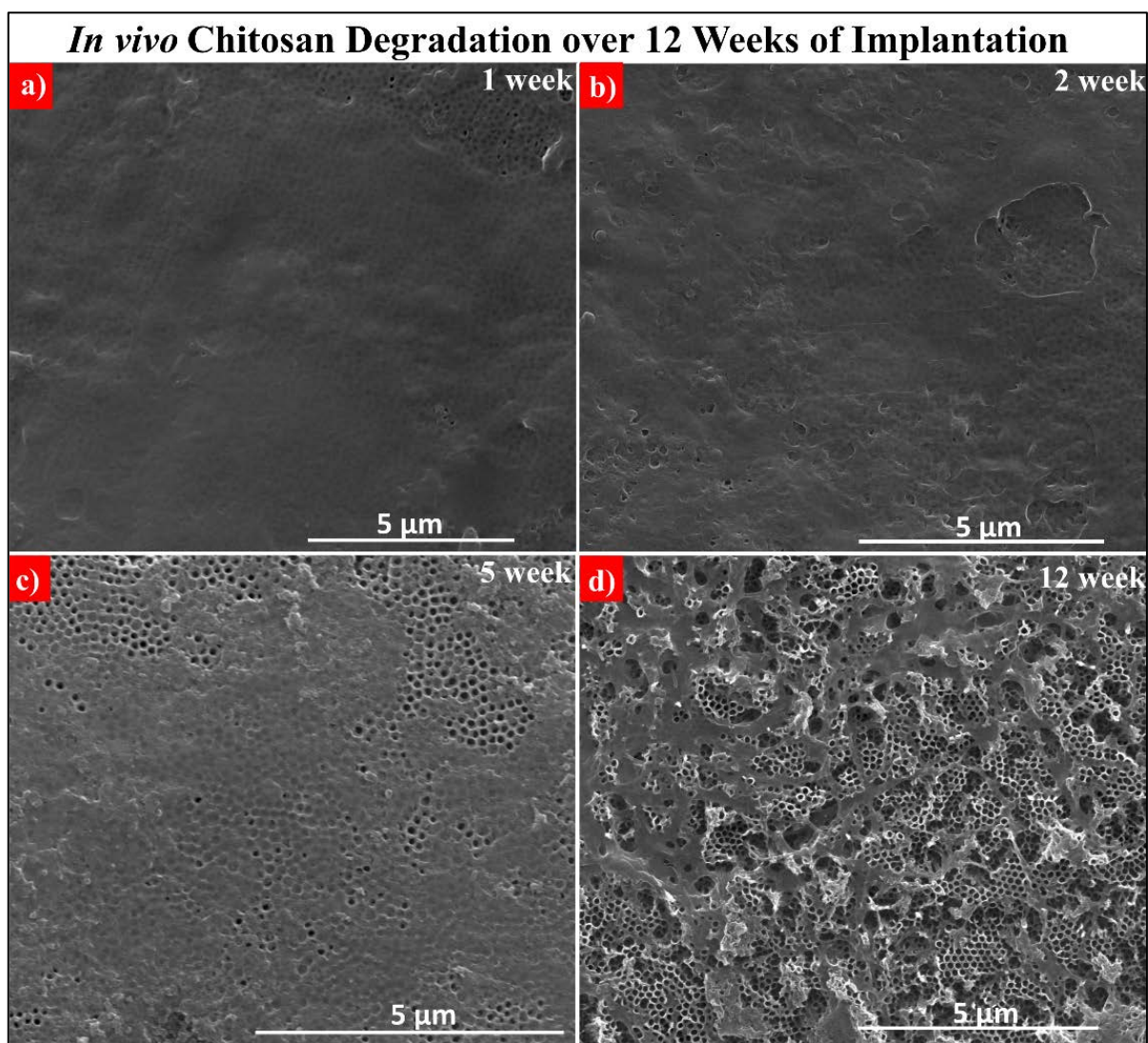
Figure 8.4. Top-view SEM images showing the degradation of chitosan spin-coated onto the TNT/Ti implants after (a) 1 week, (b) 2 weeks, (c) 5 weeks and (d) 12 weeks of implantation.

8.3.1.2. TNT-tissue interaction

No inflammatory infiltrate was present around the TNT/Ti implants. However, thin fibrous connective tissue were found at the TNT-tissue interface which led to delamination of the anodic TNT layer from the Ti surface in certain cases, whilst handling/removing the implant (**Figure 8.5b**). The mechanical stability can be compromised due to a number of factors. From the fabrication perspective, the higher growth rate due to high electrolyte water content (5%) and anodisation voltage (120 V) might have enhanced the expansion coefficient (in between the oxide and metal) during anodisation, leading to less adherent anodic film [29, 30]. Presence of "weak spots" that allow electrolyte penetration to the underlying Ti could also attribute to swelling and delamination of the nanotube layer [29, 31]. However, since the TNT/Ti implants used for tissue response studies (Chapter 7) maintained their mechanical integrity throughout and after the 12 weeks implantation period, the delamination of the TNT layer is unlikely to be a fabrication error. However, the subsequent protein loading under repeated wetting and vacuum evaporation of the solvent might have weakened the interfacial barrier layer between the nanotube oxide and Ti disc. Thus, the loading step, along with the strong adhesion of the implants surface to the periosteum or the skin fibrous tissue, must have caused the thin barrier layer to coil and delaminate (surface tension dependent phenomenon) [32]. A change in anodisation parameters to obtain shorter nanotube length and an immersion loading approach may help resolve this issue in future studies.
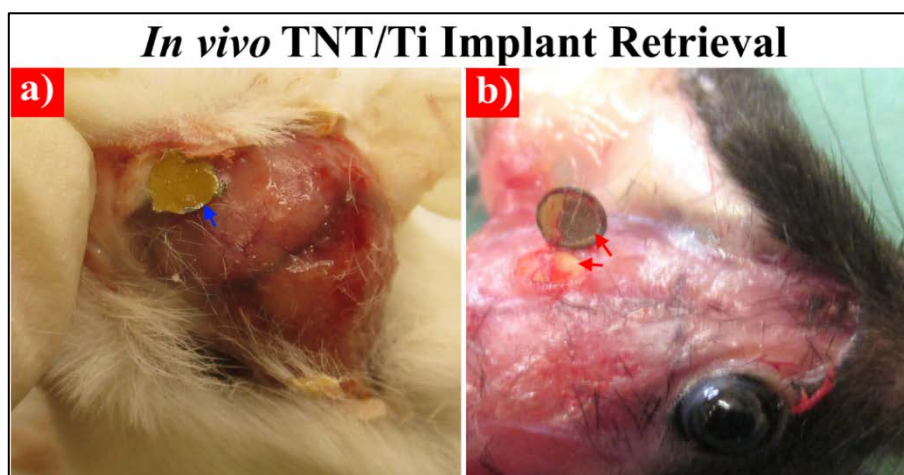
Figure 8.5. Representative images of implant retrieval showing a) well-adhered TNTs on Ti disc and b) delaminated TNTs in the defect. The blue arrow shows the intact TNT layer while the red arrows mark the partially detached TNTs on the substrate and the defect site.

The histological evaluation at the TNT-tissue interface (**Figure 8.6**) showed no adverse response such as inflammatory or multinucleated cells (macrophages or granulocytes) in the implant proximity. H&E labelled section of the whole defect at the low magnification (4×) showed extensive cellular scar tissue encapsulating the nanotubes (**Figure 8.6A-a**). Furthermore, the corresponding high magnification (40×) images of TNT interfaces with the fibrous tissue (with fibroblasts and intravascular blood cells) and bone showed absence of any chronic inflammatory cells (macrophages, foreign body giant cells or neutrophils) after 12 weeks of implantation (**Figure 8.6A-b-c**). The PAS stained sections at both 10× and 40× magnifications were negative for any neutral or acidic mucosubstances such as muco- and glycoproteins, glycogen and mucopolysaccharides (usually stained red/purple) (**Figure 8.6B-a-c**).
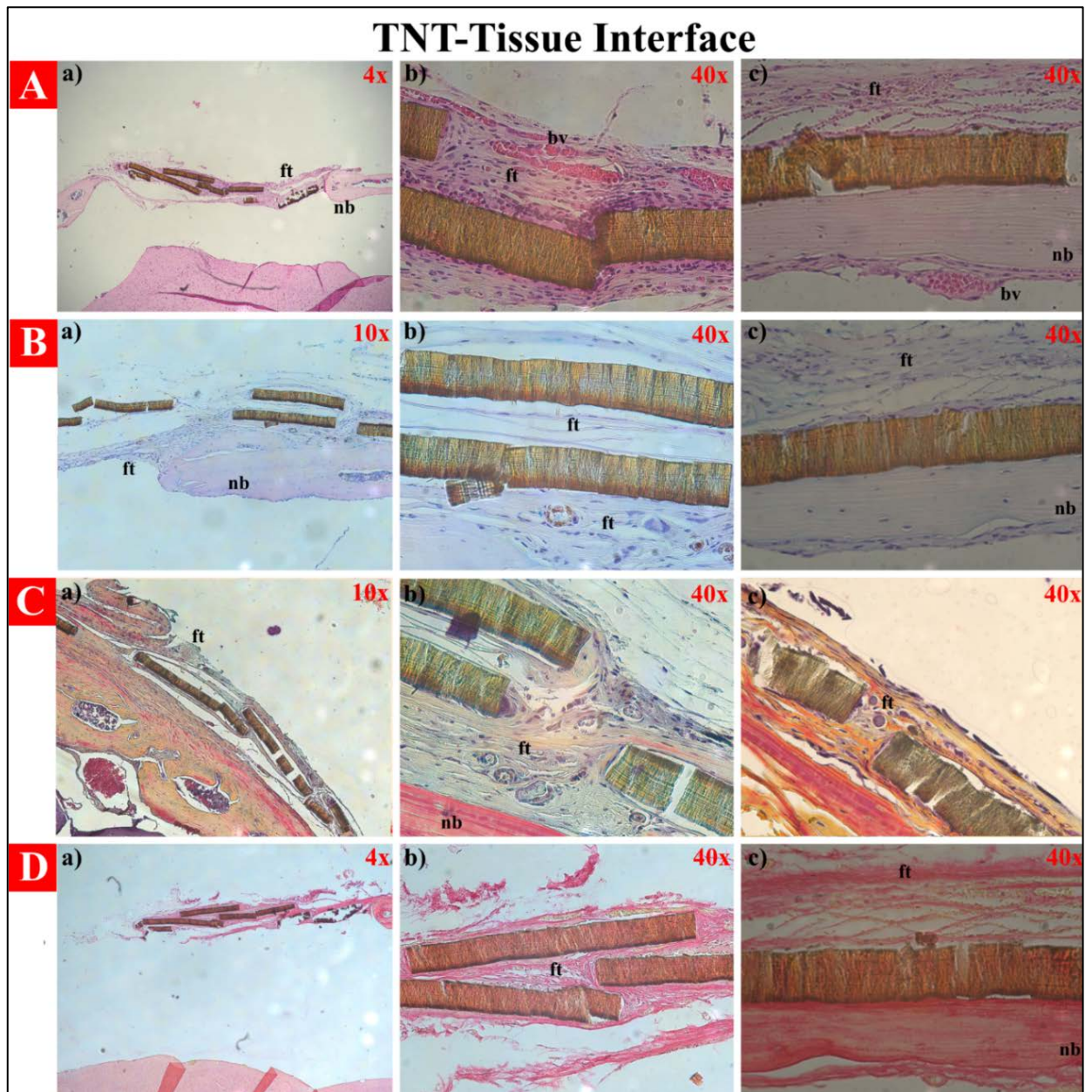
Figure 8.6. Histological evaluation of the interface between delaminated TNTs and surrounding tissue using A) H&E, B) Periodic Acid-Schiff (PAS), C) Movat Pentachrome and D) Picro-Sirius Red staining. The magnification scales are mentioned at the top corner of each panel. The low magnification images (at 4× and 10×) displayed the overall defect microenvironment while the high magnification images (at 40×) displayed the TNT interface with the fibrous tissue and the bone (nb: new bone, ft: fibrous tissue, bv: blood vessel).

The Movat pentachrome staining at 10× magnification (**Figure 8.6C-a)** distinguished the old mature bone (dark yellow) with muscles (red) from fibrous tissue with collagen (light yellow) at the defect site. The strong contrast between the fibrous tissue (collagen) surrounding the nanotubes and the dark coloured nuclei (purplish-black) at 40× magnification (**Figure 8.6C-b-c**) further allowed clear identification of existing cells (osteoblasts, osteocytes and fibroblasts). The delaminated TNTs encapsulated in connective tissue around the implantation site did not affect the bone tissue or the underlying dura. Furthermore, the absence of any blue coloured cartilage or chorondocytes indicated that the defect site had undergone intramembranous reossification.

The Picro-Sirius Red staining under bright-field microscope at 4× magnification showed the collagen (red) secreted by cells (around the implant) and deposited within the defect (**Figure 8.6D-a**). The thickness, length, density and orientation of collagen fibres differentiated collagen type I from type III. While most samples showed deposition of long, tightly packed cylinders of bone-forming collagen type I fibres within the defect (variable between different groups), the fibres around the TNTs were relatively loosely bound (**Figure 8.5D-b-c**).

Furthermore, an enzyme histochemistry staining (using TRAP marker) showed absence of eroded bone surface (resorptive pits) generated by active osteoclasts (usually marked in red). **Figure 8.7** shows the TRAP negative results for the delaminated TNTs around the bone tissue. The neutral response indicated that the implants did not cause bone resorption.
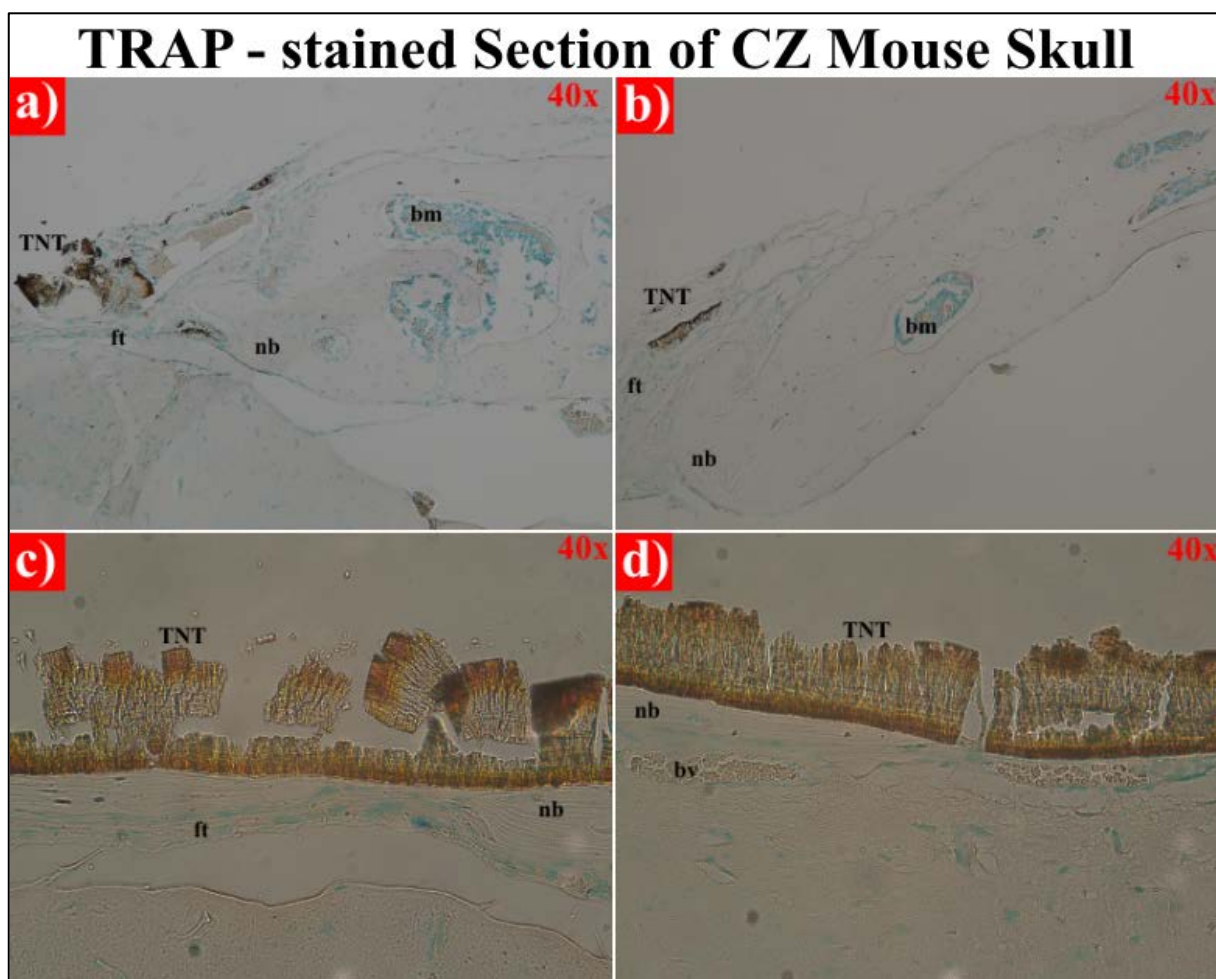
Figure 8.7. Representative Tartrate Resistant Acid Phosphatase (TRAP)-stained histological sections of cranial defects in mice following 12 weeks of TNT/Ti implantation. (a-b) The defect edge with broken delaminated TNTs surrounded by fibrous tissue and (c-d) the TNTs around new bone tissue, showing absence of TRAP positive cells (osteoclast- in red). (nb: new bone, ft: fibrous tissue, bv: blood vessel, bm: bone marrow, TNT: free standing Titania nanotubes). These images showed complete absence of osteoclasts or resorptive pits.

8.3.2. Protein release studies in murine models

8.3.2.1. Selection of the murine model

The use of animal models has made it possible to investigate bone healing in general and with therapeutically relevant TNT/Ti implants. The phenotypic differences of Crouzon mice with Fgfr2$^{c342y/+}$ mutation and their wildtype littermates with a mixed background are summarised in **Figure 8.8**.
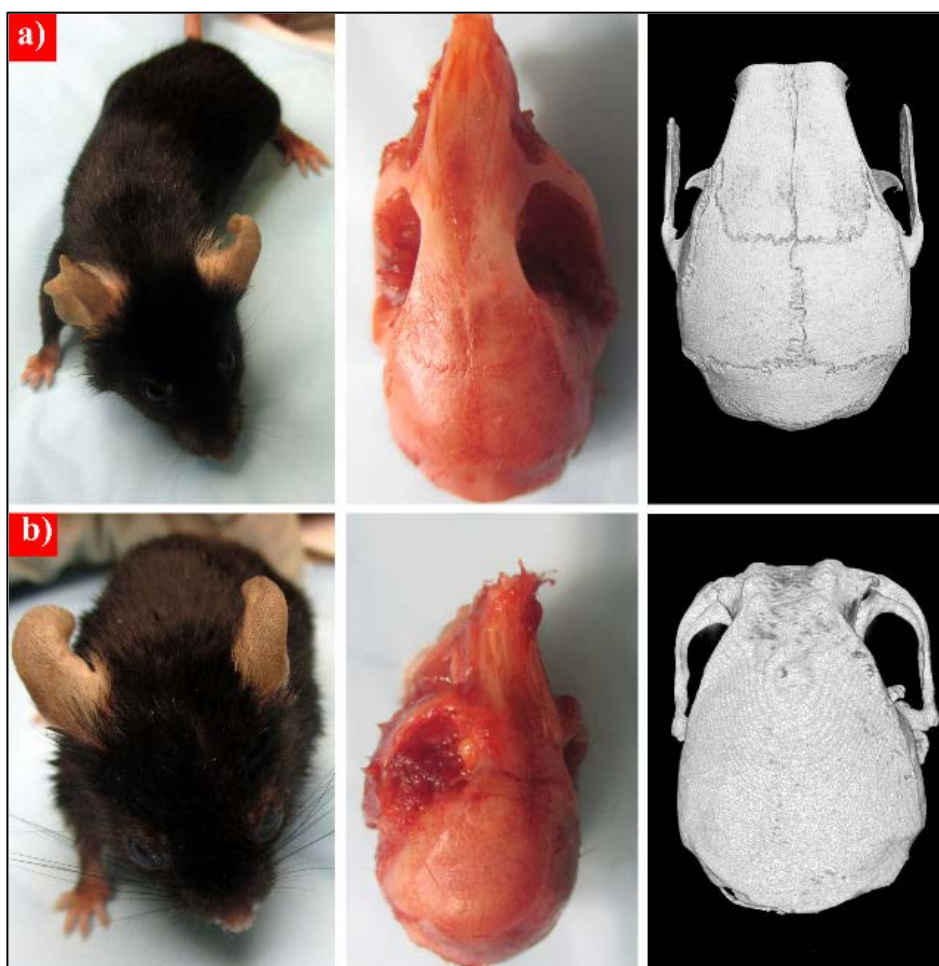
Figure 8.8. The digital and 3D micro-CT images of (a) Wildtype mouse and (b) Crouzon mouse with Fgfr2^{c342y+} mutation (with rounded calvaria, midface shortening and pansynostosis-premature fusion of all sutures).

The digital photographs and 3D micro-CT scans of the wildtype mouse (**Figure 8.8a**) revealed a normal shaped and sized skull similar to unaffected humans, with open sutures (except for frontal suture that closes early). The affected mice (**Figure 8.8b**) exhibited phenotypes that were analogous to severe human Crouzon patients, with complete fusion of all sutures (pansynostosis). They also had a characteristic flattened midface, protruding eyes, shorter snout and an overall shorter and rounded skull (along anteroposterior axis). Both these models were used to create CSDs over the left parietal bone, next to the coronal sutures.

8.3.2.2. Protein release in Wildtype murine model

The preliminary *in vivo* testing of proposed TNT/Ti protein releasing implants was conducted in wildtype murine model associated with normal bone healing and suture formation. Provided there were no intraoperative complications while creating the defect, most mice tolerated the surgical procedure well. Two mice were lost during the 12 week follow-up period from non-surgery related complications. The visual and morphological assessments of the defect sites in euthanised WT mice 12 weeks after treatment (post-operative) are summarised in **Figure 8.9**. All incision sites sealed with resorbable sutures had healed by the end of the study, with no signs of swelling, infection, abscess and wound dehiscence. A necropsy re-established implant safety with no evident tissue lesions, inflammation or purulence at and around the implantation site. **Figure 8.9A** shows the margins of the original defect with new bone originating from the edges (blue arrows). The visual analysis indicated variability in bone re-growth within the defects for the four different treatment groups (craniectomy only- wildtype control, chitosan-coated and uncoated TNT/Ti implants loaded with BSA- protein controls and TNT/Ti implants loaded with GPC3- experimental intervention).
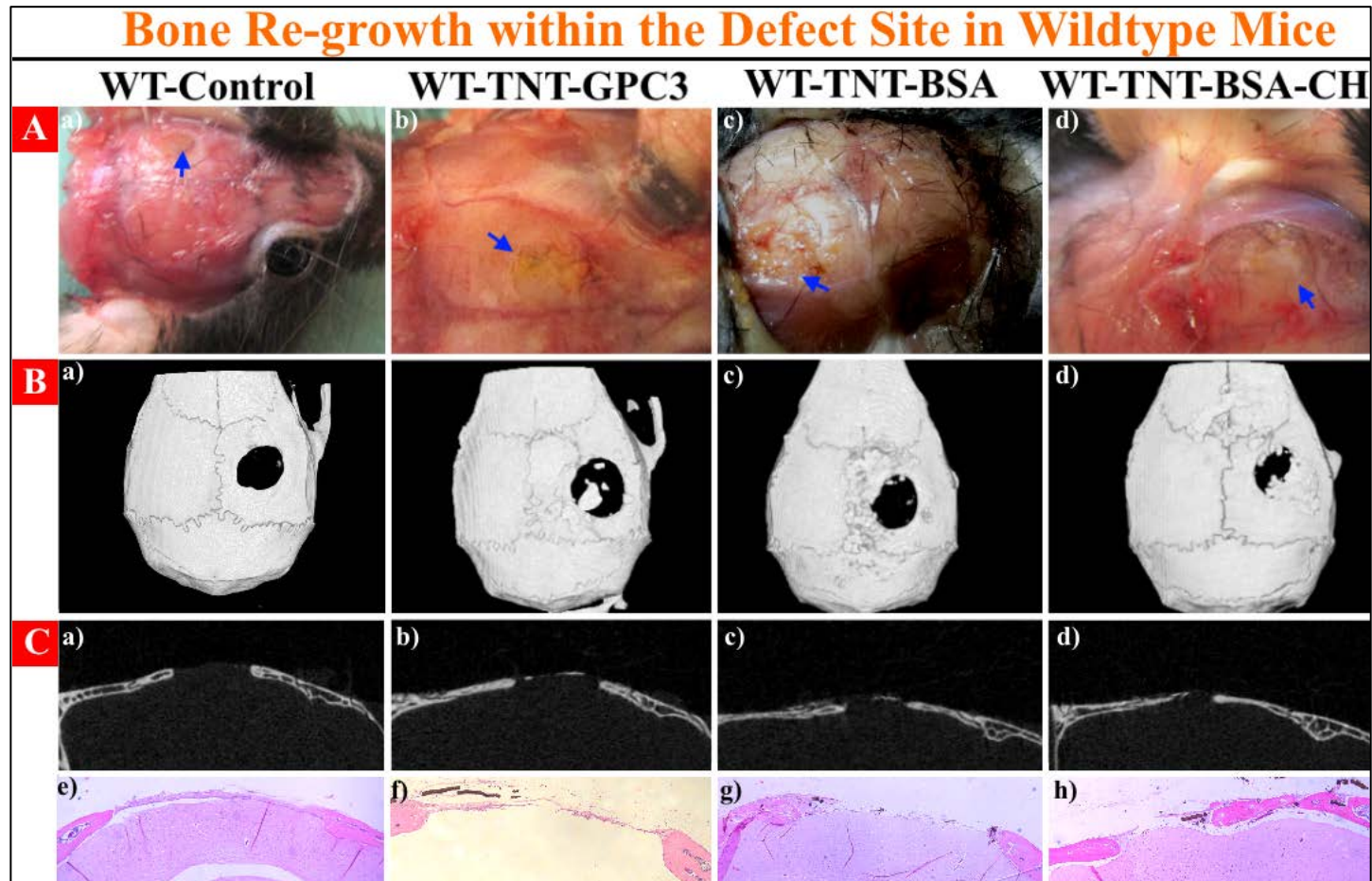
Figure 8.9. Representative images from different treatment groups of wildtype mice (craniectomy control, protein controls and experimental). A) Digital images showing bone healing at the implantation site (the blue arrows mark the defect), micro-CT images showing B) the 3D reconstructed skull with defects and C) 2D sagittal section of defect region showing bone re-growth with the comparative H&E histology (lower panel).

After 12 weeks of implantation, high-resolution micro-CT imaging was used to compare the amount and morphology of newly formed bone in harvested skulls, and the representative images from each group are shown in **Figure 8.9B-C**. The 3D renderings demonstrated that the empty defects (control craniectomies) had marked peripheral bone healing along the defect boundaries while the middle of the defect was unossified (**Figure 8.9B-a**). In contrast, the defect sites treated with GPC3 released from TNT/Ti implants showed comparatively larger defects (diminished bone volumes) with some bone formation over the dura (**Figure 8.9B-b**).

Both the protein controls (BSA-loaded TNT/Ti implants), with and without chitosan-coating, showed similar reossification patterns resulting in substantial decrease in the size of the original defect (**Figure 8.9B-c-d**). **Figure 8.9C-a-d** illustrate the 2D sagittal section of the 3D image of the skull. The 2D results were in coherence with the 3D observations showing a difference in the bony bridging across the defect sites between the groups. The comparative H&E histological images of the defect sites displayed in **Figure 8.9C-e-h** complement the 2D micro-CT sections in all treatment groups (detailed histology on p.262-266).

In addition, CT-based morphometric analysis was used to quantify the new bone volume (BV) and surface area (BS) within the defect. The mean BV, quantified in **Figure 8.10a**, was in the following order: TNT-BSA-CH (0.59 ± 0.06 mm^3) > TNT-BSA (0.49 ± 0.06 mm^3) > control day 90 (0.41 ± 0.08 mm^3) > TNT-GPC3 (0.26 ± 0.03 mm^3) > control day 0 (0.06 ± 0.02 mm^3). Mean bone surface area (**Figure 8.10b**) showed a slightly different trend in the order: TNT-BSA-CH (12.34 ± 0.53 mm^2) > control day 90 (9.64 ± 1.48 mm^2) > TNT-BSA (8.01 ± 1.75 mm^2) > TNT-GPC3 (7.68 ± 1.64 mm^2) > control day 0 (2.68 ± 1.16 mm^2).
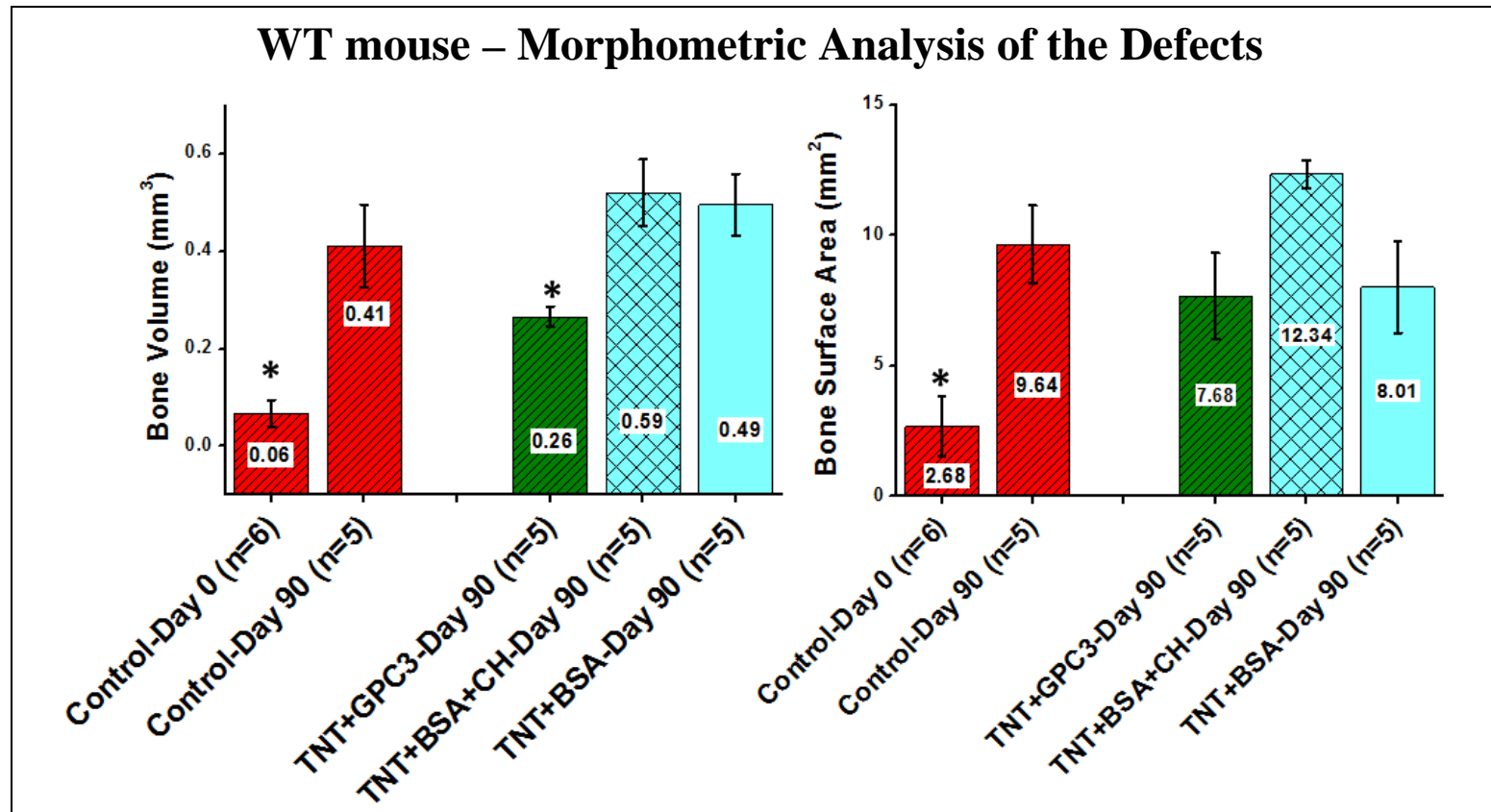
Figure 8.10. Quantitative micro-CT analyses using CTan software showing new bone volume (BV) and bone surface area (BS) within the defect in wildtype mice at 12 weeks post-operation. The GPC3-loaded TNT/Ti implants significantly (*$p<0.05$) reduced the bone formation (BV) compared with the craniectomy and protein control groups. The initial (control day 0) and final (control day 90) bone growth parameters correspond to original defect and the naturally healed defect, respectively.

The Shapiro-Wilk test of normality was non-significant for the variables (BV and BS) within each group. One-way ANOVA showed a significant effect of the GPC3 treatment on BV but not on BS. The pairwise comparisons with Bonferroni post-hoc tests revealed that the BV for GPC3-treated groups was significantly lower than the craniectomy and protein controls ($p<0.05$). The diminished bone volume confirms the ability of GPC3-loaded TNT/Ti implants to therapeutically downregulate the BMP2 activity and hence the bone morphogenesis. There were no statistically significant differences within and between the chitosan-coated and uncoated BSA-control and the empty defects. This further reinforces the delivery potential of TNTs and justifies the use of BSA as a control protein with no therapeutic action. However, in most samples, the chitosan coating showed slightly more bone regeneration when compared to the uncoated implants and the control group. The GPC3 treated group also showed non-significant difference to the baseline control (day 0, original defect), indicating successful bone-inhibition.

The micro-CT data was supported by the qualitative microscopic analysis of histological sections. Non-bony, fibrous tissue was evident within the defect regions, regardless of the treatment. **Figure 8.11** presents the histological analysis of bone regeneration in control group (craniectomy only) after 12 weeks of surgery. The H&E staining at 4× magnification (**Figure 8.11a**) revealed a thick band of fibrous connective tissue within the defect, along with newly woven bone at the defect edges connected to mature osseous bone, narrowing the defect. **Figure 8.11b** displays the 20× magnified image of the edge of the new, non-vascularised bone with limited bone marrow.
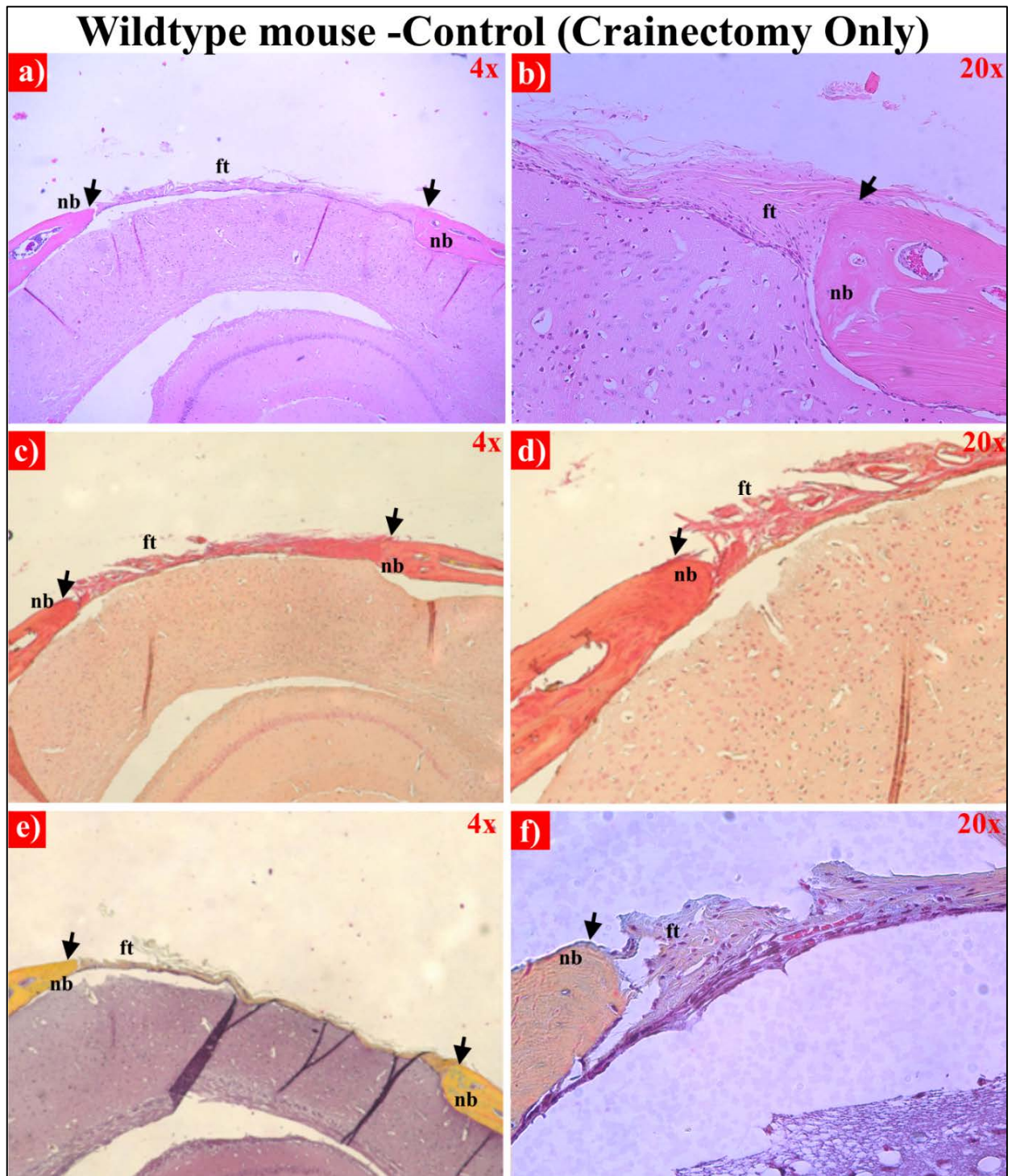
Figure 8.11. Histological analysis of bone regeneration in 3 mm cranial defect after 12 weeks of healing in wildtype craniectomy control model. Representative low and high magnification histology images of the defect site and its edge with (a-b) H&E, (c-d) Picro-Sirius red and (e-

f) Movat Pentachrome staining. The magnification scales are mentioned at the corner of each panel; black arrows mark the new bone edge (nb: new bone, ft: fibrous tissue).

The Picro-Sirius red labelling showed the thick disorganised collagen fibres bridging the defects. The 4x magnification (**Figure 8.11c**) showed the decrease in original defect width due to the formation of new bone along the margins (**Figure 8.11d**). The firm fibrous tissue emanating from the new bone were clearly visible at 20x magnification. The Movat Pentachrome staining further differentiated the bone from fibrous tissue. The low magnification image (**Figure 8.11e**) showed the collagenous fibres lining the dura while the 20x magnification image (**Figure 8.11f**) presented a layer with few fibroblasts. The black arrows at the periphery mark the new defect edge, showing narrowing of the original defect.

The histological observations of the defect sites in protein control groups were also consistent with the micro-CT data. **Figure 8.12** presents the H&E labelled sections of wildtype mice with BSA-loaded TNT/Ti implants. At $4\times$ magnification, prominent bone reossification was observed (**Figure 8.12a**) while at $20\times$ magnification, a section cut across the defect margin showed prominent defect healing with thick acellular fibrous tissue (**Figure 8.12b**). In **Figure 8.12c**, the new bone around the defect edge can clearly be seen. **Figure 8.12d** displays the unfused sagittal suture in the wildtype skull and shows that the delaminated TNTs did not pose any adverse effect on the surrounding tissue.

Figure 8.12. Histological analysis of bone regeneration in 3 mm cranial defects implanted with BSA-loaded TNT/Ti discs, after 12 weeks of healing. Representative H&E images of the defect site and edge at (a) low and (b-c) high magnifications; (d) the unfused sagittal suture in the wildtype mouse. The magnification scales are shown at the top right corner of each panel; black arrows mark the margin of the new bone (nb: new bone, ft: fibrous tissue, bv: blood vessel, TNT: free standing Titania nanotubes, ss: sagittal suture).

Furthermore, the H&E labelled sections of wildtype mice skull with chitosan-coated BSA-loaded TNT/Ti discs implanted within the defect are shown in **Figure 8.13** (in increasing order of magnification)**.** These mice displayed significant wound healing with some bony bridging (**Figure 8.13a-b**). Isolated bony islands over the dura interpolated with few strands of tightly packed fibrous tissues were also evident (**Figure 8.13c-d**).
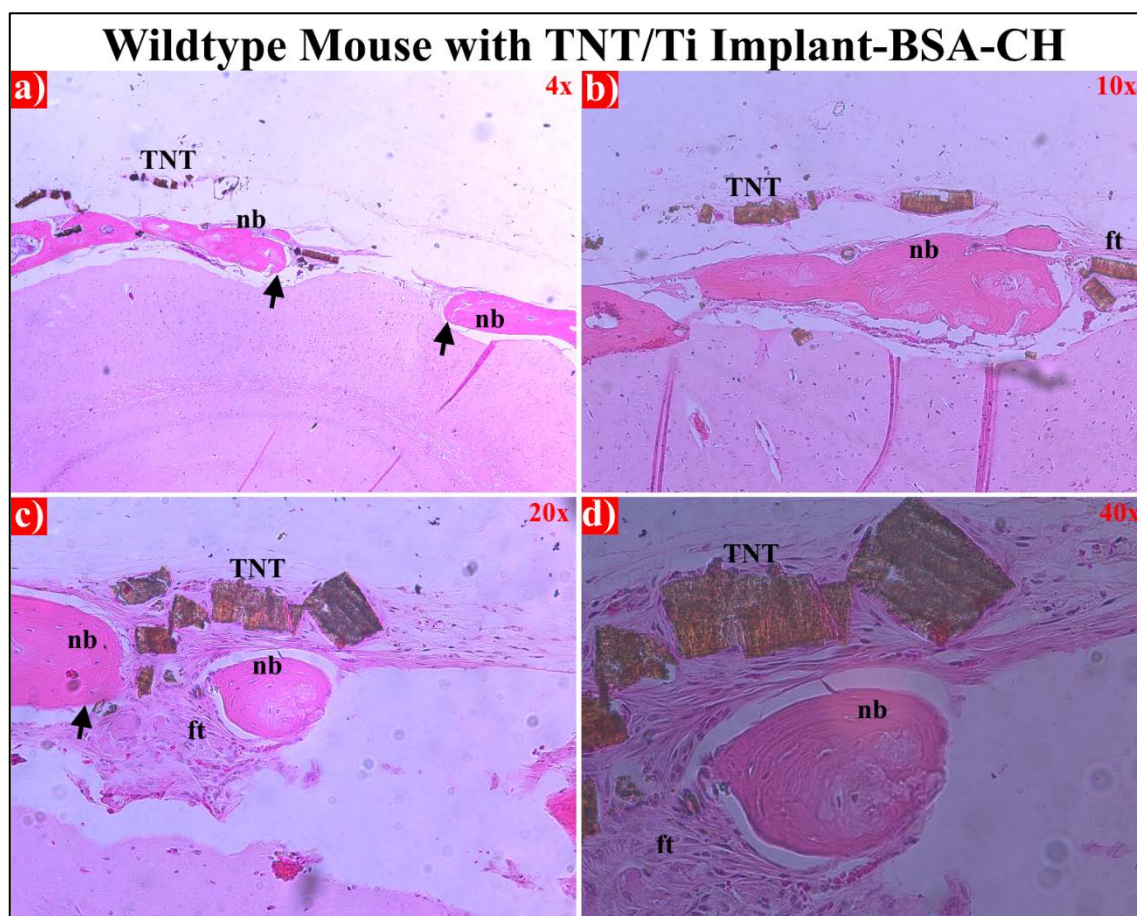
Figure 8.13. . Histological analysis of bone regeneration in 3 mm cranial defects implanted with chitosan-coated BSA-loaded TNT/Ti discs, after 12 weeks of healing; (a-d) Representative H&E images of the defect site, the bone edge and the newly formed bony islands in increasing degree of magnification demonstrating significant bone healing (nb: new bone, ft: fibrous tissue, TNT: free standing Titania nanotubes).

The histological data further supported the notion that the defects implanted with GPC3-loaded TNT/Ti discs caused bone inhibition, evident by the marginal bone re-growth. **Figure 8.14** presents the H&E and Movat pentachrome labelled slices of this experimental group with more fibrous than bony defect edges. Both H&E (**Figure 8.14a-c**) and Movat pentachrome (**Figure 8.14d-f**) stained images (from low to high magnification) revealed larger, unhealed and less ossified defect sites in comparison with other treatment groups.
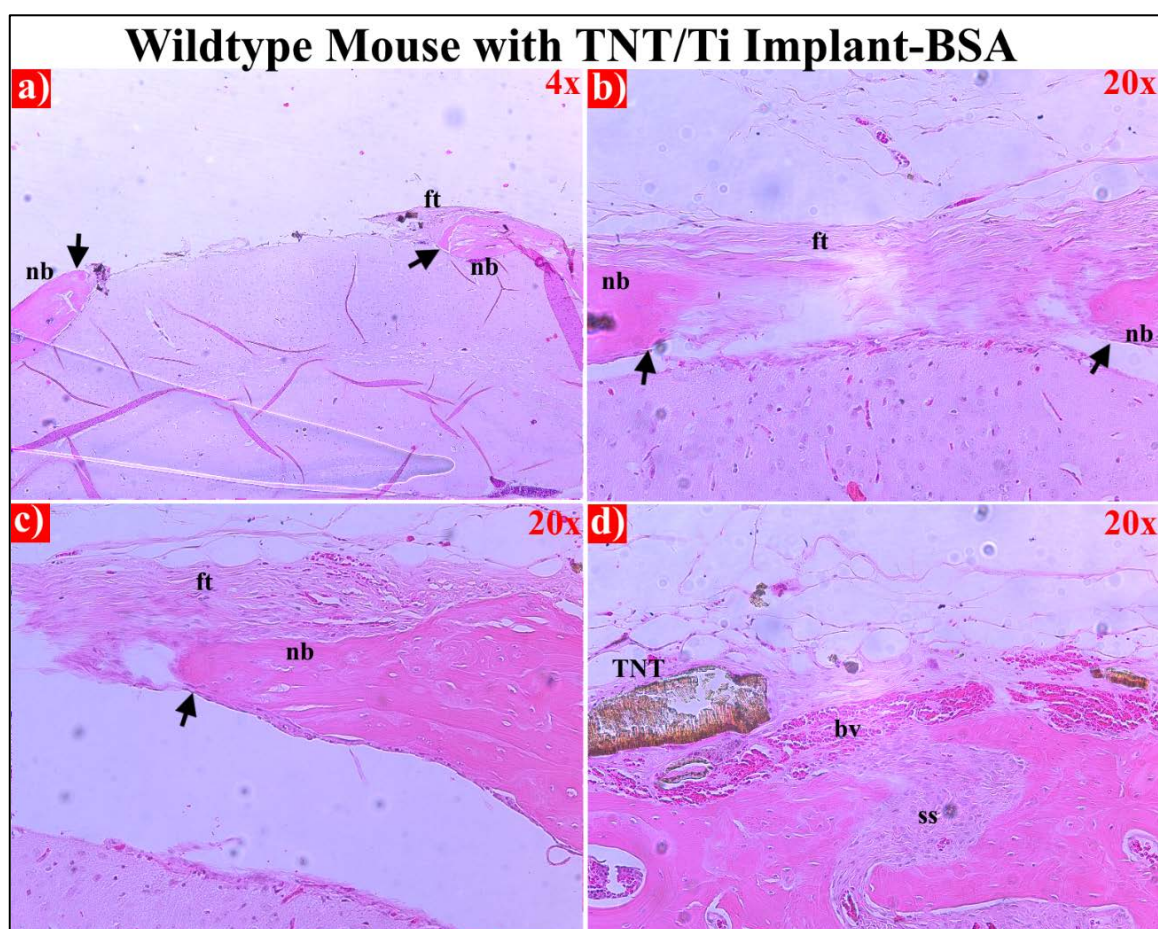
Figure 8.14. Histological analysis of bone regeneration in 3 mm cranial defect after 12 weeks of healing in defects implanted with GPC3-loaded TNT/Ti discs as therapeutic intervention. Representative images of the defect site, the bone edge and the newly formed bone in increasing degree of magnification with (a-c) H&E and (d-f) Movat pentachrome staining. The magnification scales are shown at the top right corner of each panel; black arrows mark the margin of the new bone (nb: new bone, ft: fibrous tissue, TNT: free standing Titania nanotubes).
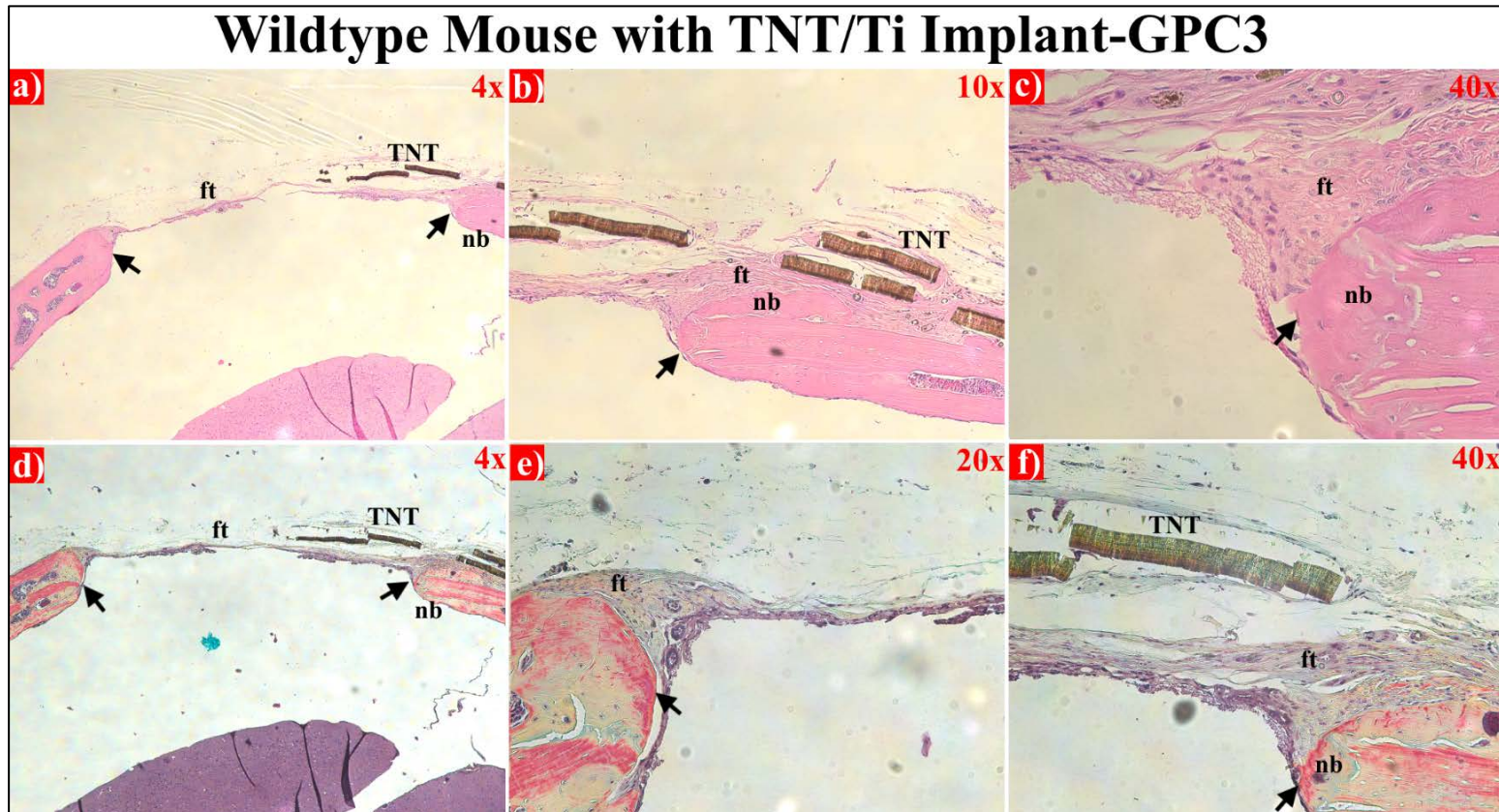
8.3.2.3 Protein release in Crouzon murine model

This section illustrates the delivery potential of GPC3-loaded TNT/Ti implants to stop ectopic bone growth in pathological Crouzon defect model. This model recapitulates the features of human Crouzon patients. All Crouzon mice tolerated the surgery well and only three post-operative deaths (at 1, 2 and 5 weeks) occurred due to non-surgical complications. **Figure 8.15** summarises the digital and micro-CT images of mouse skulls harvested after 12 weeks of implantation. Upon visual observation, the skin wounds appeared to have completely healed with no signs of infection or wound dehiscence. The peculiar features of the syndromic craniosynostosis, such as rounded skull, flattened midface, protruding eyes, shorter snout and wideset eyes, were consistent across all the affected mice, with the variable number of fused sutures. Retrieval of TNT/Ti implant discs from the euthanised animals showed no visible implantation damage to regional vascularity. Moreover, the variation in the extent of bone healing within the CSD between the groups was clearly visible (**Figure 8.15A**).

The 3D reconstructed micro-CT data revealed that, at 12 weeks post-operation, the craniectomy control group had almost completed bone healing, with majority of the defect covered with substantial ossified bone tissue (**Figure 8.15B-a**). This observation in mice is consistent with the accelerated bone reossification after primary surgery in human patients (without any therapeutic intervention) [33]. The defects that were treated with GPC3 via nanoengineered release system (TNT-GPC3) in the present study showed drastically diminished bone volume with minimal peripheral bone re-growth (**Figure 8.15B-b**). However, the experimental group with chitosan-coated implants demonstrated scattered bony islands over the dura, whilst maintaining comparatively larger defects than the control group (**Figure 8.15B-c**). The 2D renderings of appropriate sagittal sections of the micro-CT images are shown in **Figure 8.15C**. In the control group, a thick bony bridge obliterated the defect (**Figure 8.15C-a**), while the

experimental groups showed either largely open defect (TNT-GPC3, **Figure 8.15C-b**) or ectopic bone formation over the dura (TNT-GPC3-CH, **Figure 8.15C-c**). These observations reinforced the delivery results from the wildtype model by displaying significant bone inhibition in the GPC3-treated experimental groups. The comparative histological images of the defect sites displayed in **Figure 8.9C-e-g** complement the 2D micro-CT sections in all treatment groups (detailed histology on p.272-274).
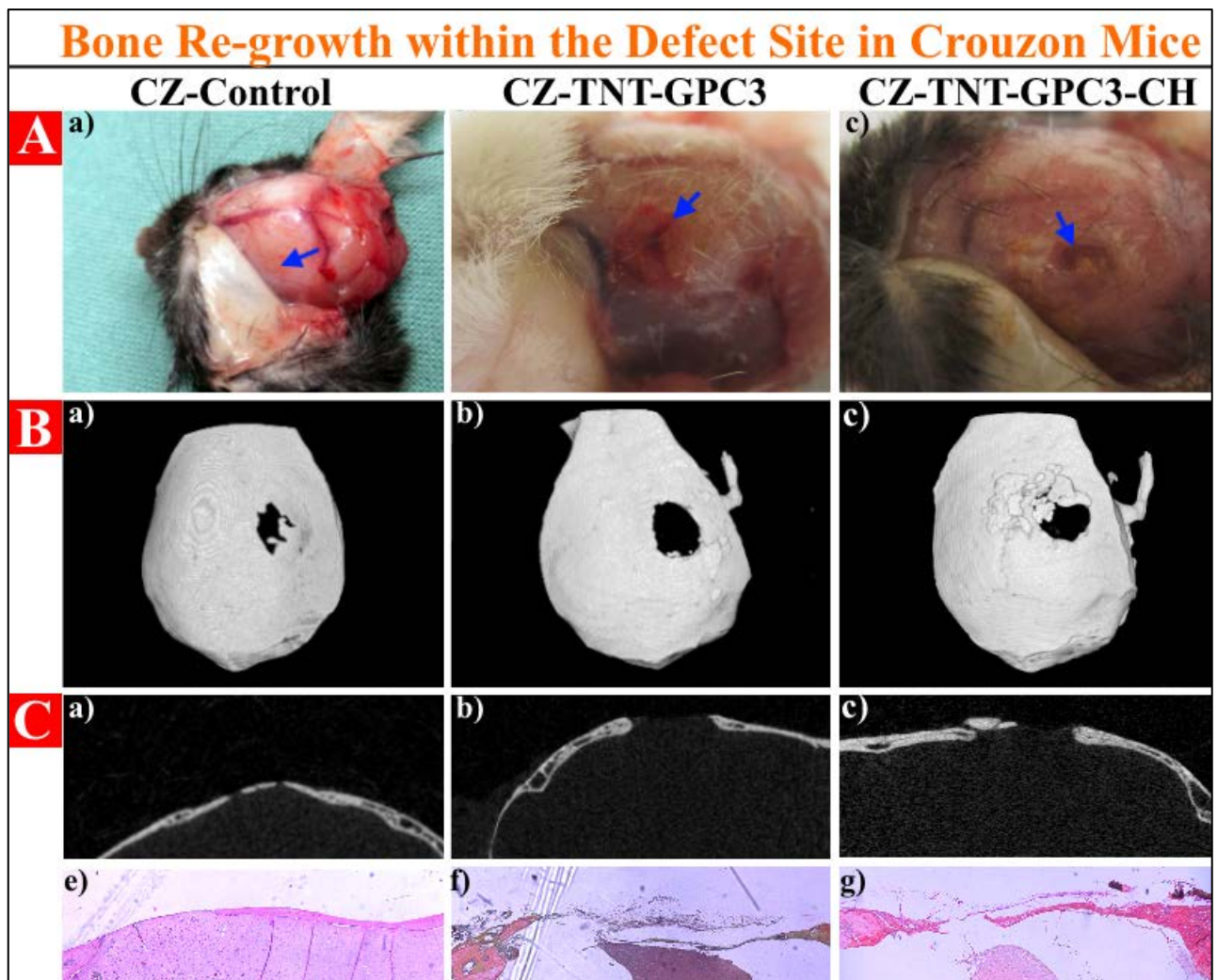
Figure 8.15. Representative images from different treatment groups of Crouzon mice (control and experimental), after 12 weeks of implantation. Digital images showing A) bone healing at the implantation site (the blue arrows mark the defect). Micro-CT images showing B) the 3D reconstructed skull with defects and C) 2D sagittal section of defect region showing bone re-growth with the comparative histology (lower panel).

The morphometric analysis of BV and BS enabled comparison of the bone-inhibiting potential of the released GPC3 across the groups. The mean BV, quantified in **Figure 8.16a,** was in the following order: control day 90 (0.68 ± 0.04 mm^3) > TNT-GPC3-CH (0.34 ± 0.06 mm^3) > TNT-GPC3 (0.18 ± 0.04 mm^3) > control day 0 (0.07 ± 0.02 mm^3). Mean bone surface area (**Figure 8.16b**) showed the same trend in this order: control day 90 (15.98 ± 1.26 mm^2) > TNT-GPC3-CH (9.14 ± 2.11 mm^2) > TNT-GPC3 (7.60 ± 1.43 mm^3) > control day 0 (4.62 ± 1.00 mm^2).

The Shapiro-Wilk test of normality was non-significant for the variables (BV and BS) within each group. One-way ANOVA showed a significant effect of the GCP3 treatment (released from chitosan-coated and uncoated TNT/Ti implants) on both BV and BS. The pairwise comparisons with Bonferroni post-hoc tests between the groups and the dependent variables (BV and BS) revealed that both the experimental groups (TNT-GPC3 and TNT-GPC3-CH) had significantly lower mean BV and BS than the craniectomy controls ($p<0.05$ for each comparison). The quantitative parameters for uncoated TNT-GPC3 group showed non-significant difference to the original defects (control-day 0), indicating successful bone inhibition within the defects.

The defects implanted with chitosan-coated TNT/Ti discs showed relatively greater bone regeneration than the uncoated groups. This may be attributed to non-uniform degradation of chitosan exerted by lysozymes in the cranial environment (failing to provide continuous protein release [34]. Alternatively, bone growth might have occurred centripetally towards the chitosan surfaces. Even with a low degree of acetylation, the positively charged coating could have stimulated osteoblast adhesion and differentiation, generating few bony islands [35, 36]. However, it seemed to be counteracted by GPC3 therapeutic action.
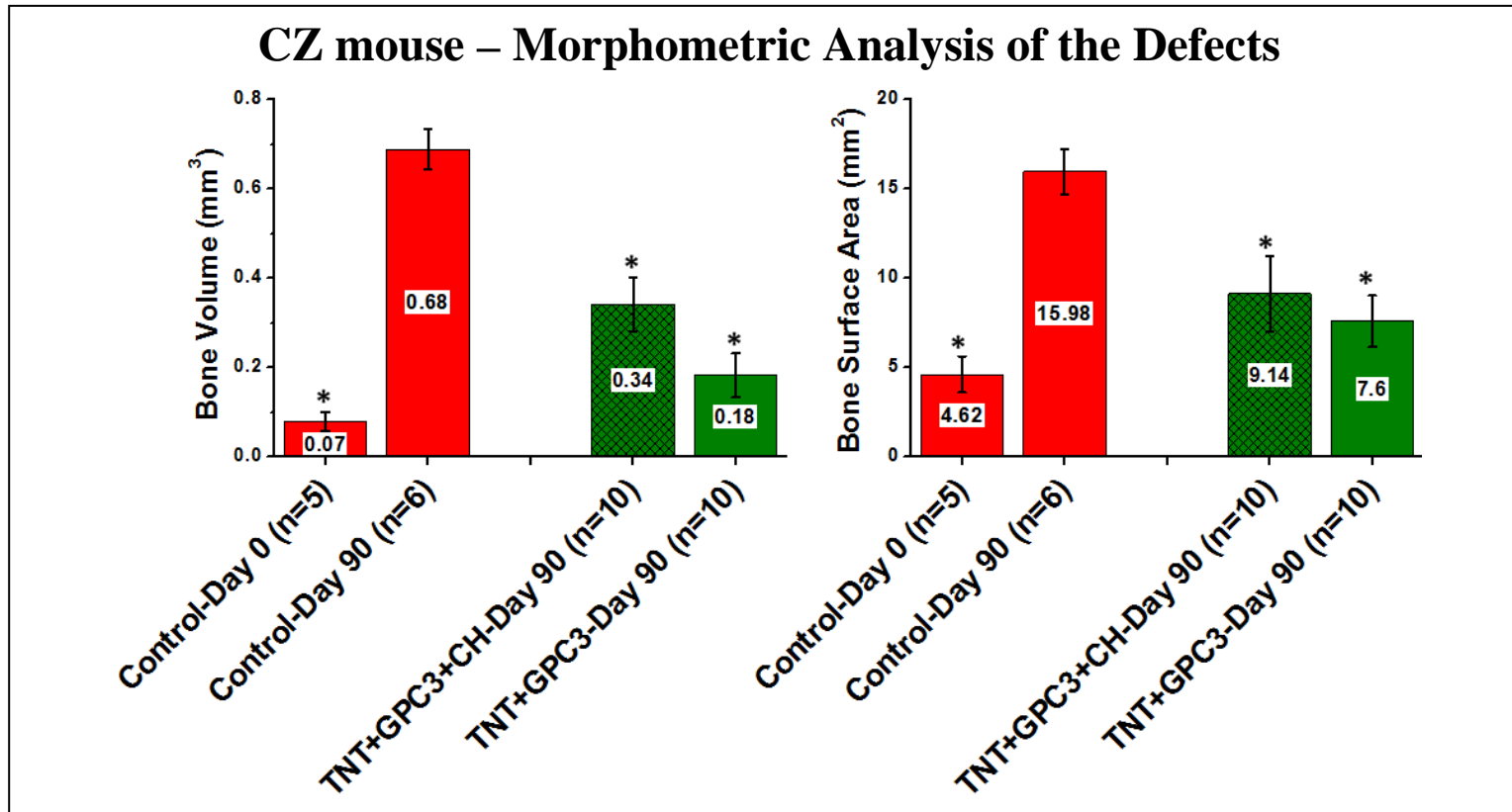
Figure 8.16. Quantitative micro-CT analyses using CTan software showing new bone volume (BV) and bone surface area (BS) within the defect in Crouzon mice at 12 weeks post-operation. The GPC3-loaded TNT/Ti implants (both uncoated and chitosan-coated) significantly (*p<0.05) reduced the bone formation compared with the craniectomy control group. The initial (control day 0) and final (control day 90) bone growth parameters correspond to original and the naturally healed defects, respectively.

The histological examination correlated well with different degrees of new bone formation after 12 weeks of implantation. **Figure 8.17a-c** show the control defect (craniectomy only) with H&E staining in increasing order of magnification displaying primarily mature lamellar bone covering the majority of the defect, along with thick band of fibrous tissue bridging the rest of the gap. The black arrows mark the new bone edges. The Picro-Sirius red staining at low and high magnification (**Figure 8.17d-e**) displayed the new bone and its margin emanating connective tissue with tightly packed collagen clusters. The Movat Pentachrome staining (**Figure 8.17f**) further confirmed new bone regeneration across the defect.

The defects implanted with GPC3-loaded TNT/Ti discs showed reduced bone healing, with a large region of the defect containing thin and scattered fibrous tissue. **Figure 8.18** presents the H&E, Movat pentachrome and Picro-Sirius red stained sections from this experimental group. The low magnification images with all three stains (**Figure 8.18a**, **d** and **g**) showed that most of the original craniectomy site remained unossified. The H&E and Movat pentachrome labelled sections at 20× (**Figure 8.18b**, **e** and **f**) and 40× (**Figure 8.18c**) showed small newly-formed wedge-shaped bone (woven with limited bone marrow) lined with thick fibrous tissue, encompassing few bony islets. The Picro-Sirius red labelling revealed a band of aligned collagen bridging the defect, overlaid by several short fibres with few red blood cells (**Figure 8.18g-i**).
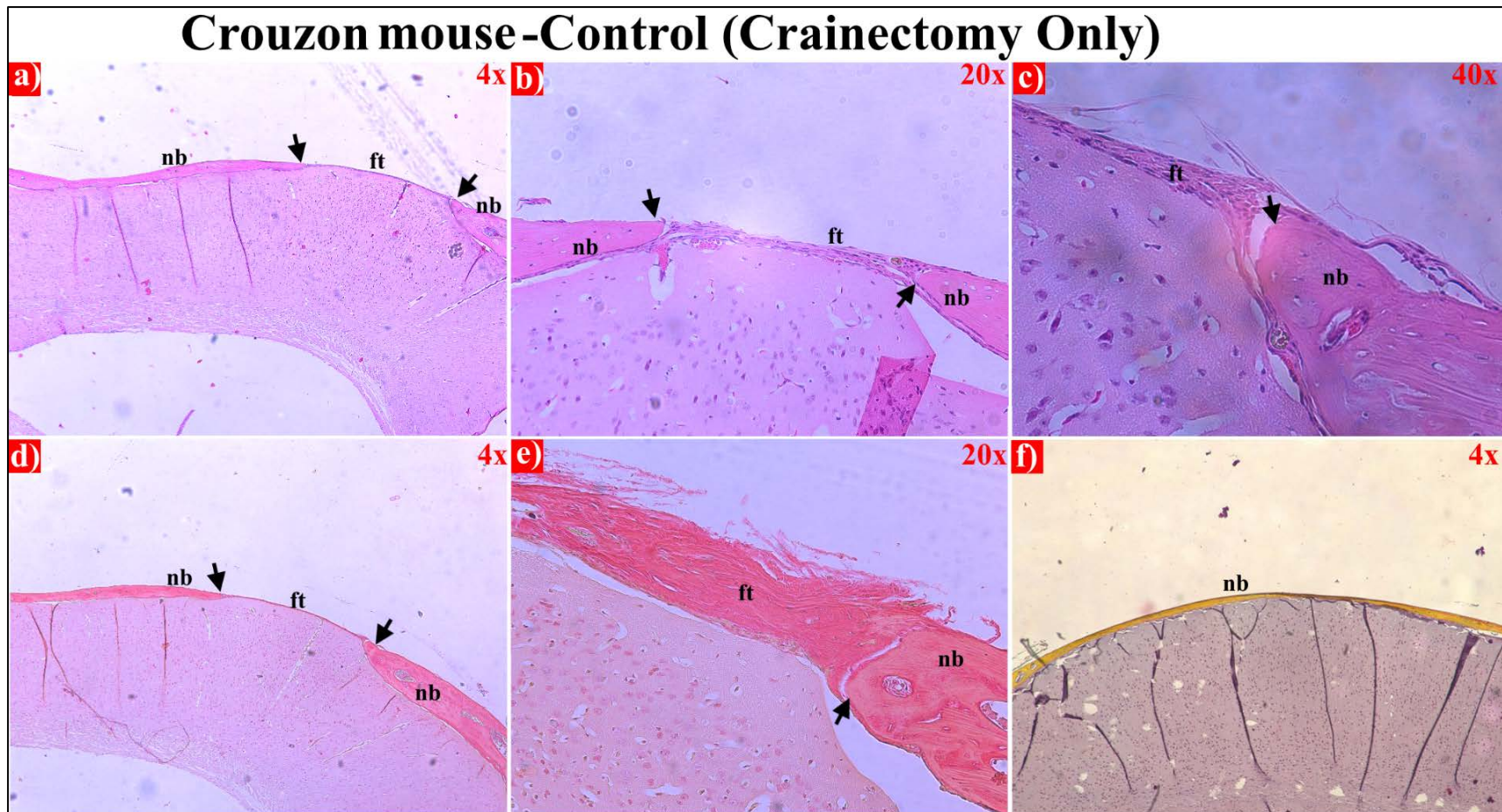
Figure 8.17. Histological analysis of bone regeneration in 3 mm cranial defect after 12 weeks of healing in Crouzon craniectomy control model. Representative histology images of the defect site and its edge with (a-c) H&E, (d-e) Picro-Sirius red and (f) Movat Pentachrome staining. The magnification scales are shown at the top right corner of each panel; black arrows mark the margin of the new bone (nb: new bone, ft: fibrous tissue).
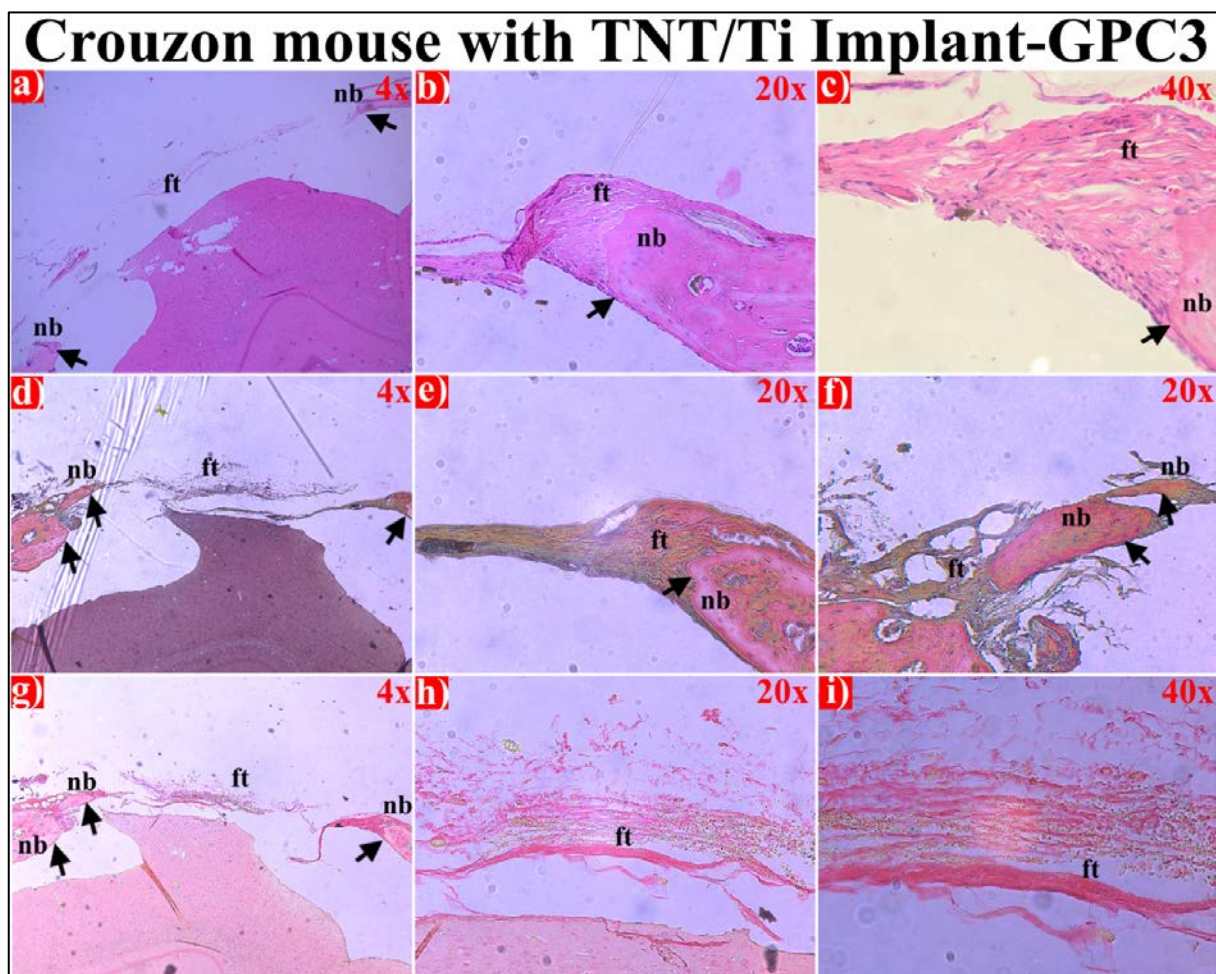
Figure 8.18. Histological analysis of bone regeneration in defects implanted with GPC3-loaded TNT/Ti discs as therapeutic intervention, after 12 weeks of healing. Representative images of the defect site (with thin discontinuous fibrous tissue), the bone edge and the newly formed bone with (a-c) H&E and (d-f) Movat pentachrome and (g-i) Picro-Sirius red staining. The magnification scales are shown at the top right corner of each panel; black arrows mark the margin of the new bone (nb: new bone, ft: fibrous tissue).

The H&E, Movat and Picro-Sirius red labelled sections of Crouzon mice with chitosan-coated GPC3-loaded TNT/Ti discs implanted within the defect are shown in **Figure 8.19**. The group displayed an incompletely healed defect with ectopic bone formation. These results correlated well to slightly increased bone volume in the micro-CT findings. The low magnification images

with all three stains (**Figure 8.19a, b, d** and **g**) showed decrease in original defect width with discontinuous new bone and thick fibrous tissue around the edge. The H&E, Movat pentachrome and Picro-Sirius red labelled sections at 20× (**Figure 8.18e** and **h**) and 40× (**Figure 8.18c, f** and **i**) displayed the newly regenerated bone edge with ectopic bony island interweaved within the collagen fibres. A combination of micro-CT and histology is useful to estimate the osseous tissue formation and the extent of mineralisation.
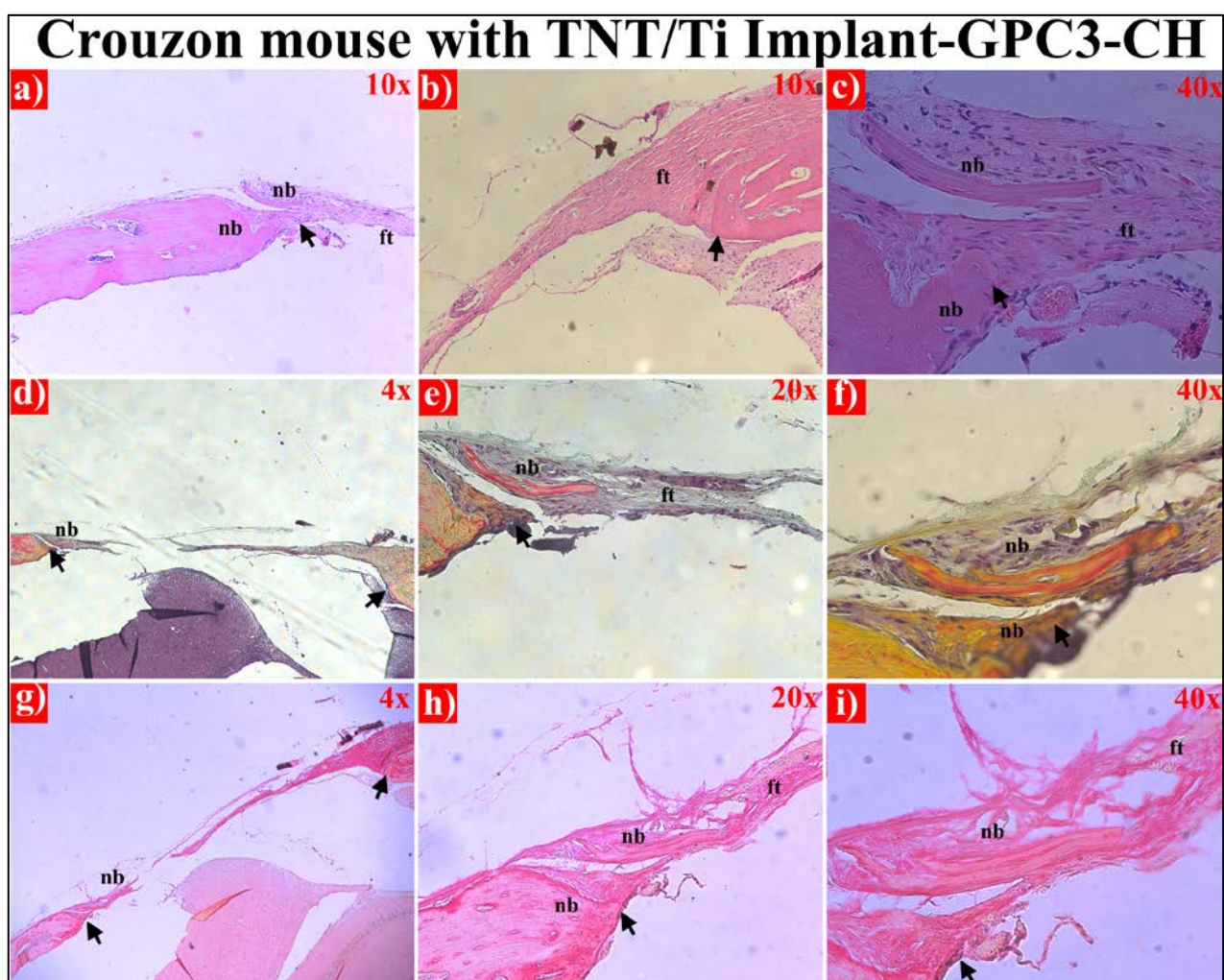
Figure 8.19. Histological analysis of bone regeneration in defects implanted with chitosan-coated GPC3-loaded TNT/Ti discs as therapeutic intervention, after 12 weeks of healing. Representative images of (a-c) H&E and (d-f) Movat pentachrome and (g-i) Picro-Sirius red

stained defect sites showing ectopic bone growth. The magnification scales are shown at the top right corner of each panel; black arrows mark the margin of the new bone (nb: new bone, ft: fibrous tissue).

8.3.2.4. Comparison between Crouzon and Wildtype murine models

The comparative CT morphometric analysis results between the wildtype and Crouzon control and experimental (TNT-GPC3) groups are shown in **Figure 8.20**. Two-way ANOVA was conducted to investigate whether the mean of BV and BS values were significantly different between the groups. The output revealed statistically significant differences in BV and BS between control and experimental groups, with therapeutically intervened CZ and WT mice inhibiting the bone re-growth when compared to their control groups. Furthermore, the bone regeneration (after 12 weeks) in the Crouzon control model was significantly greater than the wildtype control littermates ($p < 0.05$ for all comparisons) as represented by bone volume and bone surface area values. The significant difference between the genotypes reaffirmed the need of using a pathological murine model to test therapeutics for craniosynostosis therapy.
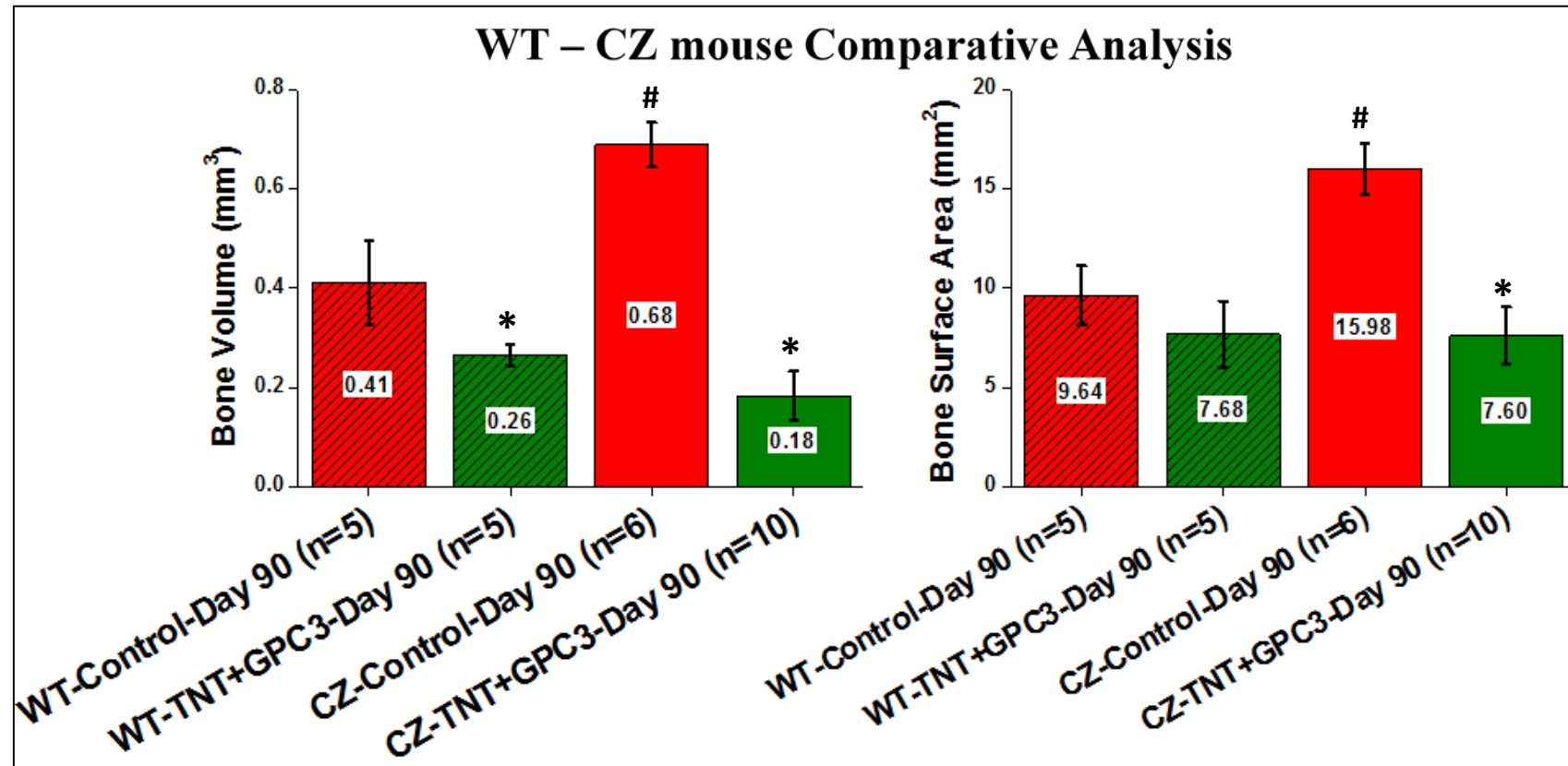
Figure 8.20. Comparative analysis (CTan) between mean BV and BS in Wildtype and Crouzon models for control and experimental (TNT-GPC3) groups. The statistical difference in BV and BS between experimental and control groups in both WT and CZ model is denoted by * and between the two genotype controls is denoted by # (p<0.05 for all comparisons).

The Picro-Sirius red labelled slides were assessed under linear polarised light to observe the resultant collagen-associated birefringence. The Crouzon control group (**Figure 8.21A**) with almost complete healing had a thin layer of tightly aligned collagen type I fibrils (in bright orange) in the unossified gap. In the wildtype control group (**Figure 8.21B**), the defect edges emanated a thick mesh of deep red and orange type I (bone generating) fibres. Since the slides were analysed under plane polarised light, the shorter fibres did not show any birefringence. A rotation of the slide base or use of circularly polarised light could have given better contrast among type I and type III collagen. The experimental (CZ-TNT-GPC3) group displayed thin, loosely bound, yellow to orange fibres radiated from the edge and scattered across the defect site (**Figure 8.21C**). These observations were consistent with the previously described histological and micro-CT results.
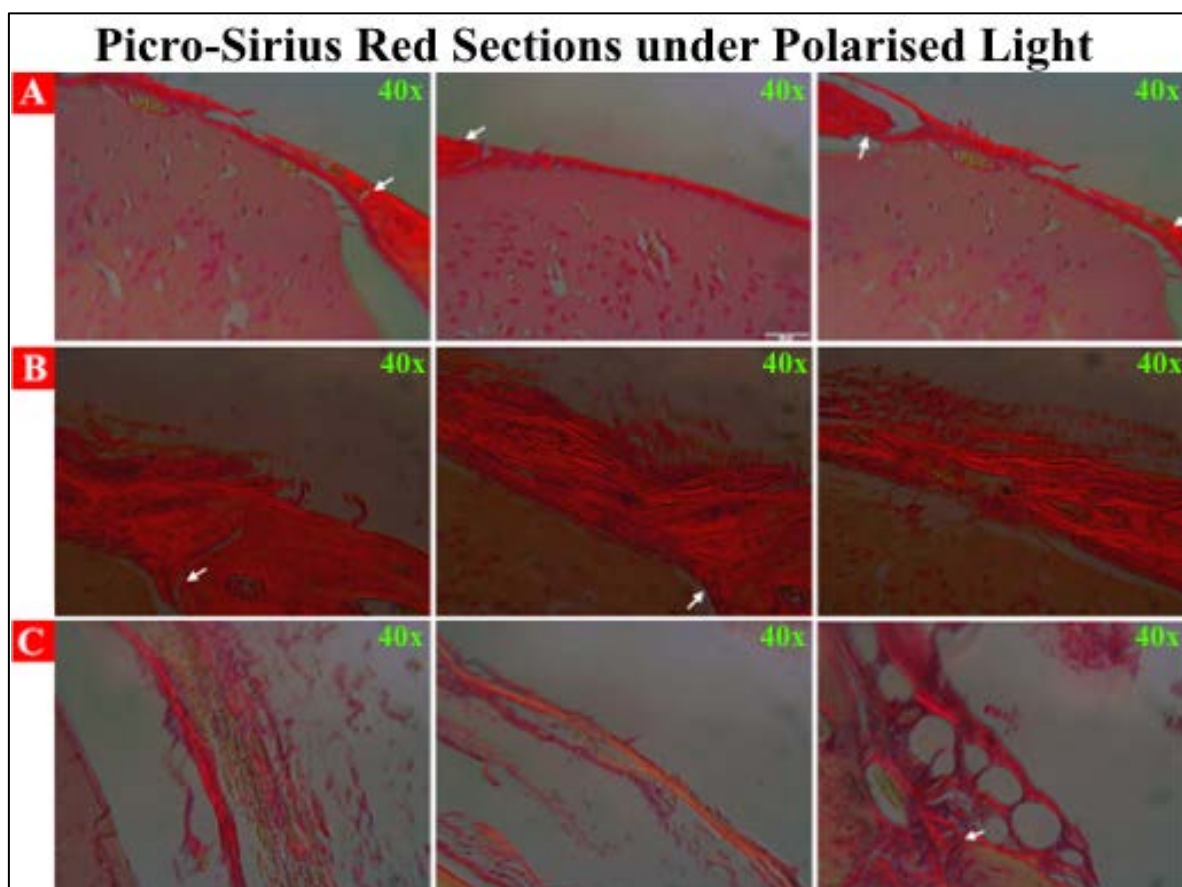
Figure 8.21. Representative images of Picro-Sirius red labelled sections under polarised light. A) Crouzon-control, B) Wildtype-control and C) Crouzon-experimental (TNT-GPC3) with variable

amount, length, thickness and orientation of collagen type I fibrils. The white arrow marks the defect margins on either side.

8.4. Conclusion

In an attempt to develop a molecular adjunct to standard surgical intervention for craniosynostosis, this study demonstrated the ability of TNT/Ti (chitosan-coated and uncoated) implants for controlled delivery of model proteins (control-BSA and experimental-GPC3) locally over the craniectomy site. After 12 weeks of implantation, the nanotube layer and the implant structure seemed robust and stable in most animals, with intact porous structure. The chitosan layer covering the nanopores gradually degraded (over weeks) via hydrolysis by lysozymes present in the cranial interstitial fluid and extracellular matrix.

In some cases, the TNT layer delaminated off the underlying Ti substrate while retrieving the implant. The histological evaluation (using H&E, PAS, Movat Pentachrome and Picro-Sirius Red labelling) of the TNT-tissue interface at the defect site showed no discernible difference to the normal tissue, with absence of any local inflammatory reaction (such as large, multinucleated cells). A TRAP labelling further confirmed the implant safety by presenting negative results pertaining to osteoclasts and resorptive pits.

The TNT/Ti delivery system and its bone-inhibiting potential was tested by surgically implanting them into critical-sized defects in wildtype and Crouzon mouse models. The wildtype mice expressed unfused sutures and normal bone healing, while the Crouzon mice displayed pathologically fused sutures, dome shaped head and other characteristics that were analogous to human Crouzon syndrome. There were no intra-operative complications and the incision sites healed well in all the mice. Digital imaging, micro-CT scanning and histological evaluations of

the implantation sites revealed variable degrees of defect healing across various subgroups in both the models.

As observed in 3D and 2D micro-CT renderings, the wildtype mice implanted with GPC3-loaded TNT/Ti discs demonstrated significantly lower new bone volume within the defect, when compared with control defects (without any therapeutic intervention). This confirmed that TNT/Ti implants releasing bioactive bone antagonising GPC3 at the craniectomy site could act as post-operative treatment to inhibit normal bone reossification. Furthermore, the wildtype mice treated with control BSA released from the TNTs (both chitosan-coated and uncoated) did not reduce new bone re-growth and showed highly ossified defects. This justified the use of BSA as a non-therapeutic protein, whilst showcasing the delivery potential of the nanoengineered implants. The morphometric analysis from the micro-CT data quantified the mean new bone volume (BV) and surface area (BS) across the subgroups and only the BV was significantly less in the GPC3-treated groups. These findings were consistent with the qualitative histological evaluations of the defect sections, 12 weeks post-implantation. The histological stained sections for control (day 90) showed substantial peripheral bone growth, narrowing the defect. Rest of the defect was bridged by a dense layer of collagen fibres. The protein control groups showed prominent bone reossification and reduction in the original defect in both chitosan-coated and uncoated TNT/Ti implantation sites, with the former group displaying isolated bony islands interpolating the fibrous tissue in the defect. As expected, the experimental treatment group with GPC3 releasing implants showed more fibrous than bony defects, with small amount of proximal bone re-growth.

The micro-CT data collected from the defect sites of Crouzon mice with craniectomy *i.e.* control group demonstrated an almost obliterated defect site, with large amount of ossified bone tissue, due to accelerated bone morphogenesis in this pathological model. On application of GPC3 releasing implants (chitosan-coated and uncoated TNTs) at the craniectomy site, there was a

significant reduction in re-ossification. The morphometric data collected from different cohorts of animals, in terms of mean BV and BS were quantified to be significantly lower in experimentally intervened groups, when compared to the control group. Both the GPC3 implanted sites maintained a large defect but the presence of chitosan induced some ectopic bone formation over the dura. These results were asserted by the histological assessment of the defect sites at 12 weeks, post-operation. The control group displayed an almost complete bridging of the defect region, while the GPC3 delivery changed the rate of healing and the defects contained thin and scattered fibrous tissue in the middle and thicker ones at the margins. The chitosan-coated TNT/Ti implants showed scattered bony islands over the dura and marginal defect healing.

The CZ and WT comparative analysis showed statistical significant difference between the treatments within the groups as well as in between the control groups. Picro-Sirius Red stained sections observed under polarised light determined the presence of bone forming collagen type I fibres lining the unossified defects with variable hue, amounts and thickness between the control and experimental groups.

The outcomes of this study provide insight into the *in vivo* protein release capability of TNT/Ti cranial implant. Overall, the results demonstrated that a molecular adjunctive postoperative treatment of craniectomy sites with GPC3 released from TNT/Ti implants significantly inhibited the bone formation within the defect in both normal and pathological model. Although this work needs further investigations and animal trials to achieve more controlled regulation of new tissue formation, it is the first attempt to develop a nanoengineered implant for molecular inhibition of bone re-growth in craniosynostosis treatment. It is envisioned that this technology combined with glypican-based therapy may improve surgical outcomes by targeting the BMP2 signalling pathway in secondary surgical sites and potentially avoid primary fusion. The TNT-based system has a potential

to form a generic delivery platform which can further be tested with different bone antagonising proteins such as noggin, gremlins *etc*.

8.5. References

1. Panchal, J. and Uttchin, V. Management of craniosynostosis. *Plastic and Reconstructive Surgery*, **2003**. 111, 2032-48.

2. Coussens, A.K., Wilkinson, C.R., Hughes, I.P., Morris, C.P., Van Daal, A., Anderson, P.J., and Powell, B.C. Unravelling the molecular control of calvarial suture fusion in children with craniosynostosis. *BMC Genomics*, **2007**. 8, 458-83.

3. Ai-Aql, Z., Alagl, A.S., Graves, D.T., Gerstenfeld, L.C., and Einhorn, T.A. Molecular mechanisms controlling bone formation during fracture healing and distraction osteogenesis. *Journal of Dental Research*, **2008**. 87, 107-18.

4. Wilkie, A.O. Craniosynostosis: genes and mechanisms. *Human Molecular Genetics*, **1997**. 6, 1647-56.

5. Coussens, A.K., Hughes, I.P., Wilkinson, C.R., Morris, C.P., Anderson, P.J., Powell, B.C., and Van Daal, A. Identification of genes differentially expressed by prematurely fused human sutures using a novel in vivo–in vitro approach. *Differentiation*, **2008**. 76, 531-45.

6. Kimonis, V., Gold, J.A., Hoffman, T.L., Panchal, J., and Boyadjiev, S.A. Genetics of craniosynostosis. in *Seminars in Pediatric Neurology*. **2007**. Elsevier.

7. Grova, M., Lo, D.D., Montoro, D., Hyun, J.S., Chung, M.T., Wan, D.C., and Longaker, M.T. Animal Models of Cranial Suture Biology. *The Journal of Craniofacial Surgery*, **2012**. 23, 1954-58.

8.   Pearce, A., Richards, R., Milz, S., Schneider, E., and Pearce, S. Animal models for implant biomaterial research in bone: a review. *European Cells & Materials*, **2007**. 13, 1-10.

9.   Siegel, M.I. and Mooney, M.P. Appropriate animal models for craniofacial biology. *The Cleft Palate-Craniofacial Journal*, **1990**. 27, 18-25.

10.   Eswarakumar, V.P., Horowitz, M.C., Locklin, R., Morriss-Kay, G.M., and Lonai, P. A gain-of-function mutation of Fgfr2c demonstrates the roles of this receptor variant in osteogenesis. *Proceedings of the National Academy of Sciences of the United States of America*, **2004**. 101, 12555-60.

11.   Perlyn, C.A., DeLeon, V.B., Babbs, C., Govier, D., Burell, L., Darvann, T., Kreiborg, S., and Morriss-Kay, G. The craniofacial phenotype of the Crouzon mouse: analysis of a model for syndromic craniosynostosis using three-dimensional MicroCT. *The Cleft Palate-Craniofacial Journal*, **2006**. 43, 740-48.

12.   Perlyn, C.A., Morriss-Kay, G., Darvann, T., Tenenbaum, M., and Ornitz, D.M. A model for the pharmacological treatment of crouzon syndrome. *Neurosurgery*, **2006**. 59, 210-15.

13.   Liu, J., Nam, H.K., Wang, E., and Hatch, N.E. Further Analysis of the Crouzon Mouse: Effects of the FGFR2C342Y Mutation Are Cranial Bone–Dependent. *Calcified Tissue International*, **2013**. 92, 451-66.

14.   Maxson, R. and Ishii, M. The Bmp pathway in skull vault development. *Frontiers of Oral Biology*, **2008**. 12, 197-208.

15. Uludag, H., D'Augusta, D., Palmer, R., Timony, G., and Wozney, J. Characterization of rhBMP-2 pharmacokinetics implanted with biomaterial carriers in the rat ectopic model. *Journal of Biomedical Materials Research*, **1999**. 46, 193-202.

16. Warren, S.M., Brunet, L.J., Harland, R.M., Economides, A.N., and Longaker, M.T. The BMP antagonist noggin regulates cranial suture fusion. *Nature*, **2003**. 422, 625-29.

17. Wu, C.J. and Lu, H.K. Smad signal pathway in BMP-2-induced osteogenesis-a mini review. *Journal of Dental Sciences*, **2008**. 3, 13-21.

18. Dwivedi, P., Grose, R., Hii, C., Filmus, J., Anderson, P., and Powell, B. Regulation of bone morphogenetic protein signalling and osteogenesis by glypicans in human cranial suture cells. *Bone*, **2011**. 48, S243.

19. Marie, P.J., Debiais, F., and Hay, E. Regulation of human cranial osteoblast phenotype by FGF-2, FGFR-2 and BMP-2 signaling. *Histology and Histopathology*, **2002**. 17, 877-85.

20. Mooney, M.P., Moursi, A.M., Opperman, L.A., and Siegel, M.I. Cytokine therapy for craniosynostosis. *Expert Opinion on Biological Therapy*, **2004**. 4, 279-99.

21. Moioli, E.K., Clark, P.A., Xin, X., Lal, S., and Mao, J.J. Matrices and scaffolds for drug delivery in dental, oral and craniofacial tissue engineering. *Advanced Drug Delivery Reviews*, **2007**. 59, 308-24.

22. Shen, K., Krakora, S., Cunningham, M., Singh, M., Wang, X., Hu, F., Post, J., and Ehrlich, G. Medical treatment of craniosynostosis: recombinant Noggin inhibits coronal suture closure in the rat craniosynostosis model. *Orthodontics & Craniofacial Research*, **2009**. 12, 254-62.

23.   Blumer, M.J., Longato, S., and Fritsch, H. Localization of tartrate-resistant acid phosphatase (TRAP), membrane type-1 matrix metalloproteinases (MT1-MMP) and macrophages during early endochondral bone formation. *Journal of Anatomy*, **2008**. 213, 431-41.

24.   Rentsch, C., Schneiders, W., Manthey, S., Rentsch, B., and Rammelt, S. Comprehensive histological evaluation of bone implants. *Biomatter*, **2014**. 4, 27993.

25.   Rich, L. and Whittaker, P. Collagen and picrosirius red staining: a polarized light assessment of fibrillar hue and spatial distribution. *Journal of Morphological Science*, **2005**. 22, 97-104.

26.   Lunt, S.J., Kalliomaki, T.M., Brown, A., Yang, V.X., Milosevic, M., and Hill, R.P. Interstitial fluid pressure, vascularity and metastasis in ectopic, orthotopic and spontaneous tumours. *BMC Cancer*, **2008**. 8, 2.

27.   Lim, S.M., Song, D.K., Oh, S.H., Lee-Yoon, D.S., Bae, E.H., and Lee, J.H. In vitro and in vivo degradation behavior of acetylated chitosan porous beads. *Journal of Biomaterials Science, Polymer Edition*, **2008**. 19, 453-66.

28.   Gulati, K., Johnson, L., Karunagaran, R., Findlay, D., and Losic, D. In Situ Transformation of Chitosan Films into Microtubular Structures on the Surface of Nanoengineered Titanium Implants. *Biomacromolecules*, **2016**. 17, 1261-71.

29.   Gulati, K., Santos, A., Findlay, D., and Losic, D. Optimizing anodization conditions for the growth of titania nanotubes on curved surfaces. *The Journal of Physical Chemistry C*, **2015**. 119, 16033-45.

30. Albu, S.P. and Schmuki, P. Influence of anodization parameters on the expansion factor of TiO$_2$ nanotubes. *Electrochimica Acta*, **2013**. 91, 90-5.

31. Di Quarto, F., Doblhofer, K., and Gerischer, H. Instability of anodically formed TiO$_2$ layers. *Electrochimica Acta*, **1978**. 23, 195-201.

32. Wang, J. and Lin, Z. Freestanding TiO$_2$ nanotube arrays with ultrahigh aspect ratio via electrochemical anodization. *Chemistry of Materials*, **2008**. 20, 1257-61.

33. Drake, D.B., Persing, J.A., Berman, D.E., and Ogle, R.C. Calvartal Deformity Regeneration Following Subtotal Craniectomy for Craniosynostosis: A Case Report and Theoretical Implications. *Journal of Craniofacial Surgery*, **1993**. 4, 85-9.

34. Tomihata, K. and Ikada, Y. In vitro and in vivo degradation of films of chitin and its deacetylated derivatives. *Biomaterials*, **1997**. 18, 567-75.

35. Oktay, E., Demiralp, B., Demiralp, B., Senel, S., Cevdet Akman, A., Eratalay, K., and Akincibay, H. Effects of platelet-rich plasma and chitosan combination on bone regeneration in experimental rabbit cranial defects. *Journal of Oral Implantology*, **2010**. 36, 175-84.

36. Lee, J.-Y., Nam, S.-H., Im, S.-Y., Park, Y.-J., Lee, Y.-M., Seol, Y.-J., Chung, C.-P., and Lee, S.-J. Enhanced bone formation by controlled growth factor delivery from chitosan-based biomaterials. *Journal of Controlled Release*, **2002**. 78, 187-97.

CHAPTER 9

CONCLUSIONS AND RECOMMENDATIONS FOR FUTURE WORK

9.1. Conclusions

This project advances the Titania nanotube (TNT) technology towards craniofacial delivery of bone antagonising proteins in order to develop a potential molecular adjunct to standard surgical treatment of craniosynostosis. The primary focus of this work was on understanding, designing, and optimising the electrochemical anodisation technique to fabricate novel nanoengineered Ti cranial implants, capable of localised and controlled release of bone inhibiting therapeutic proteins (**Chapter 3**). A series of *in vitro* studies were designed to establish the ability of TNT/Ti-based delivery systems to provide sustained release of bioactive glypicans in physiological buffer, and to modulate osteogenic BMP2 activity in C2C12 murine myoblasts (**Chapter 4** and **6**). Furthermore, the impact of nanotopography and implant surface chemistry on human suture mesenchymal cell behaviour analysed at the TNT/Ti surface (cell-biomaterial interface) underscored the plausibility of using surface-coated and uncoated TNTs as cranial implants (**Chapter 5**). The *in vivo* efficacy of TNT/Ti implants was analysed in three stages to assess the use of these nanoengineered protein delivery systems in pre-clinical situations. The preliminary experiments assessed the hard and soft tissue response to the implanted TNTs (polymer-coated and uncoated), demonstrating their biocompatibility in a wildtype mouse model. Chitosan and Pluronic-F127 coatings on the TNT/Ti surfaces also impacted the bone healing within the critical-sized cranial defect, with the later causing undesired bone induction (**Chapter 7**). The next two studies tested the glypican delivery potential of the nanoengineered implants to regulate and control the post-operative bone regeneration at the craniectomy sites in both wildtype and Crouzon mouse model of craniosynostosis. The bioactive glypicans released from the nanotubes caused significant bone inhibition in both the mouse models and minimised the ectopic bone formation within the pathological defects (**Chapter 8**). The

following sections outline the key findings drawn from the systematic investigations throughout this thesis pertaining to specific aims (**Chapter 1**), along with the perspective future work.

9.2. Key findings and significance of the work

9.2.1. Nanoengineering of the implants (Aim 1)

Optimisation of electrochemical anodisation technique and the use of Lactic acid containing ethylene glycol electrolyte at high temperature was shown to provide ultrafast fabrication of well-ordered and stable TNT/Ti implants with 120 nm pore diameter and 35 µm length. This improved fabrication method overcame the substantial limitations with traditional electrolytes (such as ageing of electrolyte, slow anodisation rate, mechanical instability *etc*.). More than 800 TNT/Ti implants were prepared throughout this project and the fabrication process was highly reproducible and repeatable. Furthermore, biopolymer deposition onto the implant surfaces via spin-coating was found to provide desirable surface properties and long-term release of subsequently loaded therapeutic molecules. This technique may enable easy integration of TNTs into the existing cranial implant technology owing to the quick and simple nanoengineering of current Titanium-based (or alloyed) implant surfaces.

9.2.2. *In vitro* protein release from TNT/Ti implants (Aim 2)

Based on the findings from this research, it was clear that these nanoreservoirs allowed loading/storage of substantial amounts of active proteins within the nanotubes and resulted in a biphasic (burst + sustained) *in vitro* release pattern. A pronounced difference in release duration between the chitosan-coated and uncoated TNT/Ti implants illustrated the ability of polymer coatings to extend protein release and improve their release pharmacokinetics. The

mathematical modelling revealing a zero-ordered sustained release profile enables this protein-release system to achieve long-term therapeutic delivery in the craniofacial regions.

9.2.3. *In vitro* protein release: Cell study (**Aim 3**)

This study demonstrated *in vitro* sustained release of bone inhibiting glypicans over 2 weeks. Moreover, the efficacy of the released glypicans in suppressing the BMP2 bioactivity significantly in transfected C2C12 cells reconsolidated the encapsulation and release capacity of the TNTs. The preservation of the biofunctionality of the loaded proteins throughout the release period is a critical requirement for the proposed craniofacial applications.

9.2.4. Pre-*in vivo* cell study (**Aim 4**)

The examination of human suture cell behaviour at the TNT-cell interface showed significant inhibition in cellular activity, adhesion and proliferation when compared with control Ti surfaces. It was confirmed that the large-diameters of TNTs led to limited cell adhesion due to unstable focal contact formation. The polymer coatings also modulated the initial protein absorption, causing a decrease in cell attachment/metabolic activity. Although the probable cause of cell behaviour modulation is debatable, it still renders the implant surface suitable for bone-inhibitory applications.

9.2.5. *In vivo* tissue response to TNT/Ti implants (**Aim 5**)

The *in vivo* interaction between implanted TNT/Ti discs and the tissues around the defect site elucidated no discernible difference to the normal tissues. Histology of the defect sections revealed the absence of inflammation, necrosis or infection, confirming implant

biocompatibility. The micro-CT images further allowed for concomitant assessments of defect width and new bone volume, and displayed substantially more bone induction in defects implanted with Pluronic-F127-coated TNT/Ti discs. Moreover, the retrieved implants showed stable, well-adhered nanotube layers.

9.2.5. *In vivo* protein release from TNT/Ti implants (Aim 6)

The *in vivo* protein delivery efficacy of TNT/Ti- based implants was confirmed by successful localised controlled delivery of incorporated proteins in both Crouzon and wildtype mice. Combined histology and micro-CT assessments showed that the untreated and BSA-treated control defects rapidly healed (to variable extent) after 12 weeks of implantation. However, the GPC3 (BMP2 inhibitors) released from the nanoengineered implants successfully inhibited post-operative bone growth in the cranial defect models. The TNT/Ti implants retrieved after the protein delivery showed a decrease in their mechanical stability causing the delamination of the TNTs from the Ti substrate. Nonetheless, the nanotubes did not leach any toxic ions/particles ascertained by absence of inflammatory cells or bone resorbing osteoclasts.

The simple fabrication, physiologically relevant nano-architecture and the capability for localised protein delivery identify TNT/Ti implants as promising interface for craniofacial applications. To our knowledge, this is the first report that combines bone inhibitory molecules with implantable TNT/Ti delivery systems to control bone regeneration in clinically relevant craniofacial models (in significant numbers). This approach has the potential to reduce the morbidity associated with cranial vault reconstruction and to improve the surgical outcomes. The TNTs can be fabricated on the existing fixation plates used in the surgical reconstruction for early intervention and normal post-operative brain and craniofacial growth. We believe that

this study is an important progress in the evolving collaborations between nanomedicine and craniofacial clinical practice and research.

9.3. Recommendations for future work

The investigation and results presented in this thesis explore the use of TNT/Ti-based implants for craniofacial therapeutic delivery. However, further research is required to increase our understanding of this interdisciplinary project and refine the implant characteristics to test the molecular adjunctive therapy. The following points outline possible future directions in the field of TNTs as craniofacial therapeutic implants:

- Although the fabricated implants showed substantial biocompatibility and provided a sustained release of glypicans to inhibit bone formation within the critical-sized defects, the delamination of TNT layers presented a potential concern. Further improvements in implant's mechanical properties by refinement of the electrochemical anodisation technique is desirable to fabricate shorter, more stable and better adhered nanotube structures. Investigating the immersion protein loading technique as opposed to vacuum drying may also improve the mechanical robustness. Moreover, larger implants and an increased amount of proteins loaded within the nanotubes may lead to better long-term osteogenic inhibition.

- While the GPC3 release from nanoengineered implants successfully down-regulated the BMP2-mediated bone reossification, the effective testing of bone-antagonising potential of GPC1 released from of TNT/Ti implants (independently and synergistically with GPC3) in mouse models is required to prove the generic applicability of this

approach. This will also provide evidence to support the *in vitro* studies in physiological buffer and cell culture.

- Since craniosynostosis is a developmental abnormality affecting children, a paediatric mouse model (instead of an adult one) may serve as a better platform to test potential therapies, as it would result in rapid bone regrowth. A more elaborate set of *in vivo* experiments (with age and sex-dependent studies) are needed to confirm the reproducibility of results from this thesis.

- Exploring the TNT/Ti-based glypican delivery in Twist mice with Saethre-Chotzen syndrome may further help develop a generic adjunctive therapy to potentially benefit many more types of syndromic craniosynostosis.

- Pathological large animal models such as rats, mini pigs and rabbits (with early or delayed-onset craniosynostosis or human familial, nonsyndromic unicoronal suture synostosis) may provide simulataneous assessment of experimental and control treatment groups on either side of the saggital suture within the same animal, resulting in better accuracy of results.

These future experiments may provide answers to fundamental questions regarding the long-term functionality of Titania nanotube implants in highly representative scenarios and direct the use of these interfaces for appropriate clinical applications.

APPENDIX A

HISTOLOGY PROTOCOL

Appendix A contains detailed protocols for histological staining throughout this research. This involves optimised procedure for H&E, Periodic Acid-Schiff (PAS), Movat Pentachrome, Picro-Sirius Red, Alcian Blue and TRAP staining.

H & E Staining Protocol

- Dewax sections in 2 changes of xylene, minimum 1 min each.

- Remove xylene by washing in 2 changes of absolute ethyl alcohol for 30 sec each.

- Immerse sections in distilled water for 15 sec.

- Stain in Lillie-Mayer's alum haematoxylin for 6 min.

- Rinse in tap water to remove excess haematoxylin.

- "Blue" sections in Scott's tap water substitute for 15 sec.

- Rinse in tap water.

- Differentiate haematoxylin stain in 0.25% acid alcohol for approximately 6-8 dips.

- Drain quickly and wash off excess acid alcohol in running tap water.

- "Blue" sections in Scott's tap water substitute for 15 sec.

- Rinse in tap water.

- Stain in alcoholic Eosin for 2 min.

- Drain well, and transfer directly to absolute alcohol, 2 changes for 30 sec each.

- Transfer to xylene, 2 changes, 1 min each. Hold in xylene until ready to coverslip.

Solutions and Reagents:

1. Lillie Mayer alum haematoxylin

   Aluminium ammonium sulphate ---- 200 g

   Haematoxylin ------------------------- 20 g

   Ethanol ------------------------------- 40 ml

   Sodium iodate ----------------------- 4 g

Acetic acid -------------------------- 80 ml

Glycerol ----------------------------- 1200 ml

Distilled water ----------------------- 2800 ml

In a 4L Erlenmeyer flask, to 1000 ml of the distilled water, add the aluminium ammonium sulphate. Place the flask on a heater/stirrer, turn on the heater and allow to mix until the alum dissolves (about 15 mins). Remove the flask from the heater/mixer, allow to cool, then add the remaining 1800 ml distilled water (to further cool the solution). Add the haematoxylin powder to the alcohol and dissolve as much of the powder as possible by shaking for a few minutes. Pour the strong alcoholic solution of haematoxylin into the cooled alum solution and stir to ensure all the haematoxylin powder is dissolved, preferably overnight. Add the sodium iodate, acetic acid, and finally the glycerol. Mix well, plug loosely and store.

2. Scott's tap water substitute

Sodium bicarbonate --- 10 gm

Magnesium sulphate ----------- 100 gm

Distilled water ------------------- 5 L

Dissolve the salts in the water. Store stock solutions at room temperature.

3. Acid alcohol 0.3% Acid Alcohol

Commercial grade ethanol ----- 2800 ml

Distilled water ------------------ 1200 ml

   Conc. hydrochloric acid --------- 12 ml

In a sufficiently large container, add the acid to the water, then add the alcohol and mix thoroughly. The generation of fine bubbles is an indication that mixing is thorough.

4.   Alcoholic acetified eosin/phloxine

   1% eosin Y --------------------- 400 ml

   1% aqueous phloxine -----------40 ml

   95% alcohol -------------------- 3100 ml

   Glacial acetic acid ---------------16 ml

Mix the above reagents together, and stir well. The solution keeps well.

Results:

Collagen----------------------pale pink

Muscle-----------------------deep pink

Acidophilic cytoplasm------red

Basophilic cytoplasm-------purple

Nuclei-------------------------blue

Erythrocytes-------------------cherry red

Sirius Red Staining Protocol

- Dewax sections in 2 changes of xylene, minimum 1 min each.

- Remove xylene by washing in 2 changes of absolute ethyl alcohol for 30 sec each.

- Immerse sections in distilled water for 15 sec.

- Stain with Weigert's haematoxylin for 8 min, and then wash the slides for 10 min in running tap water.

- Stain in picro-sirius red for one hour

- Wash in two changes of acidified water.

- Physically remove most of the water from the slides by vigorous shaking.

- Dehydrate in three changes of 100% ethanol.

- Clear in xylene and mount in a resinous medium.

Solutions and Reagents:

1. Picro-sirius Red Solution

   Sirius red F3B ------------------------ 0.5 g

   Saturated aqueous solution of picric acid ---------500 ml

Mix the above chemicals together, and stir well.

2. Acidified Water

Add 5 ml acetic acid (glacial) to 1 L of water (tap or distilled).

3. Weigert's haematoxylin

Weigert's iron haematoxylin solution, Part A ---------500 ml

Weigert's iron haematoxylin solution, Part B ---------500 ml

Mix the above reagents together, and stir well.

Results:

In bright field:

Collagen----------------------red

Background ----------------- pale yellow background

Nuclei-------------------------grey/black/brown (if stained)

In polarised light:

Large Collagen fibres (Type I) ---------------------- bright yellow or orange

Thin Collagen fibres (Type III) ------------------------- green

Russell-MOVAT Pentachrome Staining Protocol

- Dewax sections in 2 changes of xylene, minimum 1 min each.

- Remove xylene by washing in 2 changes of absolute ethyl alcohol for 30 sec each.

- Immerse sections in distilled water for 15 sec.

- Place slides in Verhoeff's Elastic Stain for 15-20 min, and then wash the slides for 10 min in running tap water.

- Differentiate sections in 2% Ferric Chloride until elastic fibres are sharply defined.

- Rinse slides in distilled water and place in 5% Sodium Thiosulphate for 1 min.

- Rinse slides in running tap water for 5 min.

- Place slides in 3% Acetic Acid for 3 min.

- Place slides directly in 1% Alcian Blue solution for 15-30 min, and then wash the slides for 1 min in running tap water.

- Place the slides in Crocein Scarlet – Acid Fuchsin for 2 min.

- Rinse slides through 3 changes of distilled water.

- Dip slides 5 times in 1% Acetic Acid.

- Place slide in 2 changes of 5% Phosphotungstic Acid for 2-5 min each.

- Dip slide 5 times in 1% Acetic Acid for 1-2 sec each.

- Dehydrate slides through 3 changes of fresh absolute alcohol, 1 min each change.

- Place slide in Alcoholic Saffron solution for 15 min.

- Dehydrate slides through 3 changes of fresh absolute alcohol, 1 min each change.

- Clear slides through 3 changes of fresh xylene, 1 min each change.

- Coverslip using a permanent mounting media.

Solutions and Reagents:

1. Verhoeff's Elastic stain

10% Alcoholic haematoxylin ----------------- 100 ml

Reagent Alcohol-------------------------------100 ml

10% Ferric Chloride ----------------------- 100 ml

 Universal Iodine solution™ ---------------- 100 ml

Mix 20 ml of above reagents together, and stir well, just prior to the use.

2. 5% Sodium Thiosulfate--------- 100ml

3. 1% Alcian Blue Solution---------100ml

4. 1% Acetic Acid -------------------200ml

5. Alcoholic Saffron Solution-------100ml

6. 3% Acetic Acid---------------------100ml

7. 2% Ferric Chloride-----------------100ml,

8. Crocein Scarlet-Acid Fuchsin-----100ml

9. Phosphotungstic Acid--------------200ml.

Results:

Collagen----------------------yellow

Muscle-----------------------red

Elastin fibres, nuclei -------black

Fibrinoid---------------------intense red

Mucins-----------------------blue to green

PAS (Periodic Acid Schiff) Staining Protocol

- Dewax sections in 2 changes of xylene, minimum 1 min each.

- Oxidize slides in 0.5% periodic acid solution for 5 min.

- Rinse slides in distilled water.

- Place slides in Schiff reagent for 15 min.

- Wash in lukewarm tap water for 5 min.

- Counterstain in Mayer's haematoxylin for 1 min.

- Wash in tap water for 5 min.

- Dehydrate and coverslip using a permanent mounting medium.

Solutions and Reagents:

1. 0.5% Periodic Acid Solution

   Periodic acid ---------------------- 0.5 g

   Distilled water -------------------- 100 ml

Mix the above reagents together, and stir well.

2. Schiff Reagent

Test for Schiff reagent: Pour 10 ml of 37% formalin into a watch glass. To this add a few drops of the Schiff reagent to be tested. A good Schiff reagent will rapidly turn a red-purple colour. A deteriorating schiff reagent will give a delayed reaction and the colour produced will be a deep blue-purple.

3. Lillie Mayer alum haematoxylin

Aluminium ammonium sulphate ---- 200 g

Haematoxylin ------------------------- 20 g

Ethanol ------------------------------- 40 ml

Sodium iodate ----------------------- 4 g

Acetic acid --------------------------- 80 ml

Glycerol ------------------------------ 1200 ml

Distilled water ----------------------- 2800 ml

Results:

Glycogen, mucin and some basement membranes --- red/purple

Background --- blue

Alcian Blue Staining Protocol

- Dewax sections in 2 changes of xylene, minimum 1 min each.

- Remove xylene by washing in 2 changes of absolute ethyl alcohol for 30 sec each.

- Immerse sections in distilled water for 15 sec.

- Stain in Alcian blue solution for 30 min.

- Wash in running tap water for 2 min and then rinse in distilled water.

- Counterstain in nuclear fast red solution for 5 min.

- Wash in running tap water for 1 min.

- Dehydrate and through 95% alcohol, 2 changes of absolute alcohol, 3 min. each.

- Transfer to xylene, 2 changes, 1 min each. Hold in xylene until ready to coverslip.

Solutions and Reagents:

1. 3% Acetic Acid Solution

    Glacial acetic acid ----------------- 3 ml

    Distilled water --------------------- 97 ml

2. Alcian Blue Solution (pH 2.5)

    Alcian blue, 8GX ------------------- 1 g

    Acetic acid, 3% solution ----------- 100 ml

    Mix well and adjust pH to 2.5 using acetic acid.

3. 1% Nuclear Fast Red Solution:

    Nuclear fast red ------------------- 0.1 g

    Aluminium sulfate------------------ 5 g

    Distilled water ---------------------100 ml

Dissolve aluminium sulfate in water. Add nuclear fast red and slowly heat to boil and cool.

Filter and add a grain of thymol as a preservative.

Results:

Strongly acidic sulphated mucosubstances -------------- blue

 Nuclei --- pink to red

 Cytoplasm --- pale pink

Tartrate-Resistant Acid Phosphatase (TRAP) Staining Protocol

- Pre-warm sufficient deionised water for a day's use to 37°C. Check temperature before use.

- Bring Fixative Solution (4% Glutaraldehyde) to room temperature (18–26°C).

- Fix slides by immersing in Fixative for 10 min.

- Rinse thoroughly by pipetting deionised water.

- Prepare TRAP solution by mixing deionised water, Naphthol AS-Bl Phosphate solution, Acetate solution and Tartrate solution in a beaker.

- Add 0.5 ml Fast Garnet GBC Base Solution and 0.5 ml Sodium Nitrite Solution in a separate test tube. Mix by gentle inversion for 30-60 sec. Let stand 2 minutes.

- Filter into a new coplin jar.

- Add slides to coplin jar and incubate for 1-2 h in 37°C water bath protected from light.

- Rinse slides thoroughly in deionised water.

- Counterstain with methyl green solution for 8 sec.

- Rinse several minutes in alkaline tap water, air dry and evaluate microscopically.

Solutions and Reagents:

1. TRAP staining solution:

    Pre-warmed water --------------------- 44 ml

    Naphthol AS-Bl Phosphate Solution -------------------- 2 ml

    Acetate Solution ----------- 2 ml

    Tartrate Solution ----------- 2 ml

    Mix well till homogeneous.

2. Fast Garnet GBC Base Solution:

    Fast garnet GBC base-----------------7.0 mg/ml,

    Hydrochloric acid with stabilizer ------------------- 0.4 mol/l

    Sodium nitrite---0.1 mol/l.

3. Methyl green Solution:

    Methyl green --------------------- 0.05 g

    Distilled water --------------------- 100 ml

Results:

Acid Phosphatase activity in leukocytes ---------------------- purplish-dark red granules

Note: All protocols were adapted/modified from either www.ihcworld.com, americanmastertech.com or sigma-aldrich.com.

APPENDIX B

ANIMAL ETHICS APPROVAL

Appendix B contains Animal Ethics Approval forms from The University of Adelaide (first page of the approved application) and Women's and Children's Animal Ethics Committee.

Appendix B: Animal Ethics Approval

The University of Adelaide Animal Ethics Committee   *of* ADELAIDE

Application for Ethical Approval of Project Involving Animals

Office Use Only:	Approval Number:	M-2014-138	Application Code:	0000019298	Approval Date:	14-10-2014	Printed Date:	21/10/2014 04:44:24 PM	Revision Number:	3

A novel treatment to prevent re-operation in craniosynostosis

	Mouse (Fgfr2c342y/+ Genetically modified mice (C57Bl/6 background), N/A)	Mouse (C57Bl/6 wildtype, N/A)
Animals Required	30	30
Animals Approved	30	30
Procedure Types	5	5
Pain Classifications	B	B
Approval Conditions	N/A	

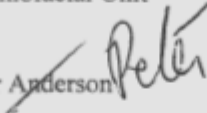|	
Animal Use to Begin	15th October 2014
Animal Use to End	31st August 2015
Project Duration	1 year
Cross Reference	M-2014-049
Type	Research and Higher Degree
Broad Purpose of Project	The Maintenance and Improvement of Human or Animal Health and Welfare
Funds Source	The work has been peer reviewed as this is to be funded by an Australian Dental Research Foundation grant, which has already been awarded. (Grant ID: 18-2013)

Primary Investigator

Name	Associate Professor Peter John Anderson ()
School	School of Dentistry, Faculty of Health Sciences
Contact details	Ph 81617235 AH 8351 6441 peter.anderson@adelaide.edu.au
Correspondence to	School of Dentistry

Role / Responsibility in this project	Supervisory

Techniques	Name	Description
	All Procedures	N/A
	Anaesthesia	N/A
	Supervision of project	N/A
	Surgery	N/A
	Breeding	N/A
	All aspects of the trial	N/A
	Humane Killing by anaesthetic overdose	N/A

Which year did this applicant complete AEC Training?	2008

10 June 2014

Professor Peter Anderson
Australian Craniofacial Unit
WCHN

Dear Professor Anderson

Re: **AE977/6/2014. "A novel treatment in Craniosynostosis".**

Thank you for your letter dated 26 May 2014 in which you responded to matters raised by the
WCHN Animal Ethics Committee at its April 2014 meeting. At its meeting on 3 June 2014 the
Women's and Children's Health Network Animal Ethics Committee **approved the protocol in full
for the period 3 June 2014 until 30 June 2017.**

The AEC is mindful of the need for responsible use of animals and to ensure that where possible,
animals are not used unnecessarily. To that end, the Committee agree that researchers should not
commence research projects until such time as adequate funding is available and that they are
confident that by commencing a project, they are able to at least undertake a phase of an experiment
(involving the use of animals) that is meaningful.

I remind you that approval is given subject to the following:

- Approval is granted for 30 Fgfr2c342y/+ genetically modified mice and 30 C57Bl/6
  wildtype mice to be used.
- **Immediate advice (within 48 hours) of any adverse or unexpected event or if, during
  the course of the experiments, the morbidity and mortality of the animals varies
  significantly from that stated in the original application form submitted to the
  Committee. The advice should include full details of the event, the reasons why this
  occurred and the strategies being implemented to minimise the mortality and
  morbidity.**
- The provision of a brief annual report on the state of progress of the study for the purpose
  of review by the Committee and collation of statistical data for the responsible Minister.
  Additionally, where relevant, a phenotype report MUST also be provided.
- Submission of any proposed changes to the original protocol. Changes must be approved
  by the Committee before they are implemented.
- Immediate advice, giving reasons, if the protocol is discontinued before its completion.
- Advice being given in the event that there is to be a change of Chief Investigator. The
  current Chief Investigator is responsible for the conduct of the project until approval has
  been granted for the new Chief Investigator.
- Any staff working on this project should be instructed in the detailed care and maintenance
  of the animals and in how their actions may affect animal wellbeing and the outcomes of
  scientific and teaching activities. Staff should be supervised until such time as they are
  competent in the procedures being used. Additionally, all personnel should have access to a
  copy of the "Australian code for the care and use of animals for scientific purposes 8th
  Edition 2013" and should attend regular ongoing education or training sessions in order to
  update their skills and knowledge.

This approval is only for those projects that are funded by the source that is stated on the application form. If the source of funding changes for any reason, the Committee must be notified of this change and the reasons.

Before commencement of your project, the enclosed 'New Project Information Sheet' must be forwarded to the Animal House.

Please note the approval number above includes the month and year in which approval expires and should be included in any future communication regarding this protocol.

Yours sincerely

Mr Philip Robinson
Chair
WCHN Animal Ethics Committee

Enc.
Cc: Lynn Marsden, Manager, WCH Animal House

Women's
& Children's
Hospital

2 June 2015

Research Secretariat
Level 2, Samuel Way Building
72 King William Road
Tel   08 8161 6390
Tel   08 8161 6521
www.wch.sa.gov.au

Professor Peter Anderson
Craniofacial Unit
WCH

Dear Professor Anderson

Re: AE999/6/2018. A novel treatment to prevent re-operation in craniosynostosis.

Thank you for your letter dated 20 May 2015 in which you responded to matters raised by the WCHN Animal Ethics Committee at its December 2014 and February 2015 meeting. At its meeting on 2 June 2015, the Women's and Children's Health Network Animal Ethics Committee approved the protocol in full for the period **2 June 2015 until 30 June 2018**.

The AEC is mindful of the need for responsible use of animals and to ensure that where possible, animals are not used unnecessarily. To that end, the Committee agree that researchers should not commence research projects until such time as adequate funding is available and that they are confident that by commencing a project, they are able to at least undertake a phase of an experiment (involving the use of animals) that is meaningful.

I remind you that approval is given subject to the following:

- Approval is granted **for 30 Fgfr2c342y/+ mice and 30 C57 Bl/6 wild type mice (as detailed in your application)** to be used.
- If you have also submitted your application for consideration by another Animal Ethics Committee in South Australia, you **must** provide a copy of the clearance (in relation to this project) from that Committee and work should not commence until you have obtained final clearance from that Institution.
- **Immediate advice (within 48 hours) of any adverse or unexpected event or if, during the course of the experiments, the morbidity and mortality of the animals varies significantly from that stated in the original application form submitted to the Committee. The advice should include full details of the event, the reasons why this occurred and the strategies being implemented to minimise the mortality and morbidity.**
- The provision of a brief annual report on the state of progress of the study for the purpose of review by the Committee and collation of statistical data for the responsible Minister. Additionally, where relevant, a phenotype report MUST also be provided.
- Submission of any proposed changes to the original protocol. Changes must be approved by the Committee before they are implemented.
- Immediate advice, giving reasons, if the protocol is discontinued before its completion.
- Advice being given in the event that there is to be a change of Chief Investigator. The current Chief Investigator is responsible for the conduct of the project until approval has been granted for the new Chief Investigator.
- Any staff working on this project should be instructed in the detailed care and maintenance of the animals and in how their actions may affect animal wellbeing and the outcomes of scientific and teaching activities. Staff should be supervised until such time as they are competent in the procedures being used. Additionally, all personnel should have access to a copy of the "Australian code for the care and use of animals for scientific purposes 8th Edition 2013" and should attend regular ongoing education or training sessions in order to update their skills and knowledge.
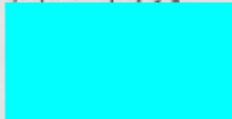
This approval is only for those projects that are funded by the source that is stated on the application form. If the source of funding changes for any reason, the Committee must be notified of this change and the reasons.

Government
of South Australia

SA Health

Before commencement of your project, the enclosed 'New Project Information Sheet' must be forwarded to the Animal House.

Please note the approval number above includes the month and year in which approval expires and should be included in any future communication regarding this protocol.

Mr Philip Robinson
Chair
WCHN Animal Ethics Committee

Enc.
Cc: Lynn Garrard, Manager, WCH Animal House

14 June 2011

Government of South Australia

SA Health

Women's & Children's Hospital

A/Prof Barry Powell
WCHRI
Level 7, Rieger Building

Research Secretariat
72 King William Road
North Adelaide SA 5006
Tel   08 8161 6521
Tel   08 8161 6390
Fax 08 8161 8177
www.cywhs.sa.gov.au

Dear Professor Powell

Re: AE884/6/2014. "Breeding colonies of mouse models of suture fusion and craniosynostosis"

Thank you for submitting the above protocol. At its meeting on 7 June 2011, the Children, Youth & Women's Health Service Animal Ethics Committee approved the protocol for the period **7 June 2011 until 30 June 2014** on the **following proviso:**

- That no C57/B1/6 mice are to be bred within the CYWHS Animal House. You should discuss this matter and your requirements for this strain of mouse with the Manager of the Animal House who will arrange for them to be sourced.

I remind you that approval is given subject to the following:

- Approval is granted for 10 breeding pairs Twist1$^{+/-}$ mice, 10 breeding pairs Fgfr2c$^{342y/+}$ mice to be used.
- **Immediate advice (within 48 hours) of any adverse or unexpected event or if, during the course of the experiments, the morbidity and mortality of the animals varies significantly from that stated in the original application form submitted to the Committee. The advice should include full details of the event, the reasons why this occurred and the strategies being implemented to minimise the mortality and morbidity.**
- The provision of a brief annual report on the state of progress of the study for the purpose of review by the Committee and collation of statistical data for the responsible Minister.
- Submission of any proposed changes to the original protocol. Changes must be approved by the Committee before they are implemented.
- Immediate advice, giving reasons, if the protocol is discontinued before its completion.
- Advice being given in the event that there is to be a change of Chief Investigator. The current Chief Investigator is responsible for the conduct of the project until approval has been granted for the new Chief Investigator.
- Any staff working on this project should be instructed in the detailed care and maintenance of the animals and in how their actions may affect animal wellbeing and the outcomes of scientific and teaching activities. Staff should be supervised until such time as they are competent in the procedures being used. Additionally, all personnel should have access to a copy of the "Australian code of practice for the care and use of animals for scientific purposes 7th Edition 2004" and should attend regular ongoing education or training sessions in order to update their skills and knowledge.

This approval is only for those projects that are funded by the source that is stated on the application form. If the source of funding changes for any reason, the Committee must be notified of this change and the reasons.

Before commencement of your project, the enclosed 'New Project Information Sheet' must be forwarded to the Animal House.

Please note the approval number above includes the month and year in which approval expires and should be included in any future communication regarding this protocol.

Mr Philip Robinson
Chair
CYWHS Animal Ethics Committee

Enc.
Cc: Lynn Marsden, Manager, WCH Animal House

APPENDIX C

AUSTRALIAN DENTAL RESEARCH FOUNDATION (ADRF) GRANT APPROVAL

Appendix C contains the grant approval acknowledgement for this project from Australian

Dental Research Foundation (ADRF).

Australian Dental Research Foundation Inc.

ABN 54 963 830 138 (Incorporated in the ACT)

14-16 Chandos Street, St Leonards, NSW 2065 Telephone: (02) 9906 4412 Facsimile: (02) 9906 4676
Address all correspondence to: Honorary Secretary, PO Box 520, St Leonards, NSW 1590

20 November 2013

Email: adrf@ada.org.au   Website: www.ada.org.au

Ms Manpreet Bariana
School of Dentistry
University of Adelaide
Colgate Dental Research Centre
ADELAIDE SA 5005

Dear Ms Manpreet Bariana

ADRF GRANT APPLICATION : 18-2013

At their Annual Meeting held on 19 November 2013, the Directors of the Australian Dental Research Foundation considered your application for a grant to support the project entitled:

"The application of novel nanoengineered implants for craniosynostosis therapy"
Ms Manpreet Bariana
Dr Sarbin Ranjitkar
A/Prof Peter Anderson
A/Prof John Kaidonis
Prof Dusan Losic
Prof Grant Townsend

It was agreed that your application be supported to the extent of $6,000.00 for one year. Subject to your agreement to the Conditions, the Directors have specified your research grant will take effect from January 2014. Australian Dental Research Foundation grants are normally paid in arrears. However, the Directors recognise that applicants may incur some unavoidable expenses in commencing their projects, particularly where equipment is to be purchased, and would be willing to make an initial payment available to you on receipt of a tax invoice with a detailed statement of the requirements.

I enclose a document setting out the Conditions of your research grant and I would be grateful if you would sign the attached acknowledgment form (page 4 of Conditions) and return it to this office. This exchange will represent the contract between you, your co-workers and the Foundation. **Please ensure that the acknowledgement form is returned to this office no later than 1 March 2014, or the offer of funds may be withdrawn.**

At the conclusion of the project the attached Final Report Coversheet shall be submitted to the Foundation, together with the abstract (in Word format as only electronic submission will be accepted) in a form suitable for publication in the Special Research Supplement of the *Australian Dental Journal* as described in the Conditions Governing Research Grants. Please note that these have recently been updated to facilitate streamlining of the Supplement. Publication of the abstract in the *Australian Dental Journal* shall not prevent the author(s) from submitting more detailed or specialised manuscripts to other scientific journals. It is permissible also to submit the primary manuscript to another scientific journal, provided that an abstract is supplied to the Foundation.

It was the recommendation of the Research Advisory Committee that summaries of comments from referees and the RAC be made available to you and a copy is enclosed.

May I take this opportunity to wish you every success with your research undertaking.

I am also taking this opportunity to enclose a Supporter's Form seeking your support. This has been a difficult year for the Foundation financially and as you no doubt know, it is difficult to attract funding for dental research as it has to compete with other research disciplines, which often have a much higher public profile, and the Foundation depends largely on donations from the profession and the dental industry. Your assistance in considering support of the Foundation would be much appreciated. Please feel free to copy and pass on the application form to others who may be interested.

With kind regards

Yours sincerely

Robert N Boyd-Boland
Honorary Secretary

Encls: